Analytical Study of Alternative Bridge Deck Models for use on Movable Bridges

Project Number: WPI-0510856

Final Report

Submitted to
Florida Department of Transportation
Mr. Jose A. Quintana, P.E. (Project Manager)

by

Dr. Okey Onyemelukwe, P.E.

Civil & Environmental Engineering Department
University of Central Florida
Orlando, Fl. 32816

March 25,1999

Technical Report Documentation Page

1.Report No. WPI 0510856	2.Government Accession No.	3. Receipient's Catalog No.
4. Title and Subtitle Analytical Study of Alternative Bridge Deck Models for use on Movable bridges.		5. Report Date 03/99
7. Author(s) Okey U.Onyemelukwe,Ph.D.,PE.		6. Performing Organization Code 8. Performing Organization Report
9.Performing Organization name and address University of Centeral Florida Civil & environmental Engineering Dept. 4000 Central Florida Blvd. Orlando,Fl. 32816		10. Work Unit No. 11. Contract or Grant No. B-B536 99700-3555-119
12. Sponsoring Agency name and address Florida Department of Transportation 605 Suwannee Street Tallahassee, FL 32399-0450		13. Type of Report and Period Covered Research 08/97 - 01/99 14. Sponsoring Agency Code
15.Supplementary Notes		

16. Abstract :
This report consists of the analytical studies involved in the development of efficient and optimized Fiber Reinforced Polymer (FRP) bridge decks for use on movable bridges.The study is presented in two parts,Part A: "Tube" and "sheet" Models,and Part B:"Monolithic"models.The two parts follow a parametric study approach,while utilizing the Finite Element Software ANSYS for all the analysis.The bridge deck systems developed are subjected to both static and dynamic loading conditions,amongst other variations in cross-sectional parameters,boundary conditions,and load combinations. The study concludes that while the existence of high-localized shear stresses is a critical consideration,especially with regards to designing a suitable connection between the bridge deck and the underlying stringers,the "monolithic" models were found to be structurally more efficient.

17. Key Words	18. Distribution Statement
Movable Bridge Deck Systems Fiber Reinforced Polymer (FRP) composites FRP-Bridge Deck Models Finite Element Model of Bridge Decks Alternative Bridge Deck Systems	

19. Security Classif.(of this report)	20. Security classes (of this page)	21. No. of pages	22. Price
Unclassified	Unclassified	200	

Disclaimer Sheet

The opinions, findings and conclusions expressed in this publication are those of the authors and not necessarily those of the Florida Department of Transportation or the US Department of Transportation.

This publication was prepared in cooperation with the state of Florida Department of Transportation & the US Department of Transportation.

SI* (MODERN METRIC) CONVERSION FACTORS

APPROXIMATE CONVERSIONS TO SI UNITS

Symbol	When You Know	Multiply By	To Find	Symbol
LENGTH				
in	inches	25.4	millimeters	mm
ft	feet	0.305	meters	m
yd	yards	0.914	meters	m
mi	miles	1.61	kilometers	km
AREA				
in^2	square inches	645.2	square millimeters	mm^2
ft^2	square feet	0.093	square meters	m^2
yd^2	square yards	0.836	square meters	m^2
ac	acres	0.405	hectares	ha
mi^2	square miles	2.59	square kilometers	km^2
VOLUME				
fl oz	fluid ounces	29.57	milliliters	ml
gal	gallons	3.785	liters	l
ft^3	cubic feet	0.028	cubic meters	m^3
yd^3	cubic yards	0.765	cubic meters	m^3

NOTE: Volumes greater than 1000 l shall be shown in m^3.

MASS				
oz	ounces	28.35	grams	g
lb	pounds	0.454	kilograms	kg
T	short tons (2000 lb)	0.907	megagrams	Mg
TEMPERATURE (exact)				
°F	Fahrenheit temperature	5(F-32)/9 or (F-32)/1.8	Celcius temperature	°C
ILLUMINATION				
fc	foot-candles	10.76	lux	l
fl	foot-Lamberts	3.426	candela/m^2	cd/m^2
FORCE and PRESSURE or STRESS				
lbf	poundforce	4.45	newtons	N
psi	poundforce per square inch	6.89	kilopascals	kPa

APPROXIMATE CONVERSIONS FROM SI UNITS

Symbol	When You Know	Multiply By	To Find	Symbol
LENGTH				
mm	millimeters	0.039	inches	in
m	meters	3.28	feet	ft
m	meters	1.09	yards	yd
km	kilometers	0.621	miles	mi
AREA				
mm^2	square millimeters	0.0016	square inches	in^2
m^2	square meters	10.764	square feet	ft^2
m^2	square meters	1.195	square yards	ac
ha	hectares	2.47	acres	mi^2
km^2	square kilometers	0.386	square miles	
VOLUME				
ml	milliliters	0.034	fluid ounces	fl oz
l	liters	0.264	gallons	gal
m^3	cubic meters	35.71	cubic feet	ft^3
m^3	cubic meters	1.307	cubic yards	yd^3
MASS				
g	grams	0.035	ounces	oz
kg	kilograms	2.202	pounds	lb
Mg	megagrams	1.103	short tons (2000 lb)	T
TEMPERATURE (exact)				
°C	Celcius temperature	1.8C + 32	Fahrenheit temperature	°F
ILLUMINATION				
lx	lux	0.0929	foot-candles	fc
cd/m^2	candela/m^2	0.2919	foot-Lamberts	fl
FORCE and PRESSURE or STRESS				
N	newtons	0.225	poundforce	lbf
kPa	kilopascals	0.145	poundforce per square inch	psi

* SI is the symbol for the International System of Units. Appropriate rounding should be made to comply with Section 4 of ASTM E380.

(Revised August 1992)

DISCLAIMER

This document contains

tone-on-tone or color

graphs, charts and/or pictures

which have been reproduced in

black and white.

EXECUTIVE SUMMARY

Problem Statement

Several of the FDOT Movable bridges are made of steel structures with open deck grating, and are approaching the end of their design service life or may be obsolete in design. Often, these bridges require high rehabilitation and maintenance costs, either to upgrade them to meet current standards, or in most cases to combat deterioration of the steel members, caused by exposure to highly corrosive environments. Over the years, some of the notable problems that have been identified from a structural point of view, include, but are not limited to:

- **Corrosion** of steel structures and concrete reinforcing bars
- **Open deck designs are noisy**, provide less traction, and produce a disconcerting "feel" to the motorist. It also offers no environmental protection to steel members below.
- **Conversion from open to a closed deck design** through the addition of concrete and reinforcement may significantly increase the bridge weight. A significant increase in weight may require the redesign of structural and mechanical systems, and will definitely reduce the live load capacity of the bridge.
- **The need to satisfy current traffic conditions and design standards may require bridges to meet higher load criteria.** At the same time, fatigue and deterioration may decrease the usable capacity of such bridge structures and mechanical systems.

Project Objectives

To mitigate some of the above-mentioned problems, it is the objective in this project to analytically investigate the use of Fiber Reinforced Polymer (FRP) composites as an alternative bridge deck material. The ultimate goal being the provision of the necessary analytical background and support data, for the development of a prototype FRP composite bridge deck system, to be fully load tested in a subsequent project. This project may thus be considered as an exploratory one into the future development and use of FRP deck systems, as a viable alternative on movable bridges. An optimized modular closed deck design using finite element techniques will be developed in this study.

The investigation consists of two parts, in which a "tube" and "sheet" bridge deck model is first developed from readily available FRP production materials and shapes, and secondly, the development and analysis of an optimized "monolithic" FRP deck system. The analytical models are designed to conform to practical and actual bridge deck systems and configurations. In this case, the Sunrise Boulevard Bridge in Fort Lauderdale served as a typical movable bridge. Finite element analysis of the deck systems utilizes AASHTO HS-20 truck live load, ML80 military load, and wind load criteria. The models are investigated for stress, deflection and dynamic behavior.

Project Findings

This report is divided into two parts, Part A: Tube and Sheet Models, and Part B: Monolithic Models, and a parametric study approach is used in both investigations.

The effects of varying parameters such as: boundary conditions, vehicular live load, single span vs. multiple span deck units, orientation of cover sheet fibers, and existence of free edges and joint discontinuities, top the investigations of Part A of the study. In Part A, two models, a 10.1cm x 10.1cm (4" x 4") tube with 2.5cm (1") top and bottom cover sheets, and a 12.7cm x 17.8cm (5" x 7") tube with 1.9cm (3/4") top and bottom cover sheets, emerge as the most viable systems. The study determined that the changes in boundary condition, representing plausible design and application of the deck to bridge attachments, has a significant impact on the adequacy of the models. On the other hand, the joint discontinuity models produced significant increases in the shear and bending stresses in the web of the tubes. However, both "tube" and "sheet" models performed poorly with respect to the deflection criteria used in the study.

In Part B, an optimized model consisting of a "monolithic" or continuously formed, thin-walled FRP deck system was developed. This new system evolved as an improvement over the "tube" and "sheet" model, and four of them were developed and analyzed for both static and dynamic load conditions, along with one model of Part A. Some of the parameters considered, in addition to those mentioned in Part A, include: the effect of inclining the webs, varying the distance between the webs, and variation of the web thickness. The static analysis indicated remarkable improvements in the performance of these shapes over those of Part A, with respect to stresses and deflection. The free vibration analysis used to establish the dynamic properties of the models, also show that these models were far from exhibiting resonance behavior under normal traffic conditions. Finally, dynamic load factors ranging from 0.239 to 1.49 were determined for these models at normal traffic loads, based on a forced vibration analysis.

Project Conclusions

The most significant conclusion from the "tube" and "sheet" models of Part A is the existence very high-localized shear stresses in the region of the boundary nodes. This condition thus calls for absolute care in treating the deck to bridge attachment points, both in the finite element modeling and in constructing a prototype for load testing. In addition to high web shear stresses, web buckling was also identified as a potential problem for this type of FRP model. It was also recommended that joint discontinuities in the deck be located over the underlying stringers for good engineering practice.

Comparison of the "monolithic" models with the "tube" and "sheet" models indicate the former out performed the latter under both static and dynamic load conditions. However, the parametric studies point out that the changes in web thickness and the spacing between the webs affect the stresses and deflection more. These "monolithic" models are thus recommended for further use in any load testing research.

TABLE OF CONTENTS

LIST OF TABLES

LIST OF FIGURES

CHAPTER 1

INTRODUCTION

1.1 Background

A critical issue, which has been receiving increased public awareness, is the deteriorated state of roads and bridges within the United States. There are over 570 thousand registered bridges in the US[1]. Nearly half of these are either structurally deficient, in various stages of decay or are considered obsolete . Bridges may be located in humid and corrosive environments. The corrosion of steel structure and concrete reinforcing bar has rendered many bridges structurally deficient. Corrosion remains a major concern for bridge owners with respect to the high preventative maintenance costs and costs of rehabilitation.

Bridge deterioration has been caused in part by increasing budget constraints coupled with the high cost of repair. It has been estimated that the cost to the Federal Highway Administration to correct bridge deficiencies would be over 90 billion dollars [1]. The cost of infrastructure renewal has prompted the federal government to encourage research and investigation into new infrastructure technologies.

The deteriorated state of many bridges in the United States, coupled with the high cost of maintenance and rehabilitation, has promoted a need for new innovative and economical materials and methodologies for infrastructure applications. Fiber reinforced polymer (FRP) composites, which have been used for structural applications in the

military and aerospace industries for years, are currently being investigated for various infrastructure applications, including their use as structural elements in bridges. This investigation focuses on the use of FRP composites as an alternative to conventional movable highway bridge decks.

1.2 Issues Related to Movable Bridges

Since the early 1900's movable bridges have consisted of an open steel deck-grating configuration. In most cases, these movable bridges are located over waterways. One disadvantage of using the open steel deck configuration is that it allows road salts and other debris to fall through and corrode the underlying substructure of the bridge. Also, the deck and superstructure may have steel components that can corrode as well. Another problem with open deck grating is the discomfort it causes to motorists due to reduced amount of traction between the car and deck. In some cases, these movable bridges are located in areas close to condominiums or hotels, in which case, the high noise level created by the open steel deck, as the vehicle rides over the surface, may become an environmental nuisance to residents. However, to accommodate this problem, dampers may be connected to the decking which reduces the noise. An example of these noise reduction dampers can be seen on the Sunrise Boulevard Bridge in Fort Lauderdale, shown as tan strips in Figures 1-1 and 1-2. Also, the corrosion of existing structural members, as seen in Figure 1-3, mainly the deck, causes costly repairs to be required frequently. These repairs result in closure of the bridges and can become an inconvenience to the motorists and residents, as well as the water traffic below.

to be required frequently. These repairs result in closure of the bridges and can become an inconvenience to the motorists and residents, as well as the water traffic below.

Figure 1-1 -- Example of Noise Dampers in the Sunrise Boulevard Bridge, Fort Lauderdale, Florida

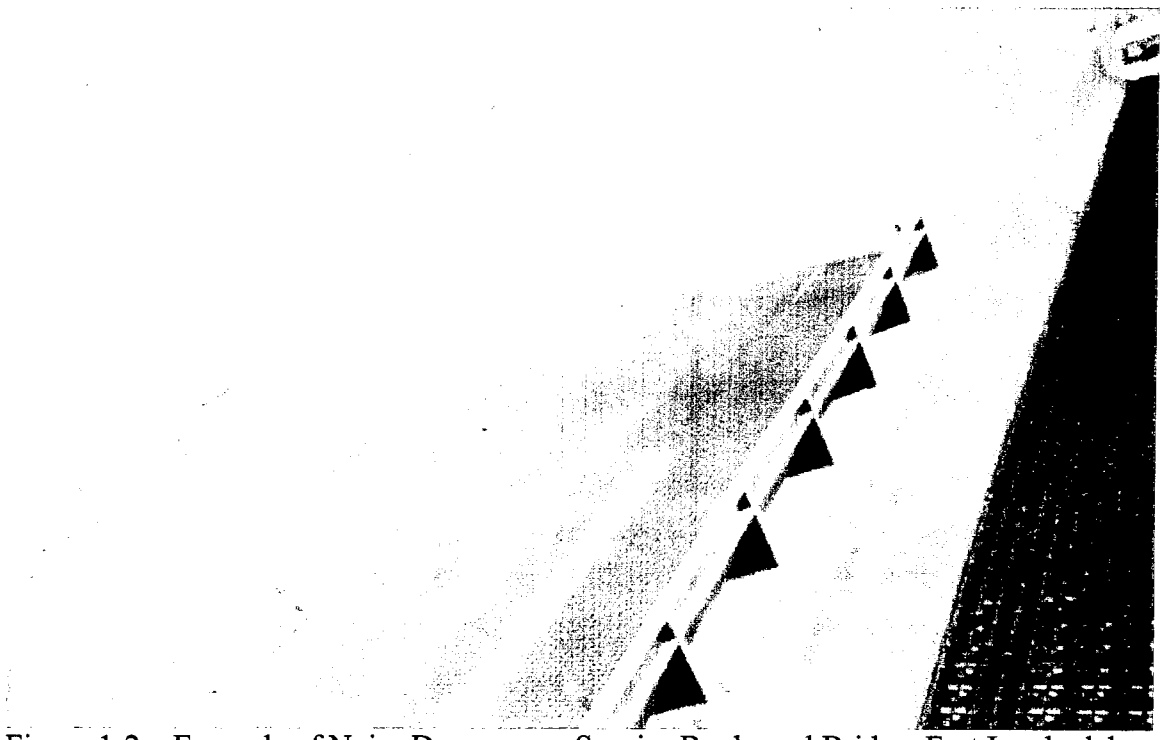

Figure 1-2 – Example of Noise Dampers on Sunrise Boulevard Bridge, Fort Lauderdale, Florida

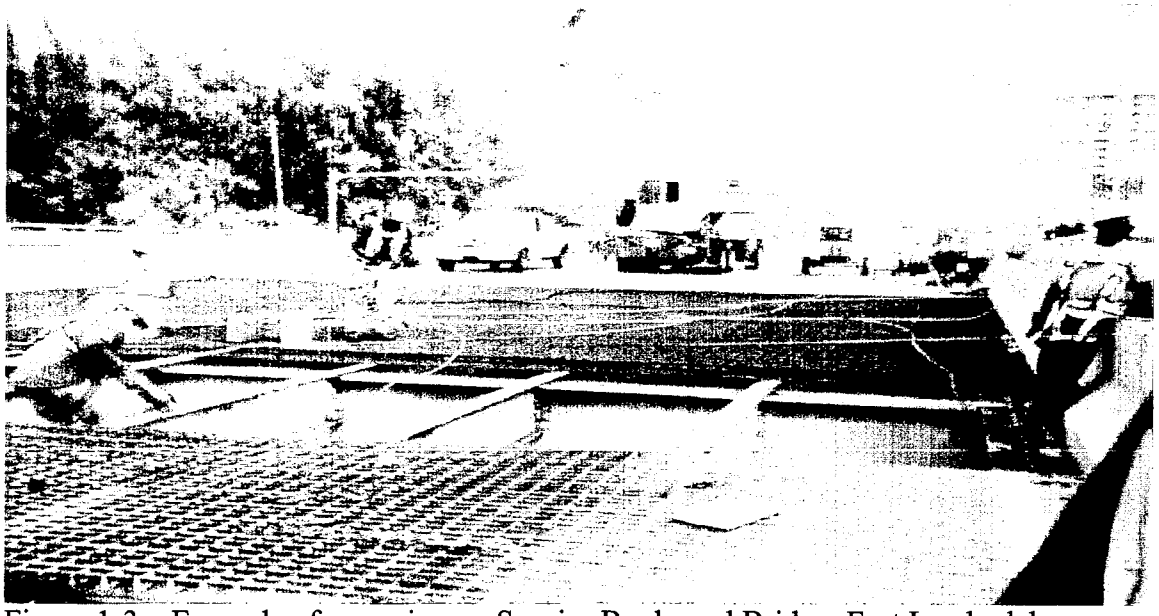

Figure 1-3 – Example of corrosion on Sunrise Boulevard Bridge, Fort Lauderdale, Florida

In addition, wear and tear, fatigue and deterioration resulting from corrosion may result in a reduction of the live load capacity of a bridge. These problems may be compounded by the need to meet current AASHTO bridge standards that may require an increase in live load capacity or traffic volume. These bridges will require costly rehabilitation and upgrading in order to meet current AASHTO standards. Also, costs are increased by the need to maintain corrosion preventative measures.

A critical issue with regard to movable bridges is weight. In order to reduce wear and tear and minimize maintenance costs associated with the bridge lift operation, the movable span weight must be kept to a minimum. The movable span weight also effects the live load capacity of the bridge. Conventional rehabilitation and upgrading of movable bridges may increase the self-weight of movable spans. Hence, the span lifting mechanism may in turn require upgrading to handle the increased load requirements.

In addition, steel grating decks consist of a large number of welds to secure the various components of the grating. Welds produce material discontinuities that are susceptible to fatigue and stress corrosion cracking. Periodic weld repairs are often necessary in order to maintain the deck system.

For the reasons listed above, it is often desirable to replace deteriorated steel grating with a closed deck design. Several deck systems are available for this purpose, most of which require the addition of concrete. One system that is often applied over an existing deck grating is referred to as an exodermic deck system. Installation of this system involves the addition of vertical studs welded to the original grating. The studs protrude above the original grating and provide an anchor for the concrete. Sheet metal is

positioned over the grating to support the uncured concrete. Next, concrete reinforcing bar is positioned and a concrete slab is poured. A diagram of the exodermic deck system is shown in Figure 1-4.

While the exodermic deck system is strong and allows for the use of existing steel grating, a number of disadvantages has become apparent. The concrete slab thickness may range from 7.6cm to 12.7cm (3" to 5") [2] resulting in a dramatic increase in weight. In addition, the system requires the attachment of numerous welded studs to the steel grating. This process is expensive and time consuming and as mentioned earlier, the welds are subject to fatigue and stress corrosion cracking. Also, since welds would be buried beneath the concrete, inspection and repair would not be possible. Another problem would be that existing bridges would be put out of operation for an extended period of time in order to allow for the attachment of the hold down studs and to allow for the curing of concrete.

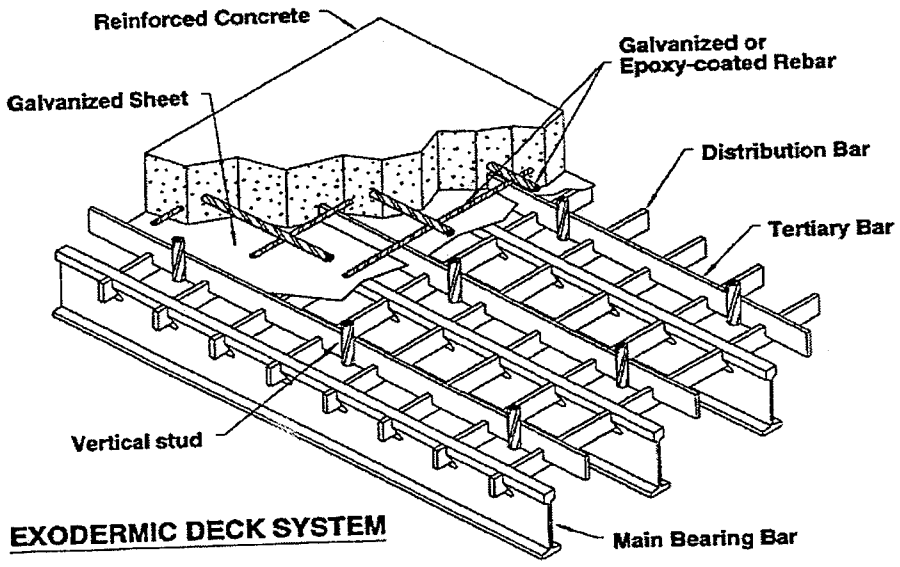

Figure 1-4 -- Diagram of Exodermic Deck System from Reference [2]

Another system involves the installation of a specially designed deck grating which can support a metal tray at either the mid-depth or bottom of the grating system. Concrete reinforcing bar is then passed through holes in the grating. The grating may be either half filled or entirely filled with concrete to its full depth. This system, while strong and typically lighter than some exodermic deck systems, has some of the same disadvantages as the exodermic system. For this system, a significant increase in weight results, the bridge must be taken out of service while cast-in-place concrete cures and the ability to inspect and repair welds is diminished. The filled and half filled grating and concrete deck system is shown in Figure 1-5.

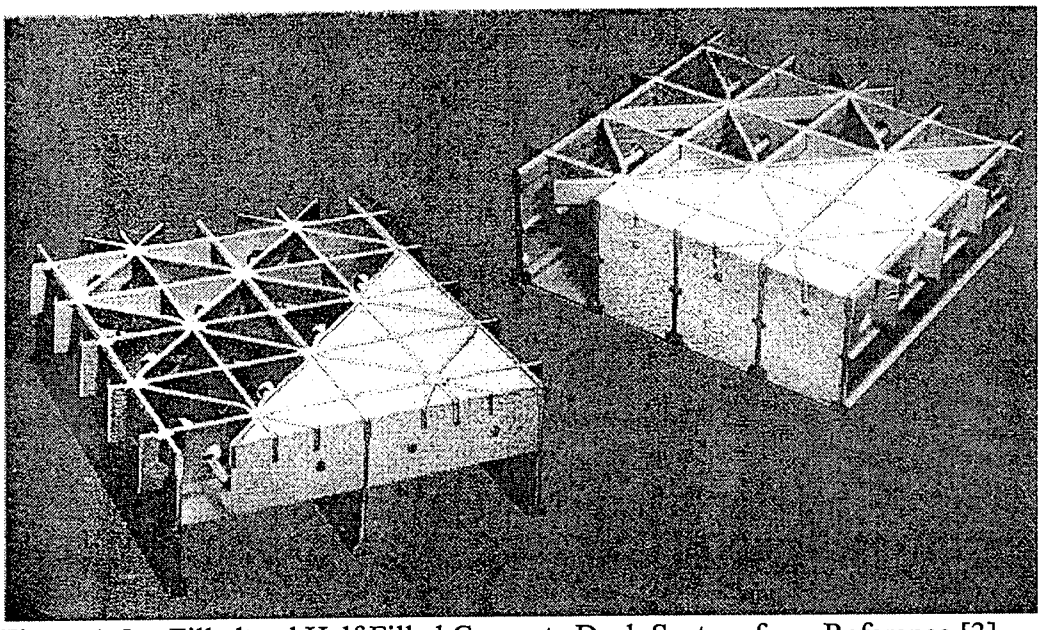

Figure 1-5 -- Filled and Half Filled Concrete Deck System from Reference [3]

1.3 Rational for the Design of FRP Composite Movable Bridge Decks

While the above systems provide a viable and strong closed deck system, they both require the addition of concrete resulting in a substantial increase in weight. In

addition, since the concrete is cast-in-place, the structure cannot be used until the concrete cures. This may result in extended traffic flow interruption and blockage of a waterway. A potential solution to the above problems could be found through the use of FRP composites. FRP composites have several attributes that would be beneficial for movable bridge applications as listed below.

FRP composites are lightweight and can weigh up to 80% less than conventional steel or concrete structures. Also, they have a high strength to weight ratio in comparison to typical steel and concrete. Structural shapes can be produced with lengthwise tensile and flexural strengths of 207 MPa (30,000 psi). In addition, rods and bars can achieve tensile strengths of 689 Mpa (100,000 psi) [4].

Another advantage is that FRP structures are highly resistant to the corrosive environments that have resulted in the deterioration of many bridges. Hence, minimizing the need for corrosion preventative measures reduces maintenance costs. The addition of chemical additives and surface veil fabrics to the composite increases the resistance to ultraviolet radiation and corrosive environments. Chemical additives may also be added to enhance resistance to high temperatures and to provide color.

Additionally, FRP composite structures may be produced in lightweight modular packages allowing for the reduction of heavy lifting and staging requirements during bridge erection or rehabilitation. Lightweight FRP components can be manufactured prior to installation as opposed to cast-in-place concrete. As a result, it would not be necessary to wait for a concrete deck to cure which will result in reduced traffic and

waterway traffic interruption. It should also be noted that FRP composites are becoming more competitive in terms of cost.

Traditionally, FRP composites have been thought to be too costly for practical infrastructure application. Recent research activity [1] dealing with the use of FRP composites in infrastructure indicates that the cost of using composites is decreasing, especially as a result of its increased utility in the non-defense/aerospace industry. A project undertaken at the Lockheed Martin Palo Alto Research Laboratory involved the development of an FRP bridge section which was produced at a cost of $11/kg ($5/lb) and a weight of about $1/5^{th}$ that of a conventional system. A traditional structural system may cost between 66 cents to $2.20 per kg (30 cents to a dollar a pound) [1].

In addition, when the weight savings and the potential for reduced life cycle costs were taken into consideration, the project was considered to have successfully demonstrated the economic viability of composite materials. It is also believed that a life cycle cost analysis would demonstrate the potential long-term benefits of using FRP composites. This could be realized mainly in the form of a substantial reduction in required maintenance cost.

1.4 Research Objectives

In this report, section 1.1 provided a brief overview of some of the problems facing infrastructure in the United States, while section 1.2 described problems related to movable bridges. Hence, the purpose of this investigation is to provide a potential solution to some of the problems discussed in sections 1.1 and 1.2.

To meet this goal, a lightweight movable FRP bridge deck design was investigated. The deck was designed as a closed deck system to avoid some of the problems associated with open deck systems as previously discussed. Since cost is often a primary issue in bridge design and rehabilitation, emphasis was placed on the use of readily available factory produced materials. Pultruded structural shapes and sheet that are manufactured in a factory and are normal stock items were used in this investigation. Various configurations involving pultruded FRP composite elements were investigated.

The FRP composite bridge deck system was evaluated by initially using hand calculations to select potential deck configurations. The hand calculations used a simplified effective width and one way action approach to evaluate potential deck configurations for deflection, bending stresses and shear stresses. Then, a more detailed static linear finite element analysis (FEA) was undertaken to evaluate the bridge deck configurations that resulted from the hand calculations.

During the finite element analysis, a number of parameters were studied that could effect the outcome of the design. Several models with different boundary conditions were analyzed to evaluate the effect of different deck to bridge attachment configurations. As discussed in Chapter 3, I-beam stringers will support the deck; as a result, the deck could consist of single or multiple span configurations. Since various bridge deck configurations could affect the outcome of the analysis, single and multiple span configurations were evaluated to determine the worst case conditions.

In addition to the above, various loading conditions were investigated in accordance with the AASHTO Standard Specifications for Highway Bridges [5] and the

AASHTO Standard Specifications for Movable Highway Bridges [6]. Also, the effect of a deck panel joint discontinuity was investigated to see if deck joints should be located over underlying structure. And finally, since FRP composite material properties are directionally dependent (orthotropic), the effects of different deck component orientations were analyzed.

1.5 The Organization of this Report

To this point, Chapter 1 of this report has provided some of the rational for the development of an FRP composite deck for movable bridges. Some of the methodologies used to develop an FRP deck were also discussed. In order to develop a suitable background, Part A Chapter 2 provides a description of FRP composite materials and presents the results of a literature survey into the use of FRP composites for infrastructure applications. The chapter also provides information on existing research and current FRP composite bridge applications The remainder portion of this report is divided into two parts as described in the following paragraphs.

Part A will discuss the static analysis of tube and sheet models where Part B will discuss the static and dynamic analyses of monolithic models. Next, Part A Chapter 3 of this report provides information related to the design of an FRP composite bridge deck. In this Chapter , criteria, material properties and geometric requirements are established for the design. In addition, the method of analysis for the initial trail hand calculations is discussed.

Then, Part A- Chapter 4 provides a description of the finite element analysis utilized for this portion of the study. The chapter details the deck configurations investigated and how the models were developed. The chapter also describes the various parameters that were investigated and the rational behind the parametric investigations. Part A-Chapter 5 presents the results of the parametric studies using tables and charts to provide comparison between the parametric results under consideration. The parametric results are then evaluated in Part A-Chapter 6 where stress contour plots are provided to illustrate some of the common critical stress locations.

Finally, Part A-Chapter 7 provides the conclusions developed as a result of this study. In addition, Part A-Chapter 7 provides recommendations for furthur study. The recommendations are also provided for the investigation of topics that were outside the scope of this study. It should be noted that this analysis was originally conducted using English units. The results were then converted to the SI units as presented along with the English units for convenience.

Part B-Chapter 8 will detail how each of the finite element models for the monolithic types were created and input into the ANSYS program that was used for the analysis. Part B-Chapter 9 will expands on details from Part B-Chapter 8 to present and discuss the data and results from the static analysis. Part B-Chapter 10 will be the data and results from the free vibration dynamic analysis, where as, Part B-Chapter 11 will detail the forced vibration dynamic analysis. In Part B-Chapter 12 a brief summary of the conclusions drawn from this portion of the research will be presented. This chapter will

also describe areas that need further research, and will present recommendations to be considered before implementing a testing program.

CHAPTER 2

BACKGROUND

2.1 Description of FRP Composites

Generally, FRP composites consist of glass, carbon or aramid fibers that are wetted and bonded together with a resin formulation and then allowed to cure. The resin matrix, which has a relatively low modulus, serves to bond the stronger higher modulus fibers together. A typical polyester resin has a tensile strength of about 40-85 MPa and a tensile modulus of 1.3 to 4.1 GPa. E-glass fiber has a tensile strength of 1.72 GPa and a modulus of 72 GPa [7]. Plastic flow of the resin results in load transfer to the higher modulus fibers, which in turn carry a higher percentage of the load. The resin also provides separation of the fibers. This helps to reduce crack propagation between fibers.

Resins come in a variety of formulations depending on the application requirements. A variety of fibers are also available. Glass, carbon and aramid fibers are typically used for structural applications. The strength of a given composite is dependent on the resin, the fiber type, the percentage of the composite consisting of fibers and fiber orientation. Fibers are significantly stronger in tension and compression than in shear. Fiber strands

are usually oriented parallel to the direction where strength is required. The fibers can be oriented to provide strength in various directions as required. Fibers may also be oriented randomly to provide quasi-isotropic properties, as shown in Figures 2.1 and 2.2. In addition, fibers may be woven into fabrics or longitudinally aligned fibers may be stitched together as shown in Figure 2.3. Many custom profiles are possible. Commonly, a percentage of a composite will consist of longitudinally oriented fibers to resist axial and bending loads while shear loads may be carried by fibers with a +/- 45 degree orientation with respect to the longitudinal axis.

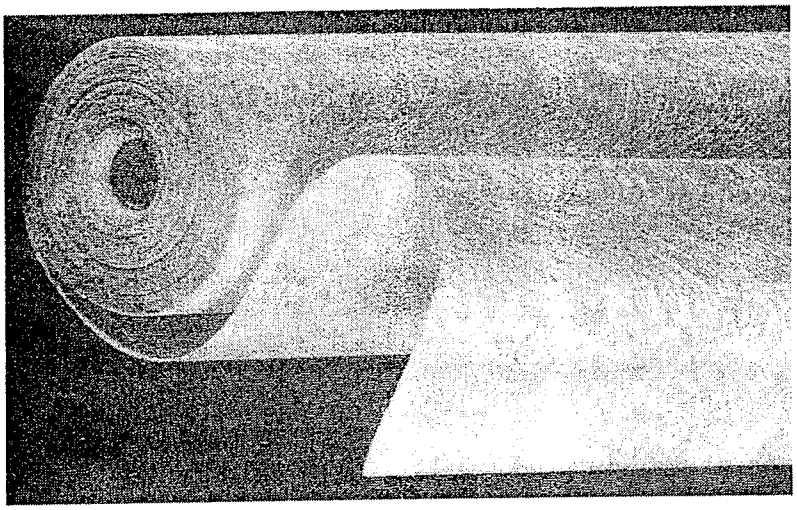

Figure 2.1 Illustration of Chopped Strand Mat from Reference [8]

Figure 2.2 Close-up View of Chopped Strand Mat from Reference [8]

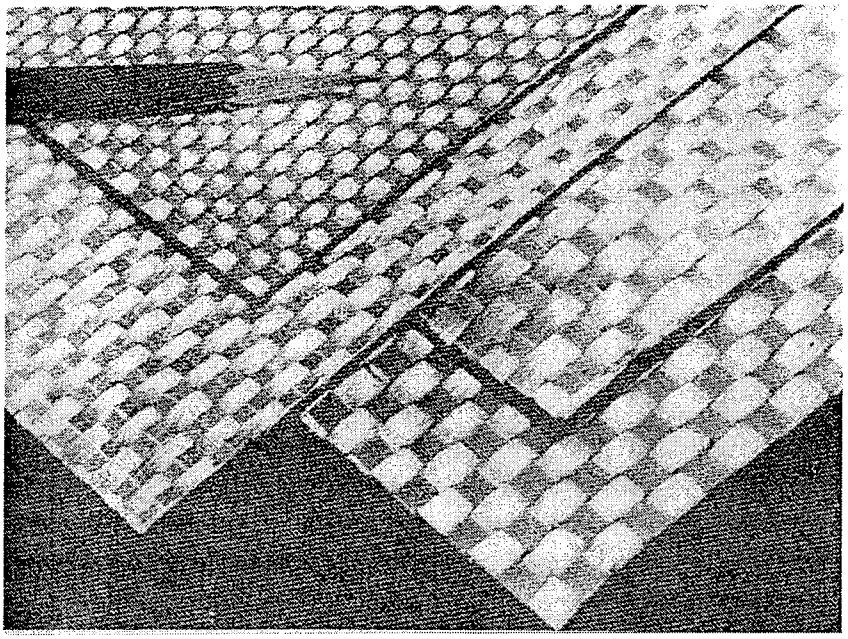

Figure 2.3 Illustration of Woven Roving Fabrics from Reference [8]

Since the strength of an FRP composite is dependent on fiber orientation, composite materials must be treated as anisotropic. Analysis is more complex for FRP composites than for homogeneous isotropic materials. Analysis must account for the directionality of material properties associated with various fiber orientations. Often, analysis of

composite materials requires that they be discretized into layers or laminae with each layer representing a given property or fiber orientation. Since the fiber orientation and properties may vary from one lamina to the next the distribution of stress may be discontinuous.

2.1.1 Pultrusion

In the past, the cost of FRP composites limited their use to military and aerospace applications. In addition, production methods were often slow with inconsistent levels of quality. New production methods have been developed which are reducing the cost of composites and providing materials with consistent levels of quality. Structural shapes are often produced by a method known as pultrusion.

The pultrusion process involves pulling fibers, which are wetted with resin, through a die of a given shape. While the fibers and resin are being drawn through the die they are heated. The FRP composite is thermally cured in a continuous process that produces the structural shape. Pultruded structural shapes usually consist of core fibers that are oriented lengthwise for tensile, compressive and bending strength. The core fibers are covered with a fabric of fibers oriented to provide shear strength. A veil of synthetic material is then added at the surface to provide corrosion and UV protection. The "surface veil" also prevents the underlying fibers from protruding or "blooming" at the

surface and prevents moisture absorption that could occur by capilary action of exposed fibers. Figures 2.4 and 2.5 illustrate the pultrusion process.

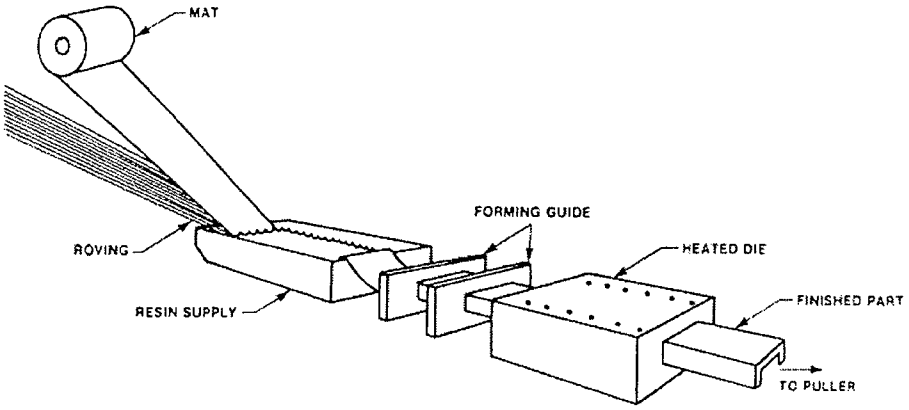

Figure 2.4 Illustration of Pultrusion Process from Reference [9]

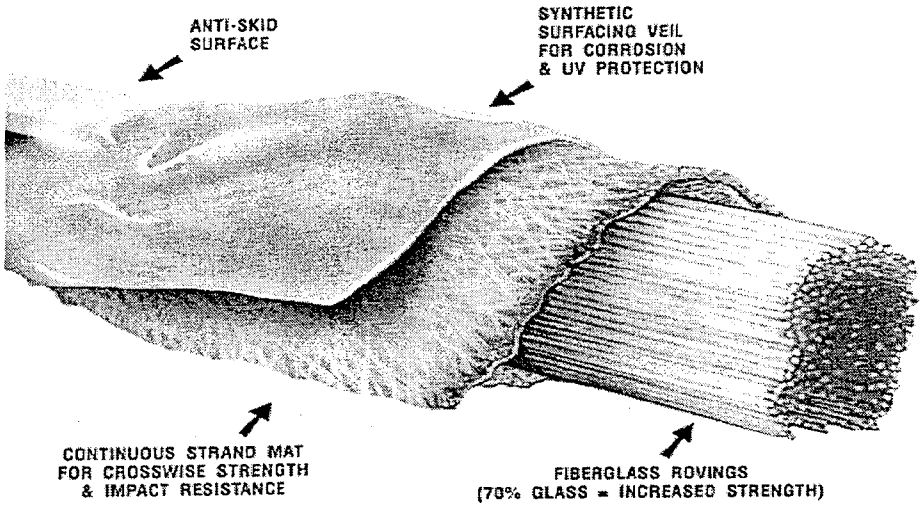

Figure 2.5 Illustration of Pultruded Shape Material Configuration from Reference [4]

2.2 Survey of FRP Composite Research with Structural Bridge Applications

The Technology Reinvestment Project (TRP) was initiated to provide for the transfer of defense and aerospace technology to other industries. As part of the project, the Advanced Research Projects Agency (ARPA) and the Federal Highway Administration (FHWA) provided funding for the development of an advanced composite bridge across Interstate 5 in San Diego. This project helped to initiate FRP composites research in a number of infrastructure related areas.

The Advanced Composite Technology Transfer Consortium and Lockheed Martin Palo Alto Research Laboratories have been conducting research and development of the advanced composite bridge at the University of California in San Diego. A 1/4 scale bridge section 9.1m (30') long and (5.5m) 18' wide has been successfully tested to 69,000 kg (130,000 lbs) [1]. One of the goals of the project was to demonstrate the potential for the economic use of FRP composites. Emphasis was placed on holding down the cost. It is expected that as the market expands increased competition and improved methods of production will result in reduced cost.

The bridge section, discussed above, is made up of longitudinal "U" shaped girders which consist of stitched, multiaxial, non-woven E-glass fiber and a resin formulation consisting of an isophthallic polyester and vinyl ester resin blend [1]. The extreme tensile bottom portion of the beam consists primarily of longitudinally oriented fibers. The deck consists of pultruded tubes of E-glass roving, mat reinforcement and polyester

resin. The tubes were bonded together with epoxy resin and sandwiched between E-glass fabric/polyester resin skins [1]. Figures 2.6 and 2.7 illustrate the experimental bridge section.

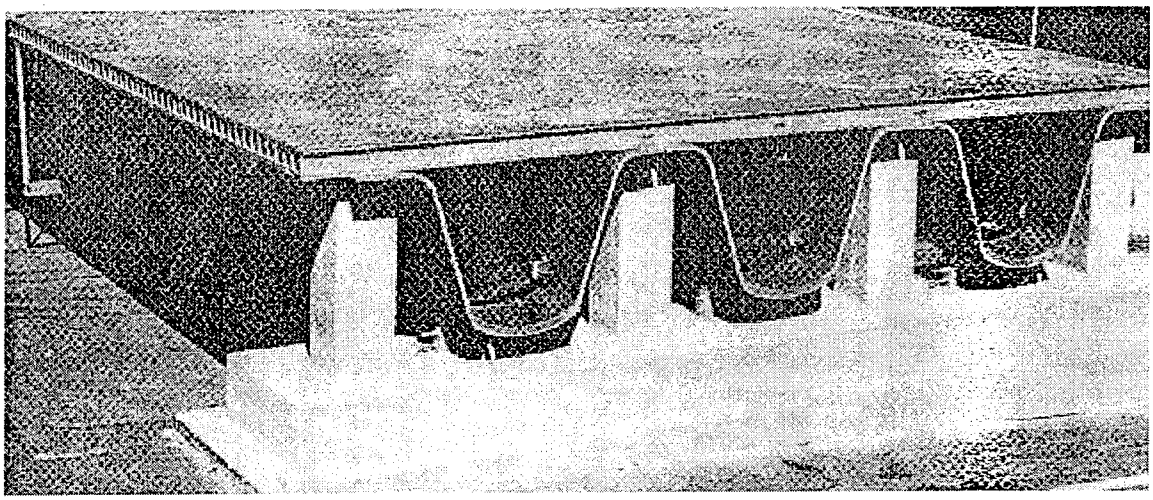

Figure 2.6 Experimental FRP Composite Bridge Section from Reference [1]

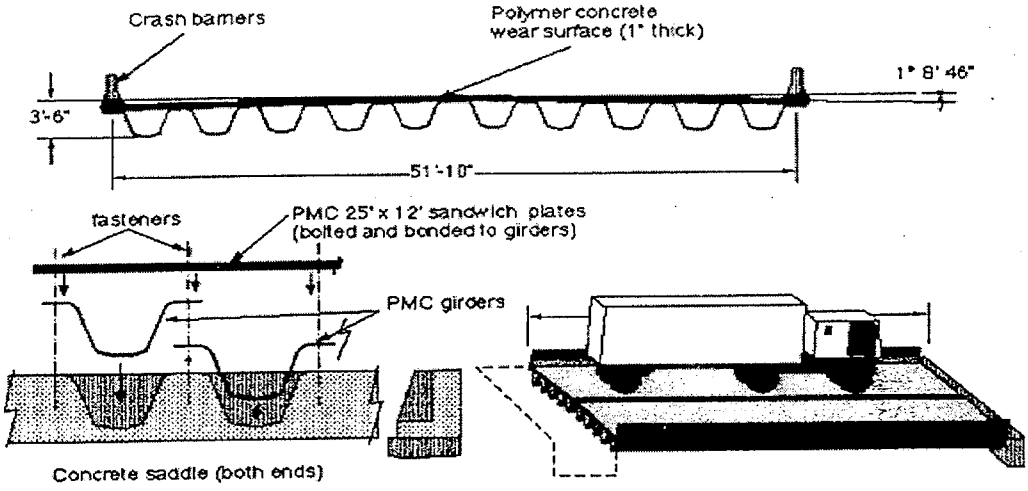

Figure 2.7 Proposed Configuration of Experimental FRP Bridge from Reference [10]

In addition to the above, a number of other FRP composite research projects with infrastructure applications are being conducted as discussed in the following paragraphs.

The Georgia Institute of Technology performed research on modular concepts for FRP bridge decks. The focus of this project was to develop models for predicting FRP structural behavior. Two reports resulted from the study, *Local Buckling of Fiber-Reinforced Polymeric Structural Members Under Linearly Varying Edge Loading* and *Preliminary Designs of Fiber-Reinforced Polymeric Bridge Decks* [11].

In addition, the Georgia Institute of Technology, Pennsylvania State University and Catholic University are investigating accelerated test methods to determine the long-term behavior of FRP structures. This project will develop test methods for evaluating a variety of environmental and loading conditions on FRP structures. The test methods are intended to provide predictions of long-term effects of up to 50 years [11]. Also, the University of California at San Diego is investigating an advanced composites cable stayed bridge. This project investigates the use of a carbon fiber shell and concrete frame system for the superstructure of a 133m (435') cable stayed bridge in San Diego [11].

The University of Central Florida and the Florida Department of Transportation have investigated FRP composite shells for the strengthening of concrete columns. The study successfully showed that FRP composite shells could be used to restrain the lateral dilation of concrete in columns by providing external confinement of the concrete. During the study, uniaxial compression tests, beam column tests and beam tests for shear

and flexural strength were conducted. Tests were conducted for both long and slender columns. The investigation demonstrated that a significant increase in strength and ductility of concrete columns could be achieved through the use of FRP composite shells [12].

Another project being conducted at West Virginia University involves the study of the use of FRP composites in Highways. The project was mandated by Congress to continue the investigation of a previously completed study of FRP rebars for the reinforcement of concrete [11]. The University of Wyoming and Pennsylvania State University are conducting research on FRP pre-stressing of highway bridges. The study is being conducted to develop tendon and anchorage systems including: designs, specifications and construction procedures for use with FRP pre-stressing tendons [11].

California State University at Long Beach is conducting a study on fiber-reinforced composite hanger cables. This project involves several studies on the performance of FRP composite cables for suspension bridges. The studies include the development of design criteria and specifications for cables and end connections. The project also includes the installation of a 3m (10'). hanger cable on the Desmond Memorial Bridge in Long Beach, California to evaluate its performance [11].

In addition, projects being conducted under the FWHA Graduate Research Program at California State University at Long Beach include: *Wearing Surface for Modular FRP*

Bridge Decks, Field Study of FRP-Reinforced Bridge Deck and *Fatigue and Anchorage Tests of FRP Hanger Cables* [11].

The University of South Florida and the Florida Department of Transportation has conducted a study of the durability of fiberglass pretensioned beams. The study investigated the affect of wet/dry (marine environment) conditions on fiberglass pretensioning bars in comparison to steel bars. Pretensioned concrete piles, both cracked and uncracked, were cyclically loaded to simulate tidal conditions. The results of the study indicated that the durability of fiberglass pretensioning bars under wet/dry conditions is significantly less that of steel steel [13].

Also, the University of Arizona is conducting research on the durability of glass fiber reinforced plastic (GFRP) rebar. The study investigates the effects of temperature, humidity, acidic and alkaline environments on the GFRP mechanical properties. The research is being funded by the National Science Foundation (NSF) [14].

The use of FRP grating as the reinforcement of concrete slabs is being investigated at the Catholic University. The project, which is being funded by the NSF, involves flexural and punch load testing of several half and full scale FRP reinforced concrete deck slabs. This project has resulted in plans to construct an 24.4m x 10.4m (80' x 34') demonstration deck [14]. In addition, the University of New Hampshire has field tested 12 FRP grid reinforced concrete deck slabs for a period of 12 months. The test included 40 ton truck traffic with a traffic volume of 300 trucks per day [14].

2.3 Survey of Existing Bridges Utilizing FRP Composites

The use of FRP composites for structural applications is not new. For years, the strength and lightweight characteristics of FRP composites have been utilized by the defense, aerospace and boating industries. New applications for the use of FRP composites in civil infrastructure are being investigated and developed around the world. This section will focus on the recently developed applications and projects considered to be pertinent to this investigation. The following is just a partial list of FRP composite projects that have been completed around the world.

The Bonds Mill bridge, completed in 1994, is an 8.2m x 4.3m (27' x 14') wide composite bascule bridge that was constructed to serve the Bonds Mill Industrial complex in Stonehouse, England. The bridge consists of interlocking rectangular pultruded composite shapes made up of isopolyester resin and reinforced with unidirectionally alligned E-glass. The interlocking shapes were glued together to form the main load carrying girders. The upper panels are filled with foam to absorb the large concentrated loads from vehicle wheels [15].

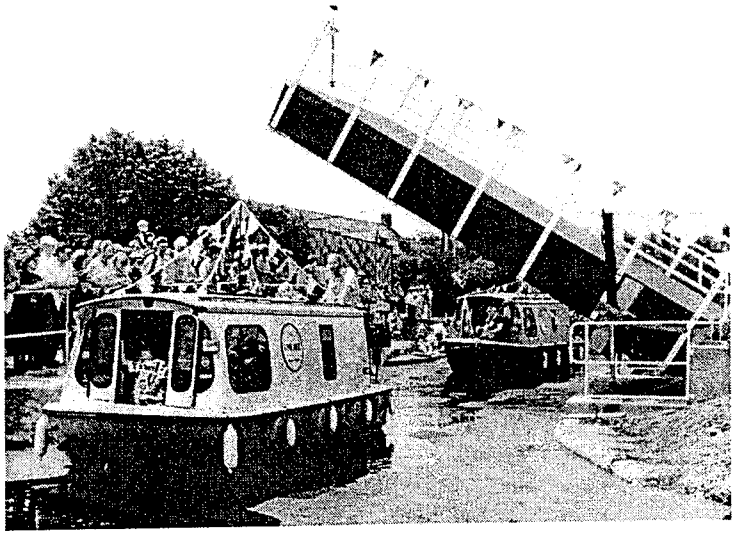

Figure 2.8 Bonds Mill Bascule Bridge in Stonehouse England, Reference [16]

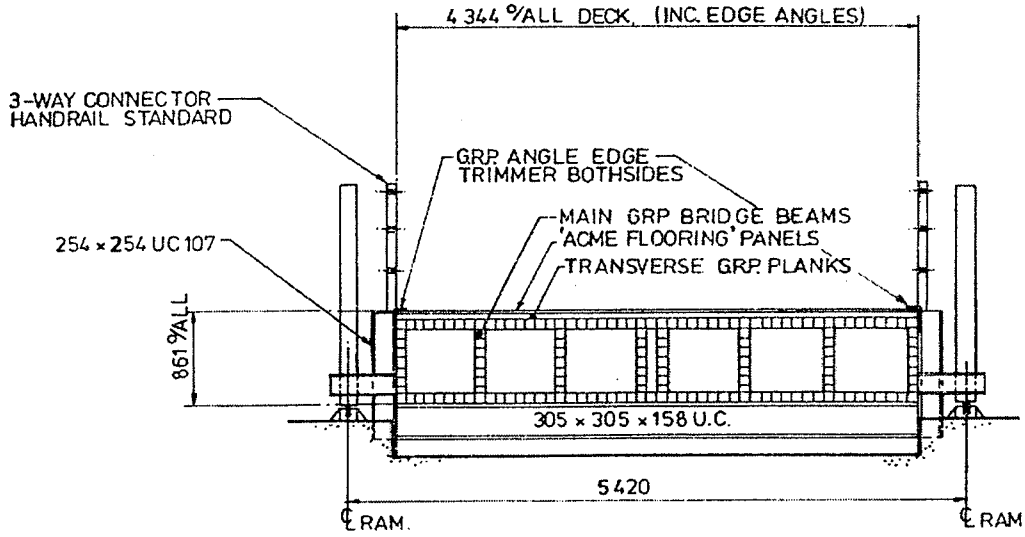

Figure 2.9 Bonds Mill Bridge Cellular Box Girder Details from Reference [17]

FRP composites have been successfully used for a number of pedestrian bridges around the world. The structures provide an essentially maintenance free alternative to conventional construction. They are lightweight enough to have entire sections fabricated off location, shipped and components installed with minimal construction time.

Two FRP bridges, a 10.7 meter and a 21.3 meter bridge were constructed to provide access to the Point Bonita Lighthouse at Golden Gate Park in San Francisco, California. The bridges consist of pultruded isopolyester composite sections that are bolted and glued together [18]. Also, a composite bridge at Antioch Illinois was constructed using pultruded E-glass/vinyl ester C-channels and square tubes. The bridge spans 3.7m (45') and is 3m (10') wide. The bridge has a load rating of 5 tons and was designed for pedestrian and gulf cart traffic. The bridge was designed by E. T. Techtonics, Philidelphia, PA [19].

Figure 2.10 Antioch Bridge, Reference [19]

In 1986 and 1988 two pedestrian bridges were completed in Chongqing, China which involved the use of steel, concrete and FRP composites. The bridge completed in 1986 consists of a concrete tower and end spans. The tower is used to support steel cables that

in turn support the main span. The main span consists of a 27.4m FRP composite box girder [20].

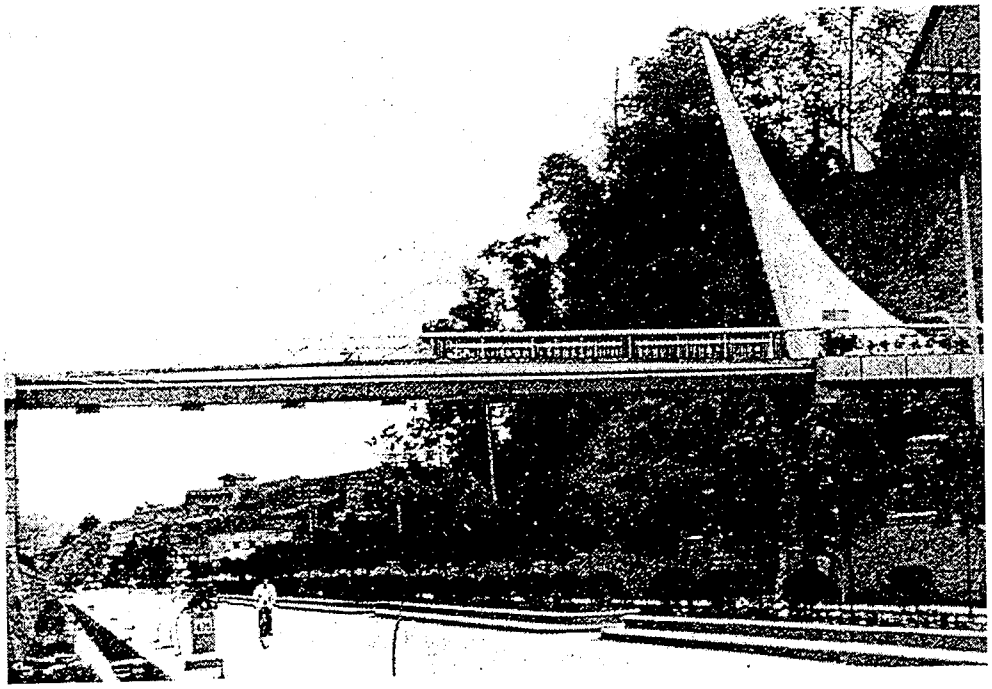

Figure 2.11 GRP Box Girder Cable-Stayed Bridge, Reference [20]

The second bridge completed in 1988 consists of a space frame and FRP composite deck girders. The deck girders are suspended from reinforced concrete frames that span 70m. The total length of the bridge is 157m. The four FRP girders span 19m each which are connected to four 9m long FRP girders. The girders are 4.3m wide and 0.9m deep.

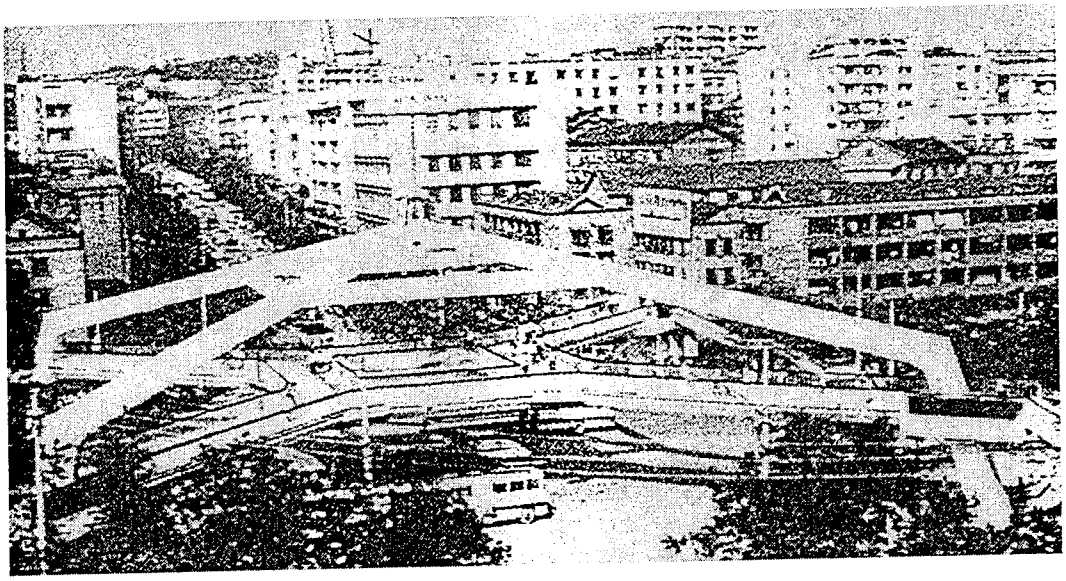

Figure 2.12 Guanyingiao Bridge, Reference [20]

PART A: STATIC ANALYSIS FOR TUBE AND SHEET MODELS

CHAPTER 3

FRP DECK DESIGN

3.1 Introduction

In order to develop suitable deck geometries for the analytical portion of this study, the characteristics of movable bridges were investigated first. As a result of the literature survey and investigation of references [21] and [22] it was concluded that the most common movable bridge types are the rolling lift bascule and trunnion bascule. Both designs are similar in geometry as far as decks are concerned, and generally only differ in the way the bridge is pivoted in its raised position. In order to have a basis for the study, the details of a typical bascule bridge were requested from the Florida Department of Transportation (FDOT). The FDOT provided the plans, reference [23], for the Sunrise Boulevard Bridge on SR 838 in Ft. Lauderdale. Framing details of the bridge are shown in Figures 3.1 and 3.2.

The Sunrise Boulevard Bridge is a double leaf bascule bridge that consists of three lanes for each traffic direction. The east and westbound roadways are separated and independent. Each leaf has an overall length of 27.7m (90'-10") and a roadway width of

11.6m (38') in addition to two 2.3m (7'-7") pedestrian walkways. The deck support system consists of longitudinal I-beam stringers (parallel to traffic flow) which are supported by transverse girders as shown in Figures 3.1 and 3.2. The worst case transverse spacing of the longitudinal I-beam stringers is 1.7m (5'- 5½"). The longitudinal spacing of the transverse girders is 5.8m (19'-1"). These dimensions represent the locations of support for the deck and were used in this study during the investigation of the FRP deck design.

As discussed previously, in order to minimize cost, the use of standard structural FRP shapes was emphasized during the study. In addition, the use of standard structural shapes was also considered to provide a more consistent level of quality and reduce variation in material properties. A number of manufacturers around the country produce pultruded FRP structural shapes including angles, channels, rectangular tubes and I-beams, in addition to a large variety of custom shapes. In order to simplify the investigation, structural shapes from the reference [4] design manual were investigated. Initially, the investigation consisted of testing various configurations of structural shapes by hand calculation. Later, a more detailed finite element analysis was performed on the selected configurations.

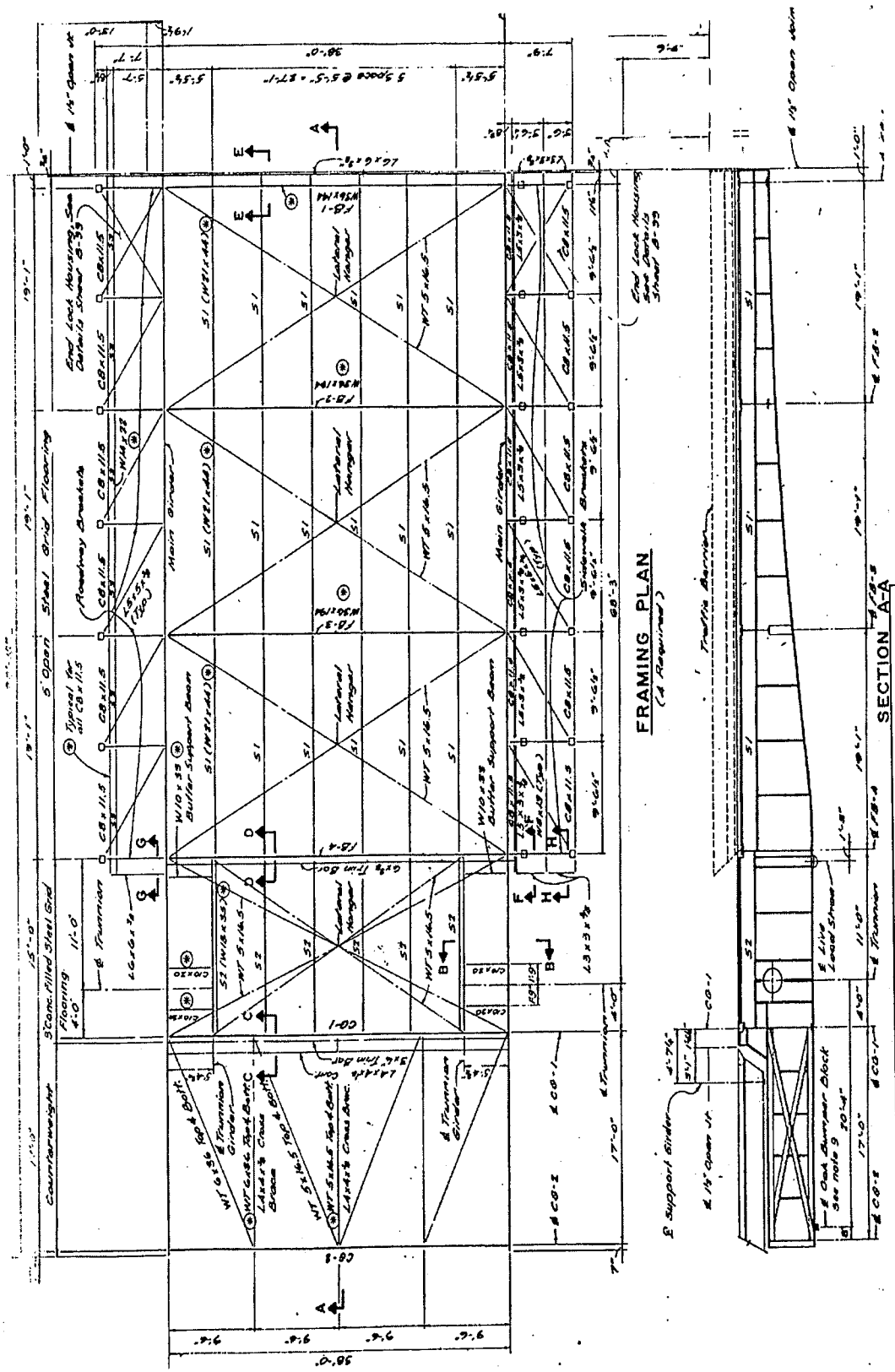

Figure 3.1 Sunrise Boulevard Bridge Framing Plan, Reference [23]

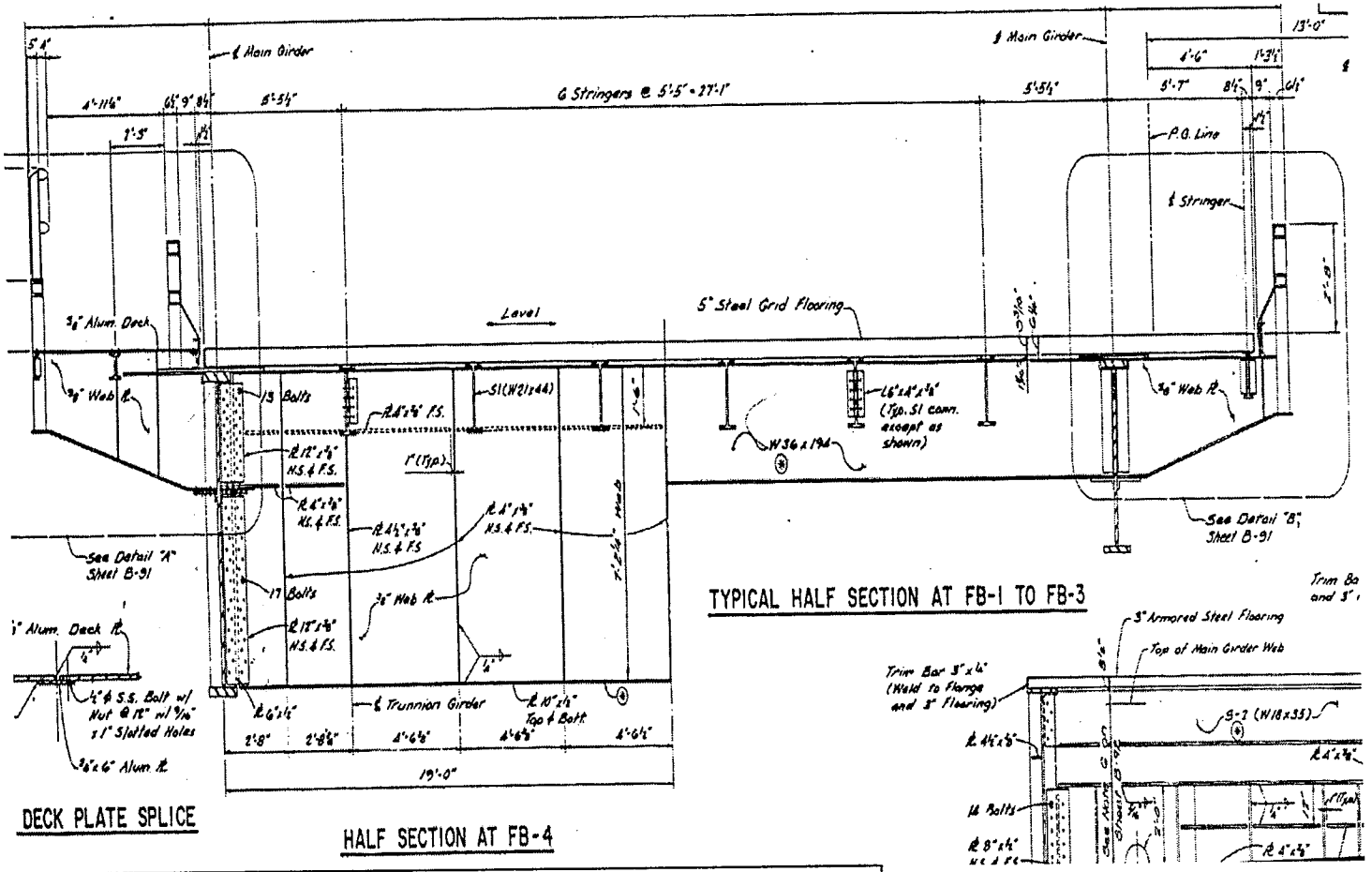

Figure 3.2 Sunrise Boulevard Bridge Framing Plan, Reference [23]

3.2 Design Criteria

The design criteria for this investigation were based on the AASHTO Standard Specifications for Highway Bridges [5], and the AASHTO Standard Specifications for Movable Highway Bridges [6]. These specifications were used to develop suitable loading criteria for the investigation. Failure criteria were based on allowable stresses and deflections. AASHTO HS20-44 and ML80 live loads with an impact factor of 30% were used for this investigation. Lane loading was not checked since the longest anticipated deck span is 5.8m (19'- 1"). For this short span it can be concluded that truck loading will govern. In addition to the truck loading specified above, the following load cases and combinations were investigated as required by AASHTO.

3.2.1 Load Cases

Case I: DL - Bridge open (Checked at 90 and 45° from horizontal)

Case II: DL - Bridge closed

Case III: DL - Bridge closed/counterweights independently supported (Not applicable for deck design).

Case IV: LL + Impact (30% of LL)

3.2.2 Load Case Combinations

Case I + W

Case I + 20% DL+ W

Case II + Case IV

Case III + Case IV (Not applicable for deck design).

Definitions:

DL: Dead Load

LL: Live Load

W (Wind):

Bridge normally open - 50 psf combined with DL at 1.33 times allowable stresses.

Bridge normally closed - 30 psf combined with DL + 20% DL for impact at 1.25 times allowable stresses.

3.2.3 Deflection

In order to prevent deterioration of the wearing surface, local deck deflection must be limited. AASHTO recommends that deflections be limited to L/800 for conventional highway bridges. AASHTO also recommends a limitation of L/1000 for bridges serving pedestrians. In addition, reference [27] suggests that L/500 be used for local deflections of orthotropic decks. During this investigation, local deck deflections were compared to

the L/800 and L/500 criteria. It should be noted that although the Sunrise Boulevard Bridge has a pedestrian walkway, the L/1000 deflection limitation was not considered, since the deck is treated as being independent of the pedestrian walkway. The walkway is supported by the primary structure of the bridge and would not be affected by deflections in the deck.

3.2.4 Material Properties

As mentioned earlier, the properties of FRP structural shapes depend on a number of factors. Properties vary depending on the direction of loading, fiber orientation, resin, fiber types and the percentage of the composite consisting of fibers. The properties and structural shapes used in this analysis were based on those presented in the reference [4] design manual. As stated in this manual, the properties listed were empirically derived using ASTM test procedures. The properties are based on either coupon testing or full section testing for minimum ultimate properties. In some cases, similar properties vary depending on the structural shape investigated.

The following minimum ultimate properties presented in Table 3.1 are from reference [4] and are based on coupon tests unless otherwise noted.

Table 3.1 Material Properties for EXTREN Structural Shapes [4]

Properties {1}, {8}	EXTREN Series 525	Vinyl Ester Rect. Shapes	Flat Sheet Series 525
Flexural Strength (LW)	206.8 MPa (30,000 Psi)	248.1 MPa (36,000 Psi) {3}	206.8 MPa (30,000 Psi) {5}
Flexural Strength (CW)	68.9 MPa (10,000 Psi)	{4}	124 MPa (18,000 Psi) {5}
Flexural Modulus (LW)	11 GPa (1.6E6 Psi)	{4}	13.8 GPa (2.0E6 Psi) {6}
Flexural Modulus (CW)	5.5 GPa (0.8E6 Psi)	{4}	9.6 GPa (1.4E6 Psi) {5}
Modulus of Elasticity Full Section {2}	19.3 GPa (2.8E6 Psi)	20.7 GPa (3.0E6 Psi)	{4}
Shear Modulus (LW)	2.9 Gpa (0.425E6 Psi)	{4}	{4}
Shear Strength (LW)	31 MPa (4500 Psi)	27.6 MPa (4000 Psi)	41.4 MPa (6000 Psi) {7}
Compressive Strength (LW) (CW)	206.7 MPa (30,000 Psi) 103.4 MPa (15,000 Psi)	241.2 MPa (35,000 Psi) {4}	165.4 MPa 24,000 Psi 137.8 MPa (20,000 Psi)
Poisson Ratio (CW) (LW)	0.33 {4}	0.2 {4}	0.29 0.31

Notes:

1. (LW) = Lengthwise, longitudinal direction of load carrying fibers.

   (CW) = Crosswise, direction perpendicular to the lengthwise direction.

2. Value is based on full section testing.

3. Listed as tensile stress (LW), flexural stress not listed.

4. Not listed in Reference [4].

5. Sheets 3/8" to 1" thick.

6. For sheets > than $1/8^{th}$ inch thick.

7. Listed as perpendicular shear stress.

8. Reference [4] recommends the following factors of safety for the above properties:

   2.5 for flexure, 3.0 for compression and 3.0 for shear.

For cases where the properties for vinyl ester rectangular shapes were unavailable, the properties for series 525 shapes were assumed. This assumption was deemed reasonable for investigative purposes based on the following reasons; series 500/525 properties are typical for similar pultruded shapes, in addition, properties may be adjusted to some degree by controlling the resin to fiber ratio, the fiber type, fiber orientation and the resin mix.

3.2.5 Design Criteria for Preliminary Trial Hand Calculations

Deflection was limited to L/500 = 166.4cm/500 = 0.333cm.

Normal lengthwise stress was limited to $\sigma_u/2.5$.

Shear stress was limited to $\tau_u/3$

Wheel loading area was based on the following, as suggested in reference [24]:

Loading area = 0.01P where P = the wheel load in lbs.

The ratio of length (in direction of traffic flow) to width is 1/(2.5).

HS20-44 wheel load of 71.2 KN (16000 lbs). plus 30% for impact was used.

P = 1.3(71.2 KN) = 92.56 KN (20800 lbs)

$A = 0.01P = 0.01(20{,}800) = 208\ in^2 = \underline{1342\ cm^2}$.

$1342\ cm^2 = w(2.5\ w)$.

$w = \sqrt{(1342/2.5)} = \underline{23.1\ cm}$

$L = 23.1(2.5) = \underline{57.9\ cm}$

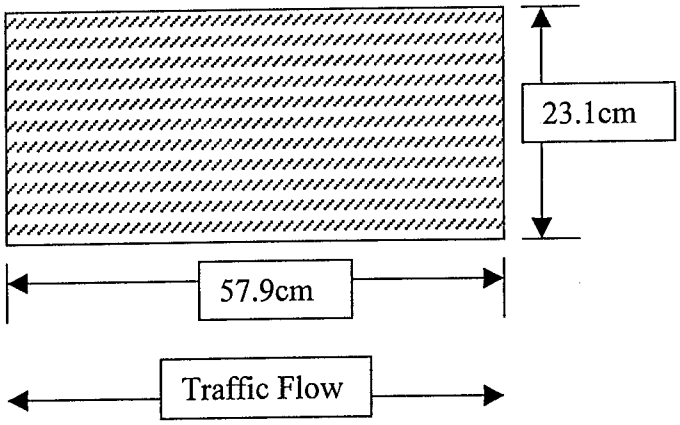

Figure 3.3 Tire Contact Area

3.3 Method of Analysis for Preliminary Trial Hand Calculations

Based on the AASHTO specification [5], the minimum required truck wheel longitudinal spacing is 4.3m (14'). The required transverse truck wheel spacing is 1.8m (6'). Since the center to center transverse spacing of the stringers supporting the deck is 1.7m (5'-5½") which is less than 1.8m (6'), the initial deck design was based on loading from a single truck wheel load of 71.2 KN (16,000 lb). In addition, AASHTO specifies that the above load be increased by 30% to account for dynamic affects (impact). The following load was used as a basis for initial design estimates.

P = 1.3(71.2 KN) = 92.6 KN (20800 lbs)

For the purposes of initial trail estimates, to simplify the analysis and since the majority of the load will be transmitted to the closest supports, a simply supported effective section spanning 1.7m (5'-5 ½") was used. For simplicity and conservatism, the panel was evaluated for one way beam action as shown in Figure 3.4.

The 92.6 KN (20,800 lb) load was placed at the center of the panel for the worst case bending moment. Since the tire contact location could occur at the panel edge (during a lane change), the load was also assumed to act over the stringer centerline (at the panel edge) for shear. Therefore, the entire 92.6 KN (20800 lb) load was used to estimate shear. It should be noted that the initial design estimates were based on live load only. This simplifying assumption was considered to be reasonable since the deck self weight represents only a small fraction of the total load.

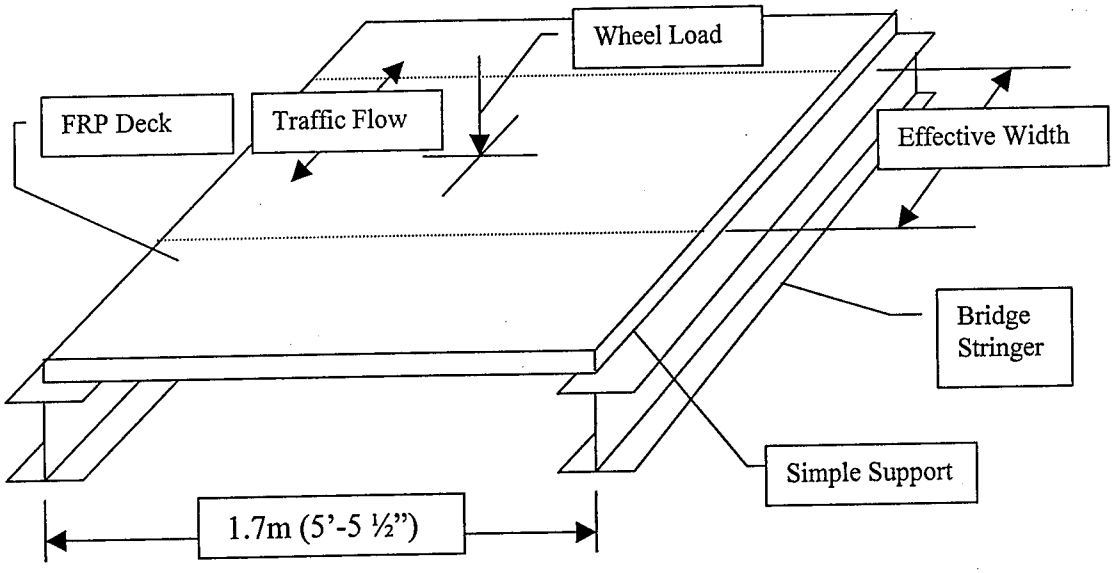

Figure 3.4 Simply Supported Span

An effective section for the panel was chosen based on the tire contact area plus an additional amount on each side equivalent to the assumed beam depth as shown below. Initially a depth of 15.2 cm (6") was assumed.

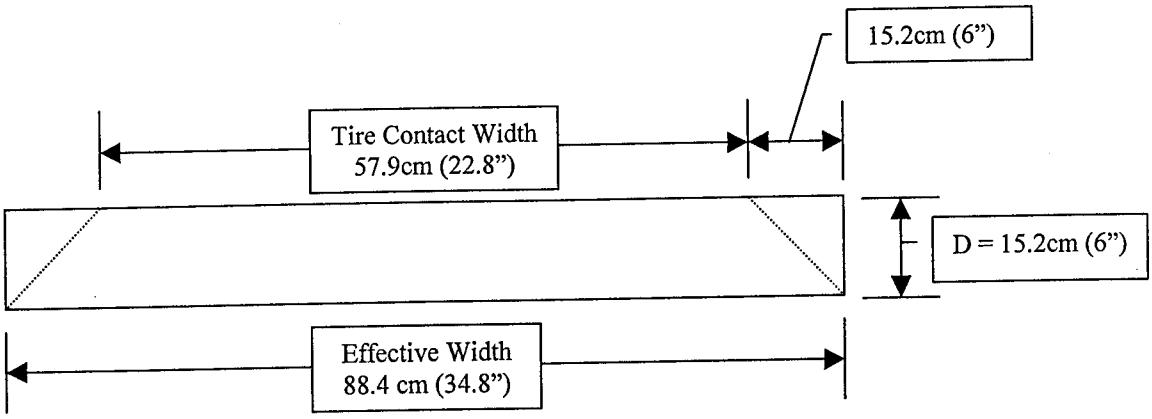

Figure 3.5 Trial Section Effective Width for Hand Calculations

The reference [4] design manual lists a variety of pultruded structural shapes. As mentioned earlier, to simplify the design and to minimize cost, the intent of this project was to utilize standard shapes that are normal stock items. As a result, the design was limited to the standard shapes offered in references [4] and [9]. It should be noted that a variety of non-standard and custom pultruded shapes are available using existing or custom designed forming dies.

Typical standard shapes in reference [4] and [9] include square and rectangular tubes, I-beams, angles and channels. Based on the results of the literature survey and after considering the following, square and rectangular tubes appear to be the best option for bridge deck construction. Also, in order to produce a continuous deck structure, the

structural shapes need to be tied together. Square and rectangular tubes are easier to stack together, and thus provide the flat surfaces needed for lamination. Other shapes offer little surface area for lamination and would rely more heavily on being tied together with cover sheets as shown in the following Figure 3.6.

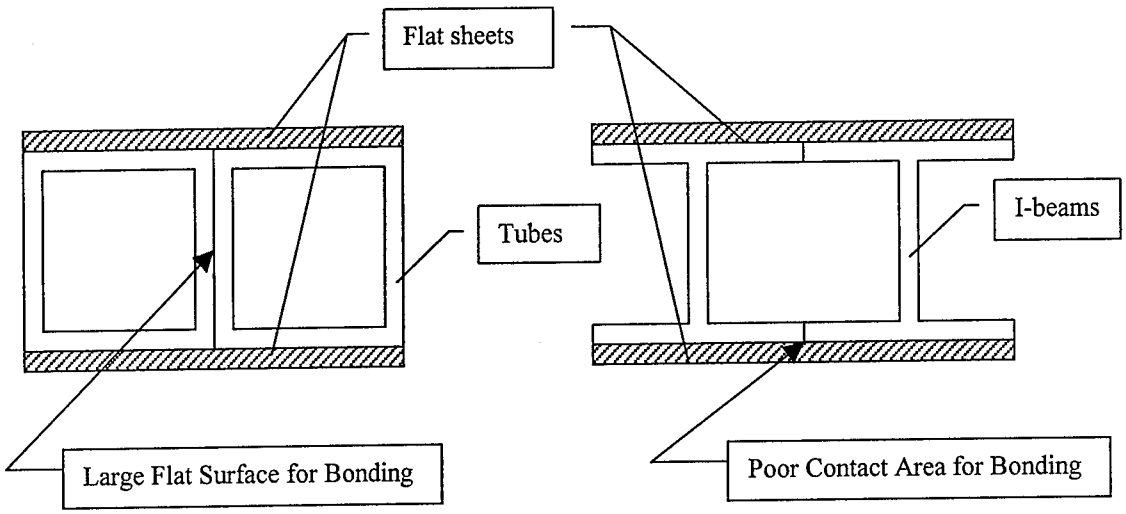

Figure 3.6 Bonding of Structural Shapes

Of the configurations shown above, for full composite action, the combination of square or rectangular tubes and flat cover sheets offer the strongest and most stable configuration, with a much reduced opportunity for local flange and web buckling (back to back tube sides form a thicker web). Also, the combination of channels and I-beams basically reproduce the rectangular configuration of tubes anyway and with a higher chance for failure where the shapes are bonded together.

In addition, since the modulus of FRP material is relatively low, it is desirable to avoid unsupported free edges, which could deflect under load. For the reasons listed

above, the design was limited to a combination of square and rectangular tubes. As an added measure of safety and to increase moments of inertia, the tubes were tied together with flat sheets. In the event of local resin failure between the tubes and in area's where the mating surfaces are imperfect, the flat sheets would provide added strength. In addition, sheets may be positioned to overlap the laminated tube sides in order to reduce the discontinuity at the joint. The tongue and groove configuration along the panel edge would also help to facilitate easy assembly of modular deck panels.

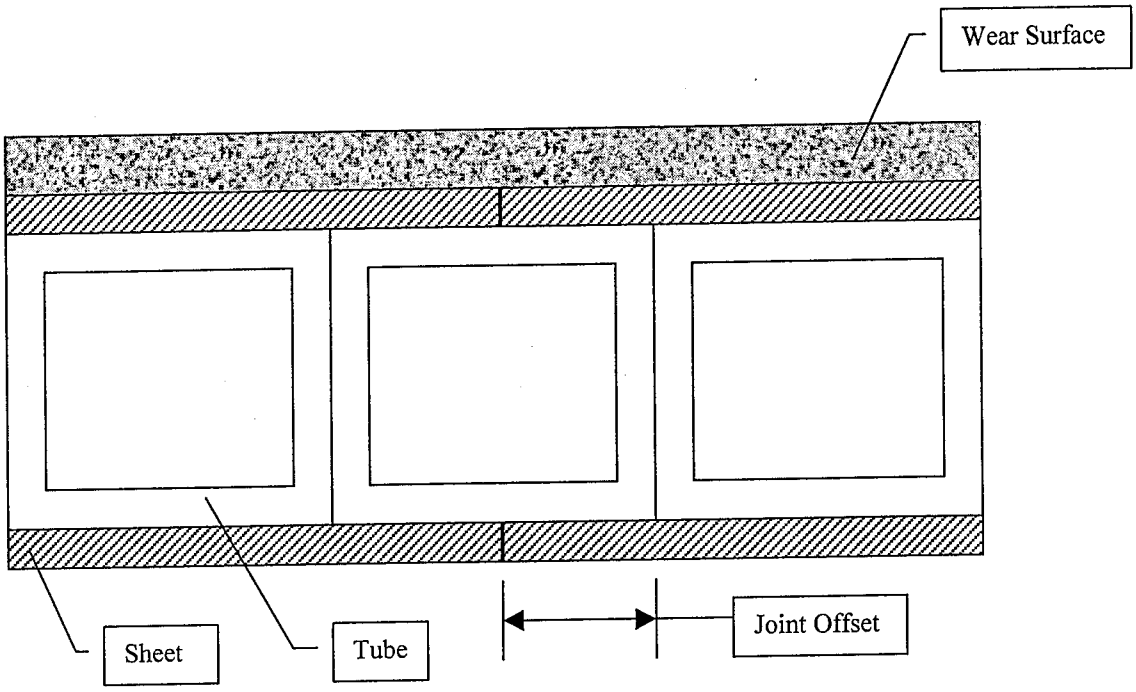

Figure 3.7 Laminated Tube and Sheet Configuration with Sheet and Tube Joint Offset

Table 3.2 lists the results of the hand calculations and the trail tube and sheet configurations investigated.

Table 3.2 Hand Calculation Results

Configuration No.	Δ mm (in)	Δ_{all} cm (in)	σ Mpa (psi)	σ_{all} Mpa (psi)	τ Mpa (psi)	τ_{all} Mpa (psi)
1	6.5 (0.256)	3.3 (0.131)	17.2 (2501)	82.7 (12,000)	9.4 (1369)	10.3 (1500)
2	4.7 (0.185)	3.3 (0.131)	12.9 (1867)	82.7 (12000)	9.0 (1306)	10.3 (1500)
3	6.5 (0.254)	3.3 (0.131)	12.4 (1805)	82.7 (12000)	19.7 (2860)	12.6 (1833)
4	1.9 (0.074)	3.3 (0.131)	9.2 (1333)	82.7 (12000)	5.2 (761)	9.2 (1333)

The following tube and sheet combinations were investigated:

1. 7.6cm x 7.6cm x .64cm (3"x 3"x ¼") tubes with 2.5cm (1") cover sheets.
2. 10.2cm x10.2cm x.64cm (4"x 4"x ¼") tubes with 2.5cm (1") cover sheets.
3. 61cm x 14cm (24"x 5 ½") Pultex construction panels [9] with 1.9cm (¾") cover sheets.
4. 12.7cm x17.8cm x 1.9cm (5"x 7"x ¾") tubes with 1.9cm (¾") cover sheets.

Based on the above initial trial results, it was decided that the 10.2cm x10.2cm x.64cm (4"x 4"x ¼") tube with 2.5cm (1") cover sheets and the 12.7cm x17.8cm x 1.9cm (7"x 5"x ¾") tube with 1.9cm (¾") cover sheets would be the best candidates for the more detailed finite element analysis. The deflections and stresses for the above tubes were either acceptable or sufficiently close to warrant a more detailed investigation. Finite element models of the above tubes and sheets were constructed and analyzed for stress and deflection using various parameters as discussed in the next chapter.

CHAPTER 4

FINITE ELEMENT ANALYSIS

4.1 Introduction

The 10.1cm x 10.1cm x 0.64cm (4" x 4" x ¼") and the 12.7cm x 17.8cm x 1.9cm (5" x 7" x ¾") tube options were evaluated using the finite element analysis package ANSYS Mutiphysics [25]. A number of models were generated in order to investigate the effect of a variety of parameters and loading conditions. The parameters investigated included: changes in boundary conditions, vehicle live load placement, orientation of cover sheets (cover sheets have orthotropic properties), the use of a simply supported panel vs. a continuous system and the use of free edge conditions to simulate the possibility of joint discontinuity. In addition, several cases were investigated in order to evaluate other loading conditions as specified by AASHTO, such as alternate military loading, wind and loading conditions for the bridge in its open position.

The finite element models were developed using the ANSYS shell 91 element as shown in Figure 4.1. The shell 91 element is a quadratic 8 noded structural shell element with 6 degrees of freedom at each node. The element allows up to 16 distinct layers, each with their own set of properties. This element was selected so that the orthotropic

properties of the sheets and tubes could be modeled using a single element. Although the sheets and tubes themselves are made up of a number of sub-layers, they were treated as equivalent single layers with orthotropic properties. In other words, the top and bottom most layers represented the sheets while the inner layers and webs represented the tubes as shown in Figure 4.2.

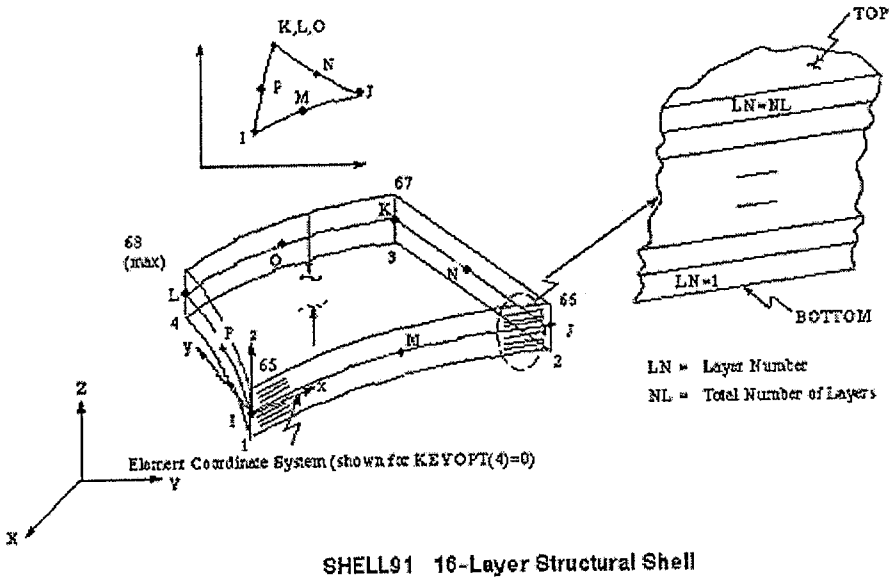

Figure 4.1 ANSYS Layered Shell 91 Finite Element [25]

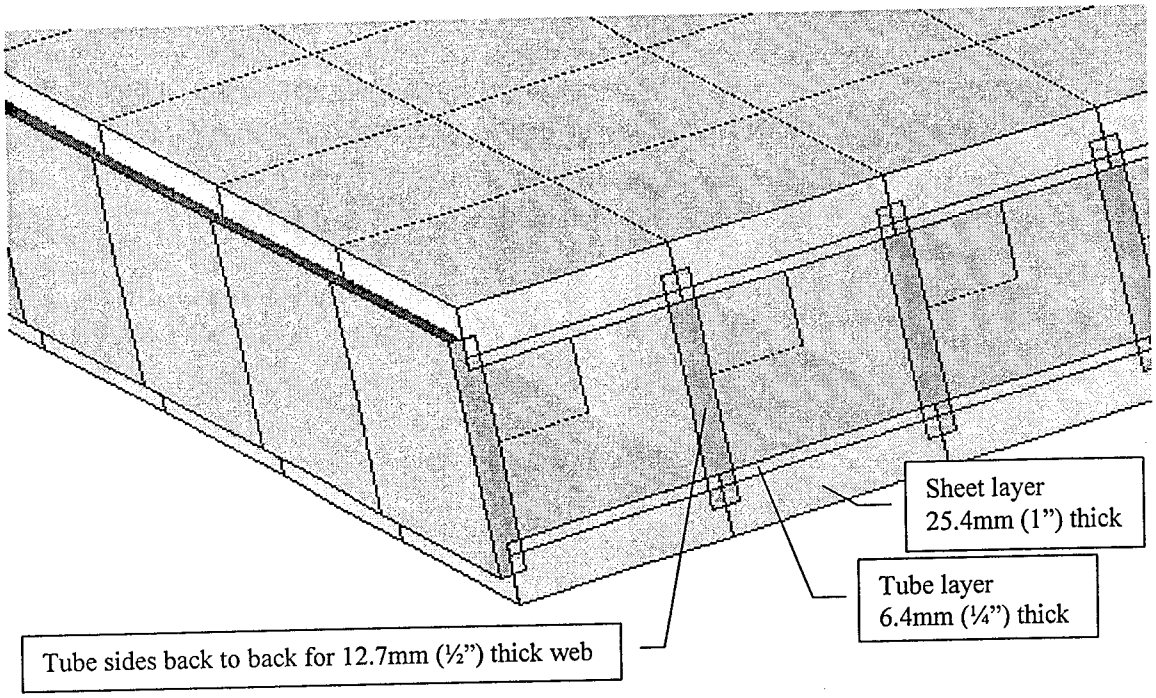

Figure 4.2 Finite Element Deck Model using ANSYS Shell 91 Elements

An alternative method to treating the material as a single layer would have been to divide the tube and sheet elements into sub-layers representing the individual laminae within the material. This methodology would have been computationally intensive and was deemed unnecessary. This assumption was considered reasonable since the properties used are based on coupon testing of the material as a single layer in accordance with ASTM procedures [4]. It should be noted that throughout the analysis it was assumed that the bond between the sheets and tubes is equivalent in strength to the bonded materials; therefore no slippage is allowed. This scenario was deemed reasonable since the properties used are the minimum ultimate values obtained from testing as stated in reference [4]. Also, the safety factors of 2.5 for flexure and 3.0 for shear were

observed. In addition, equivalent strength should be achievable through the use of good fabrication techniques, such as abrading the mated parts before bonding with a good quality resin.

4.2 10.1cm x 10.1cm (4" x 4") Tube Single Span Deck System (SSDS)

The 10.1cm x 10.1cm (4" x 4") tube modeled with 2.5cm (1") cover sheets was used to investigate the various loading and modeling parameters which will be discussed later. A single model of the 12.7cm x 17.8cm (5"x 7") tube with 1.9cm (¾") cover sheets was then modeled in a similar fashion to the 10.1cm x 10.1cm (4" x 4") tube model for comparative purposes. In the following sections of this chapter, details of the various models and approaches used for the parametric study are discussed. Then, the results of the various models are presented in Chapter 5.

The basic tube model consisted of the 10.1cm x 10.1cm (4" x 4") tubes stacked side by side and bonded together between two 2.5cm (1") thick sheets. This model was first treated as a simply supported panel spanning between a single pair of stringers and the transverse girders as shown by the finite element model of Figure 4.3.

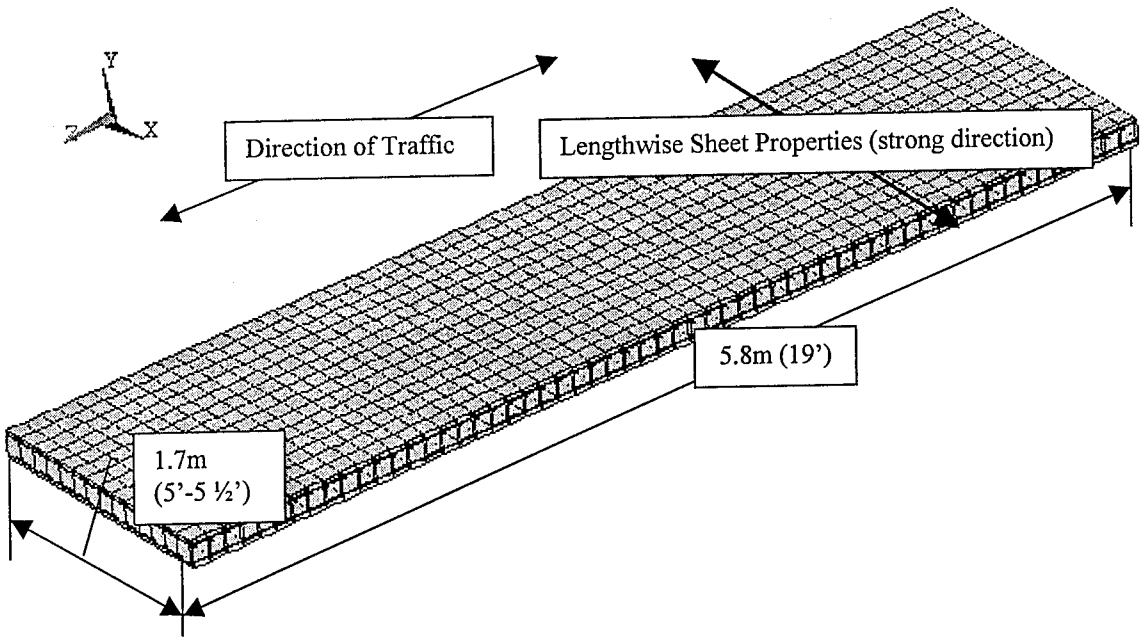

Figure 4.3 Finite Element Model of 10.1cm x 10.1cm (4" x 4") Tube SSDS

For this basic 10.1cm x 10.1cm 4"x 4" tube model, the strong axis of the cover sheets (lengthwise sheet properties) were oriented perpendicular to the direction of traffic. In other words, the strongest sheet orientation was aligned to resist bending about the sheets global Z axis (parallel to traffic). This configuration was used for the remaining deck models except for one model where the effect of rotating the sheets 90° was investigated. The upper and lower horizontal elements consist of the 2.5cm (1") thick sheets and the .64cm (¼") thick portion of the tubes for a total thickness of 3.2cm (1.25"). The webs consist of two tube sides bonded together for a total thickness of 1.3cm (½"). The material properties from Table 4.1 were used for the respective layers.

Table 4.1 Material Properties for the 10.1cm x 10.1cm (4" x 4") Tube SSDS

Properties	Material No. 1 (Tubes)	Material No. 2 (Sheets)
E_x GPa (psi)	11.0 (1.6×10^6)	13.8 (2.0×10^6)
E_y GPa (psi)	5.5 (0.8×10^6)	9.6 (1.4×10^6)
E_z GPa (psi)	5.5 (0.8×10^6)	9.6 (1.4×10^6)
ν (Poisson's Ratio)	0.33	$\nu_{xy} = 0.31$ $\nu_{yz} = 0.29$
G (Shear Modulas) GPa (psi)	2.9 (0.425×10^6)	2.9 (0.425×10^6)
γ KN/m^3 (lbs/in^3)	18.58 (0.06844)	17.48 (0.06438)

4.3 Boundary Condition Models

In order to investigate the effect of varying the number of deck to stringer attachment points, three boundary condition models were generated to envelope possible attachment configurations. At this point, details of the deck to stringer attachments had not been determined and are considered to be beyond the scope of this investigation. It was assumed that the deck will be bolted to the bridge stringers. To represent the vertical support imparted by the stringers to the deck, all three models were restrained in the vertical (model Y) direction at the bottom edge around the perimeter. To simulate the model attachment points, the models were pinned (restrained Δx and Δz with rotations unrestrained) at the deck to stringer contact points. Three scenarios were investigated: model pinned every 3rd element (BC1), model pinned every 7th element (BC2), and model

pinned at the 4 corners only (BC3). BC2, the median boundary condition case, was considered to be the most likely attachment scenario and was used for the subsequent parametric investigations. An illustration of the three boundary condition models is shown in Figure 4.4.

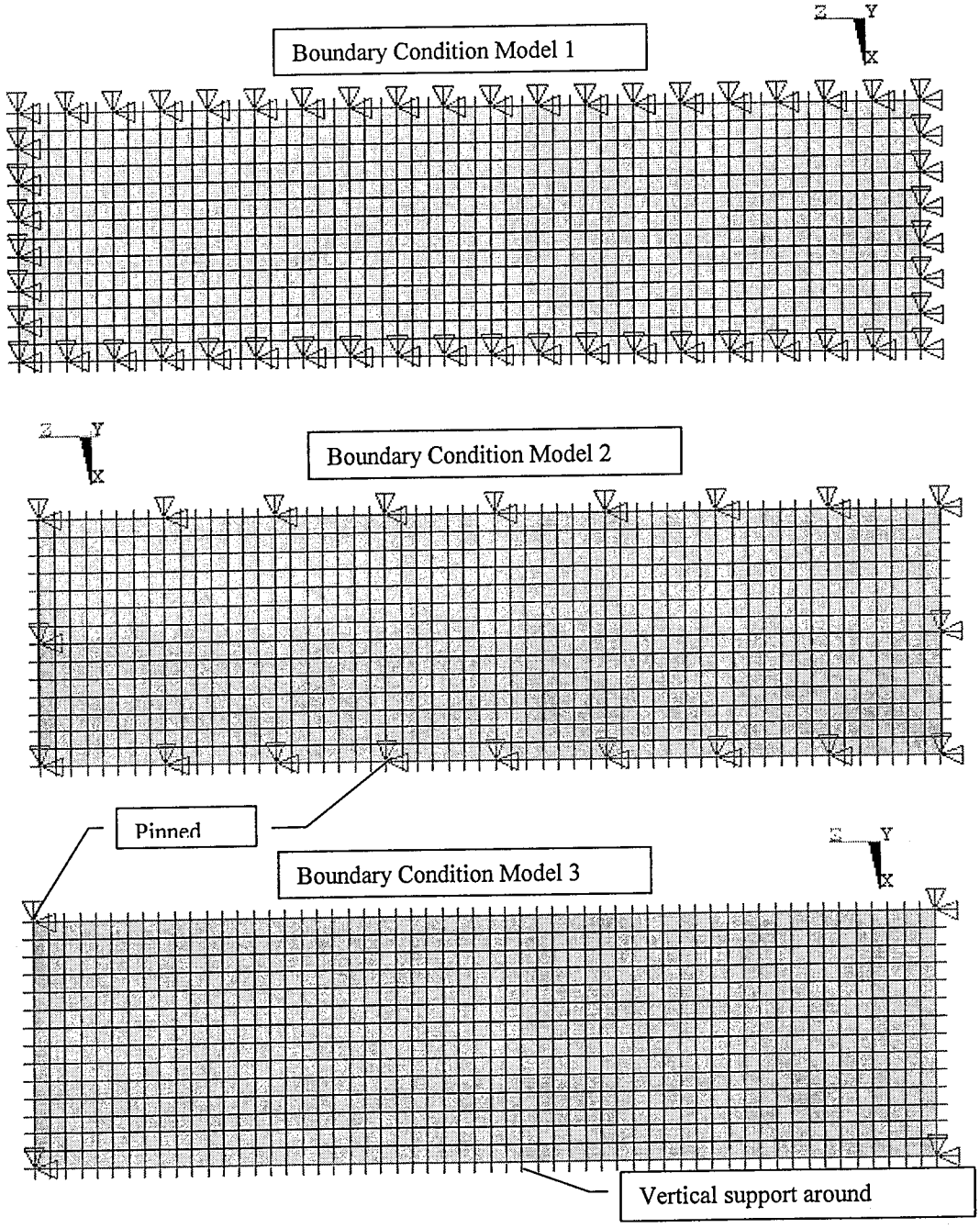

Figure 4.4 Boundary Condition Models (Plan Views)

4.3.1 Loading Conditions for the Boundary Condition Models

To obtain the worst case deflection and bending stresses, the three boundary condition cases were loaded using a single wheel load of 92.6 KN (20800 lbs). This load represents a wheel load of 71.2 KN (16000 lbs) plus 30% for impact. The load was placed in the center of the deck and was applied as a pressure load over ten elements as shown in Figure 4.5. This area is slightly different than the wheel area derived in Chapter 3 which resulted in a wheel contact area of 57.9cm x 23.1cm = 1339 cm^2 (22.8" x 9.1" = 207.5 in^2). This deviation was done to fit the existing model geometry and to avoid having to locally re-mesh the model. The actual area used was 50.8cmx23.8cm = 1208cm^2 (20"x 9.36" = 187.2 in^2). The applied pressure was 92.6/.1208 = 767 KPa (20800/187.2 = 111.1 psi). Since the applied pressure was adjusted for the area used, the difference was deemed negligible.

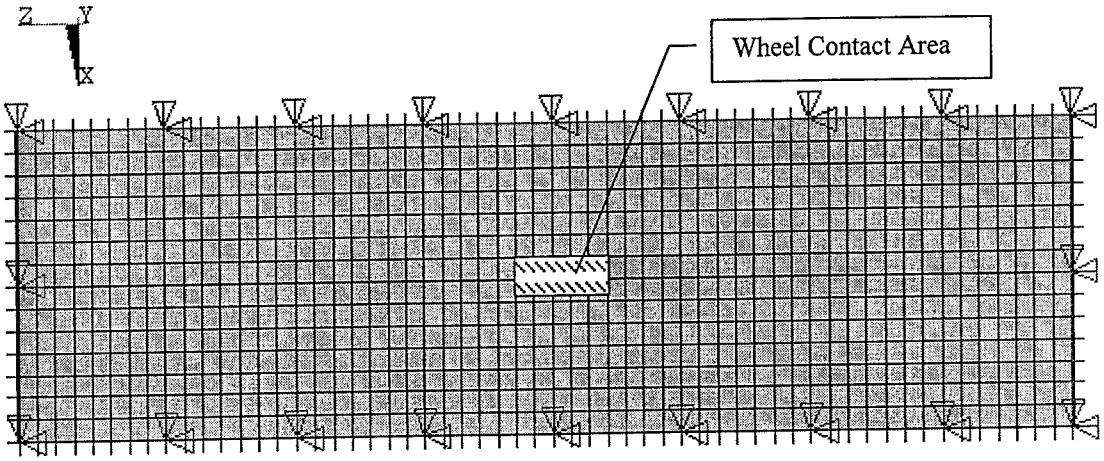

Figure 4.5 BC Model Load Area Location (HS20-44 + Impact)

4.4 Two HS20-44 Wheel Loads (BC2 Model)

The previous loading condition represented the occurrence of a single HS20-44 truck wheel located between the bridge stringers. Since the stringers are located 1.7m (5'-5 ½") apart and since the ASSHTO truck transverse wheel spacing is 1.8m > 1.7m (6' > 5'-5 ½"), only one wheel load can occur between the stringers in the transverse direction. However, the longitudinal spacing between the transverse beams is 5.8m (19'-1"), which is greater than AASHTO's minimum truck axle spacing of 4.3m (14'). For the BC2 model, a second loading condition was investigated using two wheel loads spaced 4.3m (14') apart, with the loading geometric center located over the center of the deck as shown in Figure 4.6. Each wheel load (including impact) was applied over the same model area as was described in the previous section.

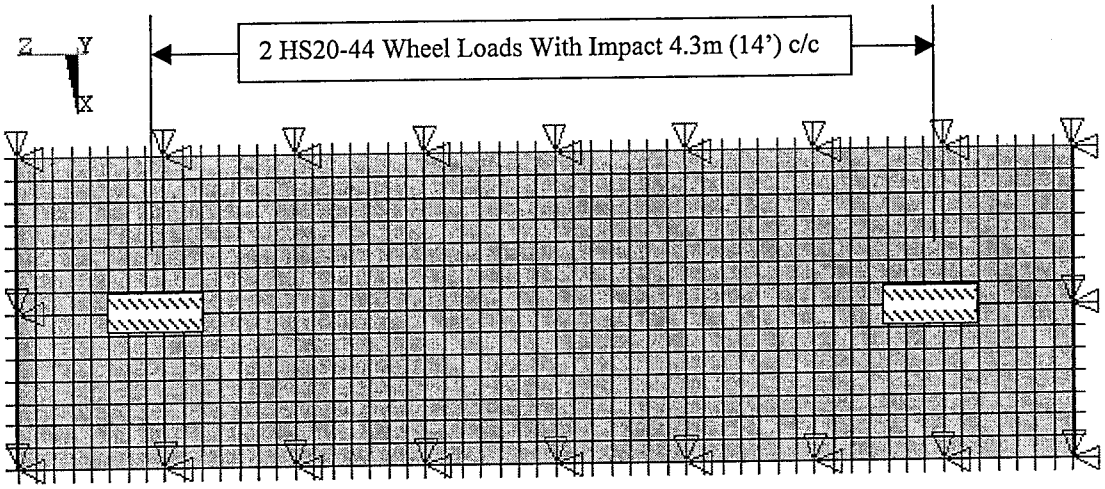

Figure 4.6 BC2 Model with Two HS20-44 Wheel Loads

4.5 Alternate Military Loading (ML-80)

A third loading condition was investigated with the alternate military loading (ML-80) as specified by AASHTO. Two 69.4 KN (15,600 lb) loads were applied 1.2m (4') apart. The 69.4 KN (15,600 lb) load represents the required 53.4 KN (12,000 lb) load plus 30% for impact. The wheel loads were applied as pressure loads in a manner similar to that used for the HS20-44 load discussed earlier. The pressure load applied was 69.4 KN /0.12m = 574.6 KPa (15600 lb./187.2 in^2 = 83.33 psi) as shown in Figure 4.7.

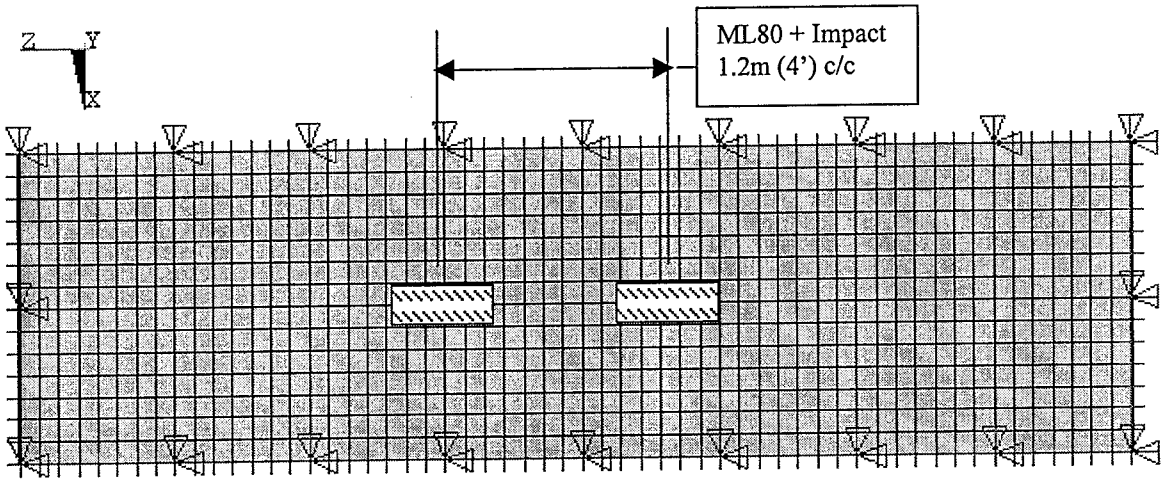

Figure 4.7 BC2 Model with Alternate Military Loading (ML80)

4.6 Shear Loading, for Single Span Deck System (SSDS)

In order to obtain the worst case shear stresses, the HS20-44 wheel loading on the BC2 model was moved to the panel edge. For this case, 4 loading conditions were evaluated. For the first condition, one HS20-44 wheel load (with impact) was placed midway down the long axis of the model with the edge of the loading area directly over the stringer centerline (Shear 3). Under this condition it was expected that some of this load would not serve to stress the model, since a portion of the load was directly over the restrained edge of the model. To assure that this condition was not significant, the load was also applied 11.9cm (4.7") away from the model edge (Shear 1). This offset from the edge represents one row of elements and was used for convenience. The next loading condition evaluated was the condition when the truck wheel was located at the end of the model, close to the transverse girders. This represents the case where the truck is about to drive off the deck panel. For this condition the load was placed directly over the model boundary (Shear 4), and also 1 row of elements inside the boundary (Shear 2), as was done for the Shear 1 loading case. The results for the shear loading conditions are discussed later in Chapter 5. Figure 4.8 shows the locations of the wheel loads that generated the worst case shear values on the single span deck system (SSDS).

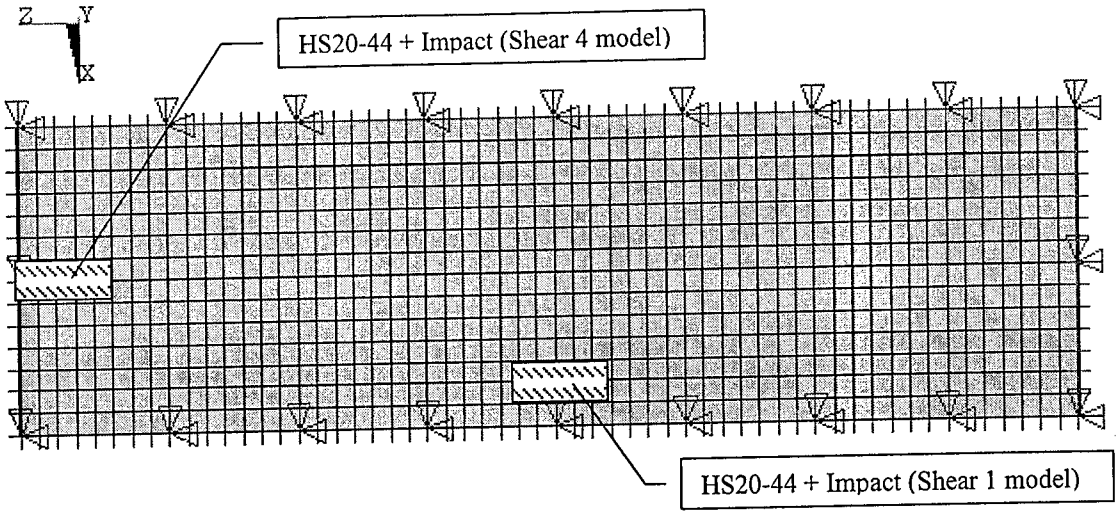

Figure 4.8 SSDS Wheel Loading for Worst Case Shear

4.7 Self-Weight and Wear Surface Loading

The effect of self-weight was evaluated by applying a model density of 18.6 KN/m^3 (0.06844 lb/in^3) for the tubes and a model density of 17.5 KN/m^3 (0.06438 lb/in^3) for the sheets. A unit vertical acceleration was then specified in order to obtain the self-weight loading. To model the wear surface loading, a 5.1cm (2") thick surface was assumed with a weight of 16.8 lb/ft^2 for (2") of polymer concrete [1]. Two additional models were generated and loaded using the deck self-weight and wear surface weight. First, to simulate the deck in a position 90° to the horizontal, unit acceleration was applied in the models global Z direction (parallel to the direction of traffic). The wear surface load was also applied in the global Z direction as joint loads distributed above the model nodes of the upper deck sheets.

The following loads were applied to each of the sheets:

$P_z = (804.7N/m^2)(5.8m)(1.7m)/(2537 \text{ nodes}) = \underline{3.1 \text{ N/node}}$

$(P_z = (16.8 \text{ lb/ft}^2)(19')(5.458')/(2537 \text{ nodes}) = \underline{0.687 \text{ lb/node}})$

The second model was loaded to evaluate the deck in a position of 45° from horizontal. Self-weight and wear surface loads were applied in a similar manner as for the 90° case with the exception that 70.7% of the joint loads and 70.7% of the unit acceleration were applied in the global Z and –Y directions.

4.8 Wind Loading

To investigate the effect of wind on a raised deck, a 344.6 KPa (50 psi) pressure load was applied normal to the BC2 deck model. The results of this loading case were then combined with the results of the 45 ° and 90° self-weight and dead load models for total stresses. In addition to the above case, AASHTO specifies a loading condition of 206.8 KPa (30 psi) combined with dead load plus 20% for impact. To check this condition, the 344.6 KPa (50 psi) model stresses were scaled by 3/5 and combined with 1.2 times the self weight plus wear surface model stresses. The results for the above load cases are presented in chapter 5.

4.9 Multi-Span Deck System (MSDS)

Since it would be possible to manufacture a deck panel that would be continuous over more than one span, it was decided to evaluate a multi-span configuration. As shown in Figure 3.2, there are seven 1.7m (5'-5") transverse spans between the longitudinal stringers that would support the deck. In order to determine the worst case load placement for the continuous cases, the computer program PcBridge [26] was used to evaluate possible loading conditions for transverse wheel placements perpendicular to the direction of traffic. PcBridge is a program for evaluating multi-span beams with moving loads.

The PcBridge program can evaluate up to ten continuous spans and will allow the user to specify the load configuration. The program generates moment, deflection and shear envelope data by stepping the user specified load configuration across the beam. Multi-span models were run for each possible span condition such as a 2 span case, a 3 span case and all other span cases up to 7 spans. Models were run for all possible load cases that could fit on a given span configuration (up to 3 trucks). For example, the 7 span model was run for the 1 truck case, the 2 truck case and the 3 truck case. Loads were spaced as recommended by ASSHTO as shown in Figure 4.9. A loading of 92.6 KN (20800 lbs) was used for each wheel. This load represents the loading of an HS20-44 truck plus impact.

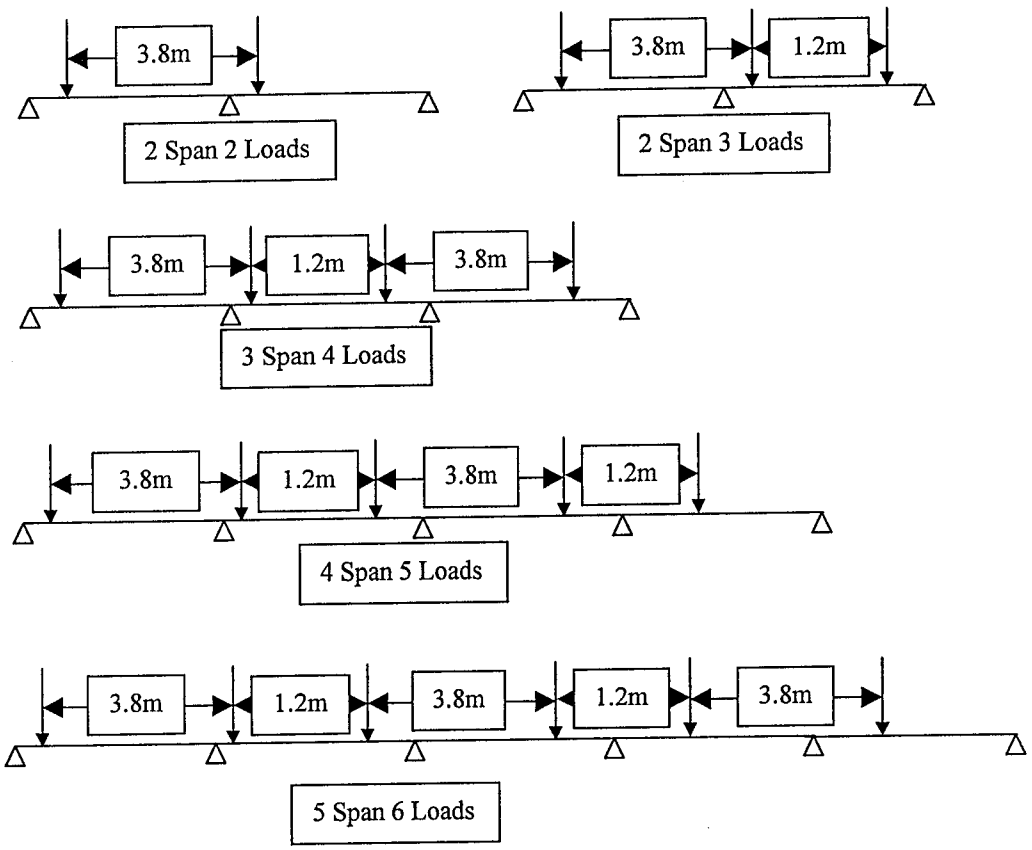

Figure 4.9 Examples of the Multi-span Beam Load Cases

Based on the results of the Multi-span beam analysis, the 2 span, 3 wheel load condition generated the worst case positive moment, negative moment, deflection and essentially the worst case shear. The 4 span 4 wheel load model generated a slightly higher number for shear but the difference (0.5%) is negligible. The resulting moment and shear envelopes are shown in Figure 4.10. To further evaluate the effect of continuity, a 2 span finite element model of the 10.2cm x 10.2cm (4"x 4") tube configuration was developed. The multi-span beam data was then used to determine the load placement location on the model that would produce the worst case positive

moment, negative moment, deflection and shear. The load locations are shown in Figures 4.11 and 4.12.

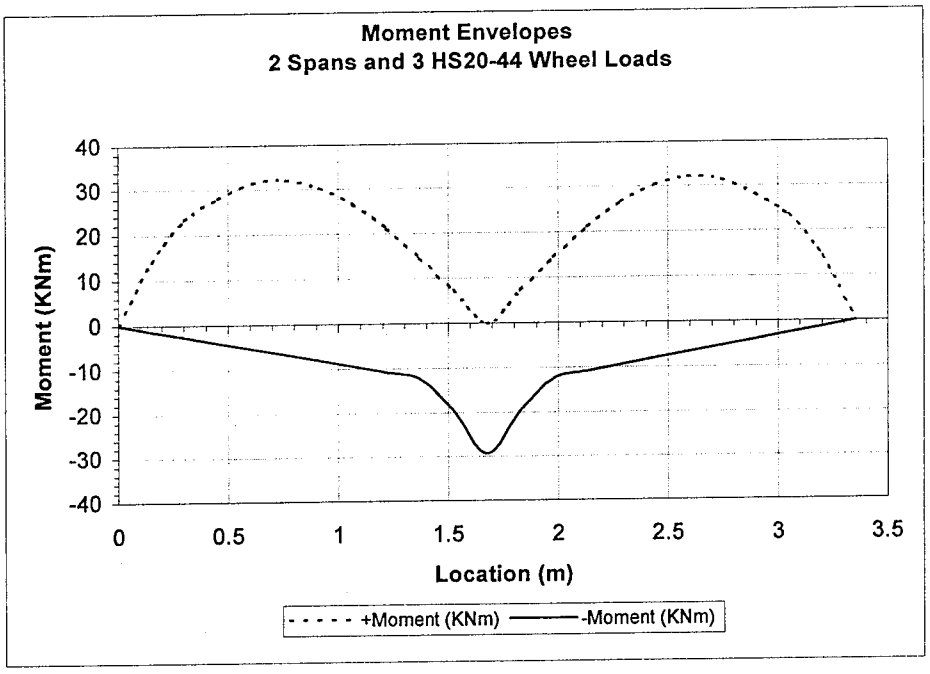

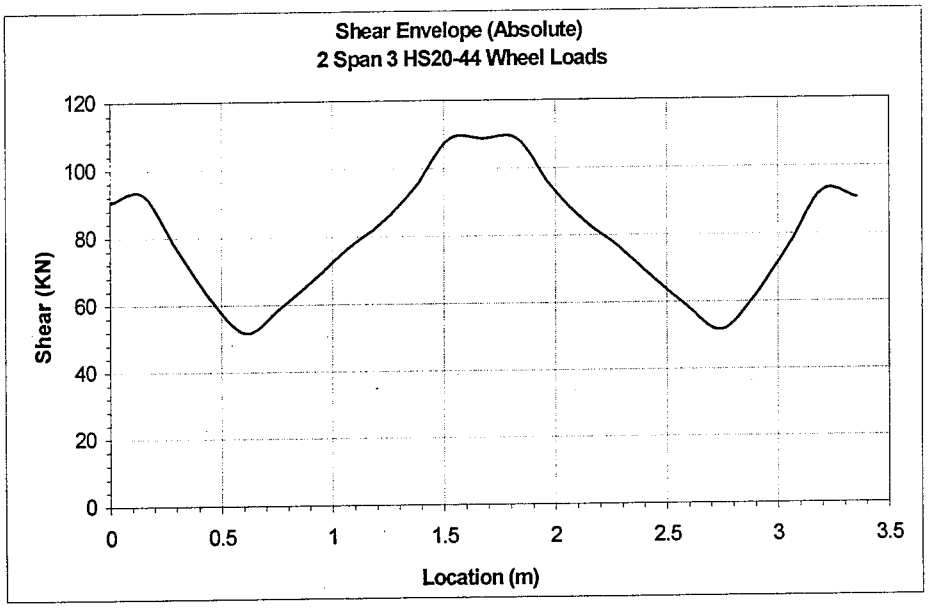

Figure 4.10 Moment and Shear Envelopes from the Multi-span Beam Analysis

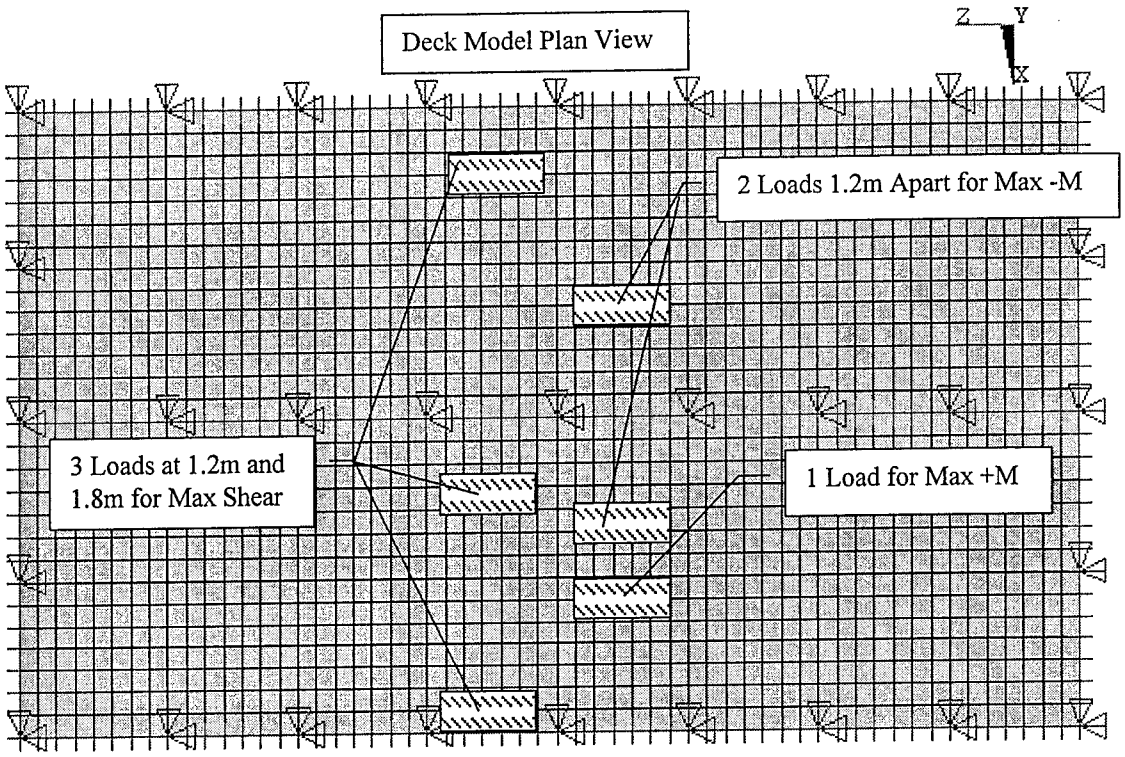

Figure 4.11 Two Span Model Load Placements for Max Moments and Shear

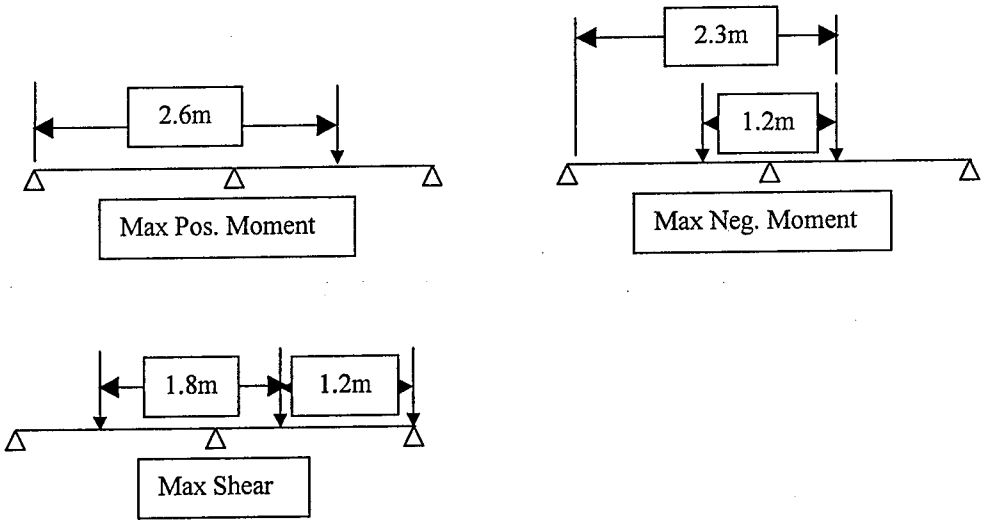

Figure 4.12 Two Span Model Load Placements for Max Moments and Shear

It should be noted that the load placements in Figure 4.11 are shown longitudinally out of position in order to show all three load cases on the same figure. Figure 4.12 shows the load locations from the multi-span moving load analysis that resulted in maximum moments and maximum shear. Loads that had moved off the span, such as one from an adjacent wheel are not shown.

4.10 Joint Discontinuity Cases

To investigate the effect of discontinuity of joints in the bridge deck, the situation where a panel to panel joint has failed or formed a hinge, two additional models were developed and evaluated. The first model consisted of a single span panel simply supported on three sides with the fourth side free. An HS20-44 wheel load, with impact, was then placed over the free edge. The second model consisted of 1½ spans with the ½ span edge unsupported acting as a cantilever. For this case another HS20-44 load, with impact, was placed at the cantilever end. Figures 4.13 and 4.14 illustrate the load locations for the joint discontinuity cases.

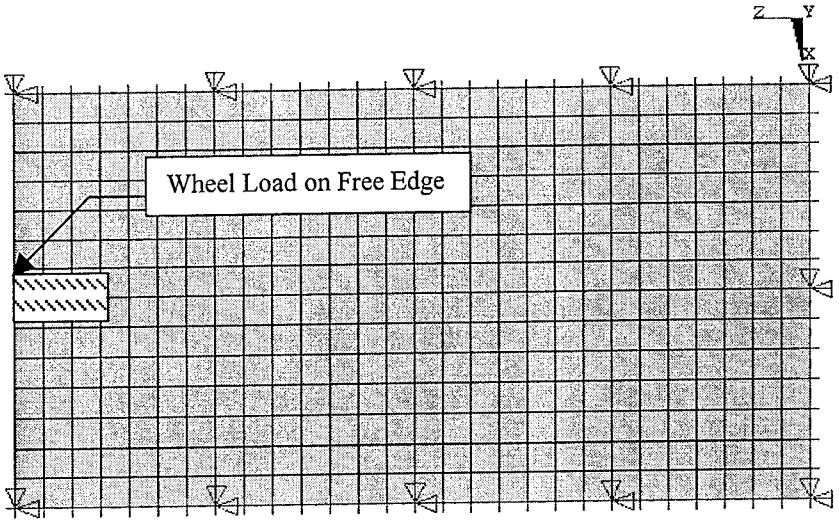

Figure 4.13 Joint Discontinuity Loading for Free Edge Model

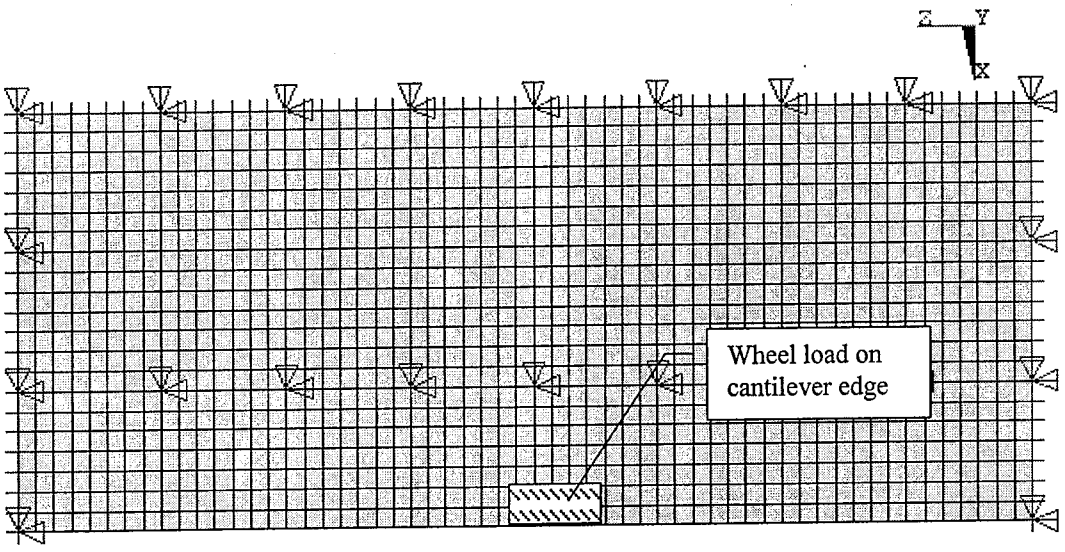

Figure 4.14 Joint Discontinuity Loading for 1 ½ Span Cantilever Model

4.11 Single Span 12.7cm x 17.8cm (5"x7") Tube Model

During the preliminary investigation presented in chapter 3, it was determined that a second tube and sheet configuration is also acceptable. To investigate this second configuration, a model of the single span panel system (Figure 4.15) was developed for the 12.7cm x 17.8cm (5"x7") tubes and 1.9cm (¾") cover sheets. The model was developed using the BC2 boundary condition case as shown in the Figure 4.16. The material properties used are shown in Table 4.2. The model was loaded in the same manner as the 10.2cm x 10.2cm (4"x 4") tube BC2 model in section 4.2. An HS20-44 (plus impact) load of 92.6 KN (20800 lbs) was applied as shown in Figure 4.16.

Table 4.2 Material Properties for 12.7cm x 17.8cm (5"x7") Tube Model

Properties	Material No. 1 (Tubes)	Material No. 2 (Sheets)
E_x GPa (psi)	11.0 (1.6×10^6)	13.8 (2.0×10^6)
E_y GPa (psi)	5.5 (0.8×10^6)	9.6 (1.4×10^6)
E_z GPa (psi)	5.5 (0.8×10^6)	9.6 (1.4×10^6)
ν (Poisson's Ratio)	0.2	$\nu_{xy} = 0.31$ $\nu_{yz} = 0.29$
G (Shear Modulas) GPa (psi)	2.9 (0.425×10^6)	2.9 (0.425×10^6)
γ KN/m^3 (lbs/in^3)	18.74 (0.06899)	17.48 (0.06438)

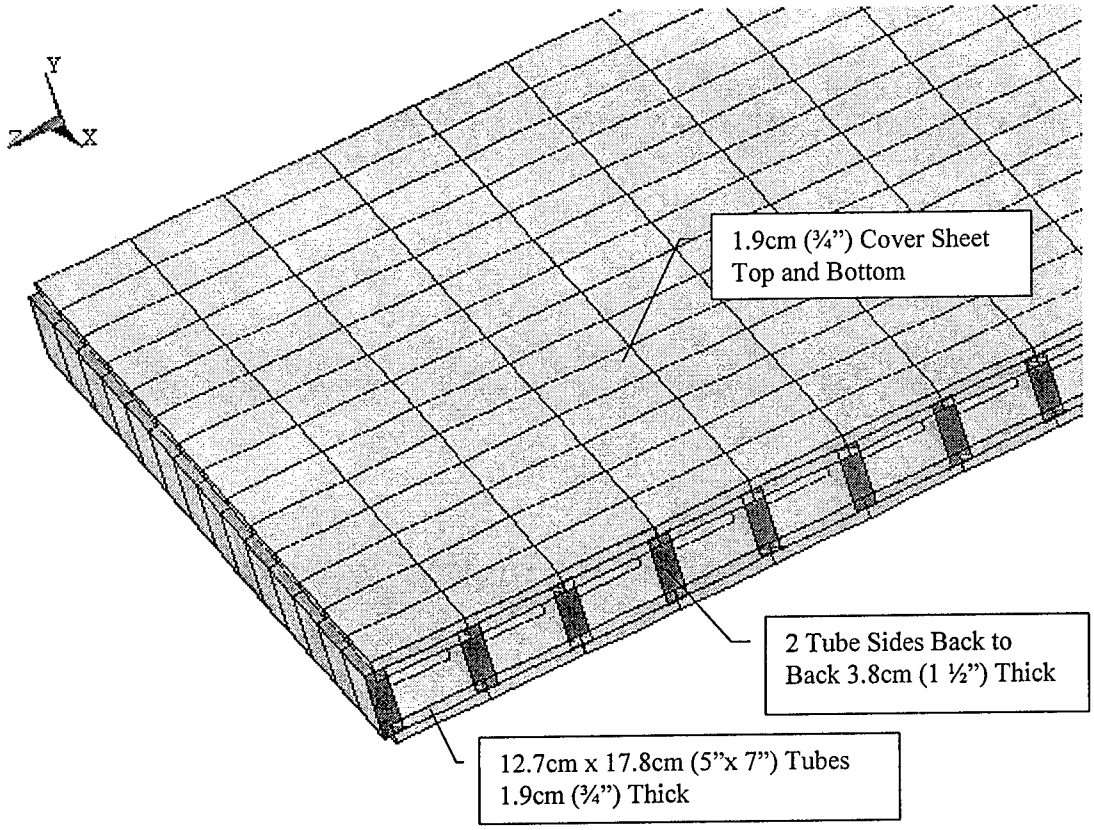

Figure 4.15 12.7cm x 17.8cm (5"x7") Tubes with 1.9cm (¾") Cover Sheets

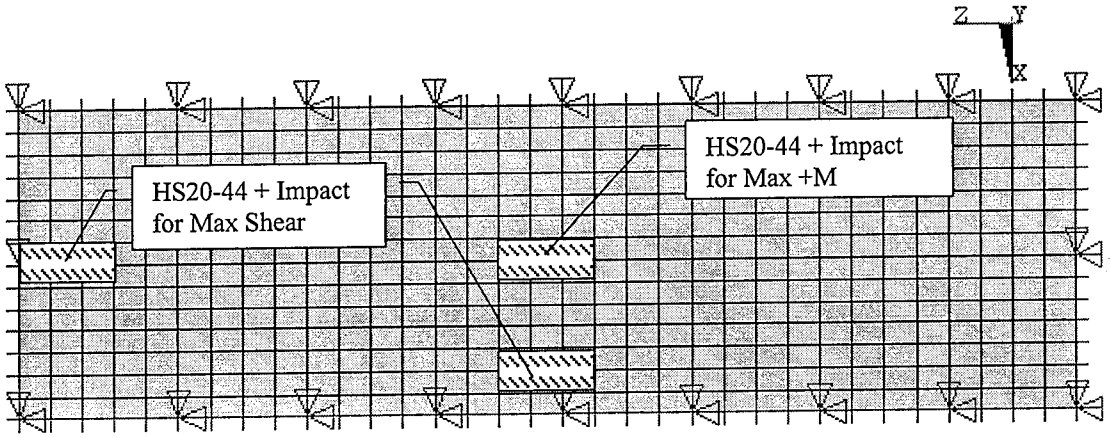

Figure 4.16 12.7cm x 17.8cm (5"x7") Tube BC2 Model Loading

CHAPTER 5

PARAMETRIC STUDIES

5.1 Introduction

As discussed in Chapter 4, a number of finite element models with various loading conditions were investigated. Stresses and deflections for each loading condition were obtained and the results are summarized in this chapter. The stresses summarized in this chapter are maximum stresses for each stress component for a given loading condition, and are not necessarily taken from the same location. In addition, both maximum positive and negative stresses are reported. For bending stresses, the positive and negative stresses represent the extreme fiber stress for the component under consideration. The stresses occur at the top and bottom of the deck where tensile stresses are positive and compressive stresses are negative. For shear stresses, differences in sign result from stresses being taken from opposite ends of the deck; that is, as a result of a positive shear force or a negative shear force.

Since the tube and sheet material properties vary, stresses are reported for both the tube layers and sheet layers. As shown in Figure 5.1, layer 1 represents the tubes and

layer 2 represents the cover sheets. Stresses are reported at the extreme fibers of each layer. The stress components reported for each layer are based on the global coordinate system of the model. In this system the X axis is in the plane of the deck and is perpendicular to traffic (longitudinal axis of the tubes). The Z axis is also in the plane of the deck and is parallel to traffic (transverse tube axis). The Y axis is normal to the deck (vertical) as shown in the following figure.

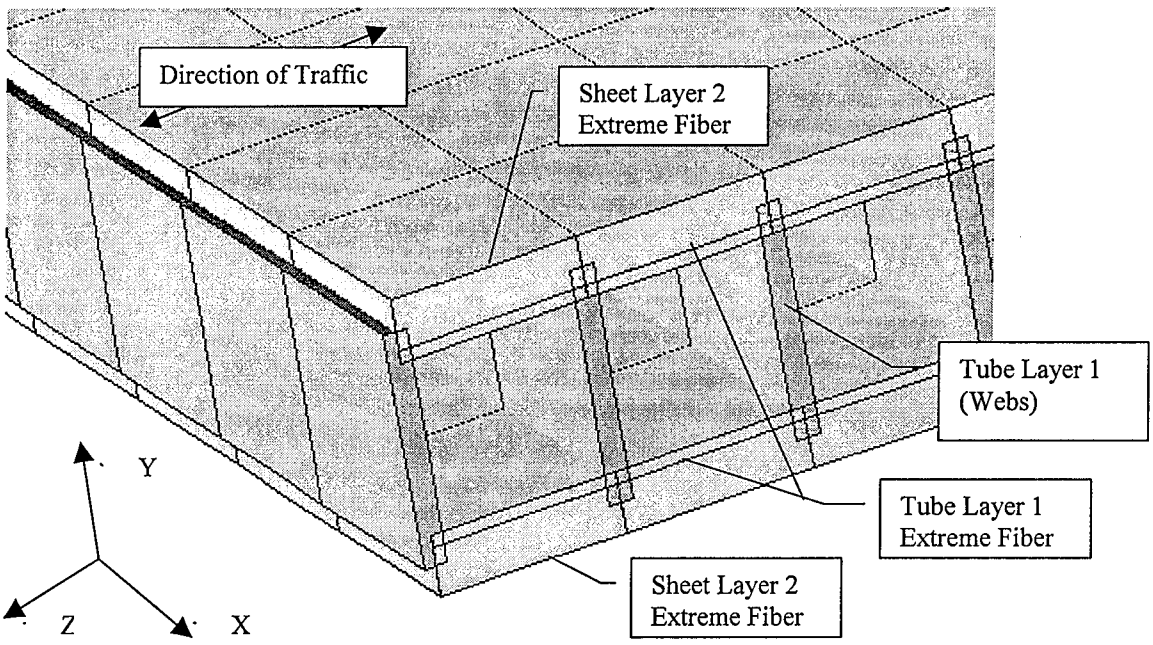

Figure 5.1 Element Layers and Global Coordinate System for the Composite Deck System

For the sheets, only σ_x, σ_z and τ_{xz} stresses are reported. Out of plane stresses such as σ_y, τ_{xy} and τ_{yz} were essentially zero. For the tubes, the σ_x, σ_y, σ_z, τ_{xy} and τ_{xz} stresses are reported. The τ_{yz} stresses in the tube are not presented since they are out of plane and

were extremely low. The τ_{xy} tube stresses occur in the tube webs (x-y plane), while the tube τ_{xz} stresses occur in the tube top and bottom (x-z plane).

The stress results in this chapter are presented as a series of charts and tables that allow for comparison of stress values between pertinent loading cases, models and allowables. Actual stresses used to develop each chart are provided in a data table below each chart. In addition, each stress component is presented as a percentage of the allowable in a second table that follows each chart.

The stresses presented in this chapter are based on the combination of live load and dead load. Dead load is based on the self-weight of the deck and an assumed 5.1cm(2") thick wear surface of polymer concrete, with a weight of 0.81kPa (16.8 psf) as was obtained from reference [1]. To simplify the analysis, the live load plus dead load stresses were obtained by adding the maximum live load stresses to the maximum dead load stresses for a given model. Although these stresses were not added based on location, the above simplifying assumption was deemed acceptable for the following reasons. The dead load stresses are only a small percentage of the live load stresses. In addition, by inspection, the maximum dead load stresses are expected to occur at or near the same locations as the maximum live load stresses. For example, in both dead load and live load cases, maximum bending stresses are expected to occur at the center of the span and maximum shear stresses are expected to occur in the webs at the ends of the deck.

5.2 Comparison of Boundary Condition Models for Single Span Deck System

As Discussed in Chapter 4, three boundary condition models were developed to investigate the effect of changing the number of attachment points to the stringer supports. The tube stresses and sheet stresses for the three models are compared in the following charts and tables. As mentioned earlier, the BC1 model boundary nodes were pinned every 3rd element, the BC2 model boundary nodes were pinned every 7th element and the BC3 model had pinned boundary nodes at the four corners only (Figure 4.4). It should also be noted that the allowable stresses are based on safety factors of 2.5 for bending and 3.0 for shear.

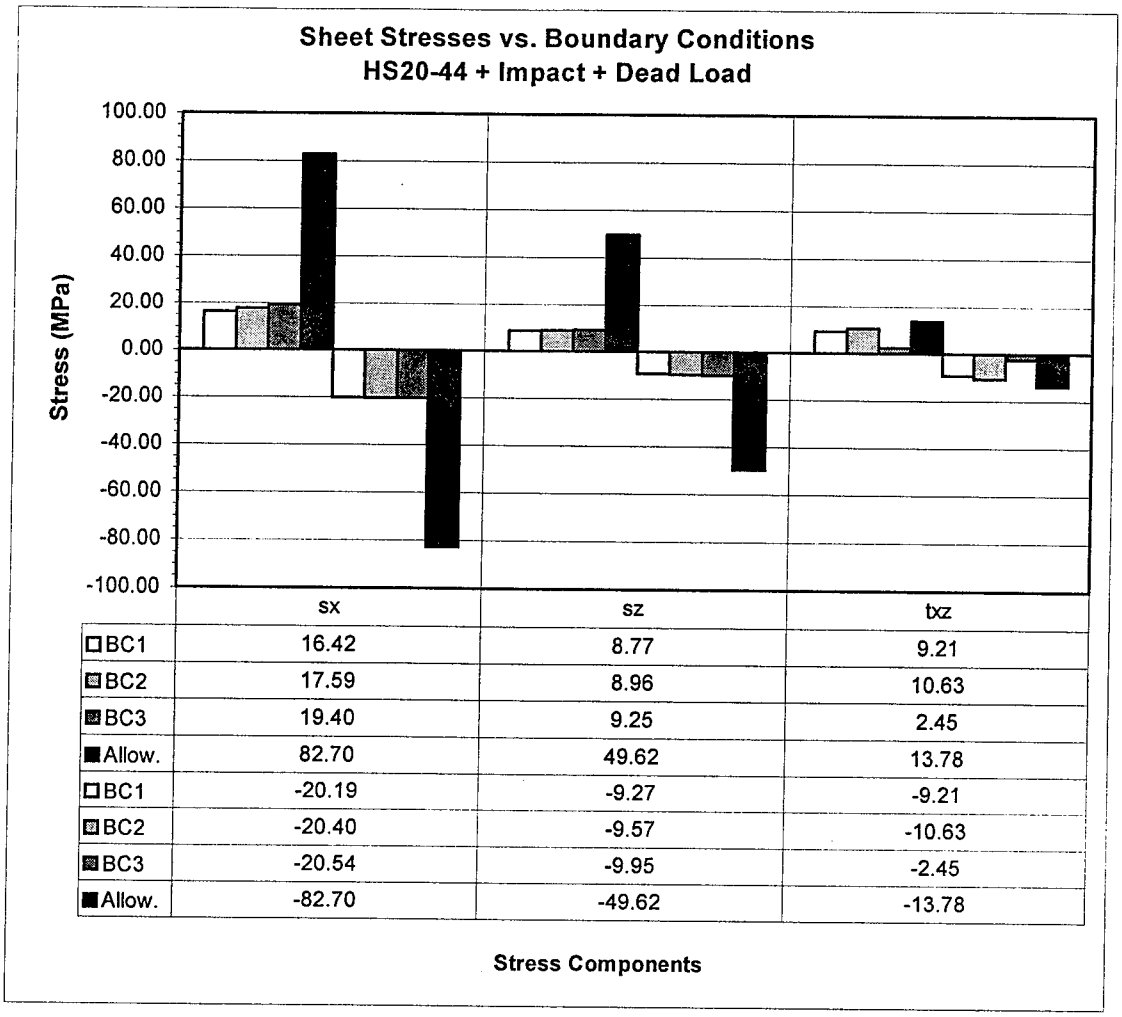

	sx	sz	txz
BC1	16.42	8.77	9.21
BC2	17.59	8.96	10.63
BC3	19.40	9.25	2.45
Allow.	82.70	49.62	13.78
BC1	-20.19	-9.27	-9.21
BC2	-20.40	-9.57	-10.63
BC3	-20.54	-9.95	-2.45
Allow.	-82.70	-49.62	-13.78

Figure 5.2.1 Sheet Stresses vs. Boundary Conditions for SSDS Models

Table 5.2.1 Sheet Stresses from Figure 5.2.1 as a Percentage of the Allowable

	σ_x (%)	σ_z (%)	τ_{xz} (%)
BC1	19.85	17.68	66.83
BC2	21.27	18.06	77.14
BC3	23.45	18.64	17.77
Allowable	100	100	100
BC1	24.41	18.68	66.82
BC2	24.66	19.29	77.12
BC3	24.83	20.05	17.77
Allowable	100	100	100

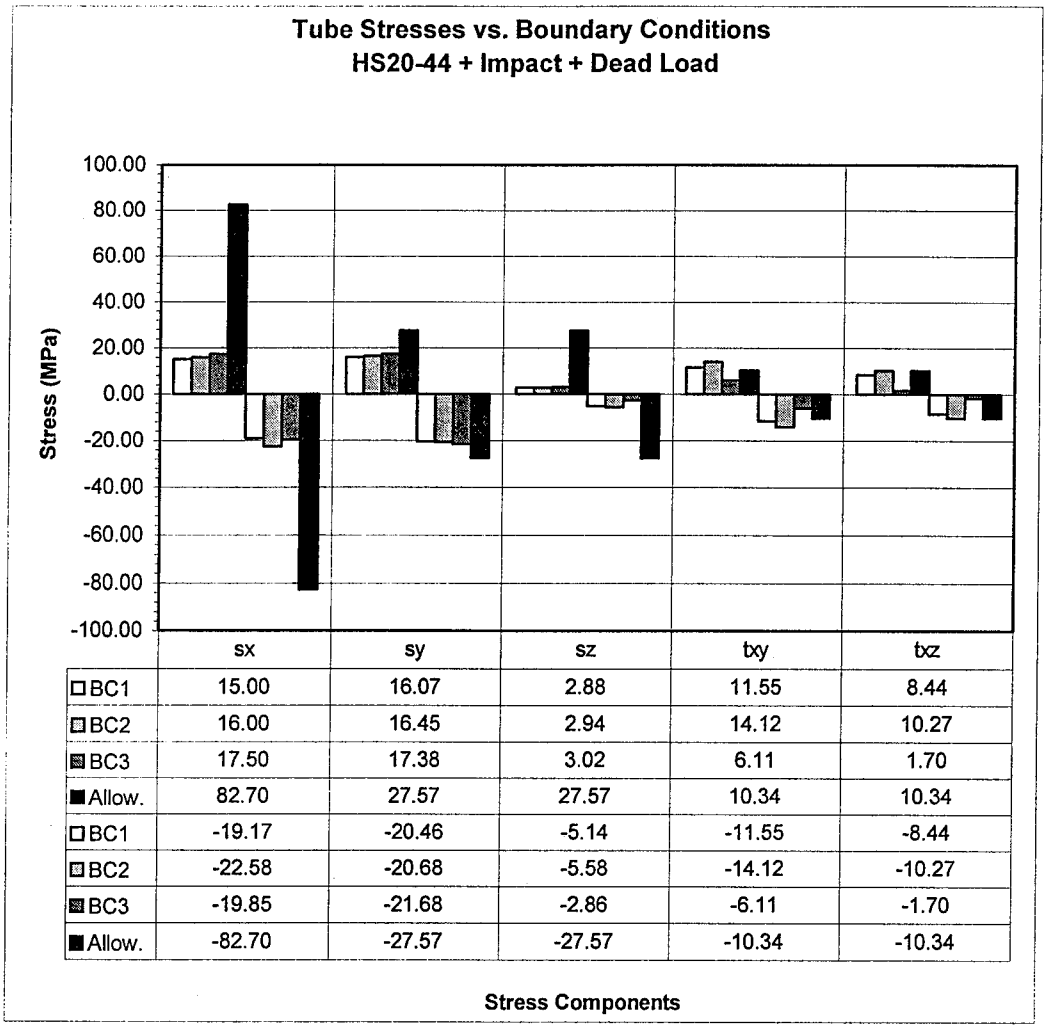

	sx	sy	sz	txy	txz
BC1	15.00	16.07	2.88	11.55	8.44
BC2	16.00	16.45	2.94	14.12	10.27
BC3	17.50	17.38	3.02	6.11	1.70
Allow.	82.70	27.57	27.57	10.34	10.34
BC1	-19.17	-20.46	-5.14	-11.55	-8.44
BC2	-22.58	-20.68	-5.58	-14.12	-10.27
BC3	-19.85	-21.68	-2.86	-6.11	-1.70
Allow.	-82.70	-27.57	-27.57	-10.34	-10.34

Figure 5.2.2 Tube Stresses vs. Boundary Conditions for SSDS Models

Table 5.2.2 Tube Stresses from Figure 5.2.2 as a Percentage of the Allowable

	σ_x (%)	σ_y (%)	σ_z (%)	τ_{xy} (%)	τ_{xz} (%)
BC1	18.14	58.28	10.46	111.72	81.63
BC2	19.35	59.68	10.66	136.58	99.29
BC3	21.17	63.03	10.96	59.06	16.43
Allowable	100	100	100	100	100
BC1	23.18	74.21	18.63	111.72	81.67
BC2	27.30	75.03	20.23	136.58	99.33
BC3	24.00	78.63	10.38	59.06	16.47
Allowable	100	100	100	100	100

5.3 Truck Loading Condition Models for Single Span Deck System

For the single span deck system and the moderate boundary condition case (BC2 model), several loading conditions were investigated. The model was loaded using a single HS20-44 wheel load at the center of the deck, two HS20-44 wheel loads spaced 4.27m (14') apart and two ML80 loads spaced 1.22m (4') apart. In addition, to investigate loading conditions that would generate the worst case shear stresses, a single HS20-44 wheel load was placed along the model boundaries. A more detailed discussion of the above loading conditions can be found in Chapter 4. The stress results for the above conditions are presented in the following charts and tables. As noted earlier, the allowable stresses are based on safety factors of 2.5 for bending and 3.0 for shear.

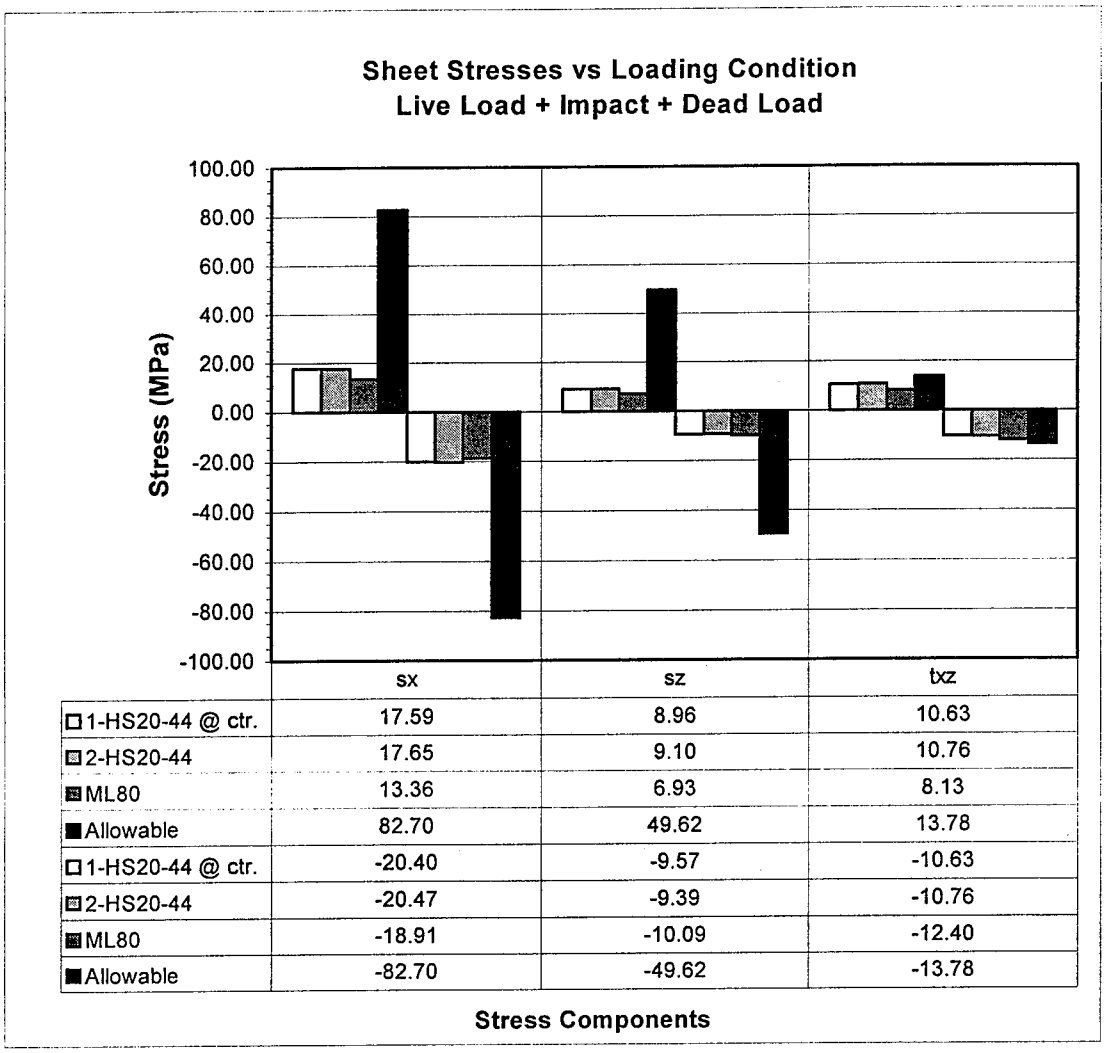

	sx	sz	txz
1-HS20-44 @ ctr.	17.59	8.96	10.63
2-HS20-44	17.65	9.10	10.76
ML80	13.36	6.93	8.13
Allowable	82.70	49.62	13.78
1-HS20-44 @ ctr.	-20.40	-9.57	-10.63
2-HS20-44	-20.47	-9.39	-10.76
ML80	-18.91	-10.09	-12.40
Allowable	-82.70	-49.62	-13.78

Figure 5.3.1 Sheet Stress Comparisons for Changes in Truck Loading Conditions (Max Moment)

Table 5.3.1 Sheet Stresses from Figure 5.3.1 as a Percentage of the Allowables

	σ_x (%)	σ_z (%)	τ_{xz} (%)
1-HS20-44 @ ctr.	21.27	18.06	77.14
2-HS20-44	21.34	18.33	78.09
ML80	16.15	13.96	59.03
Allowable	100	100	100
1-HS20-44 @ ctr.	24.66	19.29	77.12
2-HS2044	24.75	18.93	78.07
ML80	22.86	20.34	89.97
Allowable	100	100	100

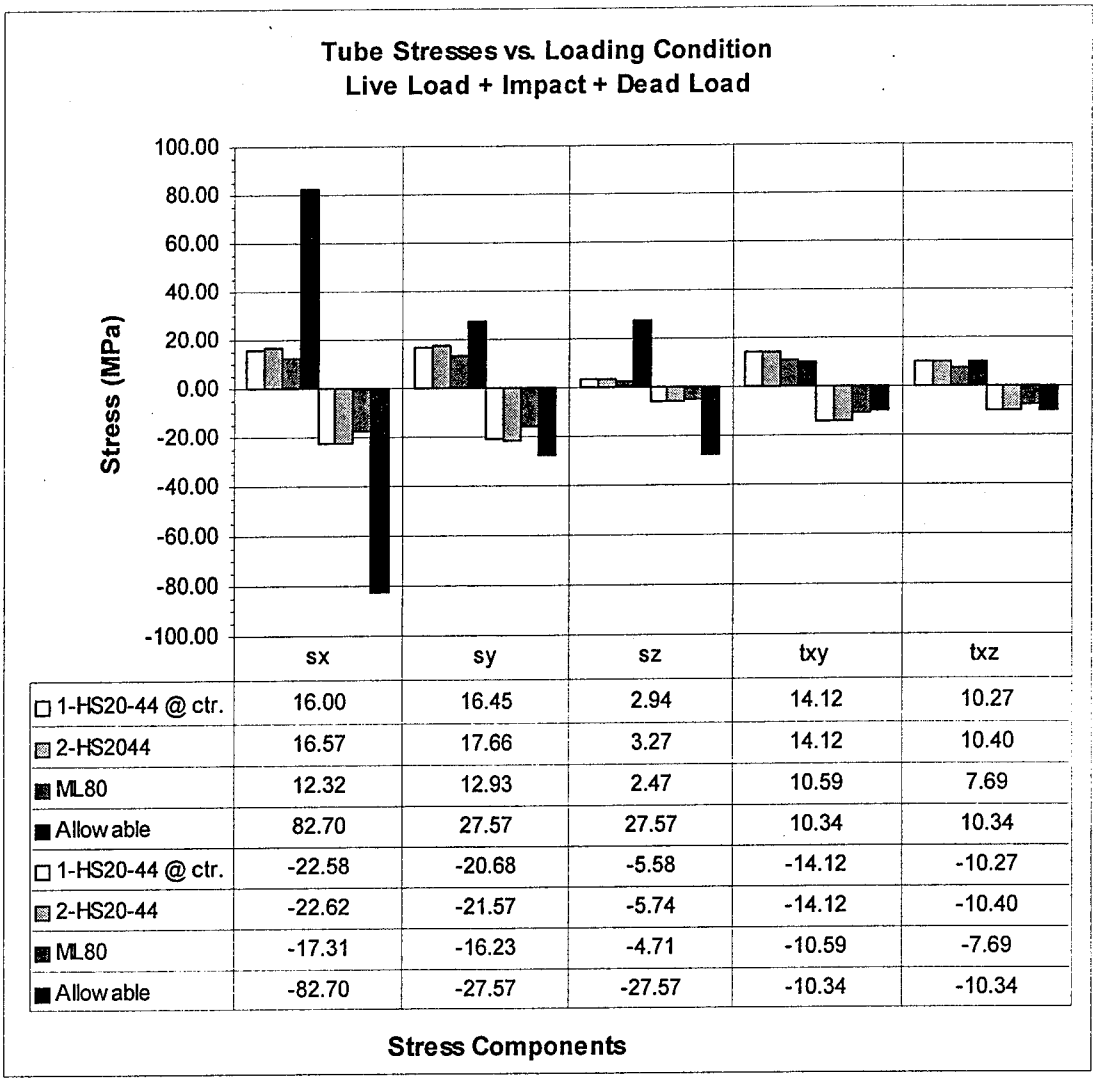

	sx	sy	sz	txy	txz
1-HS20-44 @ ctr.	16.00	16.45	2.94	14.12	10.27
2-HS2044	16.57	17.66	3.27	14.12	10.40
ML80	12.32	12.93	2.47	10.59	7.69
Allowable	82.70	27.57	27.57	10.34	10.34
1-HS20-44 @ ctr.	-22.58	-20.68	-5.58	-14.12	-10.27
2-HS20-44	-22.62	-21.57	-5.74	-14.12	-10.40
ML80	-17.31	-16.23	-4.71	-10.59	-7.69
Allowable	-82.70	-27.57	-27.57	-10.34	-10.34

Figure 5.3.2 Tube Stress Comparisons for Changes in Truck Loading Conditions (Max Moment)

Table 5.3.2 Tube Stresses from Figure 5.3.2 as a Percentage of the Allowables

	σ_x (%)	σ_y (%)	σ_z (%)	τ_{xy} (%)	τ_{xz} (%)
1-HS20-44 @ ctr.	19.35	59.68	10.66	136.58	99.29
2-HS2044	20.04	64.05	11.86	136.58	100.63
ML80	14.90	46.90	8.96	102.38	74.37
Allowable	100	100	100	100	100
1-HS20-44 @ ctr.	27.30	75.02	20.23	136.58	99.29
2-HS20-44	27.35	78.25	20.80	136.58	100.63
ML80	20.93	58.87	17.08	102.38	74.37
Allowable	100	100	100	100	100

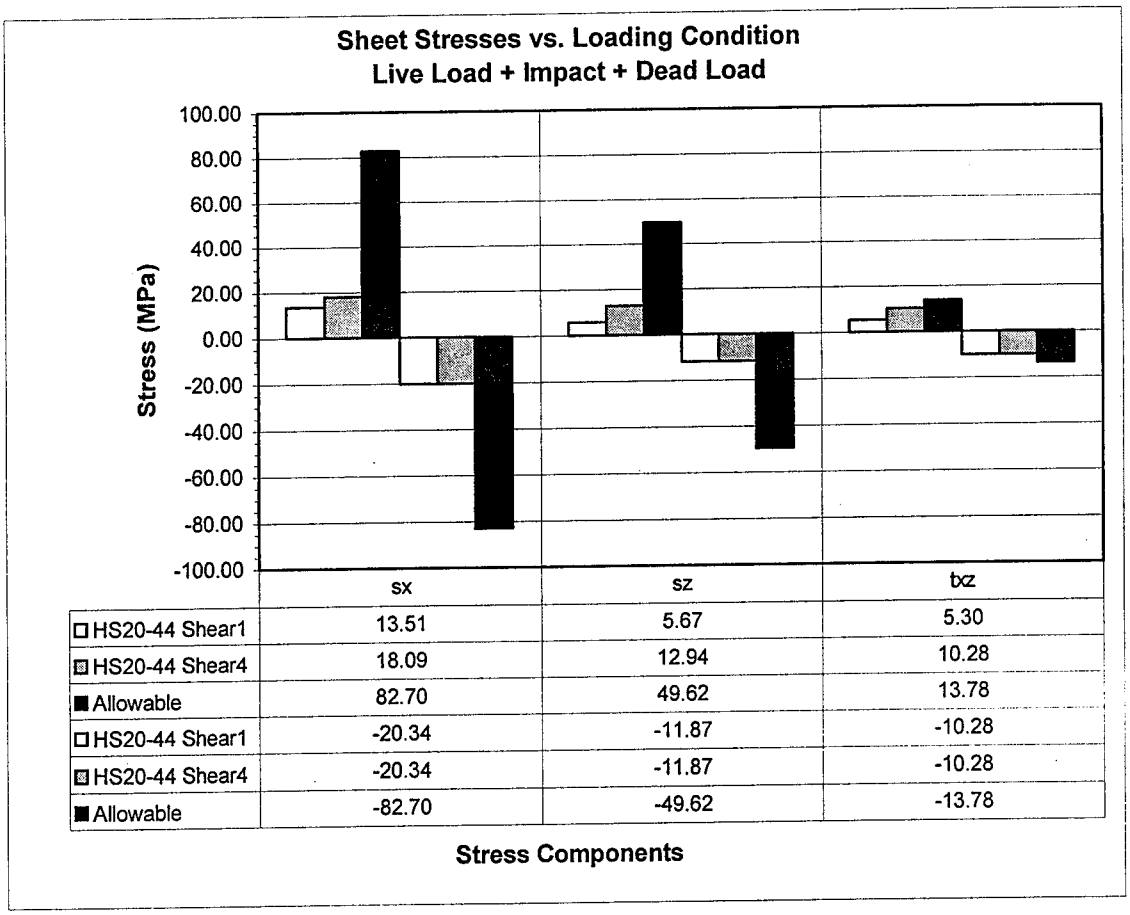

Figure 5.3.3 Sheet Stress Comparisons for Changes in Truck Loading Conditions (Wheel Load at Support)

Table 5.3.3 Sheet Stresses from Figure 5.3.3 as a Percentage of the Allowables

	σ_x (%)	σ_z (%)	τ_{xz} (%)
HS20-44 Shear1	16.34	11.42	38.46
HS20-44 Shear4	21.87	26.08	74.58
Allowable	100	100	100
HS20-44 Shear1	24.59	23.91	74.57
HS20-44 Shear4	24.59	23.91	74.57
Allowable	100	100	100

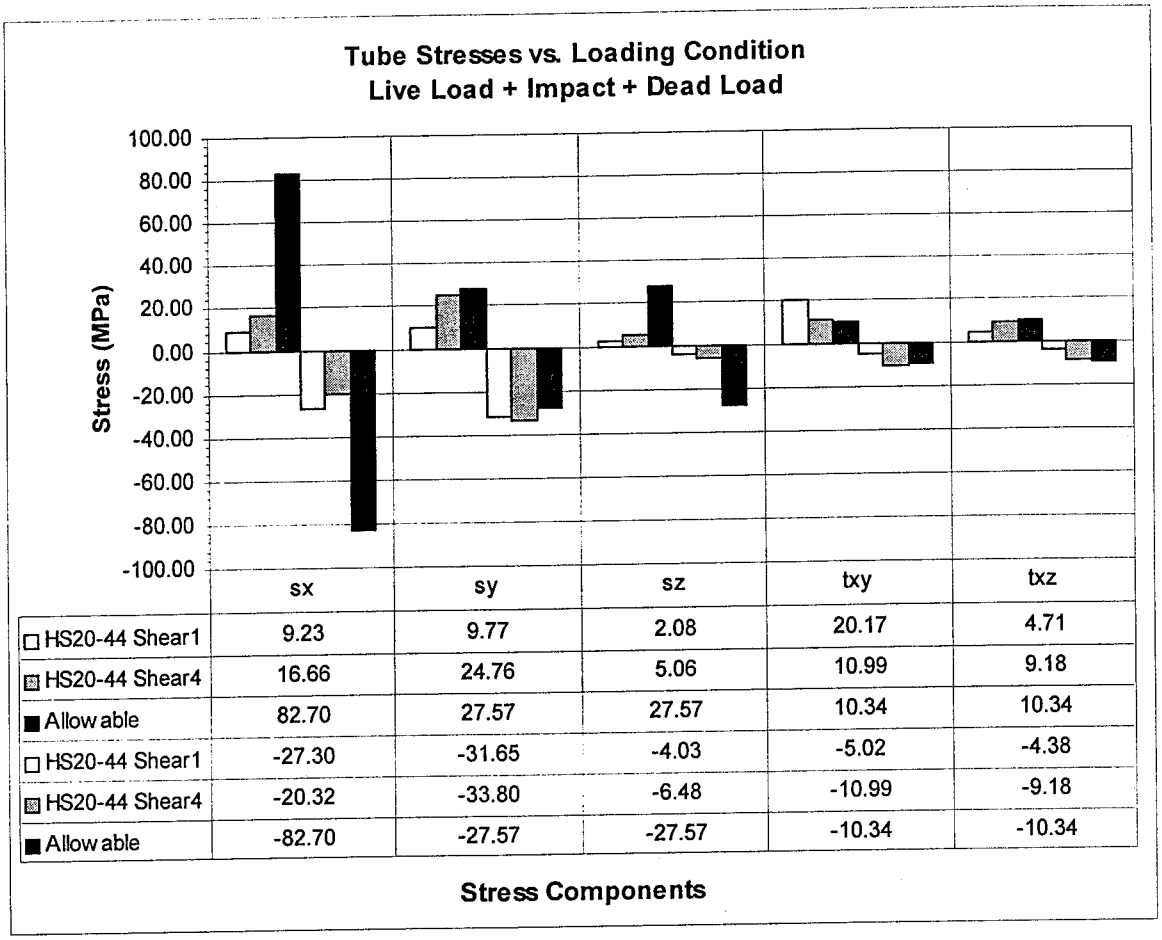

	sx	sy	sz	txy	txz
HS20-44 Shear1	9.23	9.77	2.08	20.17	4.71
HS20-44 Shear4	16.66	24.76	5.06	10.99	9.18
Allowable	82.70	27.57	27.57	10.34	10.34
HS20-44 Shear1	-27.30	-31.65	-4.03	-5.02	-4.38
HS20-44 Shear4	-20.32	-33.80	-6.48	-10.99	-9.18
Allowable	-82.70	-27.57	-27.57	-10.34	-10.34

Figure 5.3.4 Tube Stress Comparisons for Changes in Truck Loading Conditions (Wheel Load at Support)

Table 5.3.4 Tube Stresses from Figure 5.3.4 as a Percentage of the Allowables

	σ_x (%)	σ_y (%)	σ_z (%)	τ_{xy} (%)	τ_{xz} (%)
HS20-44 Shear1	11.17	35.43	7.54	195.03	45.55
HS20-44 Shear4	20.14	89.82	18.36	106.32	88.76
Allowable	100	100	100	100	100
HS20-44 Shear1	33.01	114.79	14.60	48.60	42.39
HS20-44 Shear4	24.57	122.59	23.50	106.32	88.76
Allowable	100	100	100	100	100

5.4 Single Span Deck System with Sheet Strong Axis Rotated Parallel to Traffic

As discussed in Chapter 4, the effect of placing the strong axis of the sheets perpendicular to the tube axes (parallel to traffic) was also investigated. This was done to determine if the orientation of the sheet, which has orthotropic properties, would have a significant effect on the performance of the deck. In the following tables and charts, the maximum stresses from the model with the sheet's strong axis aligned parallel to traffic are compared, to the case where the strong axis of the sheets are aligned perpendicular to traffic. As noted earlier, the allowable stresses are based on safety factors of 2.5 for bending and 3.0 for shear.

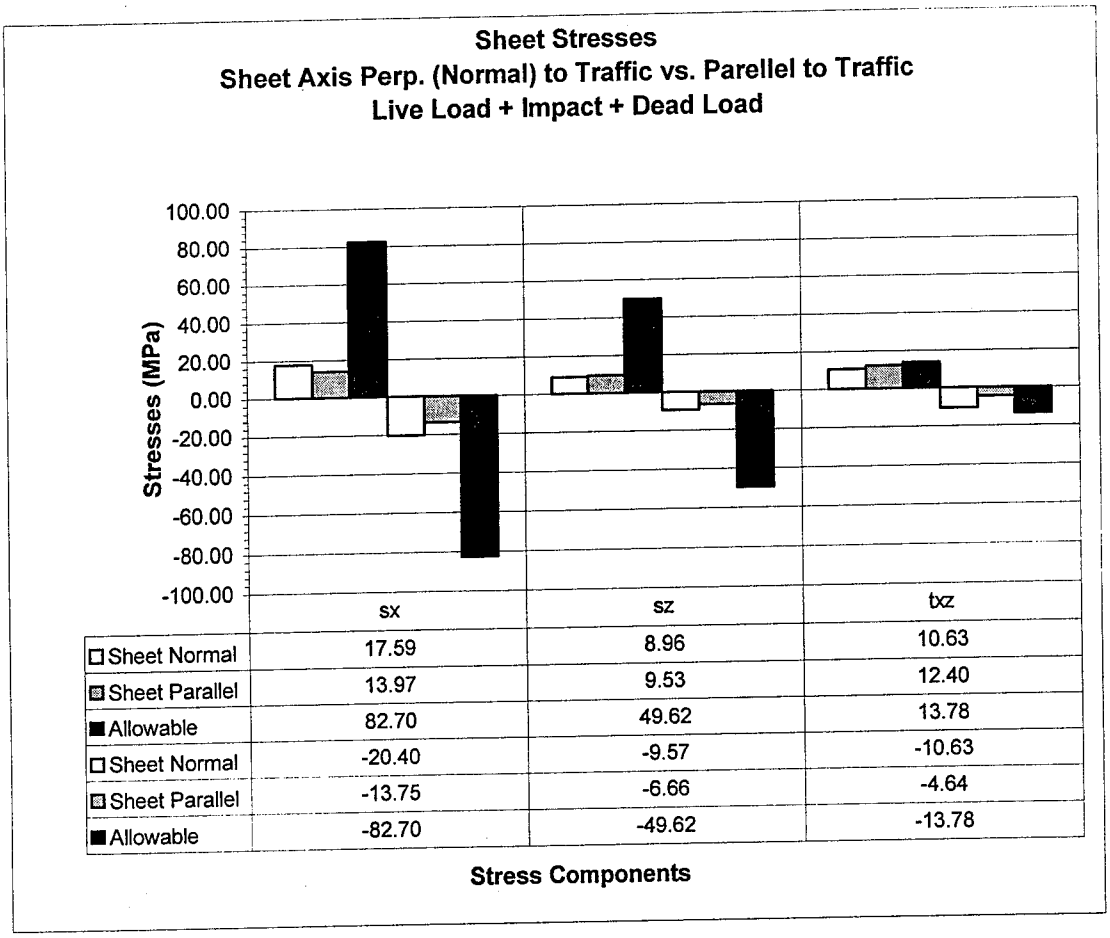

Figure 5.4.1 Comparison of Cover Sheet Orientations for SSDS (Sheet Stresses)

Table 5.4.1 Sheet Stresses from Figure 5.4.1 as a Percentage of the Allowables

	σ_x (%)	σ_z (%)	τ_{xz} (%)
Sheet Normal	21.27	18.06	77.14
Sheet Parallel	16.89	19.21	89.99
Allowable	100	100	100
Sheet Normal	24.66	19.29	77.14
Sheet Parallel	16.63	13.43	33.69
Allowable	100	100	100

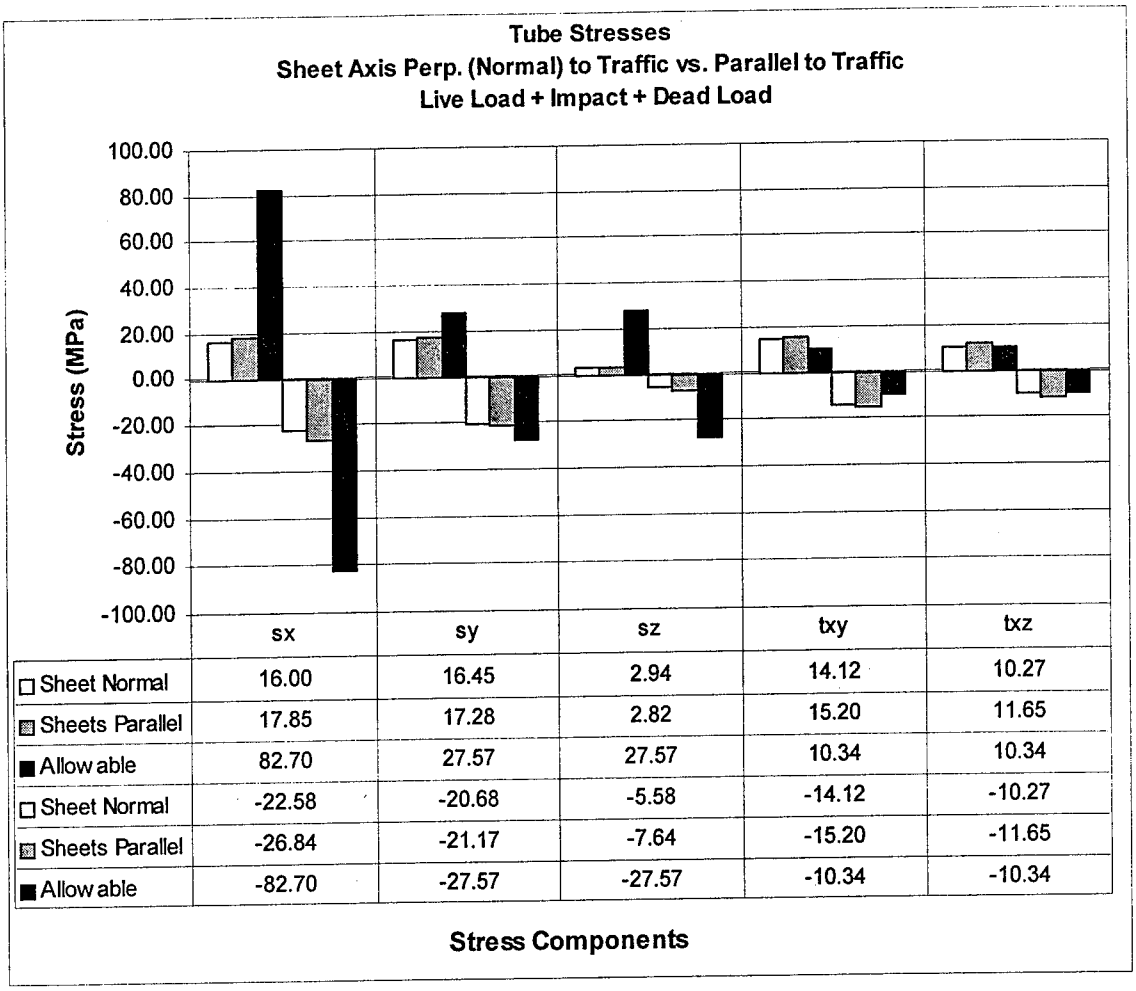

	sx	sy	sz	txy	txz
Sheet Normal	16.00	16.45	2.94	14.12	10.27
Sheets Parallel	17.85	17.28	2.82	15.20	11.65
Allowable	82.70	27.57	27.57	10.34	10.34
Sheet Normal	-22.58	-20.68	-5.58	-14.12	-10.27
Sheets Parallel	-26.84	-21.17	-7.64	-15.20	-11.65
Allowable	-82.70	-27.57	-27.57	-10.34	-10.34

Figure 5.4.2 Comparison of Cover Sheet Orientations for SSDS (Tube Stresses)

Table 5.4.2 Tube Stresses from Figure 5.4.2 as a Percentage of the Allowables

	σ_x (%)	σ_y (%)	σ_z (%)	τ_{xy} (%)	τ_{xz} (%)
Sheet Normal	19.35	59.68	10.66	136.58	99.29
Sheets Parallel	21.58	62.68	10.24	146.97	112.62
Allowable	100	100	100	100	100
Sheet Normal	27.30	75.02	20.23	136.58	99.29
Sheets Parallel	32.45	76.77	27.73	146.97	112.62
Allowable	100	100	100	100	100

5.5 Comparison of 10.2cm x 10.2cm (4"x 4") and 12.7cm x 17.8cm (5"x 7") Tube Models for SSDS

In order to investigate the use of a 12.7cm x 17.8cm (5"x 7") tube as an alternative to the 10.2cm x 10.2cm (4"x 4") tube, a single span model using 12.7cm x 17.8cm (5"x 7") tubes and 1.9cm (¾") cover sheets was developed. The model utilized the moderate boundary condition (BC2) configuration as discussed in Chapter 4.

In the following section, the 12.7cm x 17.8cm (5"x 7") model results are compared with the model with 10.2cm x 10.2cm (4"x 4") tubes and 2.5cm (1") cover sheets which used the same boundary condition configuration (BC2). Both models are loaded with the same HS20-44 wheel loading and shear loading configurations. As noted earlier, the allowable stresses are based on safety factors of 2.5 for bending and 3.0 for shear.

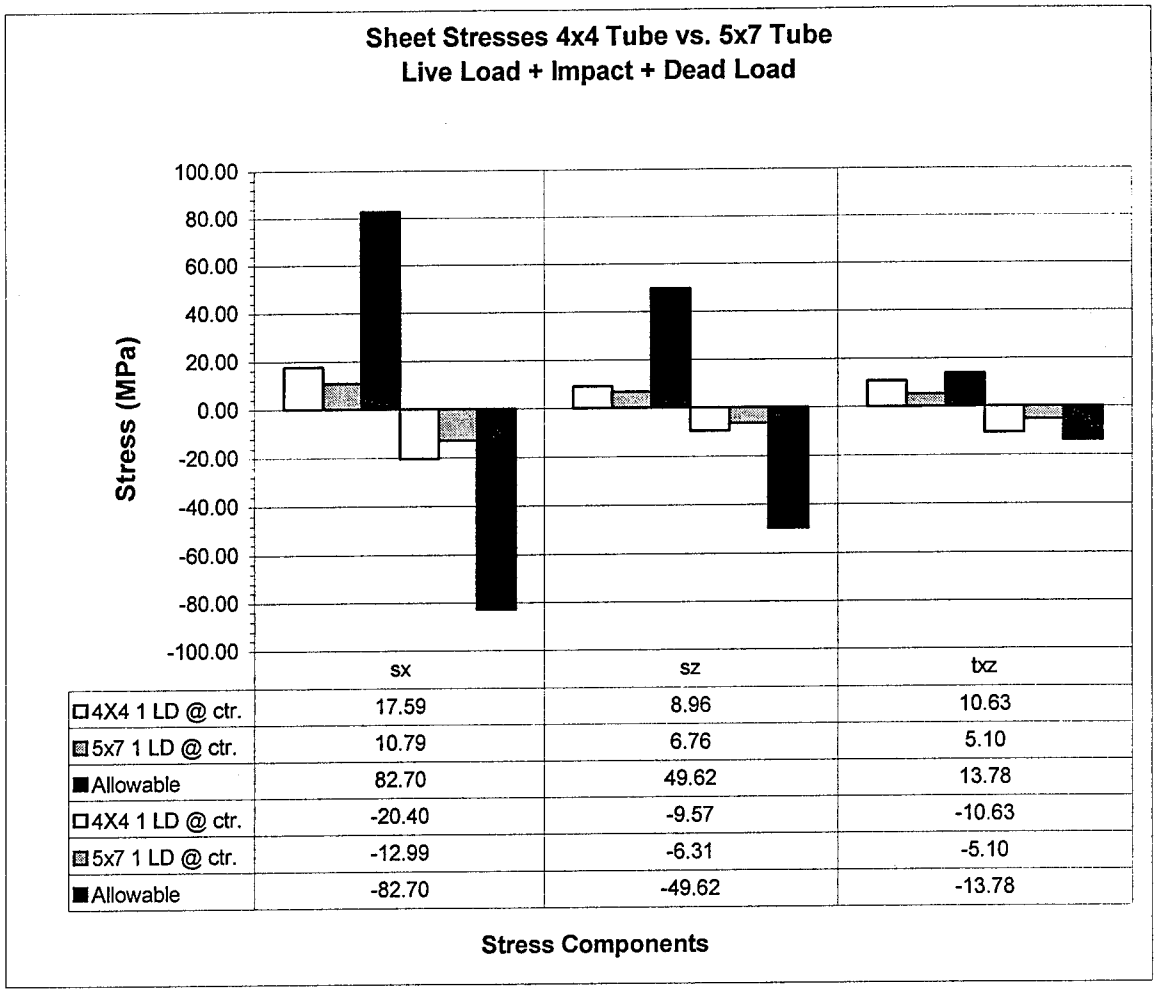

	sx	sz	txz
4X4 1 LD @ ctr.	17.59	8.96	10.63
5x7 1 LD @ ctr.	10.79	6.76	5.10
Allowable	82.70	49.62	13.78
4X4 1 LD @ ctr.	-20.40	-9.57	-10.63
5x7 1 LD @ ctr.	-12.99	-6.31	-5.10
Allowable	-82.70	-49.62	-13.78

Figure 5.5.1 Comparison of 10.2cm x 10.2cm (4"x 4") and 12.7cm x 17.8cm (5"x 7") Tube Sheet Stresses for SSDS Models (Max Moment)

Table 5.5.1 Sheet Stresses from Figure 5.1.1 as a Percentage of the Allowable

	σ_x (%)	σ_z (%)	τ_{xz} (%)
4X4 1 LD @ ctr.	21.27	18.06	77.14
5x7 1 LD @ ctr.	13.04	13.63	37.03
Allowable	100	100	100
4X4 1 LD @ ctr.	24.66	19.29	77.14
5x7 1 LD @ ctr.	15.70	12.73	37.03
Allowable	100	100	100

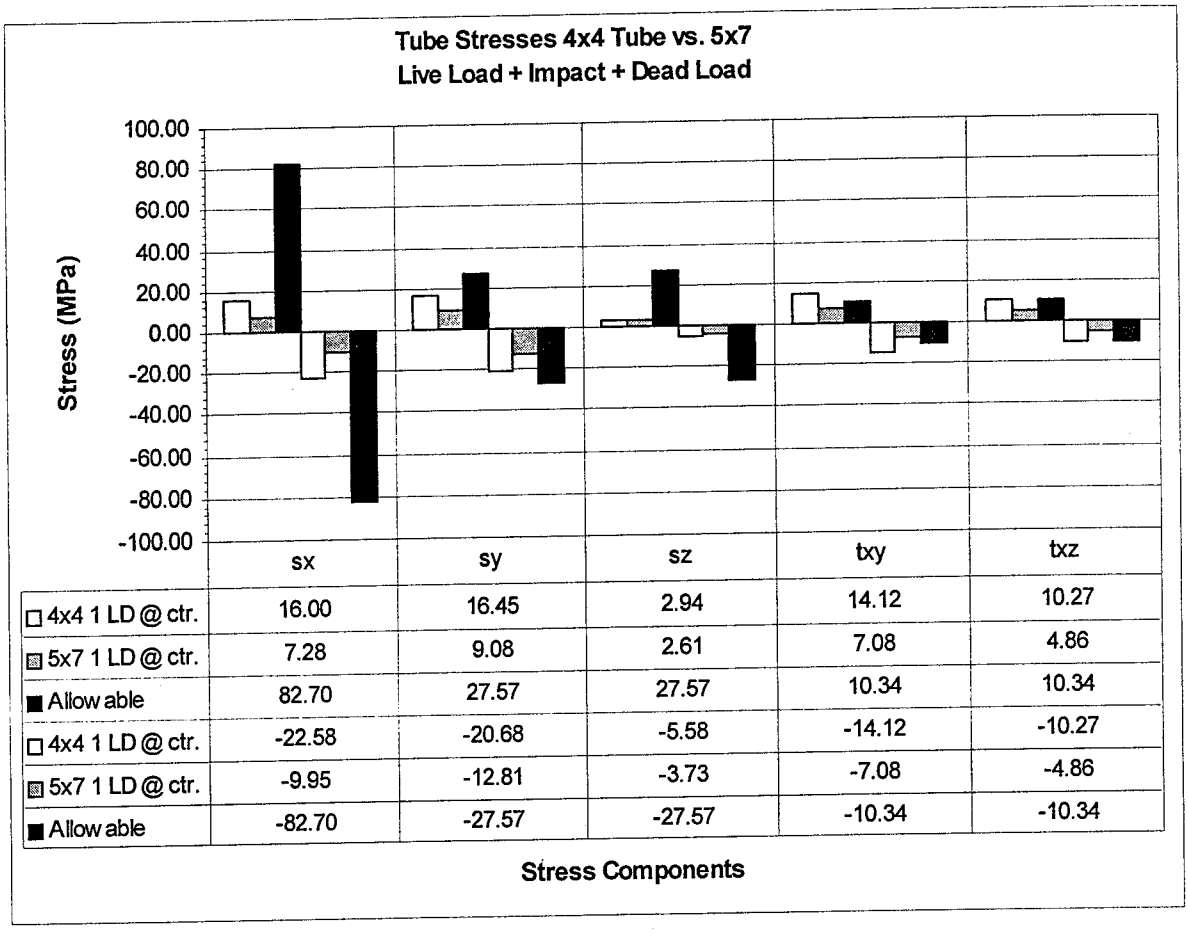

	sx	sy	sz	txy	txz
4x4 1 LD @ ctr.	16.00	16.45	2.94	14.12	10.27
5x7 1 LD @ ctr.	7.28	9.08	2.61	7.08	4.86
Allowable	82.70	27.57	27.57	10.34	10.34
4x4 1 LD @ ctr.	-22.58	-20.68	-5.58	-14.12	-10.27
5x7 1 LD @ ctr.	-9.95	-12.81	-3.73	-7.08	-4.86
Allowable	-82.70	-27.57	-27.57	-10.34	-10.34

Figure 5.5.2 Comparison of 10.2cm x 10.2cm (4"x 4") and 12.7cm x 17.8cm (5"x 7") Tube Stresses for SSDS Models (Max Moment)

Table 5.5.2 Tube Stresses from Figure 5.2.2 as a Percentage of the Allowable

	σ_x (%)	σ_y (%)	σ_z (%)	τ_{xy} (%)	τ_{xz} (%)
4x4 1 LD @ ctr.	19.35	59.68	10.66	136.58	99.29
5x7 1 LD @ ctr.	8.80	32.92	9.48	68.44	47.05
Allowabe	100	100	100	100	100
4x4 1 LD @ ctr.	27.30	75.02	20.23	136.58	99.29
5x7 1 LD @ ctr.	12.03	46.48	13.55	68.44	47.05
Allowable	100	100	100	100	100

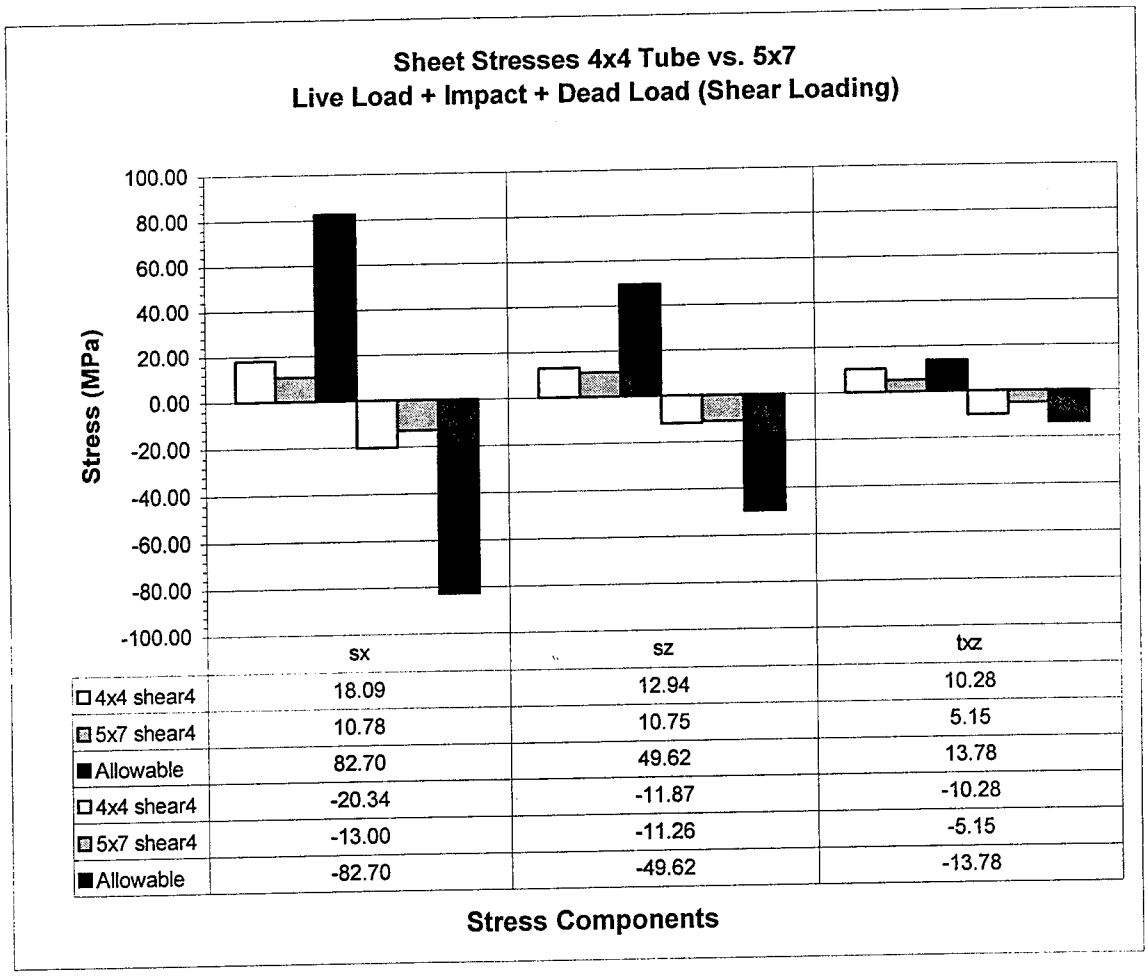

Figure 5.5.3 Comparison of 10.2cm x 10.2cm (4"x 4") and 12.7cm x 17.8cm (5"x 7") Tube Sheet Stresses for SSDS Models (Wheel Load at Support)

Table 5.5.3 Sheet Stresses from Figure 5.5.3 as a Percentage of the Allowable

	σ_x (%)	σ_z (%)	τ_{xz} (%)
4x4 shear4	21.87	26.08	74.58
5x7 shear4	13.04	21.66	37.40
Allowable	100	100	100
4x4 shear4	24.59	23.91	74.58
5x7 shear4	15.72	22.68	37.40
Allowable	100	100	100

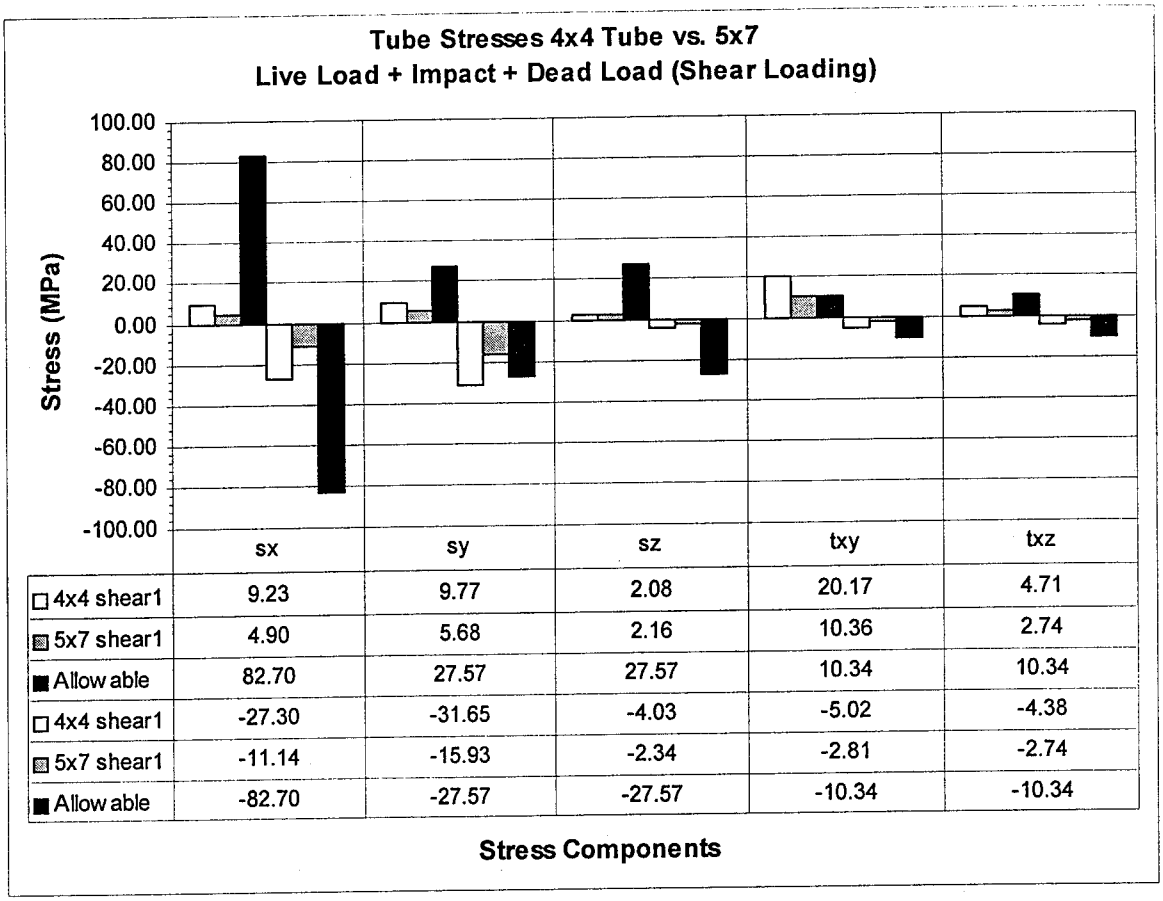

	sx	sy	sz	txy	txz
4x4 shear1	9.23	9.77	2.08	20.17	4.71
5x7 shear1	4.90	5.68	2.16	10.36	2.74
Allowable	82.70	27.57	27.57	10.34	10.34
4x4 shear1	-27.30	-31.65	-4.03	-5.02	-4.38
5x7 shear1	-11.14	-15.93	-2.34	-2.81	-2.74
Allowable	-82.70	-27.57	-27.57	-10.34	-10.34

Figure 5.5.4 Comparison of 10.2cm x 10.2cm (4"x 4") and 12.7cm x 17.8cm (5"x 7") Tube Stresses for SSDS Models (Wheel Load at Support)

Table 5.5.4 Tube Stresses from Figure 5.5.4 as a Percentage of the Allowable

	σ_x (%)	σ_y (%)	σ_z (%)	τ_{xy} (%)	τ_{xz} (%)
4x4 shear1	11.17	35.43	7.54	195.03	45.55
5x7 shear1	5.92	20.61	7.82	100.18	26.47
Allowable	100	100	100	100	100
4x4 shear1	33.01	114.79	14.60	48.60	42.39
5x7 shear1	13.47	57.78	8.48	27.17	26.47
Allowable	100	100	100	100	100

5.6 Comparison of Single Span Deck System and Multi-Span Deck System

As presented in Chapter 4, a two span model of the 10.2cm x 10.2cm (4"x 4") tube system was developed in order to investigate the effect of continuity on the deck system. In this section, the two span model is compared to the single span 10.2cm x 10.2cm (4"x 4") tube system. Both models utilize the moderate (BC2) boundary condition configuration. In addition, the models were loaded using HS20-44 wheel loads, which were located on the model to produce worst case positive moments, negative moments and shears. As noted earlier, the allowable stresses are based on safety factors of 2.5 for bending and 3.0 for shear.

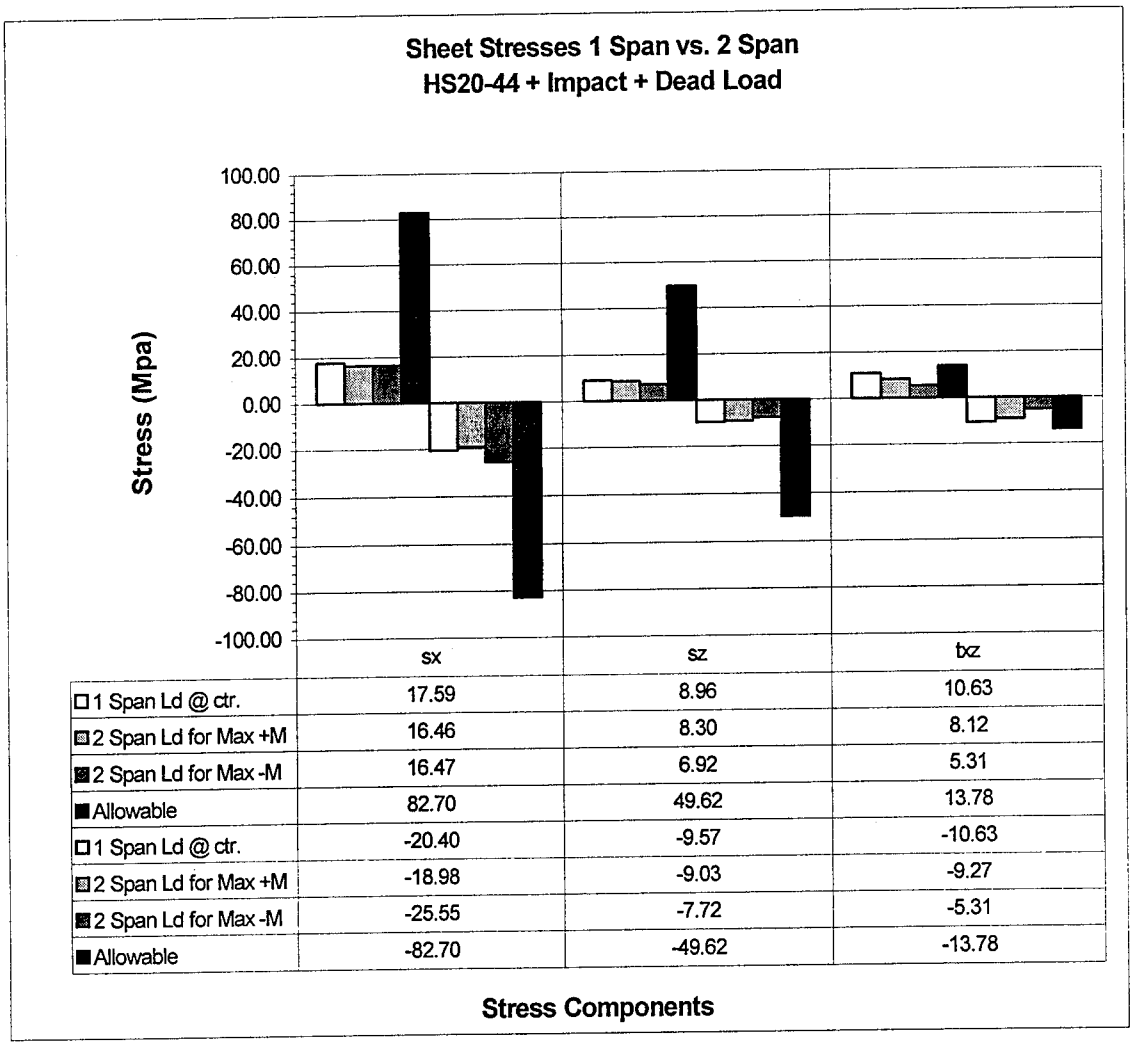

	sx	sz	txz
1 Span Ld @ ctr.	17.59	8.96	10.63
2 Span Ld for Max +M	16.46	8.30	8.12
2 Span Ld for Max -M	16.47	6.92	5.31
Allowable	82.70	49.62	13.78
1 Span Ld @ ctr.	-20.40	-9.57	-10.63
2 Span Ld for Max +M	-18.98	-9.03	-9.27
2 Span Ld for Max -M	-25.55	-7.72	-5.31
Allowable	-82.70	-49.62	-13.78

Figure 5.6.1 Comparison of SSDS and MSDS Sheet Stresses (Max Moments)

Table 5.6.1 Sheet Stresses from Figure 5.6.1 as a Percentage of the Allowable

	σ_x (%)	σ_z (%)	τ_{xz} (%)
1 Span Ld @ ctr.	21.27	18.06	77.14
2 Span Ld for Max +M	19.90	16.73	58.89
2 Span Ld for Max -M	19.91	13.94	38.54
Allowable	100	100	100
1 Span Ld @ ctr.	24.66	19.29	77.14
2 Span Ld for Max +M	22.96	18.21	67.29
2 Span Ld for Max -M	30.89	15.55	38.55
Allowable	100	100	100

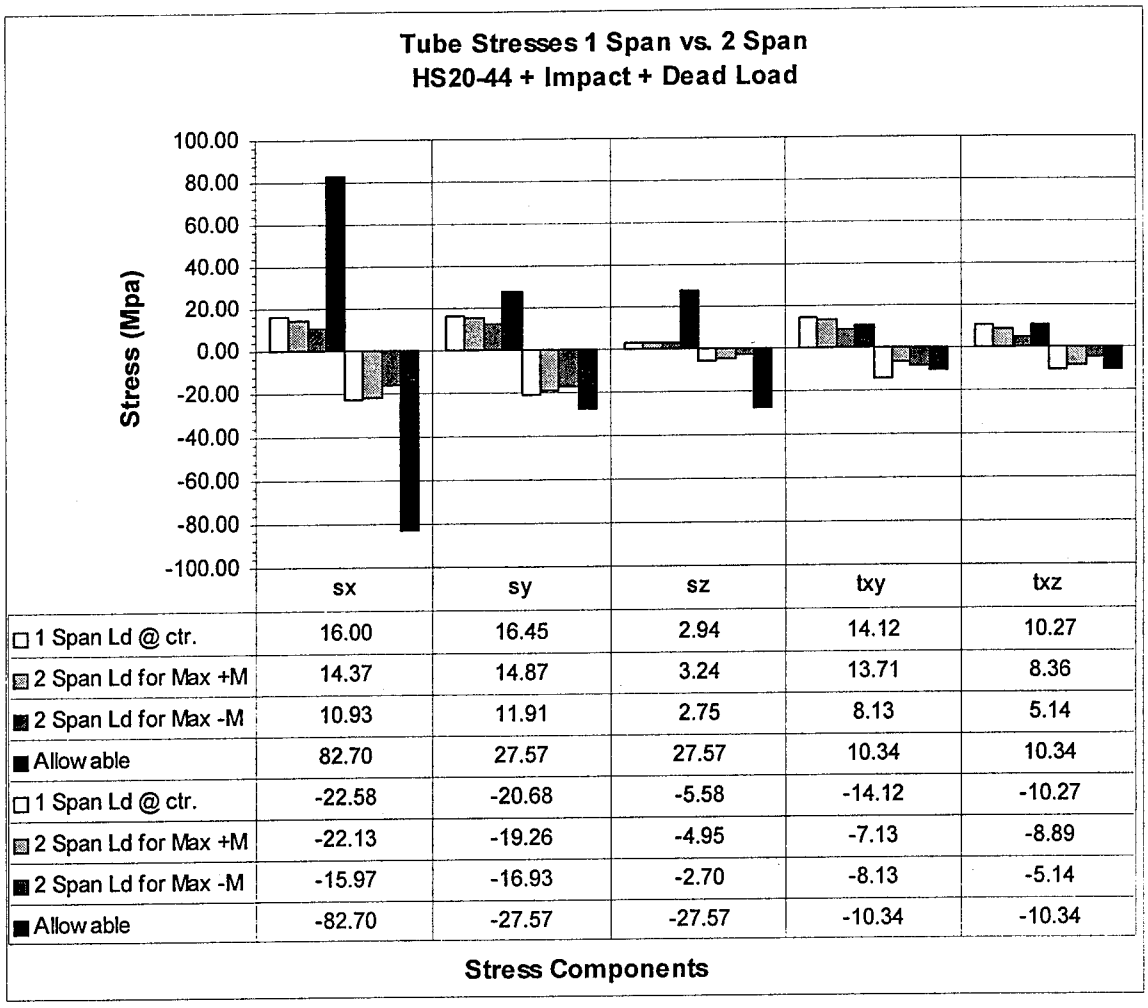

	sx	sy	sz	txy	txz
1 Span Ld @ ctr.	16.00	16.45	2.94	14.12	10.27
2 Span Ld for Max +M	14.37	14.87	3.24	13.71	8.36
2 Span Ld for Max -M	10.93	11.91	2.75	8.13	5.14
Allowable	82.70	27.57	27.57	10.34	10.34
1 Span Ld @ ctr.	-22.58	-20.68	-5.58	-14.12	-10.27
2 Span Ld for Max +M	-22.13	-19.26	-4.95	-7.13	-8.89
2 Span Ld for Max -M	-15.97	-16.93	-2.70	-8.13	-5.14
Allowable	-82.70	-27.57	-27.57	-10.34	-10.34

Figure 5.6.2 Comparison of SSDS and MSDS Tube Stresses (Max Moments)

Table 5.6.2 Tube Stresses from Figure 5.6.2 as a Percentage of the Allowable

	σ_x (%)	σ_y (%)	σ_z (%)	τ_{xy} (%)	τ_{xz} (%)
1 Span Ld @ ctr.	19.35	59.68	10.66	136.58	99.29
2 Span Ld for Max +M	17.38	53.93	11.73	132.57	80.87
2 Span Ld for Max -M	13.22	43.18	9.99	78.58	49.68
Allowable	100	100	100	100	100
1 Span Ld @ ctr.	27.30	75.02	20.23	136.58	99.29
2 Span Ld for Max +M	26.76	69.87	17.94	68.98	85.93
2 Span Ld for Max -M	19.32	61.40	9.80	78.58	49.68
Allowable	100	100	100	100	100

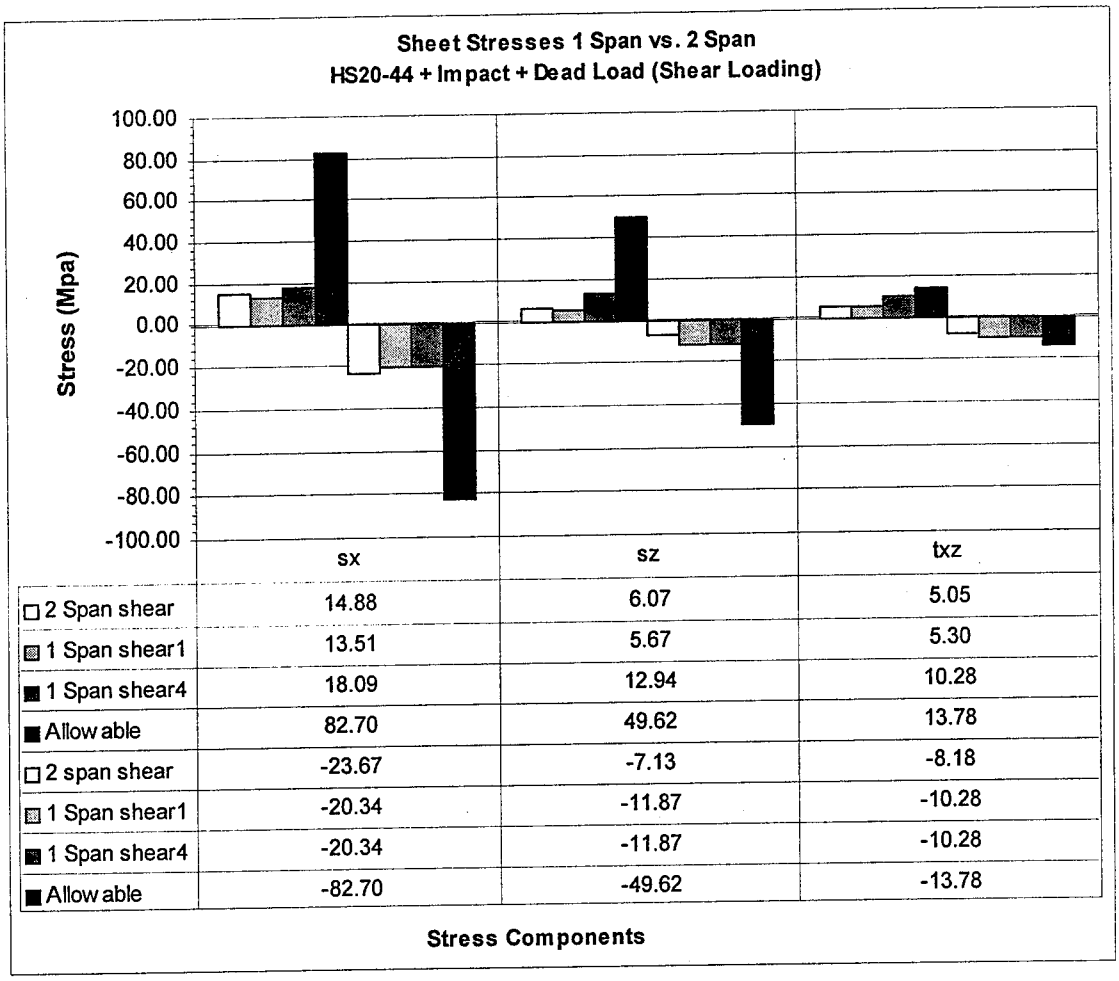

	sx	sz	txz
2 Span shear	14.88	6.07	5.05
1 Span shear1	13.51	5.67	5.30
1 Span shear4	18.09	12.94	10.28
Allowable	82.70	49.62	13.78
2 span shear	-23.67	-7.13	-8.18
1 Span shear1	-20.34	-11.87	-10.28
1 Span shear4	-20.34	-11.87	-10.28
Allowable	-82.70	-49.62	-13.78

Figure 5.6.3 Comparison of SSDS and MSDS Sheet Stresses (Shear Loading)

Table 5.6.3 Sheet Stresses from Figure 5.6.3 as a Percentage of the Allowable

	σ_x (%)	σ_z (%)	τ_{xz} (%)
2 Span shear	18.00	12.23	36.61
1 Span shear1	16.34	11.42	38.46
1 Span shear4	21.87	26.08	74.58
Allowable	100	100	100
2 span shear	28.62	14.36	59.39
1 Span shear1	24.59	23.91	74.58
1 Span shear4	24.59	23.91	74.58
Allowable	100	100	100

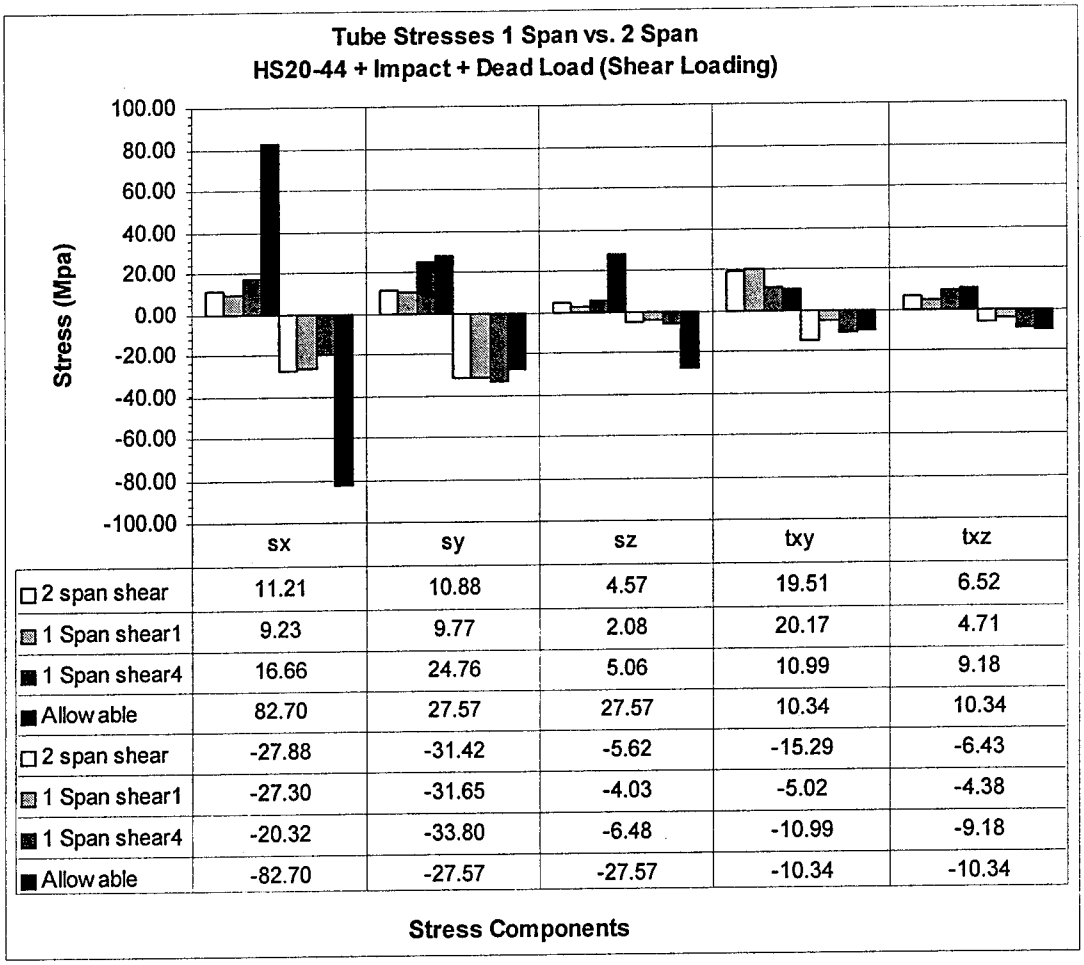

	sx	sy	sz	txy	txz
2 span shear	11.21	10.88	4.57	19.51	6.52
1 Span shear1	9.23	9.77	2.08	20.17	4.71
1 Span shear4	16.66	24.76	5.06	10.99	9.18
Allowable	82.70	27.57	27.57	10.34	10.34
2 span shear	-27.88	-31.42	-5.62	-15.29	-6.43
1 Span shear1	-27.30	-31.65	-4.03	-5.02	-4.38
1 Span shear4	-20.32	-33.80	-6.48	-10.99	-9.18
Allowable	-82.70	-27.57	-27.57	-10.34	-10.34

Figure 5.6.4 Comparison of SSDS and MSDS Tube Stresses (Shear Loading)

Table 5.6.4 Tube Stresses from Figure 5.6.4 as a Percentage of the Allowable

	σ_x (%)	σ_y (%)	σ_z (%)	τ_{xy} (%)	τ_{xz} (%)
2 Span shear	13.55	39.46	16.56	188.69	63.02
1 Span shear1	11.17	35.43	7.54	195.03	45.55
1 Span shear4	20.14	89.82	18.36	106.32	88.76
Allowable	100	100	100	100	100
2 Span shear	33.71	113.96	20.39	147.83	62.23
1 Span shear1	33.01	114.80	14.60	48.60	42.39
1 Span shear4	24.57	122.6	23.50	106.32	88.76
Allowable	100	100	100	100	100

5.7 Comparison of Single Span, Free Edge and 1½ Span (Cantilever) Models

To investigate the possibility of a panel system joint becoming discontinuous, two additional models were investigated. As discussed in Chapter 4, the free edge model consists of the 10.2cm x 10.2cm (4"x 4") tube system supported on only three sides. An HS20-44 wheel load was placed over the free edge. The second model, which consisted of the same tube system as the free edge model, was continuous over 1½ spans. This configuration results in a cantilevered edge midway between two spans. The 1½ span system was loaded in the same manner as the free edge model. In the following section, both systems are compared to the single span 10.2cm x 10.2cm 4"x 4" tube deck system. All three systems utilized the moderate boundary condition configuration (BC2). As noted earlier, the allowable stresses are based on safety factors of 2.5 for bending and 3.0 for shear.

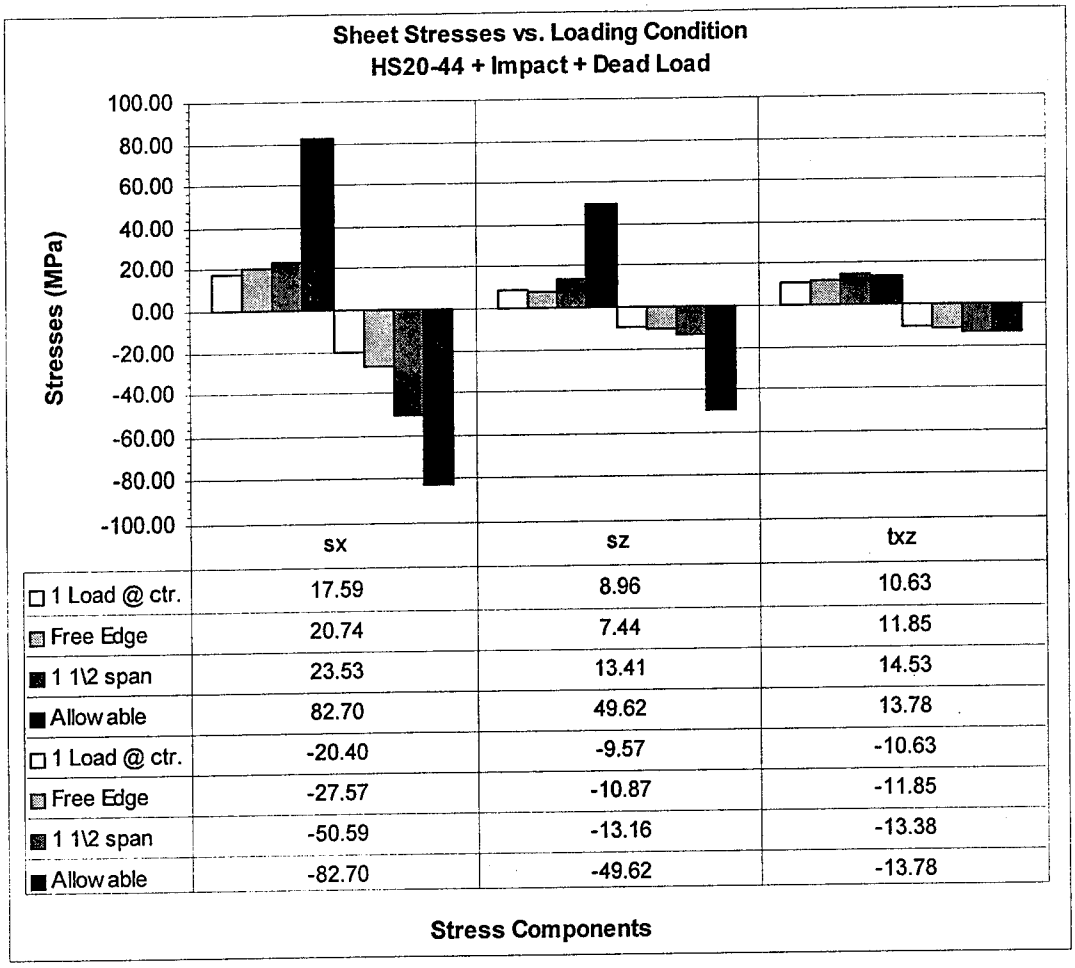

	sx	sz	txz
1 Load @ ctr.	17.59	8.96	10.63
Free Edge	20.74	7.44	11.85
1 1\2 span	23.53	13.41	14.53
Allowable	82.70	49.62	13.78
1 Load @ ctr.	-20.40	-9.57	-10.63
Free Edge	-27.57	-10.87	-11.85
1 1\2 span	-50.59	-13.16	-13.38
Allowable	-82.70	-49.62	-13.78

Figure 5.7.1 Comparison of Sheet Stresses for Single Span, Free Edge and 1½ Span (Cantilever) Models

Table 5.7.1 Sheet Stresses from Figure 5.7.1 as a Percentage of the Allowable

	σ_x (%)	σ_z (%)	τ_{xz} (%)
1 Load @ ctr.	21.27	18.06	77.14
Free Edge	25.08	14.99	85.99
1 1\2 span	28.45	27.03	105.46
Allowable	100	100	100
1 Load @ ctr.	24.66	19.29	77.14
Free Edge	33.34	21.90	85.99
1 1\2 span	61.17	26.53	97.09
Allowable	100	100	100

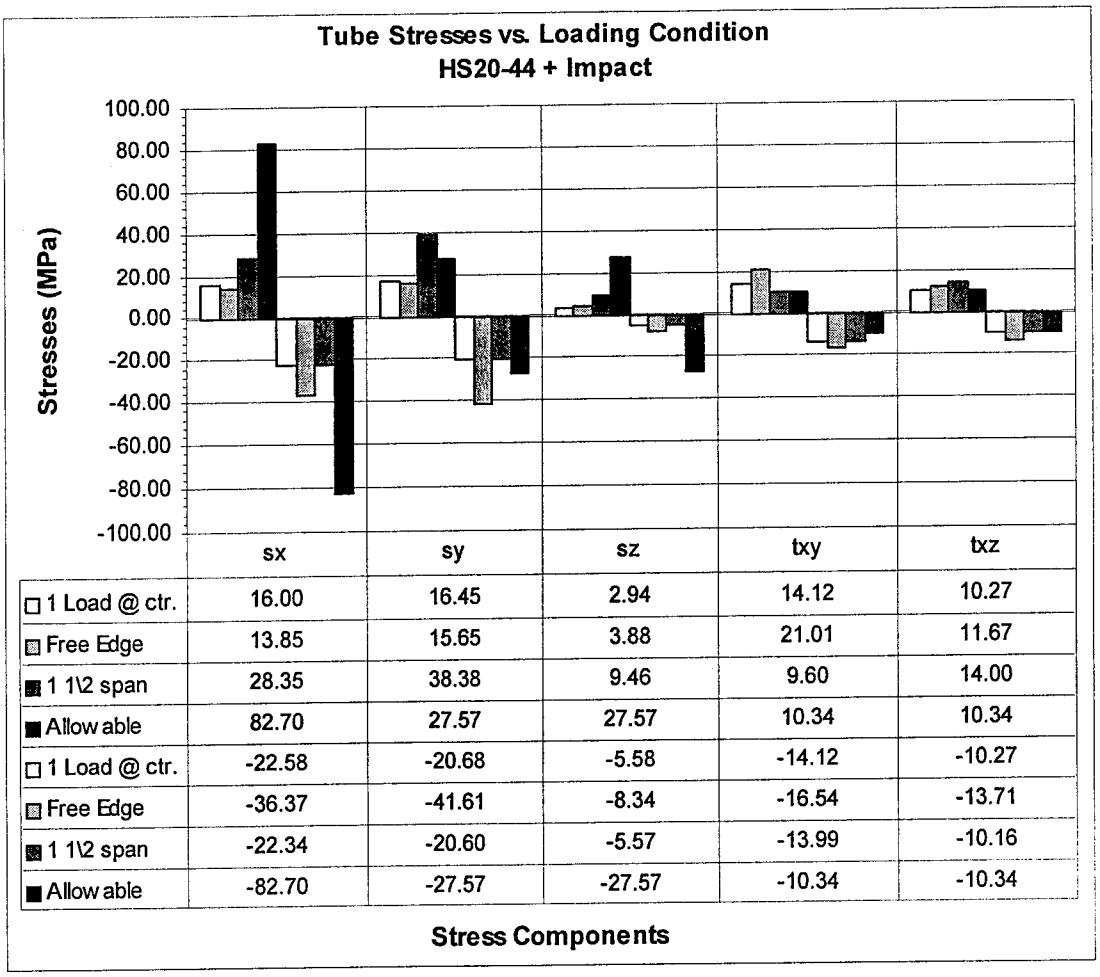

	sx	sy	sz	txy	txz
1 Load @ ctr.	16.00	16.45	2.94	14.12	10.27
Free Edge	13.85	15.65	3.88	21.01	11.67
1 1\2 span	28.35	38.38	9.46	9.60	14.00
Allowable	82.70	27.57	27.57	10.34	10.34
1 Load @ ctr.	-22.58	-20.68	-5.58	-14.12	-10.27
Free Edge	-36.37	-41.61	-8.34	-16.54	-13.71
1 1\2 span	-22.34	-20.60	-5.57	-13.99	-10.16
Allowable	-82.70	-27.57	-27.57	-10.34	-10.34

Figure 5.7.2 Comparison of Tube Stresses for Single Span, Free Edge and 1½ Span (Cantilever) Models

Table 5.7.2 Tube Stresses from Figure 5.7.2 as a Percentage of the Allowable

	σ_x (%)	σ_y (%)	σ_z (%)	τ_{xy} (%)	τ_{xz} (%)
1 Load @ ctr.	19.35	59.68	10.66	136.58	99.29
Free Edge	16.75	56.75	14.06	203.19	112.91
1 1\2 span	34.27	139.21	34.33	92.80	135.40
Allowable	100	100	100	100	100
1 Load @ ctr.	27.30	75.02	20.23	136.58	99.29
Free Edge	43.98	150.92	30.25	159.93	132.57
1 1\2 span	27.02	74.72	20.22	135.26	98.23
Allowable	100	100	100	100	100

5.8 Deck System Vertical Deflections

The following charts and tables illustrate the various deck system deflections under live load, impact and dead weight loadings. For each model, nodal deflections were recorded from the model edge (boundary), to the center of the deck panel at the location of load application. Deflections were also taken from the dead load model (gravity + wear surface) at the corresponding nodes. Live load deflections were then added to the dead load deflections. To evaluate the deflection performance of the various models, the corresponding values of L/Δ are provided to the right of the tables.

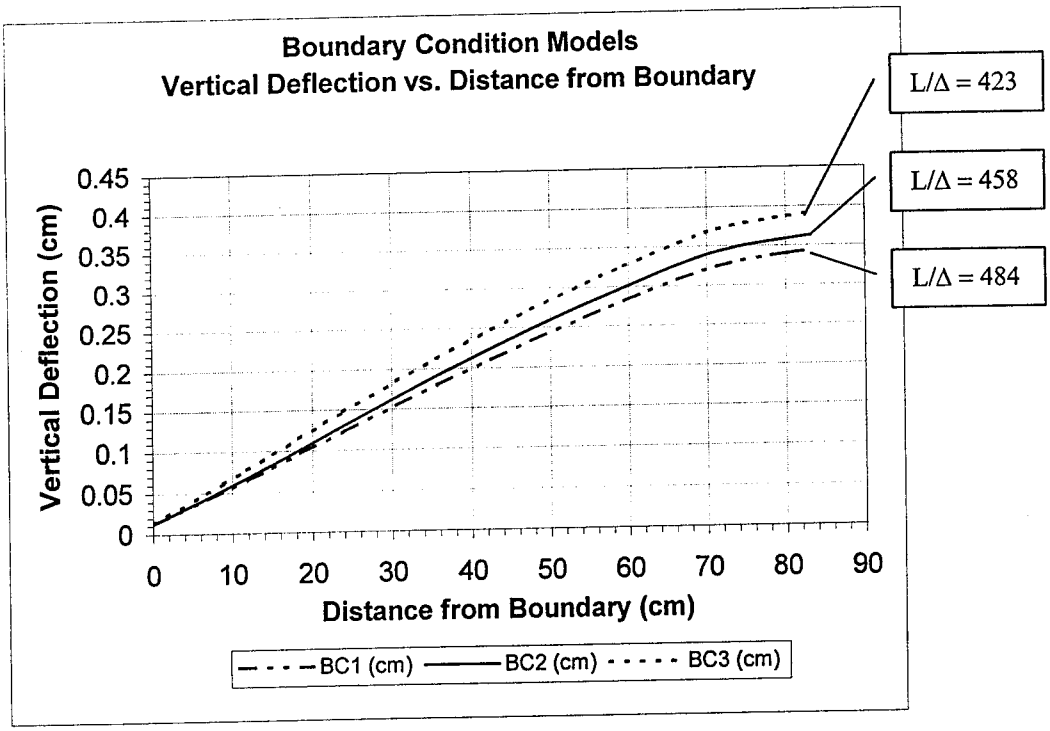

Figure 5.8.1 Deflections vs. Distance from Edge for BC Models

Table 5.8.1 Values of Deflections vs. Distance from Edge for BC Models

X (cm)	BC1 (cm)	BC2 (cm)	BC3 (cm)
0.000	0.013	0.013	0.014
11.884	0.065	0.067	0.078
23.767	0.122	0.129	0.147
35.651	0.179	0.191	0.213
47.535	0.233	0.248	0.274
59.418	0.282	0.299	0.327
71.302	0.325	0.343	0.372
83.186	0.344	0.363	0.393
Max L/Δ	484	458	423
Ortho. [27] L/Δ	500	500	500
AASHTO L/Δ	800	800	800

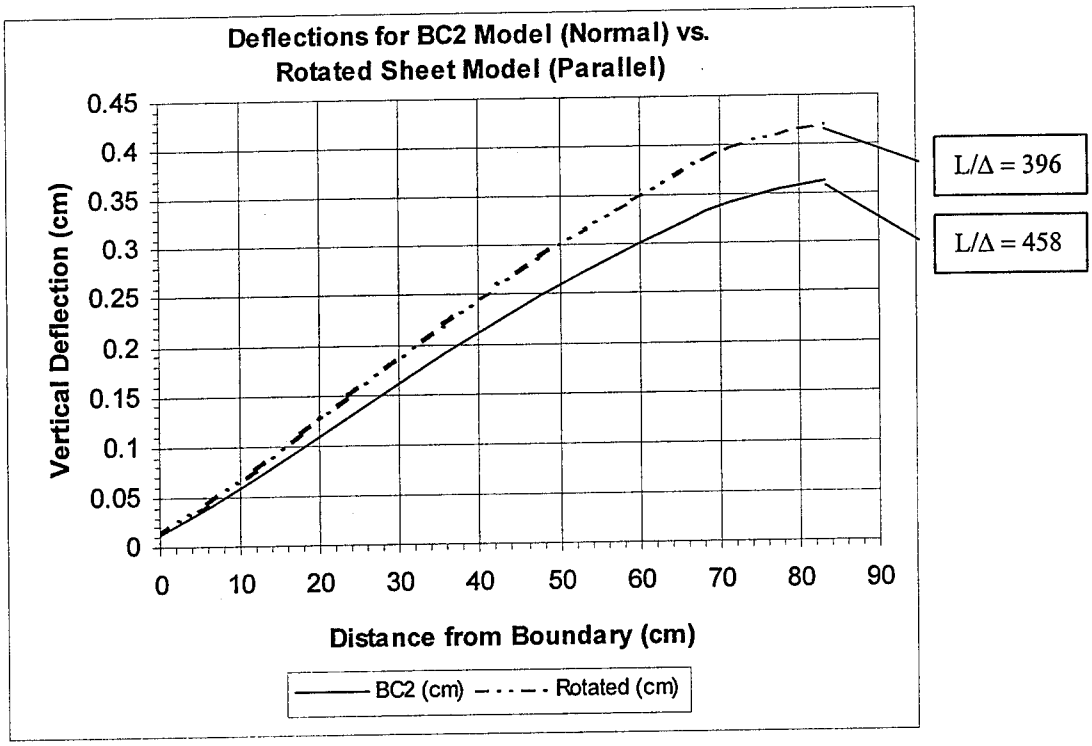

Figure 5.8.2 Model Deflections vs. Distance from Edge for Different Sheet Orientations

Table 5.8.2 Model Deflections vs. Distance from Edge for Different Sheet Orientations

X (cm)	Normal (cm)	Parallel (cm)
0.000	0.013	0.012
11.884	0.067	0.076
23.767	0.129	0.149
35.651	0.191	0.221
47.535	0.248	0.288
59.418	0.299	0.347
71.302	0.343	0.397
83.186	0.363	0.420
Max L/Δ	458	396
Ortho. [27] L/Δ	500	500
AASHTO L/Δ	800	800

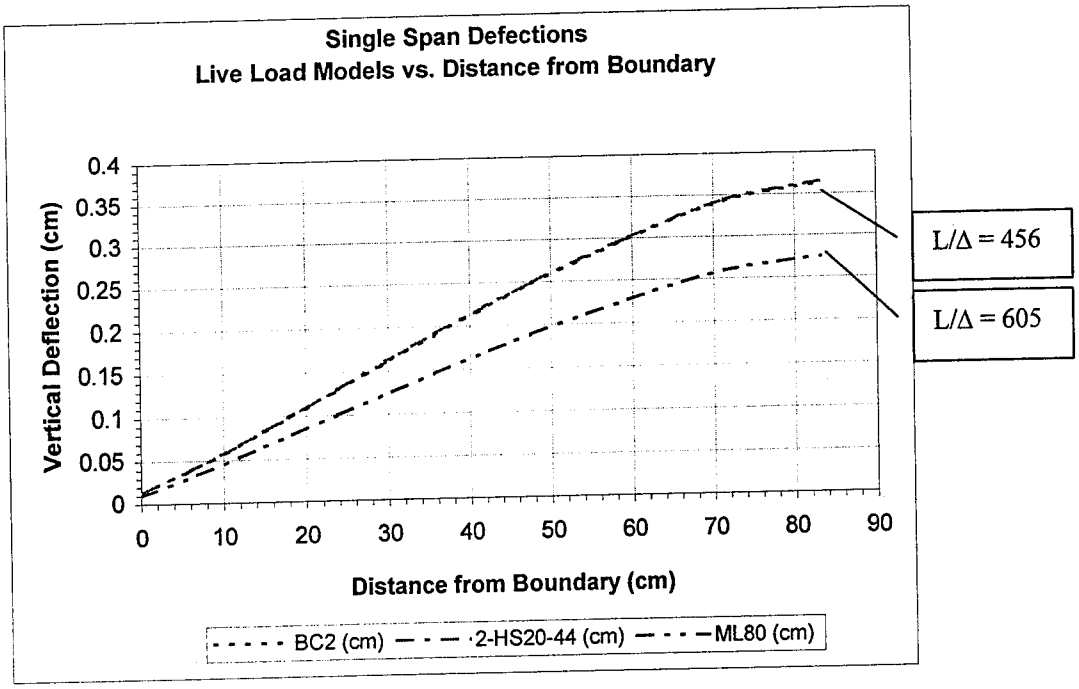

Figure 5.8.3 Live Load Model Deflections vs. Distance from Model Edge

Table 5.8.3 Live Load Model Deflections vs. Distance from Model Edge

X (cm)	BC2 (cm)	2-HS20-44 (cm)	ML80 (cm)
0.000	0.013	0.013	0.010
11.884	0.067	0.068	0.053
23.767	0.129	0.130	0.100
35.651	0.191	0.192	0.146
47.535	0.248	0.249	0.189
59.418	0.299	0.301	0.227
71.302	0.343	0.345	0.260
83.186	0.363	0.365	0.275
Max L/Δ	458	456	605
Ortho. [27] L/Δ	500	500	500
AASHTO L/Δ	800	800	800

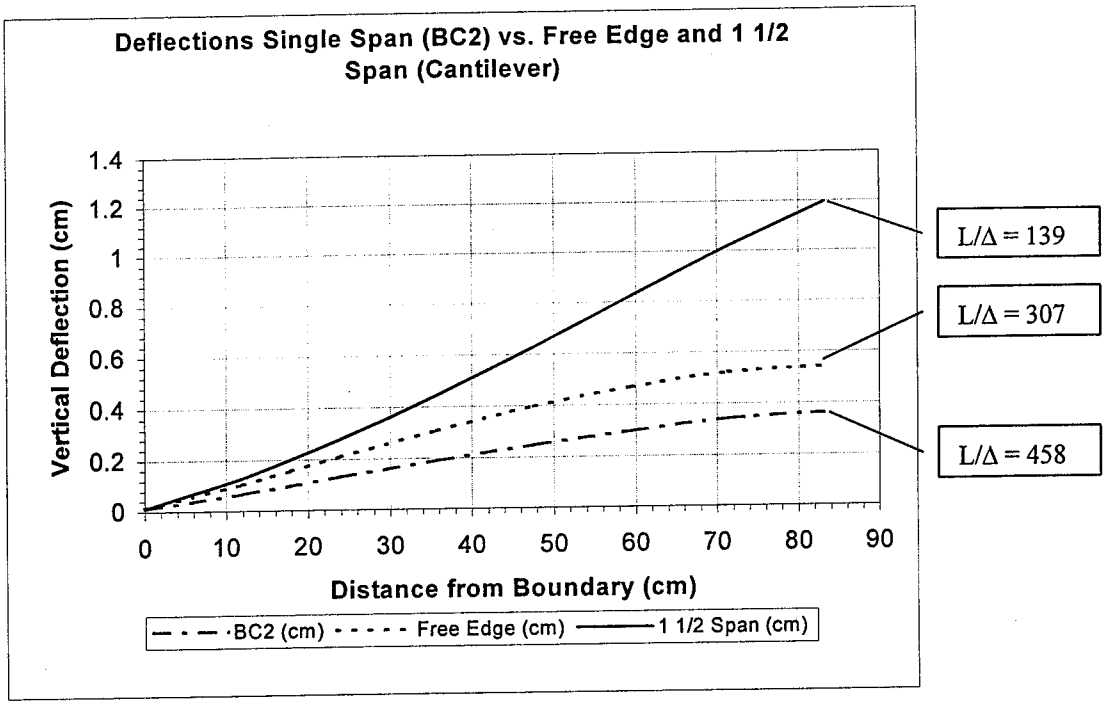

Figure 5.8.4 SSDS Deflections vs. Joint Discontinuity Deflections

Table 5.8.4 SSDS Deflections vs. Joint Discontinuity Deflections

X (cm)	BC2 (cm)	Free Edge (cm)	1 1/2 Span (cm)
0.000	0.013	0.013	0.013
11.884	0.067	0.106	0.128
23.767	0.129	0.209	0.276
35.651	0.191	0.310	0.444
47.535	0.248	0.398	0.628
59.418	0.299	0.470	0.825
71.302	0.343	0.521	1.018
83.186	0.363	0.542	1.196
Max L/Δ	458	307	139
Ortho. [27] L/Δ	500	500	500
AASHTO L/Δ	800	800	800

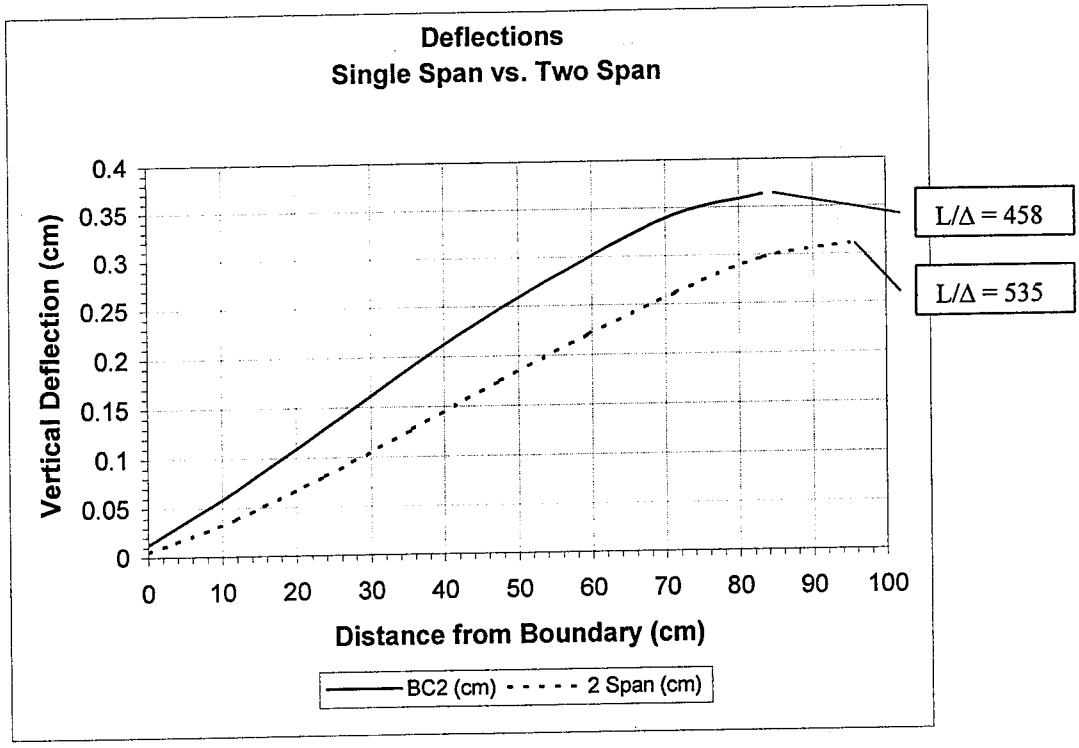

Figure 5.8.5 Single Span Model Deflections vs. 2 Span Model Deflections

Table 5.8.5 Single Span Model Deflections vs. 2 Span Model Deflections

X (cm)	BC2 (cm)	2 Span (cm)
0.000	0.013	0.006
11.884	0.067	0.039
23.767	0.129	0.081
35.651	0.191	0.128
47.535	0.248	0.175
59.418	0.299	0.221
71.302	0.343	0.262
83.186	0.363	0.297
95.072	-	0.311
Max L/Δ	458	535
Ortho. [27] L/Δ	500	500
AASHTO L/Δ	800	800

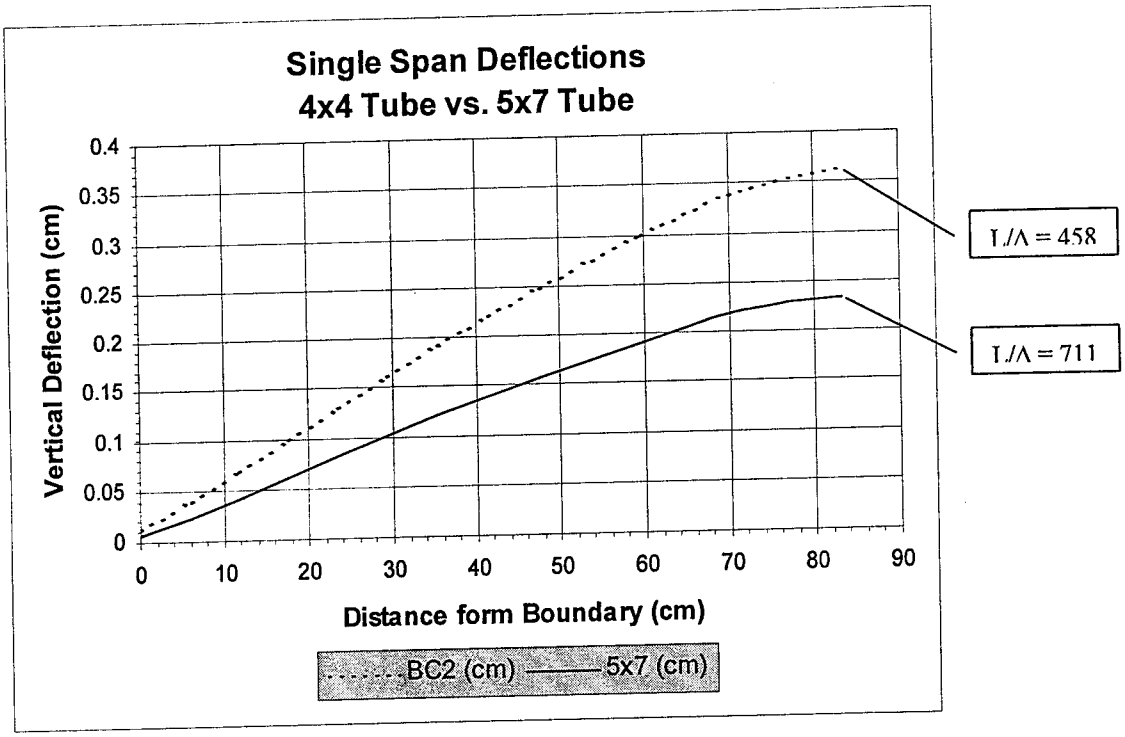

Figure 5.8.6 SSDS 4x4 vs. 5x7 Tube Model Deflections

Table 5.8.6 SSDS 4x4 vs. 5x7 Tube Model Deflections

X (cm)	BC2 (cm)	5x7 (cm)
0	0.012936	0.006292
11.88364	0.067467	0.042024
23.76729	0.129286	0.081445
35.65093	0.190729	0.120701
47.53458	0.248133	0.157483
59.41822	0.299263	0.190241
71.30186	0.343154	0.219659
83.18551	0.363372	0.233975
Max L/Δ	458	711
Ortho. [27] L/Δ	500	500
AASHTO L/Δ	800	800

5.9 Comparison of Computer Model Results vs. Hand Calculation Results

Table 5.9 provides a comparison of the hand calculation results and the computer analysis results. For comparison purposes, the stresses from the BC2 and Shear1 models were used in the table. Bending stresses are for the load applied at the center of the span. Shear stresses are for the load applied over the support. It should be noted that hand calculation shear stresses are averaged over the depth of the web, whereas the shear stresses from the computer model are concentrated at the model boundary node and include the effect of the horizontal restraints.

In addition, the modulus of elasticity of the tubes used for the hand calculations was 19.3 Gpa (2.8E6 Psi). This value was derived from full section bending tests of the tubes [4]. The modulus of elasticity applied to each individual tube element in the computer model was 11 Gpa (1.6E6 Psi). This value was derived from coupon testing of the tube material [4]. It should also be noted that the values in Table 5.9 do not include dead load.

Table 5.9 Computer Model Results vs. Hand Calculation Results

	σ_x KPa (Psi)	τ_y KPa (Psi)	Δ mm (in)
BC2 Model (4x4 tube)	19.97 (2905)	19.76 (2875)	3.6 (0.140)
Hand Calculations	17.98 (2615)	9.41 (1368)	4.7 (0.185)
% Difference	10.5	71.0	27.7

CHAPTER 6

EVALUATION OF RESULTS

6.1 Introduction

As discussed in the previous two chapters, various finite element models and loading conditions were considered in this study. The stress and deflection results from various models and parametric studies were presented in Chapter 5 in the form of charts and tables. The charts and tables presented in Chapter 5 were set up to allow for comparison of relevant parametric results. This chapter examines the parametric results and provides a more detailed interpretation of the results.

In addition, as discussed in Chapter 3, several load combinations were investigated to account for the effect of wind, and to investigate the effect of loading on the deck when the bridge is elevated to an open position. The results of the wind and dead load combinations are also presented in this chapter.

Finally, several stress contour plots are provided to demonstrate typical stress distributions from the analysis. To avoid overwhelming the report with stress contour

plots, only a few plots of some typical stress distributions are provided. The plots are intended to illustrate the character of the stresses, as opposed to providing the magnitudes of stresses for all the parameters investigated. The stress plots provided were taken from the moderate boundary condition case (BC2 model) and are based on an HS20-44 wheel load located at the center of the deck. To simplify the evaluation, the effect of dead load, which only accounts for a small percentage of the final stress, was excluded from the plots.

6.2 Stress Results

To investigate the effects of varying the number of deck to stringer attachment points, three different boundary condition models were analyzed. The stress results for the three models, which were previously described in Chapter 4, are presented in Figures 5.2.1 (sheet stresses) and 5.2.2 (tube stresses). As shown in the figures, the σ_x and σ_z stresses are well below the allowables. Also, in Figures 5.2.1 and 5.2.2, the bar charts of the σ_x and σ_z stresses show little change in magnitude. This indicates that the σ_x and σ_z stresses were not significantly influenced by the location of the pinned (Δ_x, Δ_y and Δ_z restrained) boundary constraints. The stress contour plots in Figures 6.1 and 6.2 on the following pages show stress distributions that were typical for the σ_x and σ_z stresses in both the sheets and tubes. The stress levels in the contour plots are indicated by color code, which are given in MPa at the lower left edge of the figures. A mentioned in the previous

chapter, the stress allowables are based on a factor of safety of 2.5 for bending and 3.0 for shear, as recommended by the manufacturer of the tubes and sheets [4].

For the boundary condition models, the σ_y stresses, which were less than the allowable, occurred in the top and bottom of the webs of the tubes located adjacent to the load location. From Table 5.2.2, the maximum σ_y stress occurred in the BC3 model (pinned at the 4 corners) and was 78.6% of the allowable. After examination of the σ_y stresses in the tube webs, it was determined that the σ_y stresses are transverse bending stresses. This was concluded since the stresses, which are highest at the top and bottom of the webs, are in tension on one side of the webs and in compression on the other side. Relative deflections between the top and bottom of the webs indicate that the bending in the webs is the result of relative motion between the top and bottom sheets. A color contour plot of the σ_y stresses is shown in Figure 6.3.

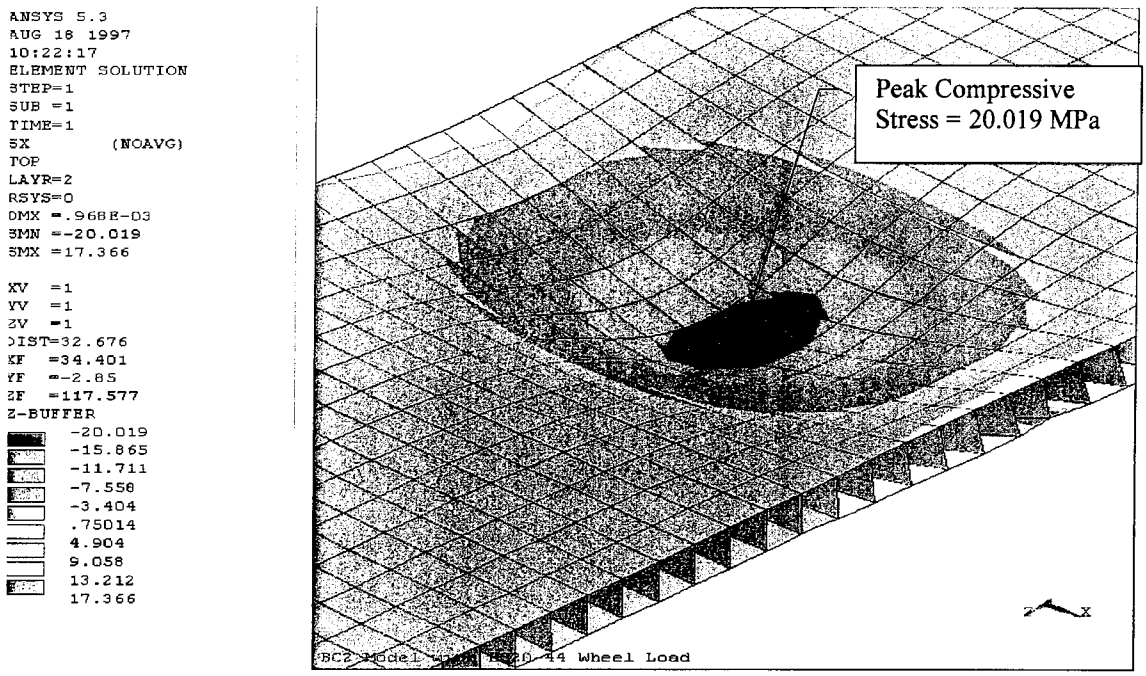

Figure 6.1 Typical Distribution of σ_x and σ_z Stresses in the Upper Deck Sheets

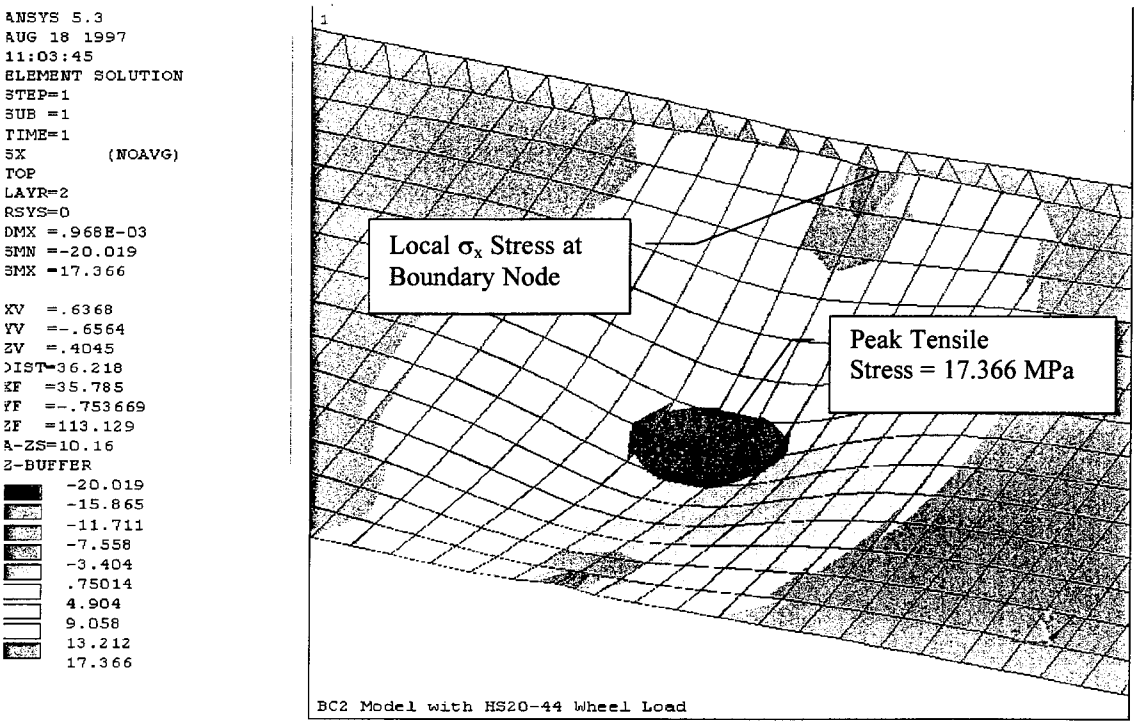

Figure 6.2 Typical Distribution of σ_x and σ_z Stresses in the Lower Deck Sheets

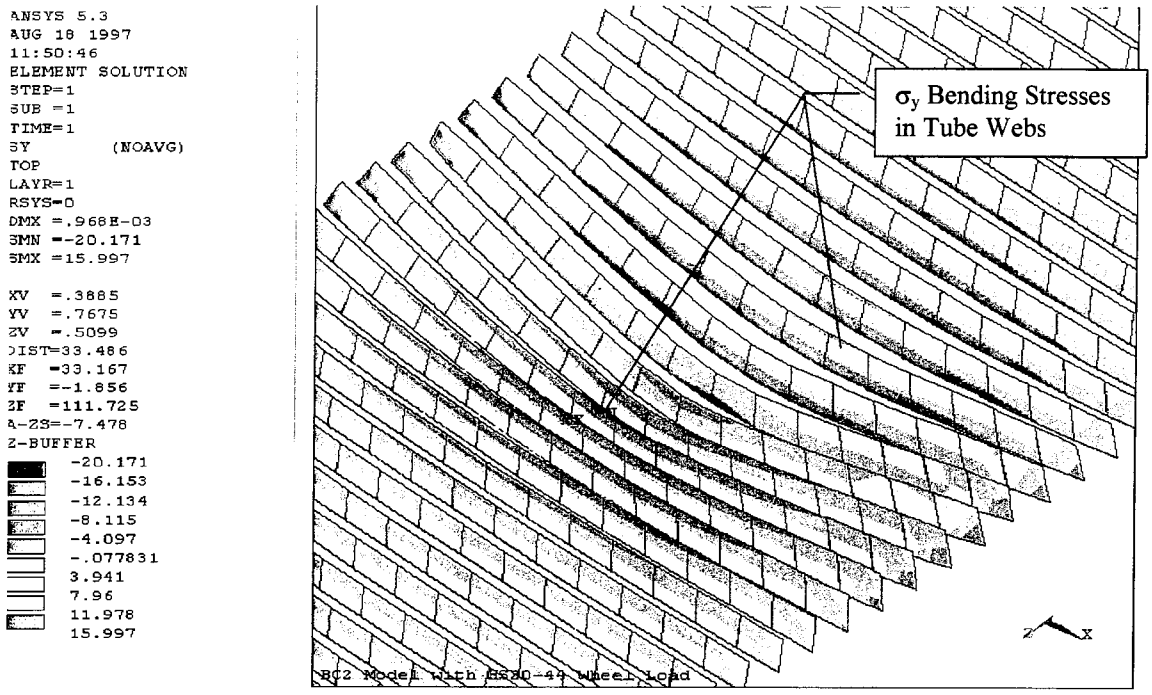

Figure 6.3 Typical Distribution of σ_y Stresses in the Webs of the Tubes

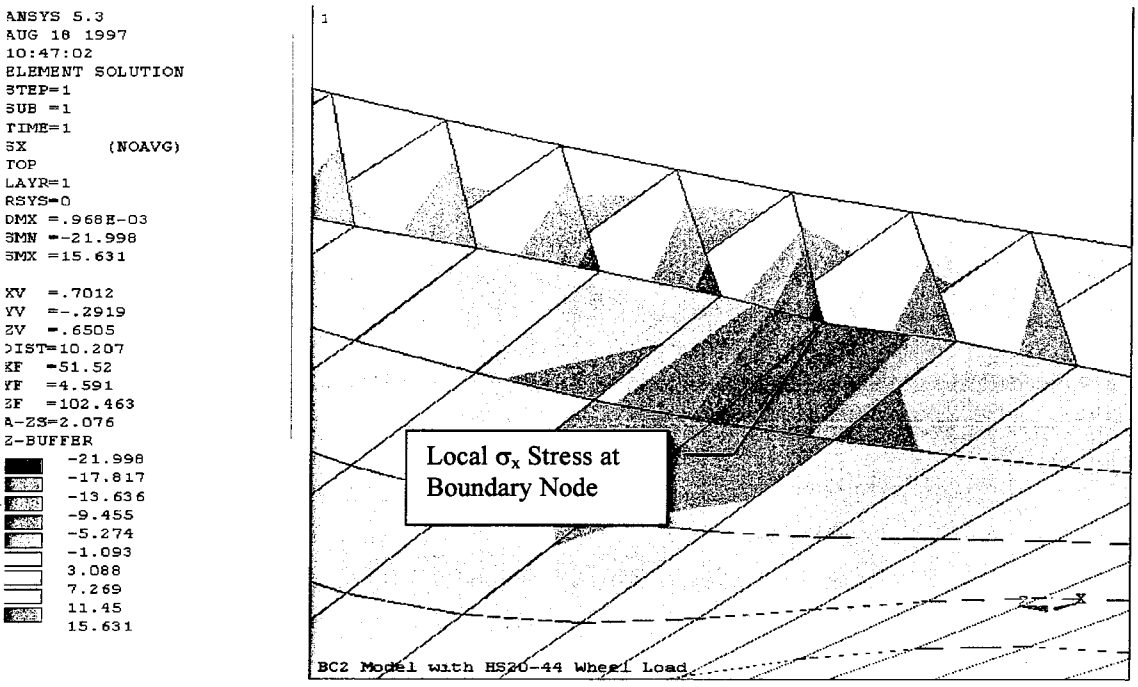

Figure 6.4 Localized σ_x Stress in the Tubes at the Model Restraint

The localized effect of the restraint at the boundary nodes is shown in Figure 6.4, which illustrates a σ_x stress concentration. This type of stress concentration had a significant effect on the shear stress results. The τ_{xz} shear stresses, which occur in the sheets and upper and lower tube elements, are less than the allowable but have little margin of safety in the BC1 and BC2 models. These stresses appear to be strongly effected by the presence of horizontal restraints (Δ_x and Δ_z restrained) at the boundary. The BC3 model, which has no horizontal restraints in the vicinity of the wheel load, has a much greater margin of safety for this stress. As shown in Tables 5.2.1 and 5.2.3, the BC3 model τ_{xz} stresses are at 17.8% of the allowable vs. 81.6% and 99.3% for the BC1 and BC2 models respectively. Figure 6.5 shows the localized influence of restrained boundaries on the τ_{xz} shear stresses.

In addition, the τ_{xy} shear stresses in the webs of the tubes were also influenced by the proximity of horizontal boundary restraints. From Table 5.2.2, the BC3 model τ_{xy} stress was 59% of the allowable. This model did not have horizontal restraints within the vicinity of the load. The BC1 and BC2 models, which had horizontal restraints adjacent to the loads, had τ_{xy} stresses of 111.7% and 136.6% of the allowable respectively. This large increase in stress in the BC1 and BC2 models demonstrates that the placement of horizontal restraints near the load causes a significant increase in τ_{xy} shear stresses. Figure 6.6 shows the localized τ_{xy} stress concentration at a pinned (Δx, Δy, Δz restrained) boundary. The local effect of the boundary restraints become even more evident with

respect to the shear stresses developed by the models that were loaded for the worst case shear as shown in Figure 6.7.

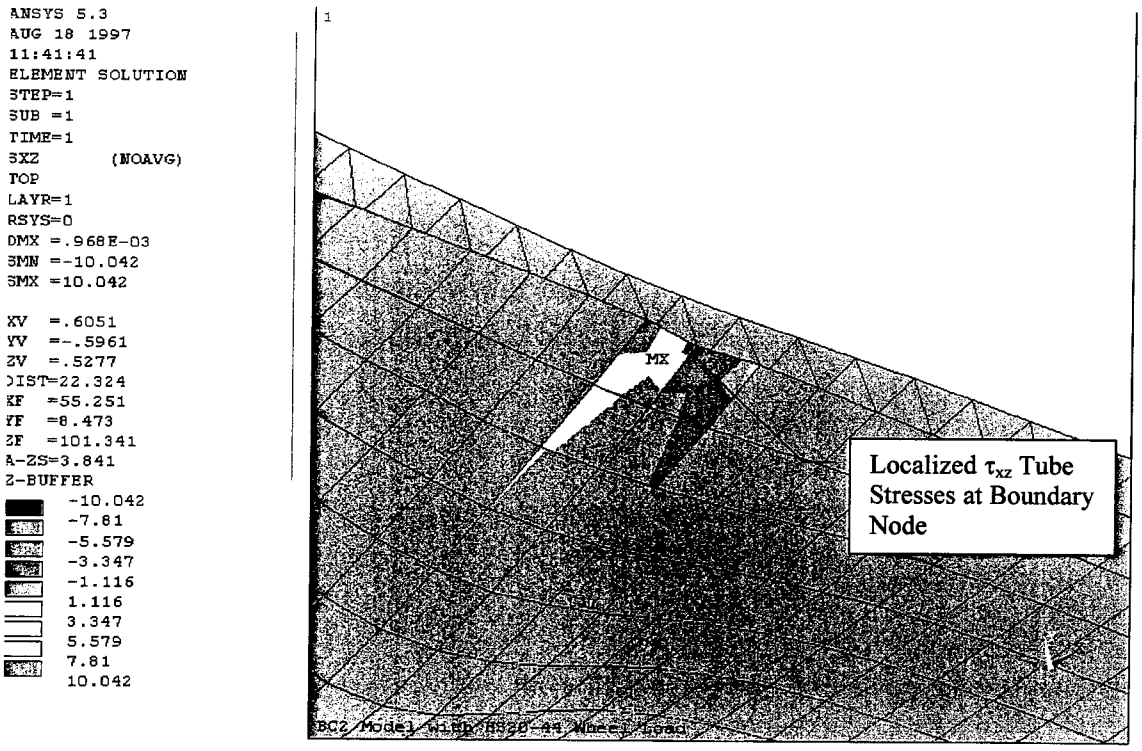

Figure 6.5 Localized τ_{xz} Stresses in Deck Sheets and Tubes

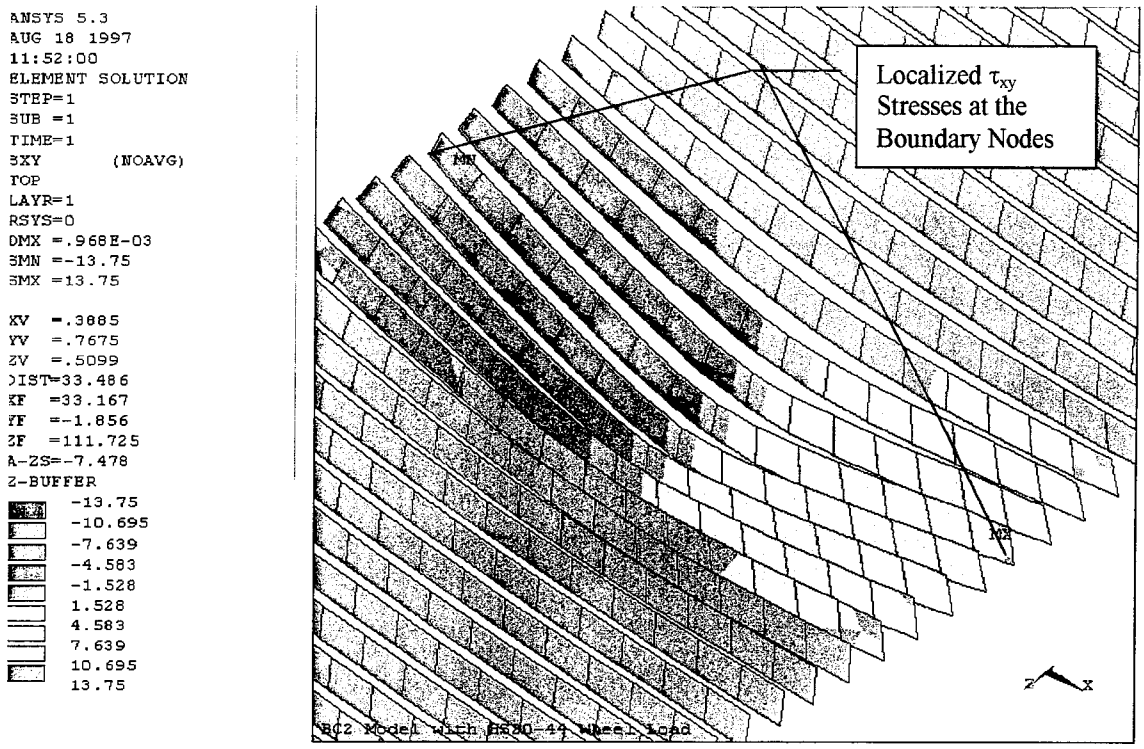

Figure 6.6 Localized τxy Stresses in Tube Webs

In order to develop the worst case shear loading, several shear models were investigated where the wheel load was placed at the model boundaries. Details of the shear models were discussed in Chapter 4. As shown in Figure 5.3.4 and Table 5.3.4 the τ_{xy} stress for the HS20-44 "Shear1" model is approximately twice the allowable at 195% of the allowable. As shown in Figure 6.7, the stress occurs at the boundary restraint and is highly localized since stress rapidly decreases away from the boundary node. The influence of restrained nodes on shear also produced high and localized shear stresses for other model loading conditions, although not as pronounced as for the "Shear1" model loading.

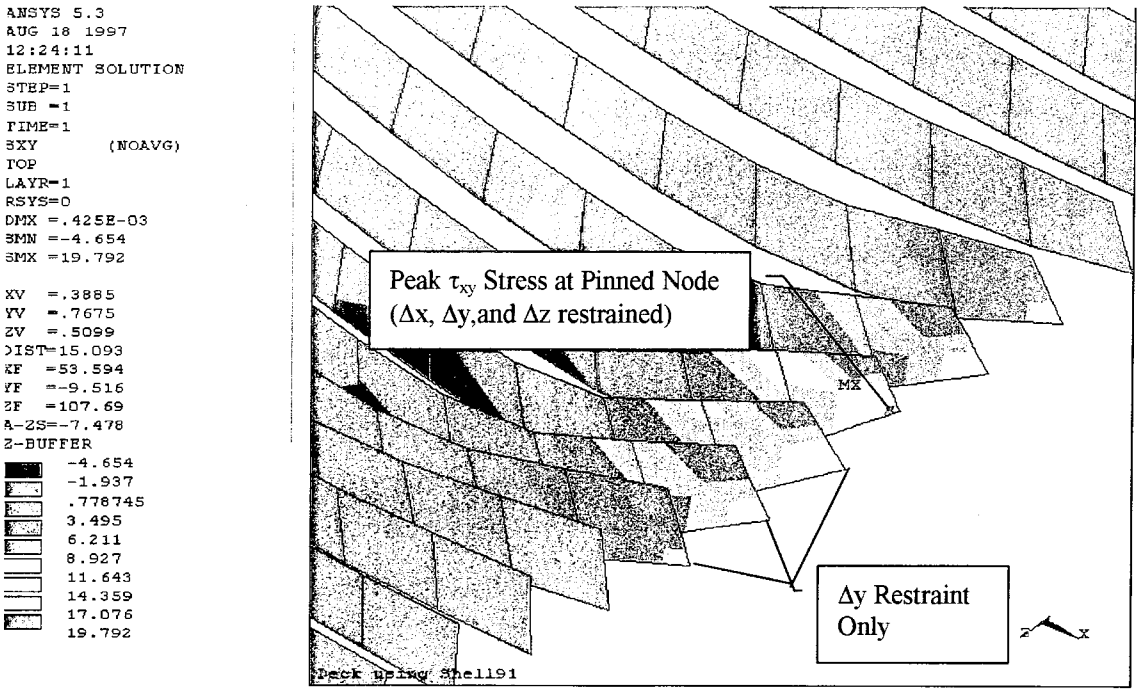

Figure 6.7 Localized τ_{xy} Shear Stress in Tube Web from Shear Model Loading

It was also noted that the models that were loaded to produce worst case shear stresses (wheel load over support) resulted in σ_y bending stresses in the tube webs that exceeded the allowable. As shown in Table 5.3.4 highest σ_y stress was 122.6% of the allowable. As discussed earlier, the bending stresses in the tube webs result from the relative motion of the upper sheets with respect to the lower sheets.

As discussed in Chapter 4, the effect of two HS20-44 loads spaced 4.27m (14') apart and two ML80 loads spaced 1.2m (4') apart were investigated. As shown by the bar charts in Figures 5.3.1 and 5.3.2, the bending stresses from the different HS20-44 loading models do not vary significantly. The charts also show that the bending stresses from the

ML80 loading model are typically lower than the stresses from the HS20-44 loading models (a negative σ_z stress was slightly higher). All bending stresses were within the allowables. Figure 6.1 demonstrates that the bending stresses decrease rapidly away from the point of load application. As a result, multiple wheel loads have little influence on one another since the resulting stresses are highly localized beneath the load. This result was also supported by the ML80 loading which was only 1.2m (4' apart).

In addition, by scaling the single HS20-44 load to account for the difference between HS20-44 and ML80 loading, it can be shown that the proximity of the two ML80 loads to one another have little influence on the resulting stresses as compared to a single load. For example, the ML80 load is 75% of the HS20-44 load. From Figure 5.3.1 the single HS20-44 load resulted in a σ_x stress of 17.6 MPa. The two ML80 loads, that were only 1.2m (4' apart), resulted in a σ_x stress of 13.4 MPa. When the HS20-44 stress is scaled to simulate the result of a single ML80 load, the resulting stress is similar to the two ML80 load case (0.75 * 17.6 = 13.2 MPa vs. 13.36 MPa for two ML80 loads). It should be noted that the shear stresses developed by the two HS20-44 loads and the two ML80 loads are similar in character to the single HS20-44 loading. The shear stresses exceeded the allowables and were highly localized at the pinned boundary nodes.

To evaluate the effect of alternative sheet orientations, models were analyzed with the strong axis of the sheets oriented either parallel or perpendicular to traffic. The details of these models were discussed in Chapter 4. Figures 5.4.1 and 5.4.2 provide a comparison of the stresses from the two models. As shown in the figures, the bending stresses only

vary slightly. When the strong axis of the sheet is rotated parallel to traffic, the sheet σ_x stresses go down while the sheet σ_z stresses go up or down slightly depending on the location of the stress. The bending stresses and shear stresses in the sheets were all lower than the allowables. However, shear stresses in the webs exceeded the allowables and were localized at the boundary nodes as previously discussed. Shear stresses in the webs increased slightly when the sheets were oriented parallel to traffic.

As previously discussed in Chapter 4, a 12.7cm x17.8cm (5"x 7") tube model was evaluated. Figures 5.5.1 and 5.5.2 provide a comparison of stresses for the 12.7cm x17.8cm (5"x 7") tube vs. the 10.2cm x 10.2 cm (4"x 4") tube model. The figures illustrate that the bending stresses for both models are below the allowables. The bending stresses for the 12.7cm x17.8cm (5"x 7") tube model are lower than those for the 10.2cm x 10.2cm (4"x 4") tube model. This result was expected since the 12.7cm x17.8cm (5"x 7") tube develops a deeper section with a higher moment of inertia.

In addition, both the 10.2cm x 10.2cm (4"x 4") tube model and the 12.7cm x17.8cm (5"x 7") tube model have localized shear stresses at the model boundaries. However, shear stresses for the 12.7cm x17.8cm (5"x 7") tube model were lower than the allowable when the load was applied at the center of the deck. The worst case shear for the 12.7cm x17.8cm (5"x 7") tube model was 68.4% of the allowable (Table 5.5.2), for the load case with the load in the center of the panel. Figures 5.5.3 and 5.5.4 provide stress comparisons for the 10.2cm x 10.2cm (4"x 4") tube model and 12.7cm x17.8cm (5"x 7") tube model for the worst case shear loading conditions where the load was placed along

the model boundary. The resulting shear stress in the 12.7cm x17.8cm (5"x 7") tube model was slightly over the allowable. The τ_{xy} stress was 100.2% of the allowable as shown in Table 5.5.4. It should also be noted that the σ_y bending stresses in the 12.7cm x17.8cm (5"x 7") tube webs were below the allowable for all loading conditions.

In addition to the above models, a two span model was investigated which was intended to evaluate the effect of continuity on the performance of the deck. Chapter 4 provided a detailed discussion on the selection of the two span model for the continuity evaluation. Stress comparisons of the two span and single span deck systems are provided in Figures 5.6.1, 5.6.2, 5.6.3 and 5.6.4. Most of stresses in the two span model were lower than the corresponding single span stress. For the loading cases that produced maximum positive and negative moments, the two span model stresses were either close to or less than the corresponding single span model stresses. Under all loading conditions, the σ_x and σ_z bending stresses for the two span model were less than the allowables. For the two span model loaded for worst case shear, the σ_y bending stresses in the tube webs were 114% over the allowable (Table 5.6.4).

As in the single span model, the shear stresses in the two span model exceeded the allowable and are the critical stress for this model. The shear stress magnitudes are similar to the single span case that demonstrated high localized stresses at the model restraints. The worst case two span shear stress was only slightly less than the single span case. As shown in Table 5.6.4, the shear stress for the two span case was 188.7% of the allowable vs. 195% for the single span case.

In addition to the models discussed to this point, two cases were also evaluated to investigate the effect of a joint discontinuity located near a wheel load. The stresses for these two model cases, which were discussed in Chapter 4, are provided in Figures 5.7.1 and 5.7.2. For both model cases, the σ_x and σ_z bending stresses in the sheets and tubes were below the allowables. For the 1 ½ span and free edge models, the σ_y stresses in the webs exceeded the allowable as shown in Table 5.7.2. The τ_{xy} shear stresses in the joint discontinuity models proved to be the most critical. This result is similar to the results of the previous models that were affected by the location of horizontal constraints at the boundary nodes. The worst case shear stress occurred in the web of the single span "free edge" model. From Table 5.7.2, the shear stress was 204% of the allowable. As in the previous model cases, the shear stresses were highly localized at the model boundary nodes. A summary of the worst case stresses for the 10.2cm x 10.2cm (4"x 4") tube model, the 12.7cm x17.8cm (5"x 7") tube model and the joint discontinuity cases is provided in Table 6.2.1.

Table 6.2.1 Summary of Worst Case Stresses and Allowables

Sheet Stresses	Lengthwise Bending (Mpa)	Crosswise Bending (Mpa)	τ_{xy} (Mpa)	σ_y (Mpa)
10.2cm x 10.2cm Tube Model	25.55 (1)	12.94 (2)	12.4 (3)	N/A
12.7cm x17.8cm Tube Model	13.0 (4)	11.26 (4)	5.15 (4)	N/A
Joint Models	50.59 (5)	13.41 (5)	14.53 (5)	N/A
(Allowable)	(82.7)	(49.62)	(13.78)	N/A
Tube Stresses				
10.2cm x 10.2cm Tube Model	27.9 (6)	7.64 (7)	20.17 (8)	33.8 (2)
12.7cm x17.8cm Tube Model	11.14 (9)	3.73 (10)	10.36 (9)	15.93 (9)
Joint Models	36.37 (11)	9.46 (5)	21.01 (11)	38.38 (5)
(Allowable)	(82.7)	(36.75)	(10.34)	(27.57)

Table 6.2.1 Notes:

(1) From two span10.2cm x 10.2cm tube model loaded for maximum negative moment.

(2) From single span 10.2cm x 10.2cm tube model with the"Shear4" loading.

(3) From single span 10.2cm x 10.2cm tube model with ML80 loading.

(4) From the single span 12.7cm x 17.8cm tube model with the "Shear4" loading.

(5) From the 1 ½ span (cantilever) 10.2cm x 10.2cm tube model.

(6) From the two span 10.2cm x 10.2cm tube model loaded for maximum shear.

(7) From the 10.2cm x 10.2cm tube model with the strong axis of the sheets rotated parallel to traffic.

(8) From the single span 10.2cm x 10.2cm tube model with the "shear1" loading.

(9) From the single span 12.7cm x 17.8cm tube model with the "shear1" loading.

(10) From the single span 12.7cm x 17.8cm tube model loading in the center of the deck.

(11) From the "Free Edge" model.

6.3 Deflections

Deflection results for the three boundary condition models are illustrated in Figure 5.8.1 and Table 5.8.1. The corresponding L/Δ values are also given for the maximum deflections. As shown in the table and figure, the deflections do not vary significantly

between the three models. The maximum deflections for the three models ranged from 3.4 mm to 3.9 mm. The L/Δ values ranged from 484 to 423. AASHTO recommends a general deflection criteria of L/800 while reference [27] recommends L/500 for the design of orthotropic bridge decks. The maximum deflections for the boundary condition models exceeded the L/Δ ratios of 800 and 500 as indicated above.

For the model with rotated sheets, the maximum deflection was 4.2 mm vs. 3.6 mm for the model with the sheets strong axis oriented perpendicular to traffic. Again, the rotated sheet model deflection exceeded the recommended L/Δ values of 800 and 500. By rotating the sheets, deflections increased approximately 17%. As shown in Figure 5.8.3, the deflections for the single HS20-44 loading and the double HS20-44 loading models are virtually identical. This reinforces the conclusion that the influence of the loads on the deck is highly localized and that multiple wheel loads have little influence on one another. It may also be noted that the ML80 loading generated deflections that were approximately 75% of the HS20-44 loadings.

Although deflections for the 10.2cm x 10.2cm (4"x 4") tube models generally do not meet the recommended L/Δ ratios, deflections for the two span model do improve somewhat. The worst case deflection for the HS20-44 loading including impact and dead load was 3.1 mm. This value represents an L/Δ ratio of 535, which is greater than the value of 500 suggested by reference [27] for orthotropic decks. Figure 5.8.5 and Table 5.8.5 provide a comparison of the two span vs. the single span model deflections.

Figure 5.8.4 and Table 5.8.4 illustrate the effect of joint discontinuity on the model deflections. The figure indicates that deflections were dramatically increased in the 1 ½ span (cantilever) model. The maximum deflection for the cantilever model was 12 mm vs. 3.6 mm for the single span model. The deflection increase for the "Free Edge" model was not as severe as the 1 ½ span model. The maximum "Free Edge" model deflection was 5.4 mm vs. 3.6 mm for the single span model.

Finally, Figure 5.8.6 and Table 5.8.6 provide a comparison of the 12.7cm x17.8cm (5"x 7") tube model deflections to those of the 4x4 tube model. As shown in the figure, the 12.7cm x17.8cm (5"x 7") tube model offers improved deflection performance over the 10.2cm x 10.2cm (4"x 4") tube model. The maximum 12.7cm x17.8cm (5"x 7") tube model deflection was 2.3 mm as compared to 3.6 mm for the 10.2cm x 10.2cm (4"x 4") tube model. The L/Δ ratio for the 12.7cm x17.8cm (5"x 7") tube model was 711. This L/Δ value meets the recommended value of 500 for orthotropic decks from reference [27] and is much closer to AASHTO's recommended L/Δ value of 800.

6.4 AASHTO Wind and Dead Load Combinations

As discussed in section 6.1, several additional load cases were investigated. In order to evaluate the effect of wind loading and to evaluate the deck for dead load stresses while in the raised position, the deck was evaluated for a 50 psi wind load and dead load from

the 45° and 90° raised positions. A more detailed discussion of the above loading cases was provided in Chapter 4.

In accordance with the criteria listed in Chapter 3, two AASHTO wind plus dead load combinations were evaluated, 50 psi wind plus dead load and 30 psi wind plus dead load plus 20% of dead load for impact. For the first load combination, the maximum stresses from the 50 psi model were added to the maximum stresses from either the horizontal, the 45° or the 90° dead load models depending on which model generated the highest stress. Then, for the 30 psi wind plus 120% of dead load combination, the 50 psi model stresses were scaled by 3/5 and added to the worst case dead load stresses which were multiplied by 1.2. The following tables illustrate the resulting stresses for the two load combinations. In addition, stresses from the live load plus impact plus dead load case are included in the tables for comparison. As shown in the following tables, the stresses for the wind plus dead load combinations are low compared to the live load case.

It should be noted that in all loading cases the σ_x and σ_z bending stresses were less than the allowables. The σ_y bending stresses in the tube webs exceeded the allowables for some of the models that were loaded for worst case shear. Also, localized shear stresses in the tube webs exceeded the allowable for models that were loaded for live load plus impact plus dead load.

Table 6.3.1 Sheet Stresses (Mpa)

	σ_x	σ_z	τ_{xz}
HS20-44+I+DL	17.59	8.96	10.63
50psiWind + DL	0.59	0.86	0.70
30psiWind +1.2DL	0.56	0.94	0.69
Allowable	82.70	49.62	13.78
HS20-44+I+DL	-20.40	-9.57	-10.63
50psiWind + DL	-0.90	-0.87	-0.70
30psiWind +1.2DL	-0.82	-0.93	-0.69
Allowable	-82.70	-49.62	-13.78

Table 6.3.2 Sheet Stresses in % of Allowable

	σ_x (%)	σ_z (%)	τ_{xz} (%)
HS20-44+I+DL	21.27	18.06	77.12
50psiWind + DL	0.71	1.74	5.10
30psiWind +1.2DL	0.68	1.89	5.01
Allowable	100.00	100.00	100.00
HS20-44+I+DL	24.66	19.29	77.12
50psiWind + DL	1.09	1.75	5.10
30psiWind +1.2DL	1.00	1.88	5.01
Allowable	100.00	100.00	100.00

Table 6.3.3 Tube Stresses (Mpa)

	σ_x	σ_y	σ_z	τ_{xy}	τ_{xz}
HS20-44+I+DL	16.00	16.45	2.94	14.12	10.27
50psiWind + DL	0.86	1.12	0.57	0.79	0.69
30psiWind +1.2DL	0.78	1.04	0.61	0.70	0.68
Allowable	82.70	27.57	27.57	10.34	10.34
HS20-44+I+DL	-22.58	-20.68	-5.58	-14.12	-10.27
50psiWind + DL	-1.33	-1.31	-0.60	-0.79	-0.69
30psiWind +1.2DL	-1.22	-1.23	-0.62	-0.70	-0.68
Allowable	-82.70	-27.57	-27.57	-10.34	-10.34

Table 6.3.4 Tube Stresses in % of Allowable

	σ_x (%)	σ_y (%)	σ_z (%)	τ_{xy} (%)	τ_{xz} (%)
HS20-44+I+DL	19.35	59.7	10.66	136.60	99.31
50psiWind + DL	1.03	4.06	2.08	7.62	6.71
30psiWind +1.2DL	0.94	3.8	2.21	6.74	6.60
Allowable	100.00	100.00	100.00	100.00	100.00
HS20-44+I+DL	27.30	75.0	20.23	136.60	99.31
50psiWind + DL	1.61	4.75	2.17	7.62	6.71
30psiWind +1.2DL	1.47	4.46	2.25	6.74	6.60
Allowable	100.00	100.00	100.00	100.00	100.00

CHAPTER 7

PART A: CONCLUSIONS AND RECOMMENDATIONS

7.1 Conclusions

The goal of this part of the investigation was to determine if a suitable movable bridge deck could be developed using fiber reinforced polymer (FRP) composite materials. In order to lower costs, an additional goal was to determine if an FRP bridge deck could be developed using readily available and stocked production materials, such as pultruded structural FRP shapes. As a means to developing a viable design, finite element models using "tube" and "sheet" configurations were created to investigate AASHTO loading conditions, and to evaluate additional parameters that could be encountered during implementation of an FRP deck design. Chapters 5 and 6 of this document presented the numerical results of the various investigations. This chapter focuses on the outcome of the numerical results and provides suggestions for future work.

Initially, trial hand calculations were used to determine preliminary structural sections for the more detailed finite element analysis. The trial hand calculations resulted in further investigation of two different structural configurations, (1) 10.2cm x 10.2cm (4"x4") tubes with 2.5cm (1") cover sheets, and (2) 12.7cm x 17.8cm (5"x7") tubes with 1.9cm (¾") cover sheets. A detailed parametric study was conducted on the 10.2cm x 10.2cm (4"x4") tube configuration. The 12.7cm x 17.8cm (5"x7") tube configuration was then evaluated for comparison with the 10.2cm x 10.2cm (4"x4") tube configuration.

The results of the investigations indicate that both configurations could offer viable solutions to the development of an FRP bridge deck. However, several issues need to be addressed concerning the results of this investigation as presented in the following conclusions.

(1) Boundary Conditions:

The initial parametric study involved the investigation of various boundary conditions in conjunction with ASSHTO recommended loads. This investigation was initiated to determine how changes in boundary conditions would affect the stresses in the deck. It was also initiated to address a variable parameter that could affect the design of the deck, as well as subsequent attachment design considerations.

Based on the results of the investigation it can be concluded that the boundary condition parameters have a significant impact on the adequacy of the 10.2cm x 10.2cm (4"x4") tube configuration. As a result, it is concluded that the design and application of the deck to bridge attachment points could have a critical impact on the viability of the deck design.

High localized shear stresses at the deck model boundary nodes resulted during the analysis. It should be noted that the high localized shear stresses were the result of intermittent horizontal restraints at the boundary nodes, as opposed to vertical shear at the nodes. The results show that the variation of the boundary conditions as prescribed by

this analysis did not have a significant impact on the σ_x and σ_z bending stresses, which were less than the allowables.

It should be noted that while the shear stress allowable was exceeded, this factor alone should not constitute a failure of the 10.2cm x 10.2cm (4"x4") tube and cover sheet concept. Since the high shear stresses were concentrated at the nodes with horizontal restraints, this localized condition could be controlled or corrected. In addition, the limitations of the modeling methodology must be considered. The application of horizontal restraints of the boundary nodes does not necessarily provide a sufficiently accurate representation of the deck behavior at the boundary. It is recognized that the actual response at the deck-to-bridge connection will be highly dependent on the methodology used to create the attachment. The actual attachment configuration may introduce flexibilities or degrees of freedom, which are not represented by the model. It is believed that additional flexibility at the attachment joint would help to reduce the localized shear stress.

It may also be concluded that the localized high shear stresses could be relieved by the addition of reinforcement at the joints or through careful design of the attachment joint. For example, a joint design that allows some horizontal movement or perhaps added flexibility in the horizontal direction could produce the desired reduction in stress. In any case, a noteworthy observation is that it is unlikely that the joint system eventually used, would introduce reactions to the deck as discretely as in the case where restraints are applied at a single model node. It is more likely that stresses would be dispersed over

a larger area and may be more significantly relieved. In conclusion, a detailed joint study involving a finer model mesh and a more accurate representation of the attachment joint is warranted.

Another stress that may have been indirectly affected by the model boundary conditions was the σ_y bending stresses in the tube webs, which were 123% of the allowable (Table 5.3.4). As discussed in Chapter 6, the σ_y bending stresses in the webs occurred as the result of relative movement between the upper and lower deck sheets. This movement may have resulted because the model boundary restraints were only applied around the lower perimeter of the deck, at the deck-to-bridge contact points. This condition left the upper deck sheets free to move relative to the lower sheets, which were restrained. A more detailed study of the deck-to-bridge attachment joint design might reveal that the attachment joints provide some restraint for the upper deck sheets, as well as for the lower sheets. Such a condition would result in lower σ_y bending stresses in the tube webs.

(2) Vehicular Loading Conditions:

In addition, to the model parameters discussed above, various AASHTO loading conditions were investigated. The 10.2cm x 10.2cm (4"x4") tube configuration, with the moderate BC2 boundary conditions, was evaluated considering dead load, live load and impact. The AASHTO live loads consisted of a single HS20-44 wheel load located in the center of the panel, two HS20-44 loads spaced 4.27m (14') apart and two ML80 loads

spaced 1.2m (4') apart. Also, multiple truck loads for the multi-span configuration were also investigated and will be discussed later.

The results of the analysis indicate that the HS20-44 truck loading governs over the ML80 loading. In addition, the application of two HS20-44 loads did not significantly influence deck stresses over the single loading configuration. The influences of the wheel loads were localized resulting in little stress overlap between points of load application. For the loading considered, localized shear stresses proved most critical as previously discussed.

The localized effect of wheel loads on the deck, as indicated by the analysis results previously discussed, resulted in little difference between the single span models and the multi-span model. The multi-span model was investigated to evaluate the effect of continuity and multiple truck loads on the design. The results indicate that the stresses are not dramatically different between the single span and multi-span conditions. As previously indicated, the presence of the multiple truck loading did not significantly affect the stresses in the deck as compared to a single wheel load. However, as indicated by the single span loading condition, the critical stresses were highly localized shear stresses at the model boundary nodes. As a result, the specification of either a single or multi-span deck design would not be significantly influenced by stress.

(3) Wind + Dead Load Condition:

As recommended by AASHTO, the effect of wind induced stresses and the effect of dead load stresses while the bridge is in the open position were evaluated. The load combinations used were discussed in detail in Chapter 6. As shown in Tables 6.3.1 to 6.3.4, the stresses for the wind plus dead load combinations were extremely low. The highest stress for the above load combinations was 7.6% of the allowable.

(4) Variation of Cover Sheet Orientation:

Added to the parameters discussed to this point, is the evaluation of the effect of changing the cover sheet fiber orientation. Since the cover sheets have orthotropic properties, it could be expected that the orientation of the strong fibers in the sheets might influence the performance of the deck. The results of the analysis indicate that stresses in the sheets were affected somewhat, while stresses in the tubes were less significantly affected. When the orientation of the strong axes of the sheets was changed to be parallel to traffic, stresses in the tubes increased slightly. For this condition, the σ_x stresses (weak direction of fiber) in the sheets decreased and the σ_z stresses (strong direction of fiber) and the τ_{xz} stresses either increased or decreased slightly depending on which side of the deck was examined.

At this point it should be noted that the deck model bending stresses were not always symmetric. In some cases, stresses in the top of the deck differed from stresses in the bottom of the deck. This condition can be attributed to the influence of the model boundary constraints, which were located around the perimeter of the lower deck

elements. For the sheet orientation models, only shear stresses proved to be critical, all other stresses were lower than the allowables. Considering that the shear stresses were localized and could be corrected as previously discussed, in terms of stress, sheet orientation would not significantly impact the performance of the deck.

(5) Deck-Panel Joint Discontinuity:

In consideration of design parameters, which could effect the performance of the deck, two additional ones were investigated to evaluate the effect of a deck panel joint discontinuity or failure. This condition would dictate whether or not the underlying bridge structure should be used to back up the deck panel joints. That is, should the joints be forced to be located over the bridge stringers and added backup structure or not? Since the panel joints were conceived as being either parallel or perpendicular to traffic, two models were evaluated. For the panel joints oriented perpendicular to traffic, the deck was supported on three sides with the wheel load applied on the free edge. For the panel joints oriented parallel to traffic the model consisted of 1½ spans with the load applied at the end of the half span, similar to a load at the free end of a cantilever.

The results indicate that stresses were significantly affected by the joint discontinuity cases. Stresses generally increased, with shear and bending stresses in the webs being the most critically affected. The critical shear stresses tended to be concentrated at the boundary nodes in a similar manner as in the other model cases. As shown in Table 5.7.2, the "Free Edge" model had the highest shear stress in the tube webs. The shear

stress was 203.2% of the allowable as compared to 137% for the model without a joint discontinuity.

In addition, the σ_x and σ_y bending stresses were lower than the allowables; however the σ_y bending stresses in the webs were over the allowable. The "Free Edge" model σ_y stress was 151% of the allowable as compared to 75% for the model without a joint discontinuity. It should be noted at this point that the allowable stresses are based on a safety factor of 2.5 for bending and 3 for shear. The ultimate properties of the materials used are based on minimum properties derived from coupon testing as described in reference [4]. It should be considered that, for the joint discontinuity models, none of the stresses exceeded the ultimate stresses values published in the Strongwell design manual for fiberglass structural shapes, reference [4].

Based on the above, it is concluded that a joint discontinuity would not necessarily constitute a catastrophic failure of the deck. It is suggested, however, that prudent design practice would employ locating the panel joints over supporting structures wherever possible. In addition, as with the previous model cases, localized shear stresses could be mitigated through the use of an attachment joint that has been designed for this stress condition or some form of deck reinforcement at the deck-to-bridge attachment points.

(6) Comparison of the Two Models:

To this point, all the modeling parameters investigated were based on the 10.2cm x 10.2cm (4"x4") tube configuration. A single span model using 12.7cm x 17.8cm (5"x7")

tubes and 1.9cm (¾") cover sheets was also evaluated. Based on the results, the 12.7cm x 17.8cm (5"x7") tube configuration offered significant improvement in stress performance over the 10.2cm x 10.2cm (4"x4") configuration. All stresses were reduced and some of the deck overstresses were resolved using the 12.7cm x 17.8cm (5"x7") tube configuration. For this configuration, all stresses were less than the allowables except for a slight shear overstress in the tube webs. The overstress was 100.18% of the allowable.

It should be noted that other model parameters investigated using the 10.2cm x 10.2cm (4"x4") tube configuration were not evaluated for the 12.7cm x 17.8cm (5"x7") tube configuration. However, based on the reduction in shear and bending stresses in the tube webs, it can be safely concluded that the 12.7cm x 17.8cm (5"x7") tube configuration would outperform the 10.2cm x 10.2cm (4"x4") tube configuration for all the parameters investigated.

In consideration of the localized nature of the overstresses at the boundary nodes, the 10.2cm x 10.2cm (4"x4") tube option could become acceptable for shear stresses after a more detailed study of the deck to bridge attachment points. In addition, the σ_y bending stresses in the tube webs could be reduced by the addition of thicker cover sheets. Also, using a more accurate model representation of the deck-to-bridge attachment, could result in reduced relative movement between the upper deck sheets and the lower deck sheets. Less movement between the upper and lower sheets would result in lower σ_y bending stresses in the webs. Finally, it may also be concluded that the 12.7cm x 17.8cm (5"x7")

tube configuration outperforms the 10.2cm x 10.2cm (4"x4") tube option, and is the most viable option if stress is used as the governing criteria.

The final performance criteria established for the deck design was deflection. For the cases considered, neither the 10.2cm x 10.2cm (4"x4") tube system nor the 12.7cm x 17.8cm (5"x7") tube system satisfied the deflection criteria of L/800 set forth by AASHTO. The 12.7cm x 17.8cm (5"x7") tube model outperformed the 10.2cm x 10.2cm (4"x4") tube model with an L/D of 711 vs. an L/D of 458 for the corresponding 10.2cm x 10.2cm (4"x4") model. It should be noted that the 12.7cm x 17.8cm (5"x7") tube configuration could possibly satisfy AASHTO's L/800 requirement if the deck were designed as a two span panel with continuity across one of the longitudinal bridge stringers. This assertion is based on the deflection results of the 10.2cm x 10.2cm (4"x4") tube model which indicated a worse case two span deflection of 85% of the single span case. Assuming a linear relationship, 711/0.85 = 836. This result indicates that a two span configuration, using 12.7cm x 17.8cm (5"x7") tubes, would probably satisfy the L/800 AASHTO deflection requirement.

(7) Deflection Considerations:

In addition to the above, reference [27] suggests a deflection criteria of L/500 for orthotropic decks. The single span 12.7cm x 17.8cm (5"x7") tube configuration meets this requirement. The two span 10.2cm x 10.2cm (4"x4") tube configuration meets this requirement with an L/D of 535. It is, therefore, concluded that both tube configurations may offer viable deck solutions depending on the deflection criteria used. It should also

be noted that the deflection and stress performance of both tube configurations could be improved simply by increasing the thickness of the cover sheets.

7.2 Recommendations for Future Work

In order to address considerations that were outside the scope of this analysis and to address some of the findings, a number of recommendations are provided. In consideration of the localized overstresses at the model boundary nodes, and the transverse bending stresses in the tube webs, it is recommended that a more detailed evaluation of the deck to bridge attachment points be performed. Such an investigation could involve the implementation of a more refined model mesh at the boundary joints. In addition, the effect of imparting horizontal flexibility in the design of attachment joints should be investigated.

Also, the improvement of deck deflections could be investigated through the use of thicker cover sheets. Several factors that were beyond the scope of this analysis should be considered as well. Tube web buckling should be evaluated which could prove to be critical at the deck reaction points and at the point of load application. It should be noted that this analysis was based on an equivalent single layer approach that does not accurately predict interlaminar shear stresses. Interlaminar shear stresses are typically critical at the model boundary. Evaluation of interlaminar shear stresses at the model boundary would involve the development of a more refined model at the deck boundaries.

PART B : STATIC AND DYNAMIC ANALYSIS OF MONOLITHIC MODELS

CHAPTER 8

BRIDGE DECK MODELING

8.1 Introduction

As mentioned in Chapter 1 of this report, the main objective of this research is to determine a structurally viable cross-section of a bridge deck made from FRP that can be fabricated and tested in a laboratory. This type of FRP-Deck can be used in place of current open steel decks being used on movable bridges. Evaluation of previous research by Ballard [29] showed that a monolithic cross-section with sloping webs might eliminate some issues that were identified in that study. Therefore, in this Part-B of the research, four monolithic models were created and compared to each other, as well as to the tube and sheet models developed by Ballard [29]. These four monolithic models have varying web slopes, varying distances between the webs, and varying uniform thicknesses. A static analysis was performed on these models to compare how each variable affects the stresses and deflections. Once this analysis had been done, the most viable models were then analyzed for their dynamic properties through a free dynamic vibration analysis. Thus, the free vibration dynamic analysis would provide the dynamic properties such as

mode shape and natural frequency of the bridge deck. These dynamic properties are in turn to be used in determining if resonance may or may not occur. Potential for resonance is determined by comparing the frequency of the bridge deck to the frequency of a moving vehicle. The closer these frequencies are to each other the more the potential for resonance.

In order to determine if the impact factor of 1.3, taken from AASHTO [6], used in the static analysis is a valid value for FRP, a forced vibration dynamic analysis was performed. From this analysis the dynamic deflection is determined and can then be used in the equation for the impact factor, or dynamic load factor (DLF), as shown in equation 8-1 as follows:

$$DLF = \frac{\delta_{dynamic}}{\delta_{static}} \qquad (8\text{-}1)$$

where δ_{static} is the static deflection determined from the static analysis and $\delta_{dynamic}$ is the dynamic deflection from dynamic analysis. Also, the stresses due to dynamic effects can be extracted and then compared to the stresses due to static effects without the DLF, as well as, the difference between using the impact factor to simulate dynamic loading versus performing a complete dynamic analysis.

8.2 Physical Model

The first step in computer modeling is to create or determine the physical model. This in turn helps the designer with the dimensions of the model, properties of the material used and cross-sectional shape. For this study, several models were initially "designed" and then analyzed for their feasibility as the model of choice in this study. The dimensions of the models in this research were patterned after the Sunrise Boulevard Bridge in Fort Lauderdale Florida (see Figures 8-1 and 8-2). This bridge has a spacing of 1.65 m (5'-5") between the stringers and 5.79 m (19'-0") span of grating (see Figure 8-3). Therefore, the deck model will have dimensions of 1.65 m x 5.79 m x 15.24 cm (5'-5" x 19'-0" x 6"), although the use of FRP might lead to a thinner deck. Next, the material

properties used for each model were obtained from the earlier work done on the same bridge by Ballard [29] and are listed in Table 8-1.

Figure 8-1 – Sunrise Boulevard Bridge, Fort Lauderdale, Florida

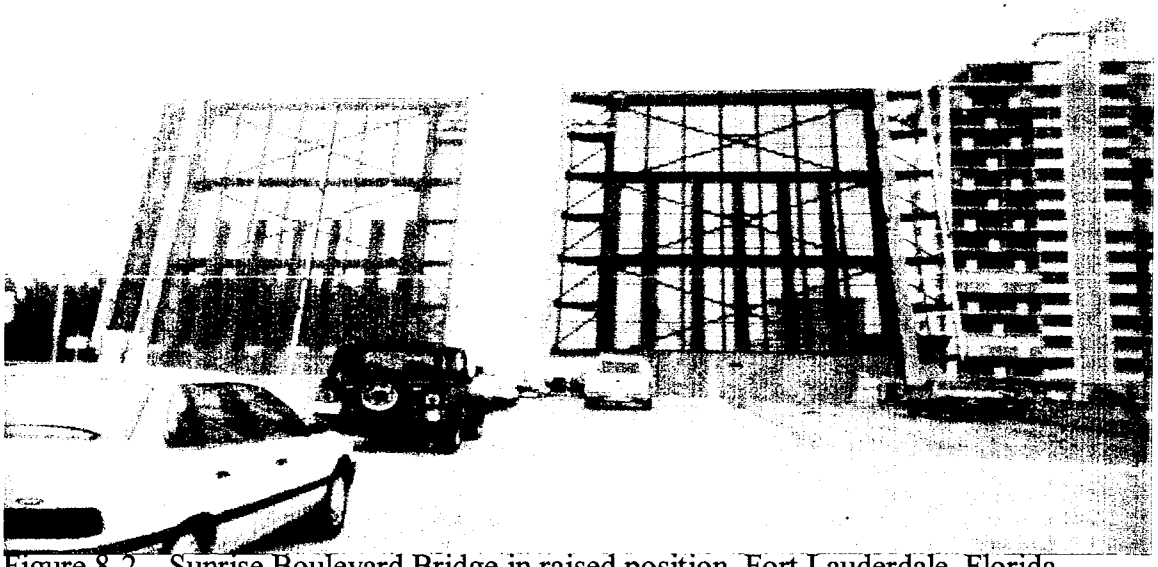

Figure 8-2 – Sunrise Boulevard Bridge in raised position, Fort Lauderdale, Florida

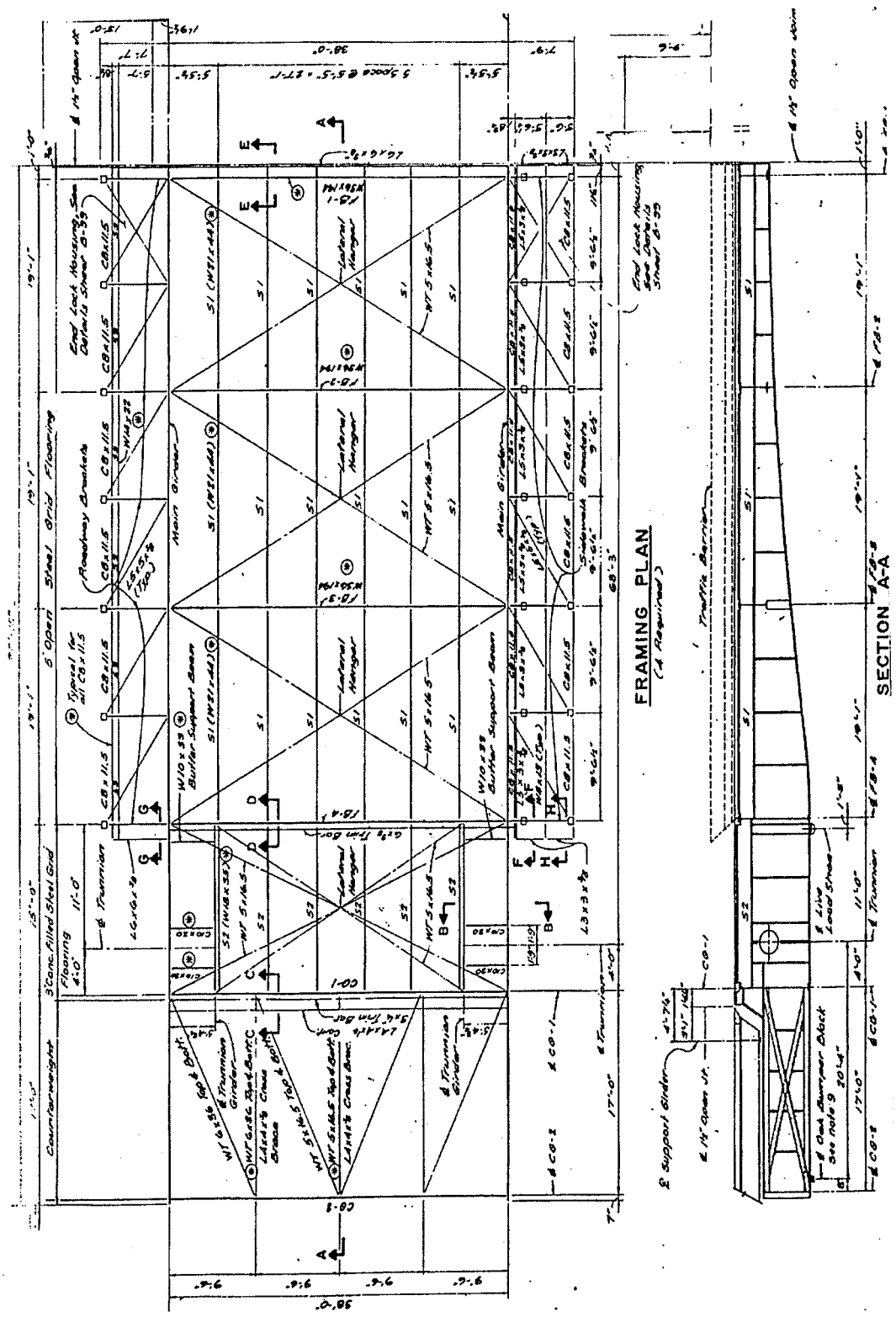

Figure 8-3 – Sunrise Boulevard Bridge Framing Plan [23]

Properties	Material
E_x (GPa) (psi)	11.0 (16×10^5)
E_y (GPa) (psi)	5.5 (8×10^5)
E_z (GPa) (psi)	5.5 (8×10^5)
ν_{xy} (Poisson's ratio) ν_{yz} ν_{xz}	0.165 0.33 0.165
G (shear modulus) (GPa) (psi)	2.9 (4.25×10^5)
γ (Kn/m^3) (lbs/in^3)	18.58 (0.0685)

Table 8-1 – Material Properties [29]

8.3 Computer Model

Determining the cross-sectional shape of each model is dependent upon many factors. In previous research [29], tube and sheet models were analyzed to determine the stresses and deflections (see Figure 8-4). Four tube and sheet models were built and two were determined to be the most feasible. These two models were 12.7 cm x 17.8 cm (5" x 7") tube with 1.9 cm (¾") cover sheets and the 10.1 cm x 10.1 cm tube with 2.5 cm (1") cover sheets. Consequently these models were then adopted and used in this investigation.

One problem discovered with the tube and sheet models was high-localized stresses at the nodes. Figure 8-5 shows an example of this high localized stress at a support where the model is supported against all three translational directions. Also, the tube and sheet models have discontinuities where the tubes connect. This discontinuity

problem could be remedied through the use of a monolithic model. High local buckling stresses would also seem to be lessened by angling the web. These two remedies are the basis for the next four models investigated in this study. Each of the following models has characteristics that can be compared to one another. Therefore, the slope of the web, the spacing between the webs, and the thickness are factors that could all be compared, to determine the most beneficial and efficient model. Table 8-2 shows the different monolithic models investigated in this study.

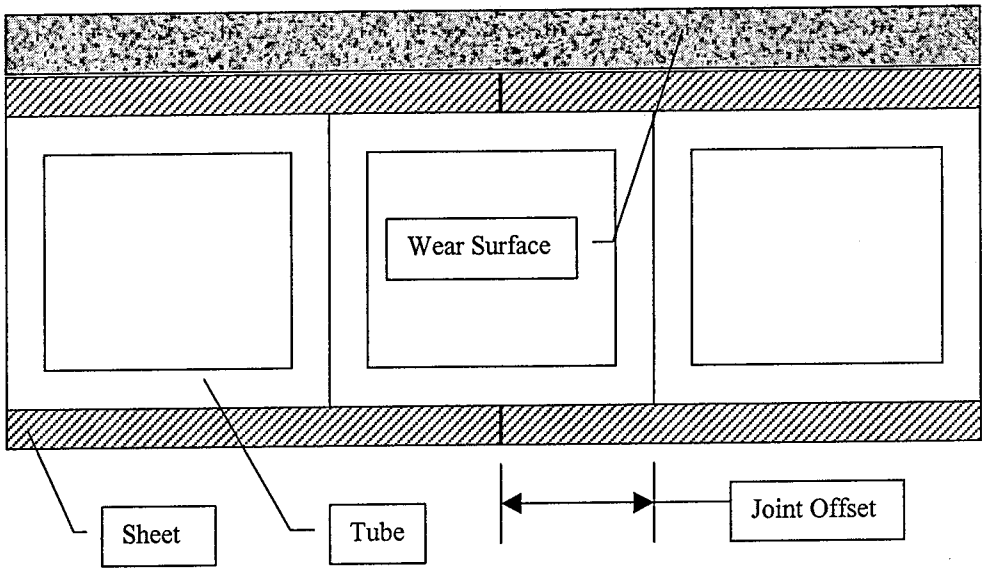

Figure 8-4 – General Tube and Sheet Model Configuration [29]

The next input that must be determined is the element type to be used in the finite element modeling. For the finite element analysis the software ANSYS 5.3 will be utilized. ANSYS 5.3 has many different element types that are very practical for this application. The element type that will be most suited for this research is one where the

thickness can be changed fairly easily and has six degrees of freedom at each node. It is desired to have a thickness that can be changed easily since the thickness will be varied in order to determine the importance of the thickness. Table 8-3 shows the properties of various elements that were investigated and the one that was chosen for this research. One property of FRP that would require a layered element, although not utilized in this research, is that FRP can have numerous layers each with a different angle of fiber. This approach will be most useful for a micro level analysis; however, this study focuses on the macro level representation of the bridge deck. Therefore, the layered element is desired in case future research is on the micro level and utilizes orientation of the fiber. The layered element that was chosen for this research is the 16-layer structural shell, shown in Figure 8-6 with the local coordinate system.

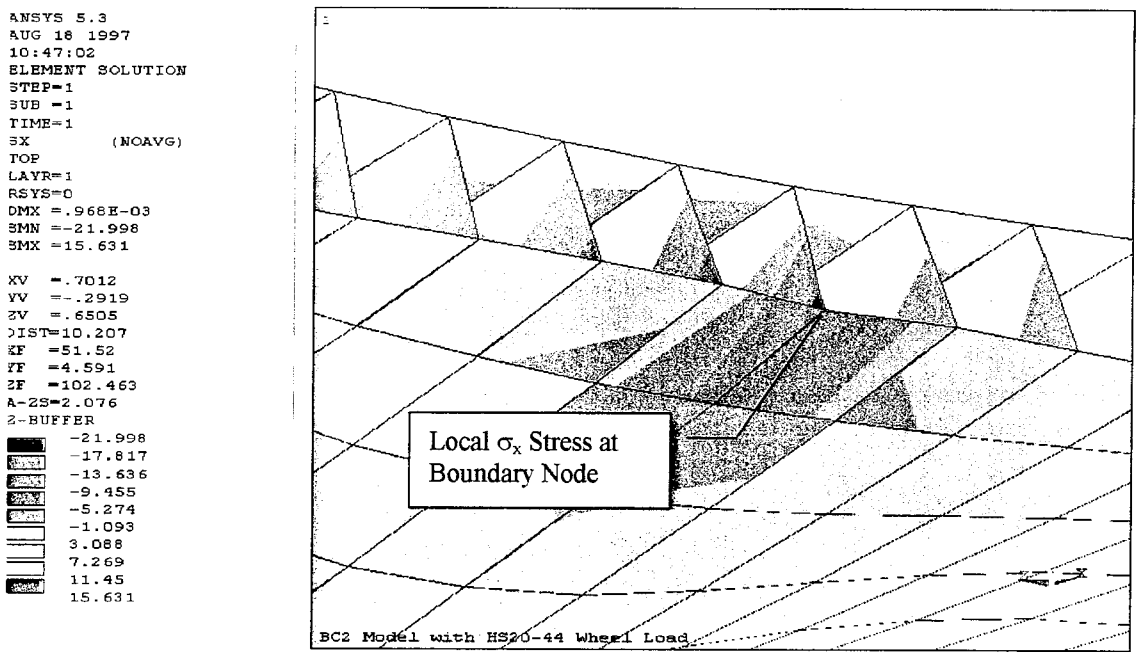

Figure 8-5 – Localized σ_x (Mpa) Stress in the Tubes at the Model Restraint [29]

Model	Slope of Web	Distance Between Webs
1	2:1	7.62 cm (3")
2	2:1	15.24 cm (6")
4	1:1	7.62 cm (3")
5	1:1	None

Table 8-2 – Model Characteristics

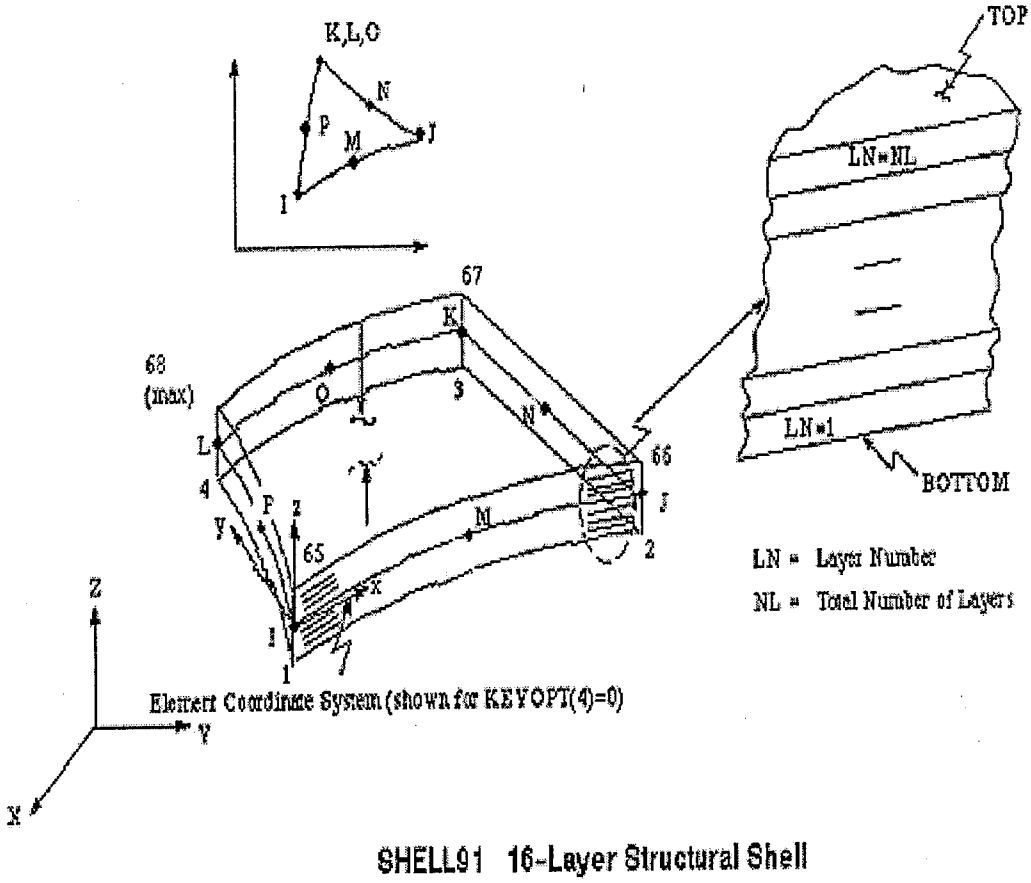

Figure 8-6 – ANSYS 5.3 16-Layer Structural Shell Element

ANSYS Element type	Degrees of Freedom	Number of Nodes	Remarks
3-D Structural Solid	3 U_x, U_y, U_z	8	Lacks rotational degrees of freedom and variation of thickness
3-D Layered Structural Solid	3 U_x, U_y, U_z	8	Lacks rotational degrees of freedom and variation of thickness
3-D, 8-node Structural Solid with Rotations	6 U_x, U_y, U_z, M_x, M_y, M_z	8	Does not allow variation of thickness
16-Layer Structural Shell	6 U_x, U_y, U_z, M_x, M_y, M_z	4	Has rotational degrees of freedom and allows for variation of thickness
100-Layer Structural Shell	6 U_x, U_y, U_z, M_x, M_y, M_z	4	Has rotational degrees of freedom and allows for variation of thickness

Table 8-3 – Element type comparison

Once the element is chosen, the next step is to create the model. In ANSYS 5.3 the models are created by forming areas or volumes, depending on the element type, and then "gluing" them together using the Boolean-glue command. For the previously mentioned monolithic models two large rectangular areas were created to be the top and bottom of the deck and then the webs were created as angled areas. The Boolean-glue command simply glues the areas, or volumes, together to form one monolithic piece. Once the model is one piece the mesh command can be performed to create nodes and elements from the keypoints and areas, or volumes, entered. Once the model has been

meshed, see Figure 8-7, the boundary conditions can be added. From previous research by Ballard [29], supporting every element in the y-direction and every 7th element in the x, y, and z-directions was the most efficient out of three boundary condition models investigated in that study (see Figure 8-8). The purpose of supporting every 7th element in 3 directions is to model a bolt or similar intermediate connection. Once all the boundary conditions are applied all that is left is to apply a static or dynamic load and perform the appropriate analysis, which is, discussed further in Chapters 9, 10, and 11.

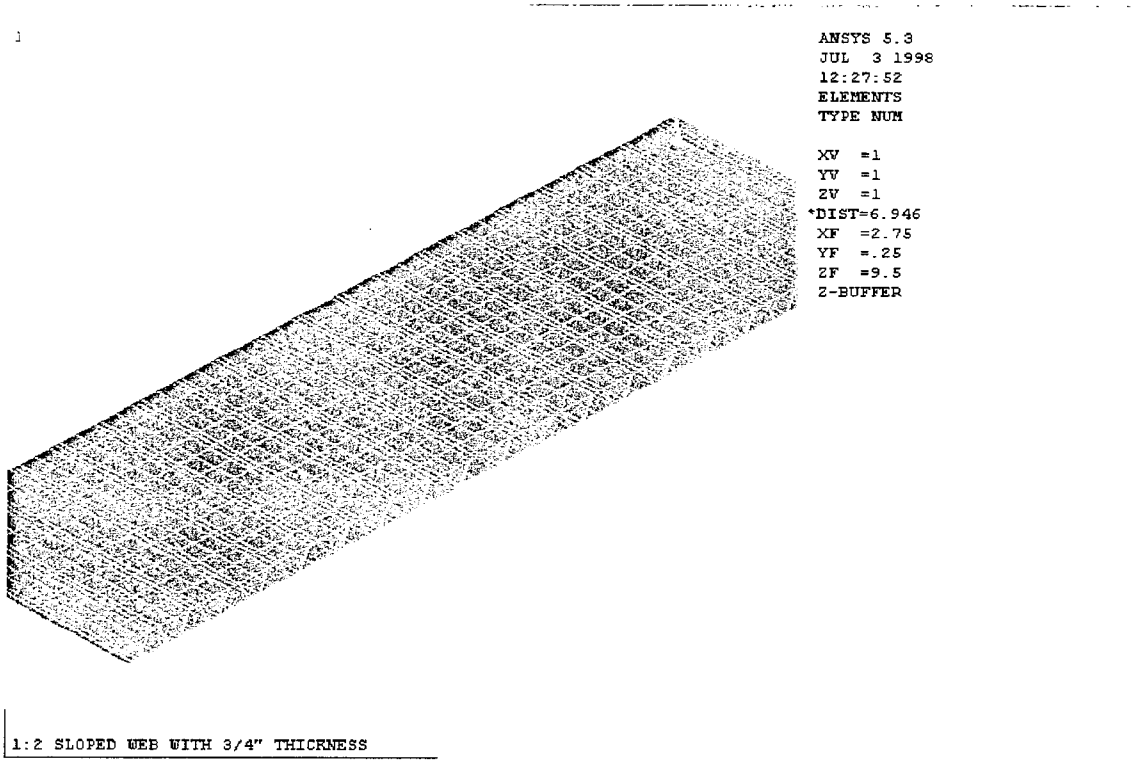

Figure 8-7 – Example of monolithic model and the orientation of the global coordinate system (Model 1)

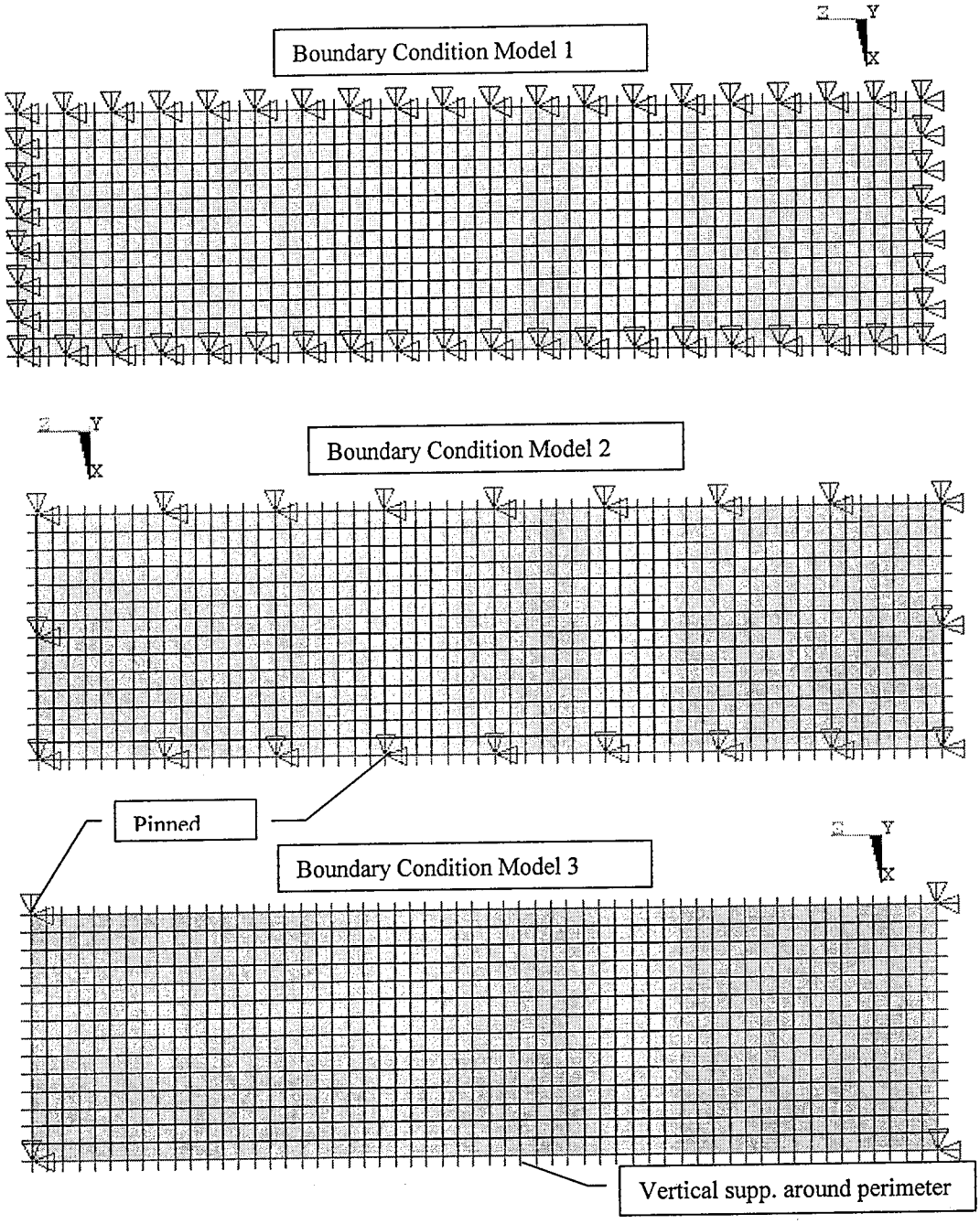

Figure 8-8 – Boundary Condition Models [36]

CHAPTER 9

STATIC ANALYSIS

The chosen initial step in determining a feasible model, in the context of this research, is to perform a static analysis on all models. This static analysis will determine the stresses, the static deflection and any local stresses that may occur in the model. Therefore, in this study, as mentioned in Chapter 8, four monolithic models are analyzed. Once the desired data has been extracted, it can then be compared to the data retrieved from the previous analysis performed on tube and sheet models by Ballard [29]. The purpose of these comparisons being to determine the model or models that will be further analyzed in the dynamic portion of this research. This chapter will focus on the results determined from the comparison of all the model data obtained from a static analysis. The specific parameters that were considered included the thickness, the slope of the webs, the distance between the webs, and the deflection of the cross section. The sections that follow will discuss the results of these comparisons.

9.1 Thickness Variation

The role that thickness plays in determining a model's feasibility will be determined by varying the thickness of the cross-section. The expectation is that the

thicker the elements are the lower the stresses will be. This study varies the monolithic model's uniform thickness from 1.27 cm to 5.08 cm (½" to 2") at incremental steps of 0.635 cm (¼"). The tube and sheet models by Ballard [29] were created from pultruded elements utilizing the Extren Design Manual [4]; therefore, the thickness was not varied. Table 9-1 shows all the model characteristics for the models compared in this section. Figures 9-1 to 9-4 show what the monolithic model cross sections look like, while Figure 8-4 of Chapter 8 shows the drawing of the tube and sheet model. Figures 9-5 to 9-10 show the maximum tensile and compressive stresses of each model for σ_x, σ_y, σ_z, τ_{xy}, τ_{yz}, and τ_{xz}. Each figure designates a different stress comparison. The designated compressive stress is in the top of the model where the tensile stress is at the bottom of the model.

Model Designation	Model Type	Cross Section	Remarks
Model 1	Monolithic	2:1 sloped webs with 7.62 cm (3") spacing	
Model 2	Monolithic	1:1 sloped webs with 15.24 cm (6") spacing	
Model 4	Monolithic	1:1 sloped webs with 7.62 cm (3") spacing	
Model 5	Monolithic	2:1 sloped webs with no spacing	
Model X	Tube and Sheet	10.2 cm x 10.2 cm x 0.64 cm (4" x 4" x ¼") with 2.54 cm (1") cover sheets	Thickness will be taken as 1.27 cm (½")
Model Y	Tube and Sheet	12.7 cm x 17.8 cm x 1.9 cm (5" x 7" x ¾") with 1.9 cm (¾") cover sheets	Thickness will be taken as 3.81 cm (1½")

Table 9-1 – Model Characteristics

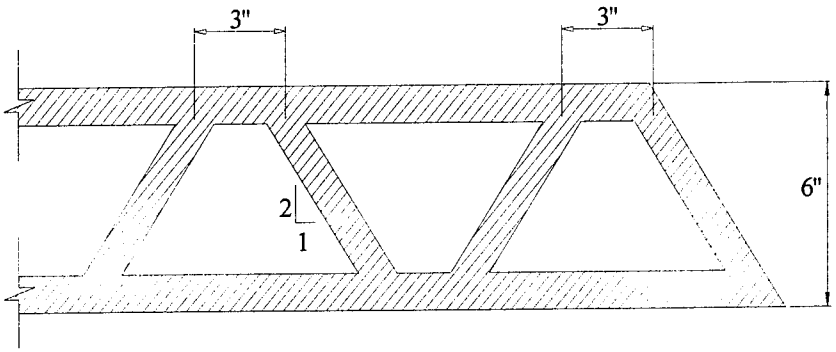

Figure 9-1 – Cross – section of Model 1

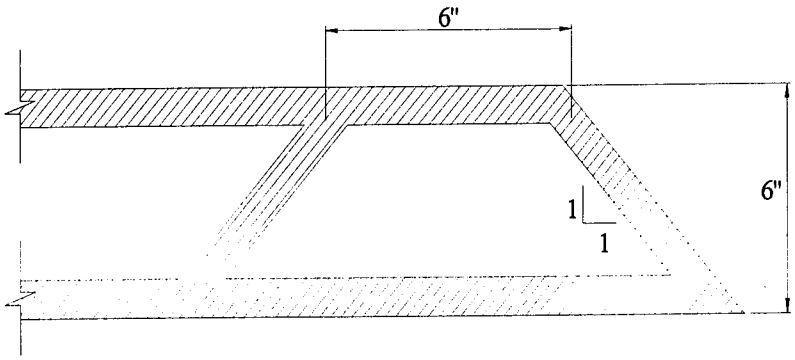

Figure 9-2 – Cross – section of Model 2

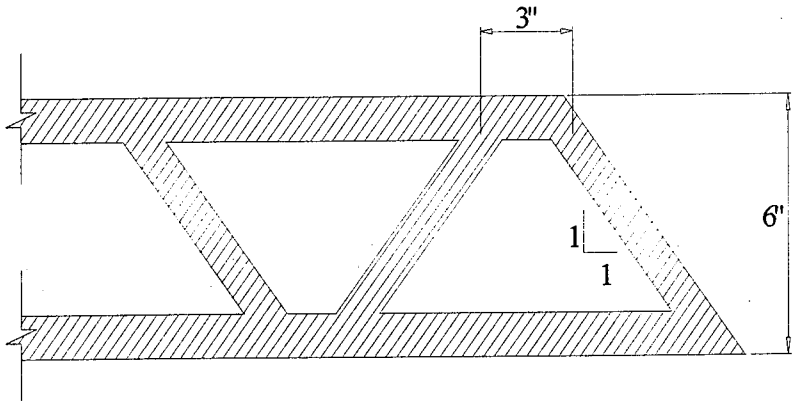

Figure 9-3 – Cross – section of Model 4

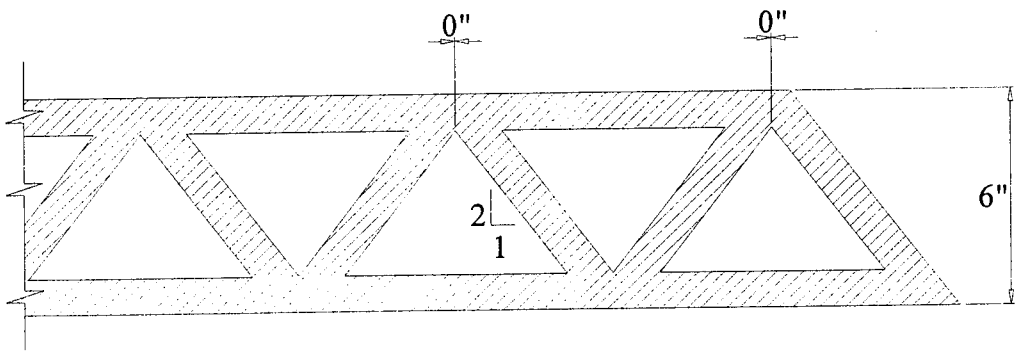

Figure 9-4 – Cross-section of Model 5

Figures 9-5 through 9-10 show that the normal stress decreases exponentially with respect to increasing thickness. The 'x' lines indicate the allowable stresses of $\sigma_u/2.5$ and $\tau_u/3$ from the Extren Design Manual [4]. The allowable stresses will help in determining the most feasible and efficient model. These figures show that the thickness of the models assume more importance in the case of the shear stresses, τ. Consistent with the exponential stress variation with thickness as the thickness is increased, the benefit becomes minor at about 3.81 cm (1½"); therefore, a thickness of between 2.54 cm and 3.81 cm (1" and 1½") appears to be the most efficient in most sections. Hence, for the rest of the comparisons a thickness of 3.81 cm (1½") will be used. However, when observing the data for τ_{yz}, it can be concluded that Models 1 and 5 will be viable candidates for use in the dynamic analysis. This is due to the stresses for both Model 1 and Model 5 falling within the allowable stress and being the closest to zero. Although, before a definite conclusion can be inferred, other comparisons must be made, as will be done in the sections that follow.

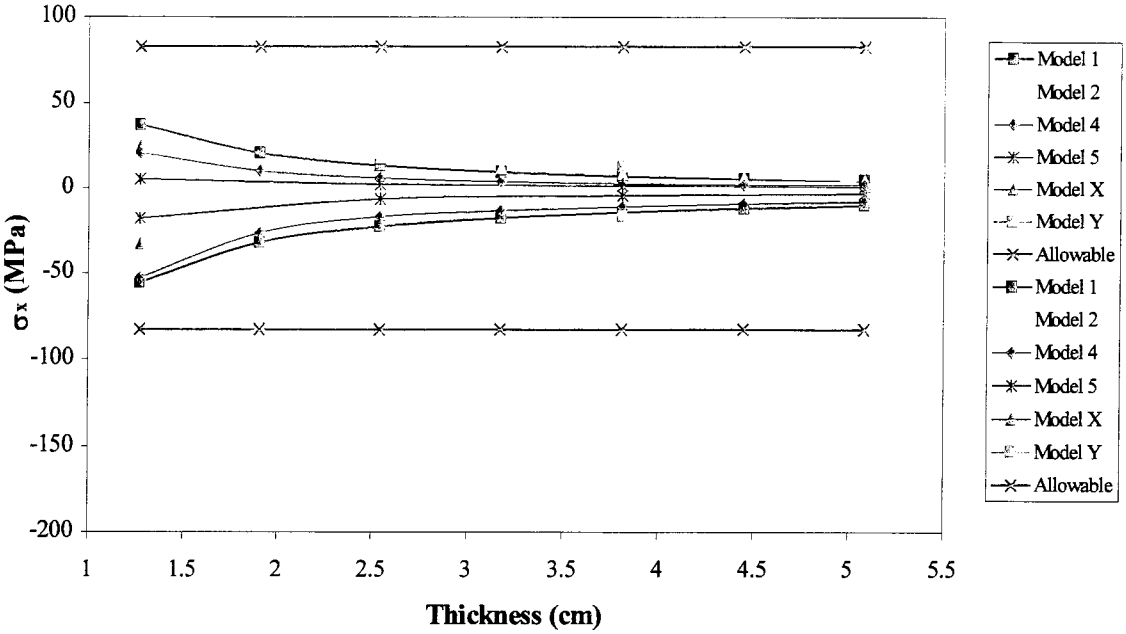

Figure 9-5 – σ_x stress comparison for varying thickness

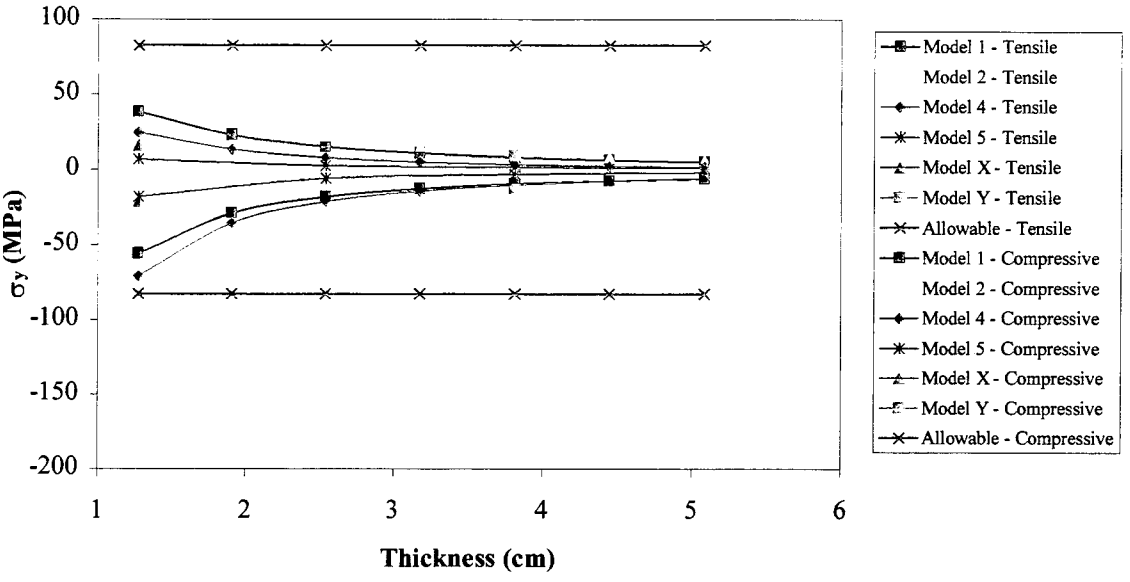

Figure 9-6 – σ_y stress comparison for varying thickness

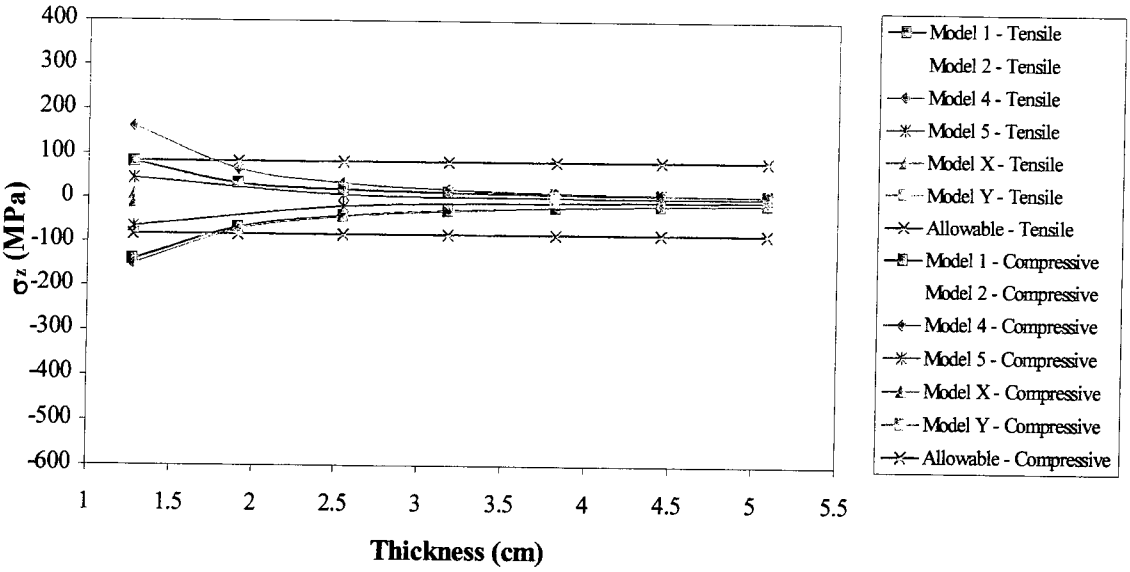

Figure 9-7 – σ_z stress comparison for varying thickness

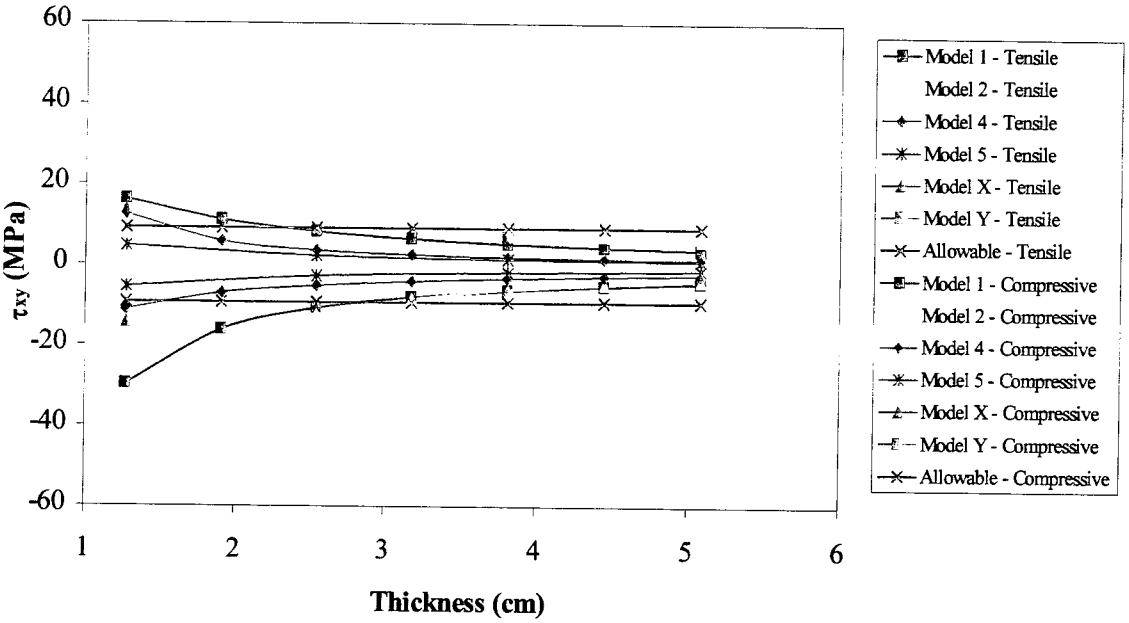

Figure 9-8 – τ_{xy} stress comparison for varying thickness

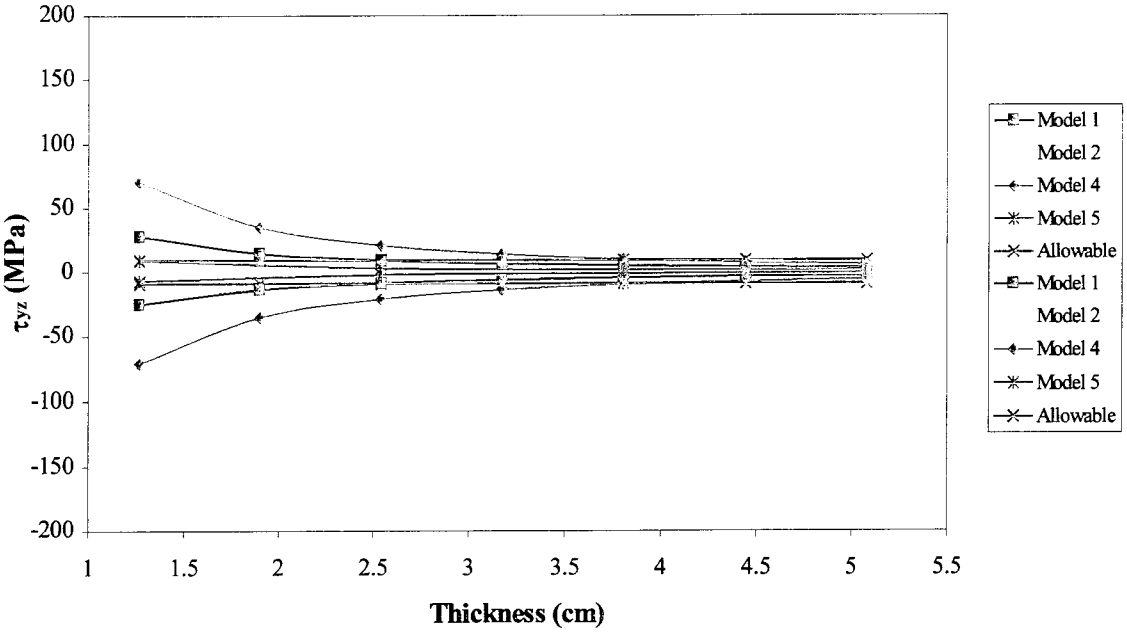

Figure 9-9 – τ_{yz} stress comparison for varying thickness

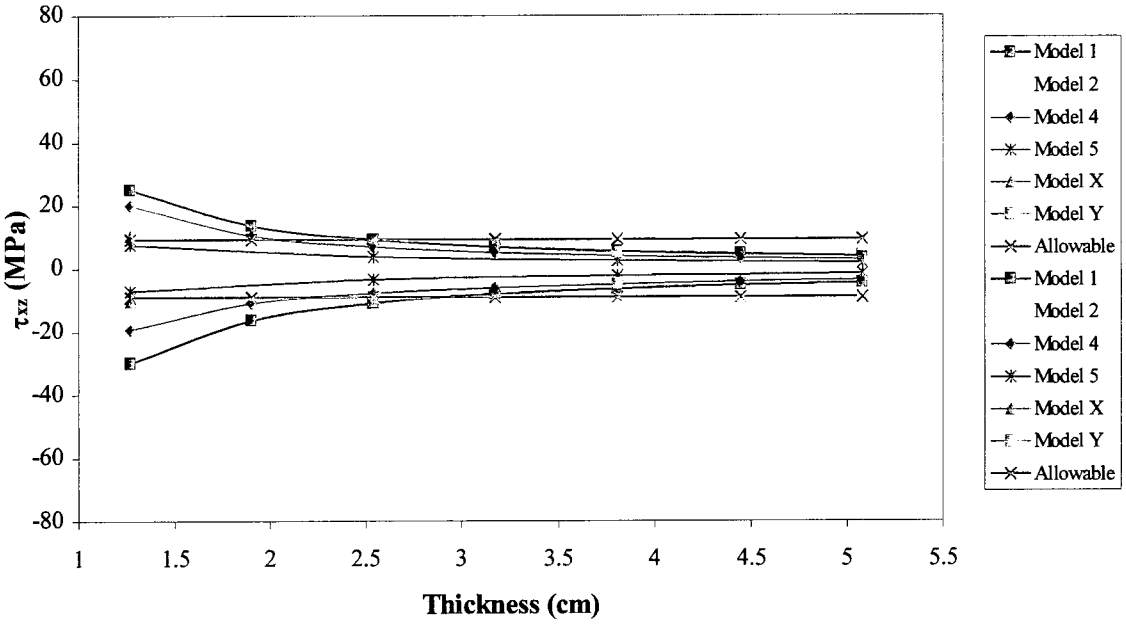

Figure 9-10 – τ_{xz} stress comparison for varying thickness

9.2 Slope of Webs

One other problem that was identified in the tube and sheet model analysis by Ballard [29] was that high local stresses occurred in some of the web locations, which was attributed to a potential web local buckling condition (See Figure 9-11). In this part of the study it was suggested that one way to remedy this problem is to angle the webs in the model. Hence, in this research two slopes were used, a 1:1 angle and a 2:1 angle. Figure 9-12 shows the comparison of the stresses between the Models 1 and 4, to determine how the angle of the web affects the stresses through out the model.

As can be seen from Figure 9-12, Model 4 performs better in some instances where Model 1 performs better in others. Therefore, it can be postulated that the angle of the web does not have a significant and clearly defined effect on the total stress. However, varying the slope of the web does improve the local stress problem that was encountered in the previous research of PART-A (See Figure 9-15). In this research, a comparison between the spacing of the webs and the stresses, as well as, the deflection needs to be done also, before a suitable model can be determined.

9.3 Distance between the webs

Another factor that can affect the stresses in the model is the spacing between the webs. The spacing between the webs does not only have a theoretical purpose, but a practical one as well. The spacing of the webs can be important when the deck may be bolted to the stringers. If a model has too little spacing between the webs, the bolts may not fit and therefore cause a constructibility problem. The models that could be compared

not fit and therefore cause a constructibility problem. The models that could be compared in this correlation are Model 2 versus Model 4 and Model 1 versus Model 5. The comparison of Models 2 and 4 are shown in Figure 9-13. In Figure 9-13 the bar graph shows that Model 4 performs better than Model 2 because the stresses are higher in Model 2, which has the webs further apart. In Figure 9-14, the comparison of Models 1 and 5 show that Model 5 performed better than Model 1 because the stresses are higher in Model 1 than Model 5, which has no spacing between the webs. Therefore, the spacing between the webs has a significant effect on the stress and from this Model 5 appears to be the most efficient, however, the deflection needs to be determined before the final choice can be made.

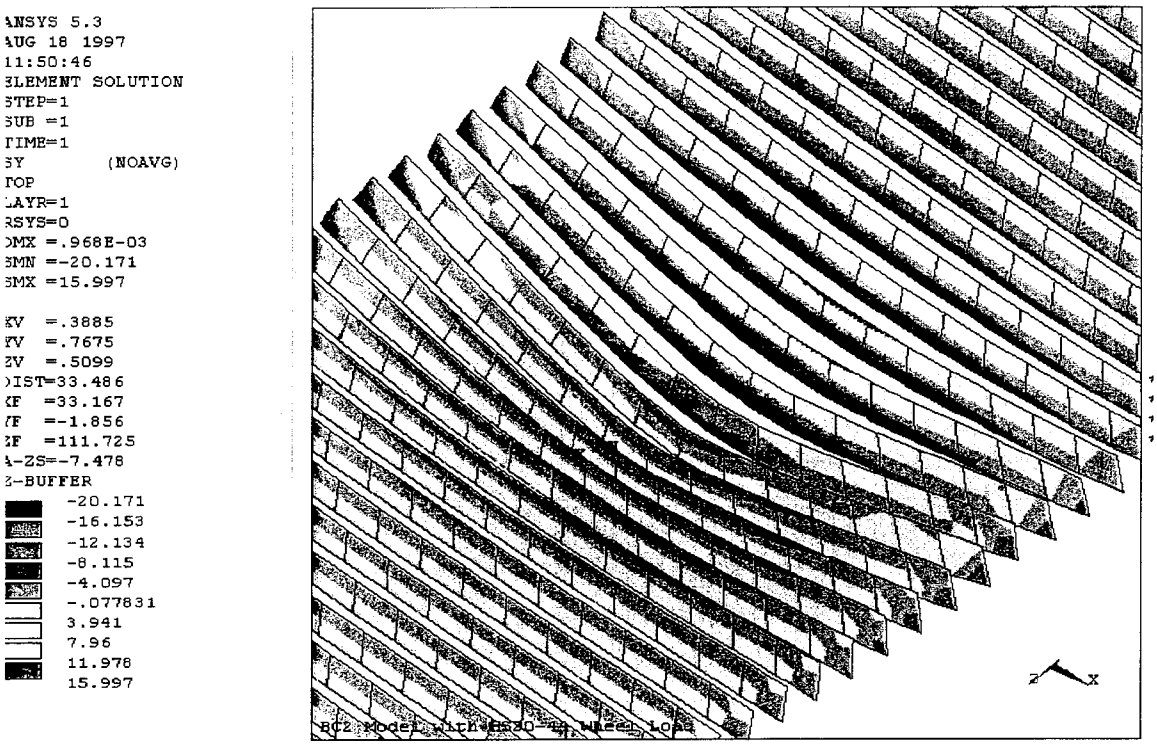

Figure 9-11 – Typical Distribution of σ_y (MPa) Stresses in the Webs of the Tubes [29]

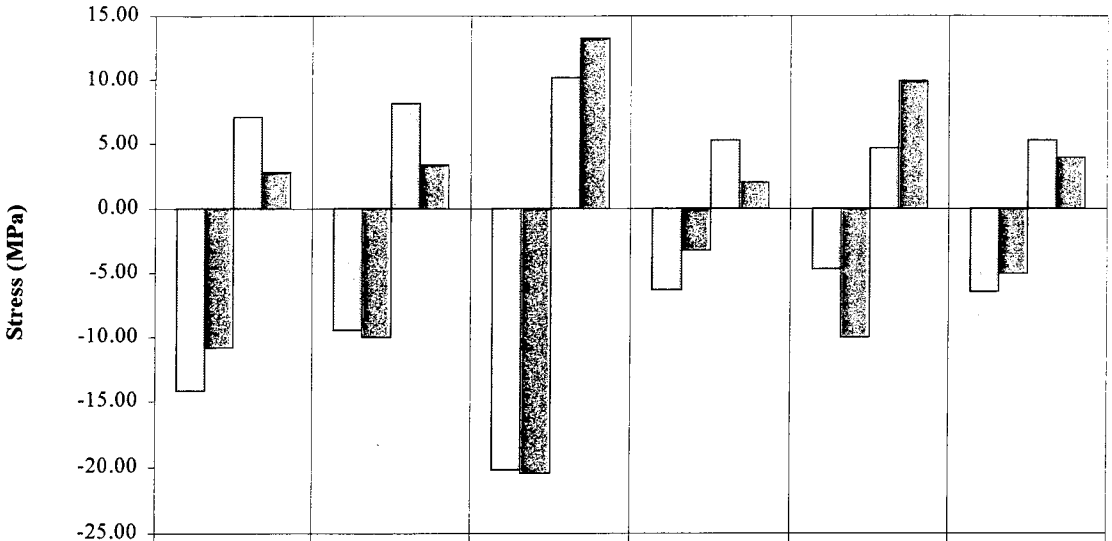

	sx (MPa)	sy (MPa)	sz (MPa)	txy (MPa)	tyz (MPa)	txz (MPa)
Model 1	-14.18	-9.42	-20.22	-6.27	-4.66	-6.45
Model 4	-10.78	-9.98	-20.48	-3.23	-9.98	-5.01
Model 1	7.10	8.18	10.18	5.31	4.71	5.31
Model 4	2.81	3.40	13.26	2.00	9.96	3.95

Figure 9-12 – Stress comparison of Model 1 and Model 4

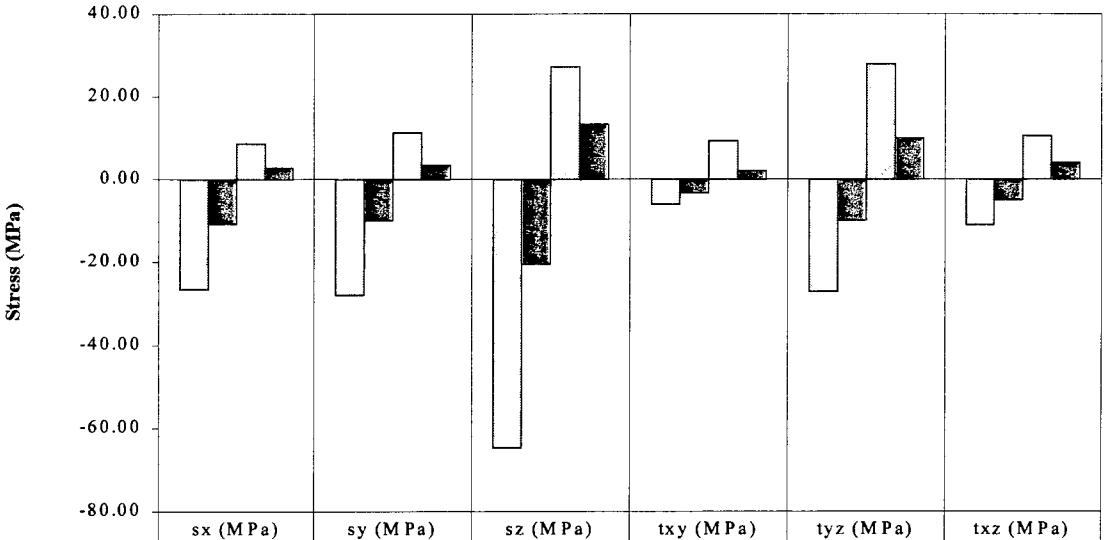

	sx (MPa)	sy (MPa)	sz (MPa)	txy (MPa)	tyz (MPa)	txz (MPa)
Model 2	-26.50	-27.95	-64.64	-6.11	-27.24	-11.03
Model 4	-10.78	-9.98	-20.48	-3.23	-9.98	-5.01
Model 2	8.69	11.22	27.27	9.20	27.95	10.55
Model 4	2.81	3.40	13.26	2.00	9.96	3.95

Figure 9-13 – Stress comparison of Model 2 and Model 4

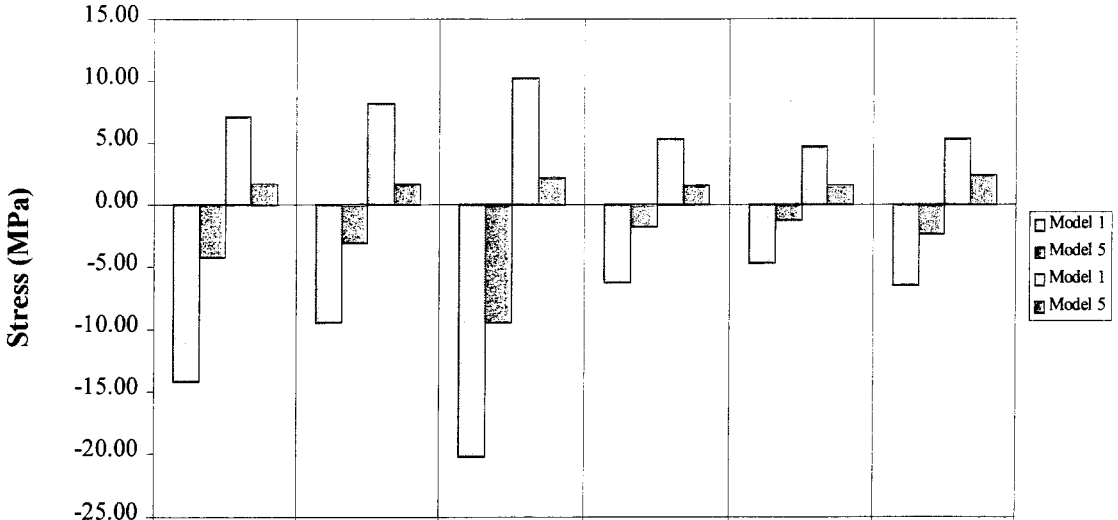

	sx (MPa)	sy (MPa)	sz (MPa)	txy (MPa)	tyz (MPa)	txz (MPa)
Model 1	-14.18	-9.42	-20.22	-6.27	-4.66	-6.45
Model 5	-4.20	-3.06	-9.44	-1.75	-1.21	-2.35
Model 1	7.10	8.18	10.18	5.31	4.71	5.31
Model 5	1.63	1.68	2.14	1.52	1.53	2.41

Figure 9-14 – Stress comparison of Model 1 and Model 5

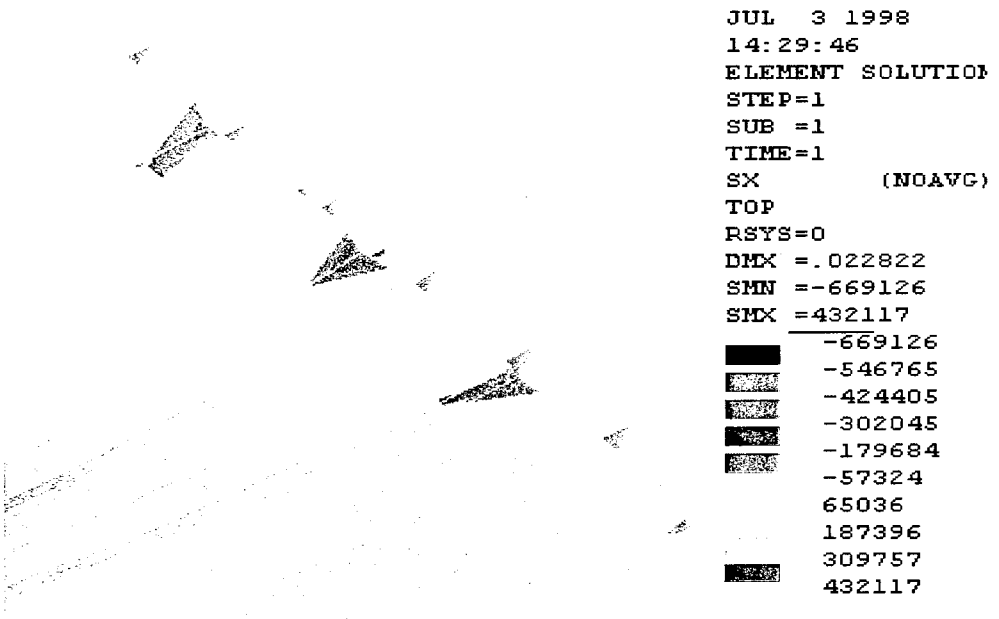

Figure 9-15 – Stresses at support for monolithic model

9.4 Deflection

Figure 9-16 is a graph of the deflection versus thickness for each model. The 'x' lines indicate an allowable deflection as per AASHTO [6] of L/500. As seen in the chart, Model 5 falls completely under the allowable deflection further emphasizing the feasibility of this model for further analysis.

The purpose of this chapter was to discuss the factors that were utilized in determining a feasible model for dynamic analysis. From the previous charts and data Model 5 has been determined to be the most reasonable monolithic section and Model Y to be the most reasonable tube and sheet model. In Chapters 10 and 11, these two models will be dynamically loaded and analyzed.

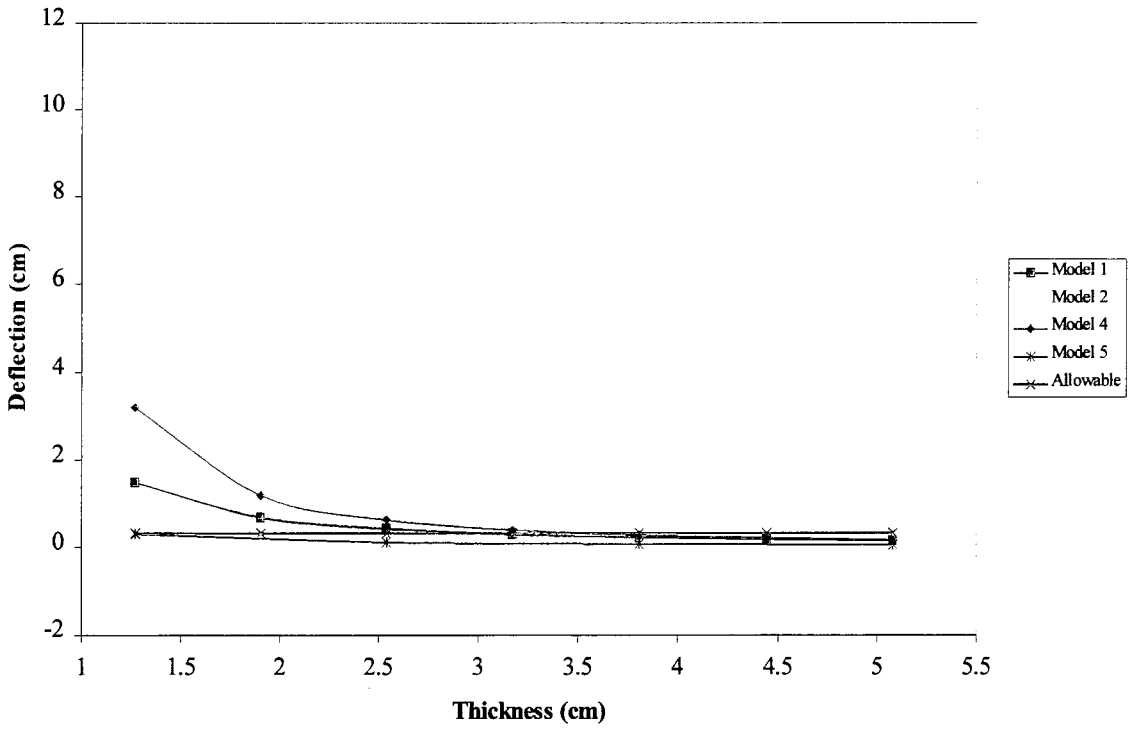

Figure 9-16 – Deflection vs. thickness comparison for all models

CHAPTER 10

FREE VIBRATION DYNAMIC ANALYSIS

In chapter 8 the importance of a dynamic analysis was discussed. As an extension of the static analysis discussed in Chapter 9, the free vibration dynamic analysis will be used to determine the mode shape and the natural frequency, where the forced vibration dynamic analysis will be used to determine the dynamic deflection in order to determine the dynamic load factor. Free vibration of a system is one with absence of external excitation [40]. The free vibration dynamic analysis data will be compared and analyzed, and a feasible section will then be chosen for the forced vibration dynamic analysis.

Every structural element has natural frequencies that can be determined without any type of load placed on it. These natural frequencies can be found by performing a free vibration dynamic analysis. The natural frequencies are crucial in determining if resonance can occur. Resonance is determined by comparing the frequency of the load on the bridge, in this instance a vehicle, to the natural frequencies of the bridge. If the frequency of the vehicle coming on to the bridge, or running across any surface irregularities, is close to any of the natural frequencies of the bridge, a calamitous failure of the bridge deck can occur which is known as resonance. This kind of failure has been popularized by the failure of the first Tacoma Narrows Suspension Bridge, popularly

known as Galloping Gertie, located over Puget Sound. The importance of determining the natural frequency can be seen in the manner that Galloping Gertie failed. (See Figures 10-1 and 10-2). This catastrophic failure was due to resonance effects caused by the bridge having a frequency close to the frequency of the wind, which was only at a speed of 19.67 m/s (44 mph). From the photos, the twisting of the bridge is obvious what eventually led to its demise and since then studies have determined that the bridge failed in resonance of one of the torsional modes.

Figure 10-1 – First Tacoma Narrows Suspension Bridge Action during Failure [39]

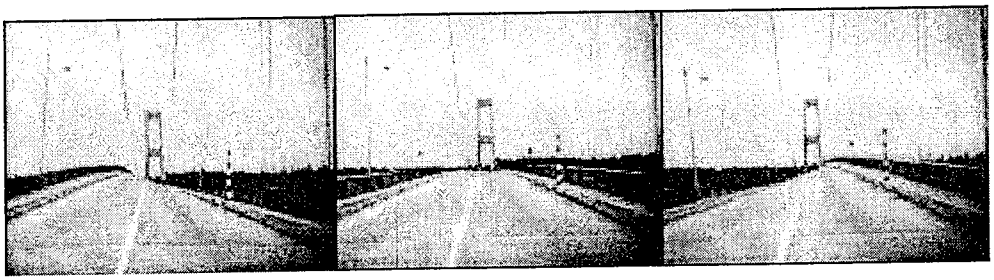

Figure 10-2 – First Tacoma Narrows Suspension Bridge Action during Failure [39]

The mode shape, which can also be determined from a free vibration dynamic analysis, corresponds to the natural frequencies. The modal shapes, or normal modes, are

the relative displacements at the coordinates of a multi-degree of freedom system vibrating at one of the natural frequencies [40]. The fundamental mode shape generally refers to the mode associated with the lowest frequency. In this study, the mode shapes and natural frequencies of the bridge deck are determined from utilizing the modal analysis command in ANSYS 5.3. The ANSYS 5.3 modal analysis command allows the extraction of several modes if necessary. Using these dynamic analysis capabilities, a free vibration analysis was performed on Model 1, Model 4, Model 5, and Model Y, which would determine an appropriate model to be further analyzed with varying spans of 11.58 m (38'-0"), and 17.37 m (57'-0"), as well as for the forced vibration analysis. The intent of studying the frequency for varying span lengths is to determine how long a bridge span made of the deck systems being studied in this project, could be before the frequency would become a major factor to its stability.

Model Designation	Uniform thickness	Span Lengths
Model 1	2.54 cm and 3.81 cm (1" and 1½")	1.65 m x 5.79 m (5'-5" x 19'-0")
Model 4	2.54 cm (1")	1.65 m x 5.79 m (5'-5" x 19'-0")
Model 5	1.91 cm and 2.54 cm (¾" and 1")	1.65 m x 5.79 m (5'-5" x 19'-0") 1.65 m x 11.58 m (5'-5" x 38'-0") 1.65 m x 17.37 m (5'-5" x 57'-0")
Model Y	3.81 cm (1½")	1.65 m x 5.79 m (5'-5" x 19'-0")

Table 10-1 – Model Characteristics for the Free Vibration Dynamic Analysis

Table 10-1 summarizes the different models and the uniform thicknesses used in this dynamic analysis. Determination of the model to be further analyzed, with varying span lengths, cannot be done by simply observing the charts in Figures 10-4 to 10-8, because the frequency does not vary greatly for the different monolithic models. However, Figure 10-7 does show that Model Y, the tube and sheet model, has a very low fundamental natural frequency, which is close to 4.0 Hz. This natural frequency could lead to possible resonance since the frequency of the vehicle is assumed to be in the neighborhood of 3.0 Hz, from the equation derived from Williams [36]. Figure 10-9 is a graph showing the variation of wheel base length to frequency, where Figure 10-3 shows the set up of an HS20-44 truck including the wheel loads and wheel base spacing per AASHTO.

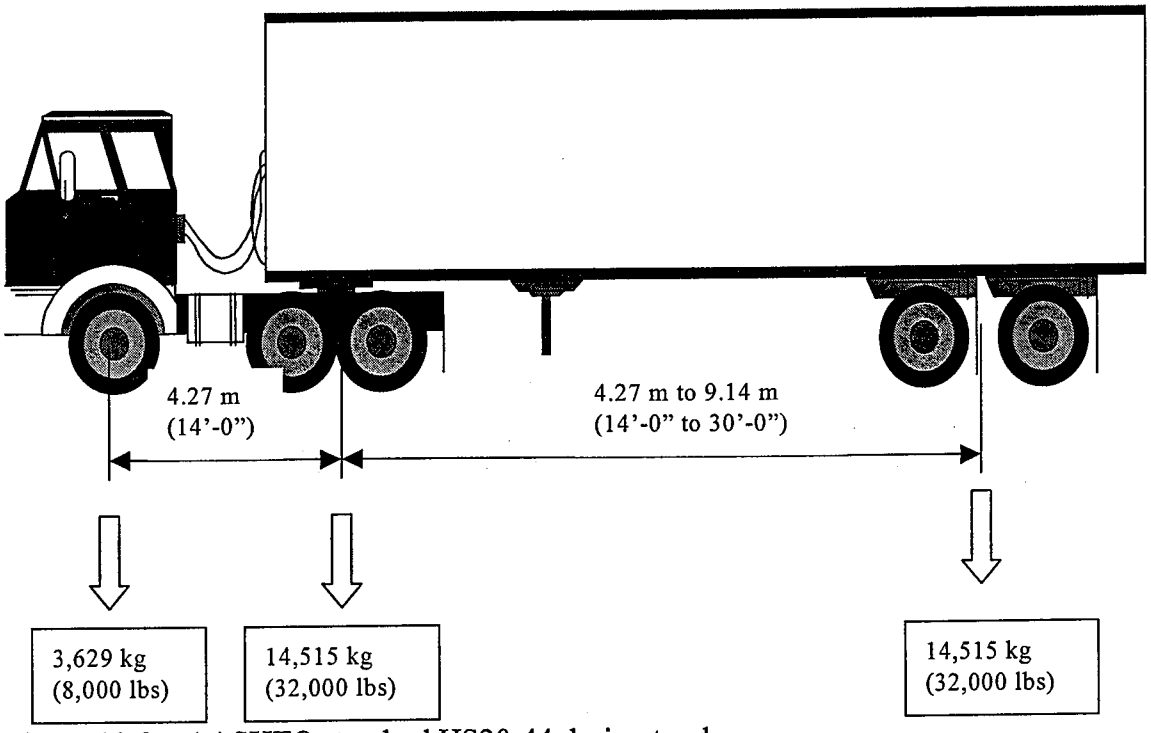

Figure 10-3 – AASHTO standard HS20-44 design truck

Since the frequency versus mode shape data for the monolithic models of various thicknesses was inconclusive, in order to determine which model is the most reasonable to further analyze, the static analysis results and conclusions will be required to determine a model that will be analyzed for different span lengths. As concluded in Chapter 9, Model 5 will be the most reasonable and will be analyzed for a 11.58 m (38'-0") span and a 17.37 m (57'-0") span. Figure 10-10 shows the projection of span length versus the frequency.

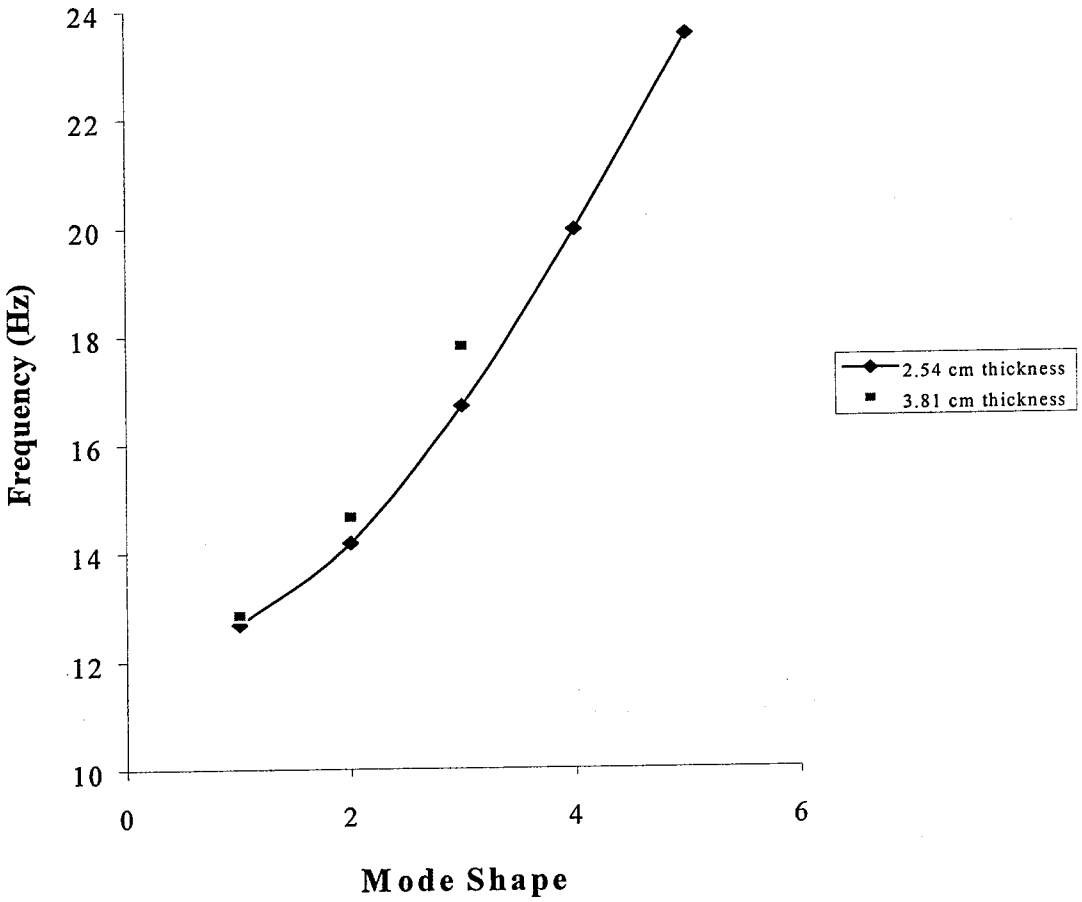

Figure 10-4 – Mode Shape vs. Frequency for Model 1

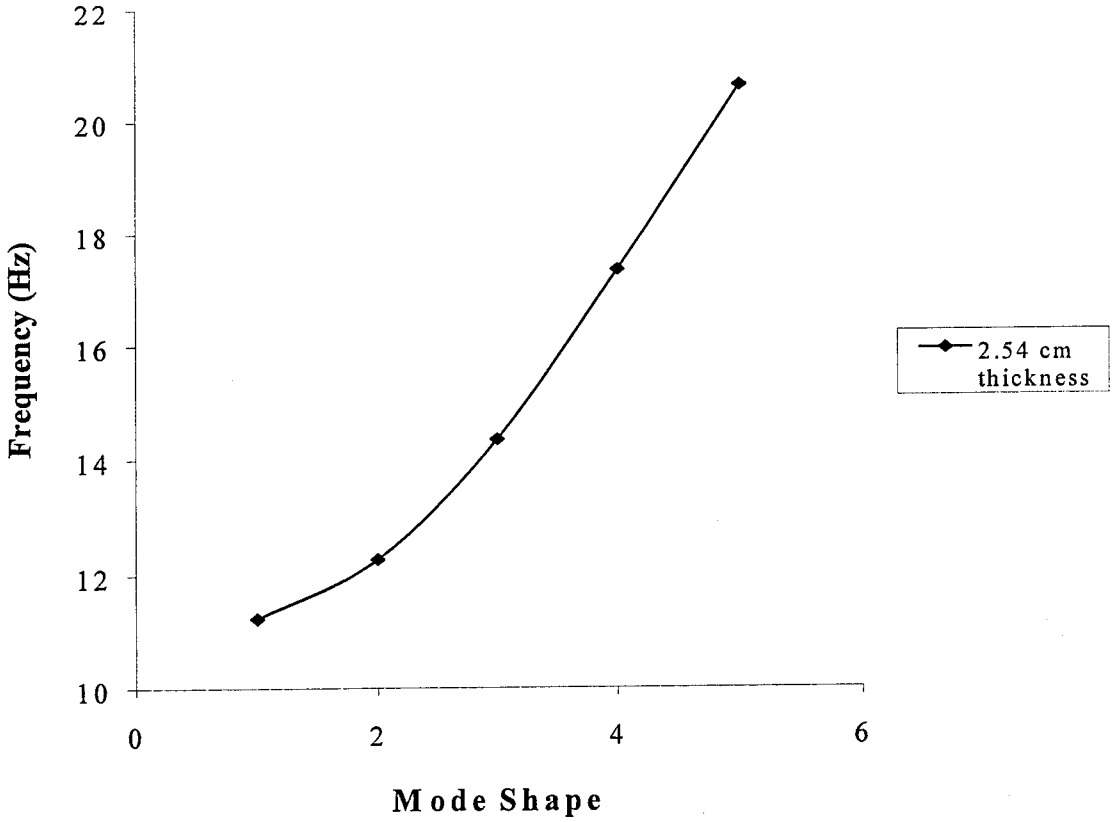

Figure 10-5 – Mode Shape versus Frequency for Model 4

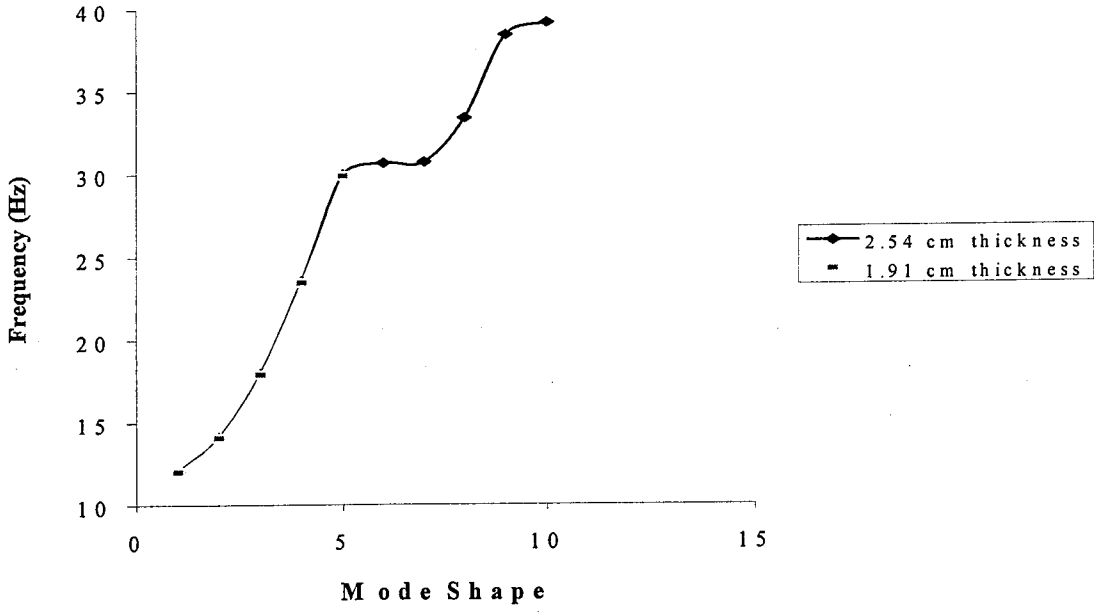

Figure 10-6 – Mode Shape vs. Frequency for Model 5

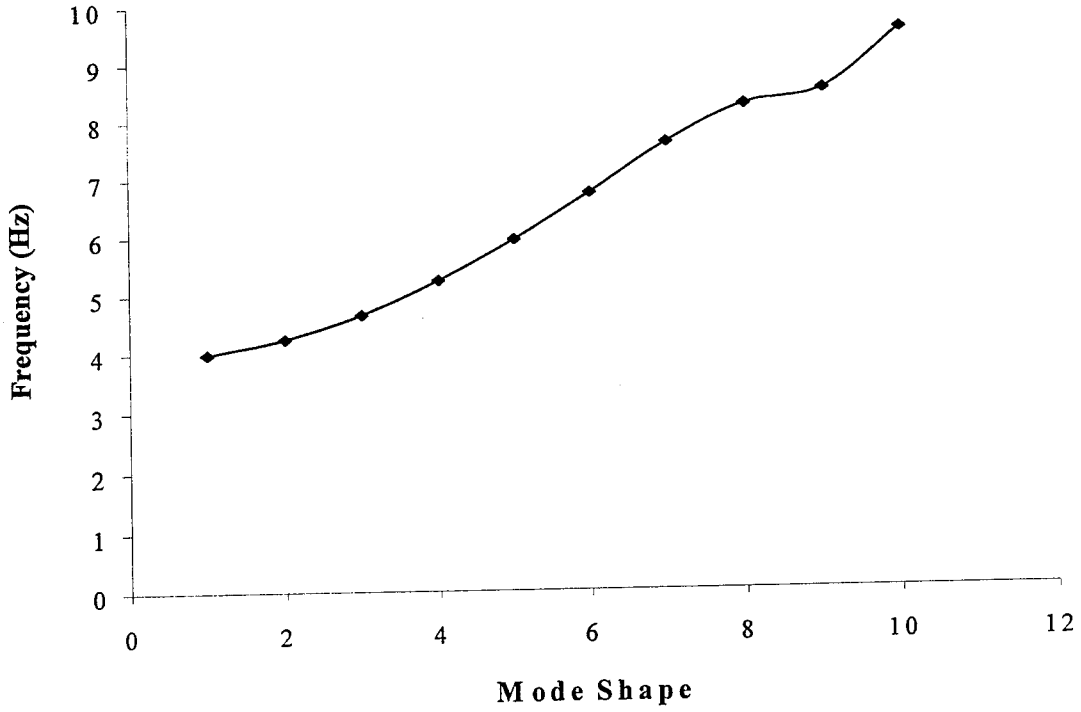

Figure 10-7 – Mode Shape vs. Frequency for Tube and Sheet Model

For Model 5 and Model Y, ten mode shapes were extracted from the dynamic analysis results. From observing Figures 10-6 and 10-7, it can be seen that after the 5^{th} mode shape the curve begins to flatten indicating that the frequency does not vary much after the 5^{th} mode shape. This phenomenon help to emphasize why the fundamental mode shape is the most important one needed in the mathematical calculation of the frequency.

Figures 10-4 through 10-8 are comparing the dynamic analysis data for the models stated in Table 10-1. From these graphs the same comparisons performed in Chapter 9 for thickness, slope of the webs, and distance between the webs can be done

for the dynamic analysis results. In observation of the graphs, it can be hypothesized that the thickness, a specific slope of the web, and distance between the webs does not have a significant effect on the fundamental frequency of the model. However, it does appear that simply sloping the webs does effect the frequency which can be seen from comparing the tube and sheet model, which has perpendicular webs, to the monolithic models that have a sloped web. The frequency for the tube and sheet model is considerably less than that of the models with sloped webs.

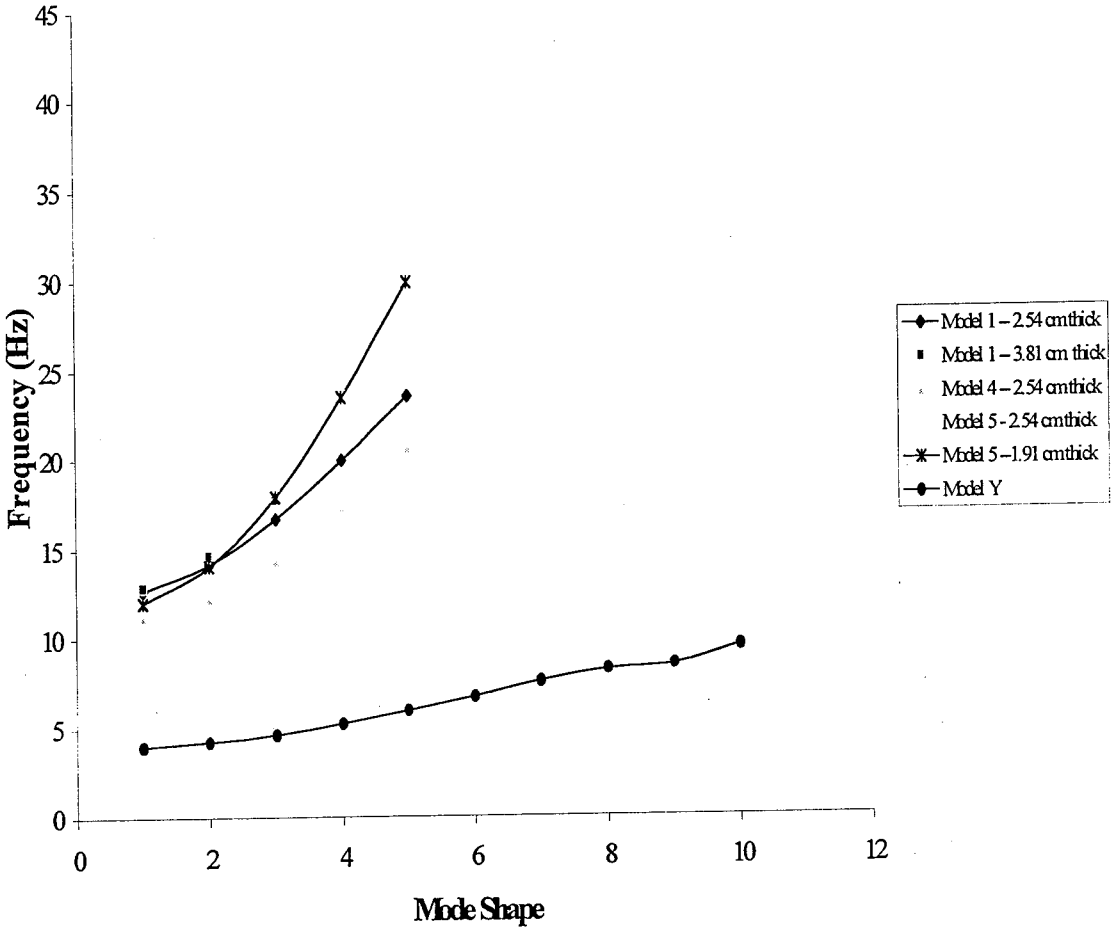

Figure 10-8 – Mode Shape vs. Frequency for all models analyzed

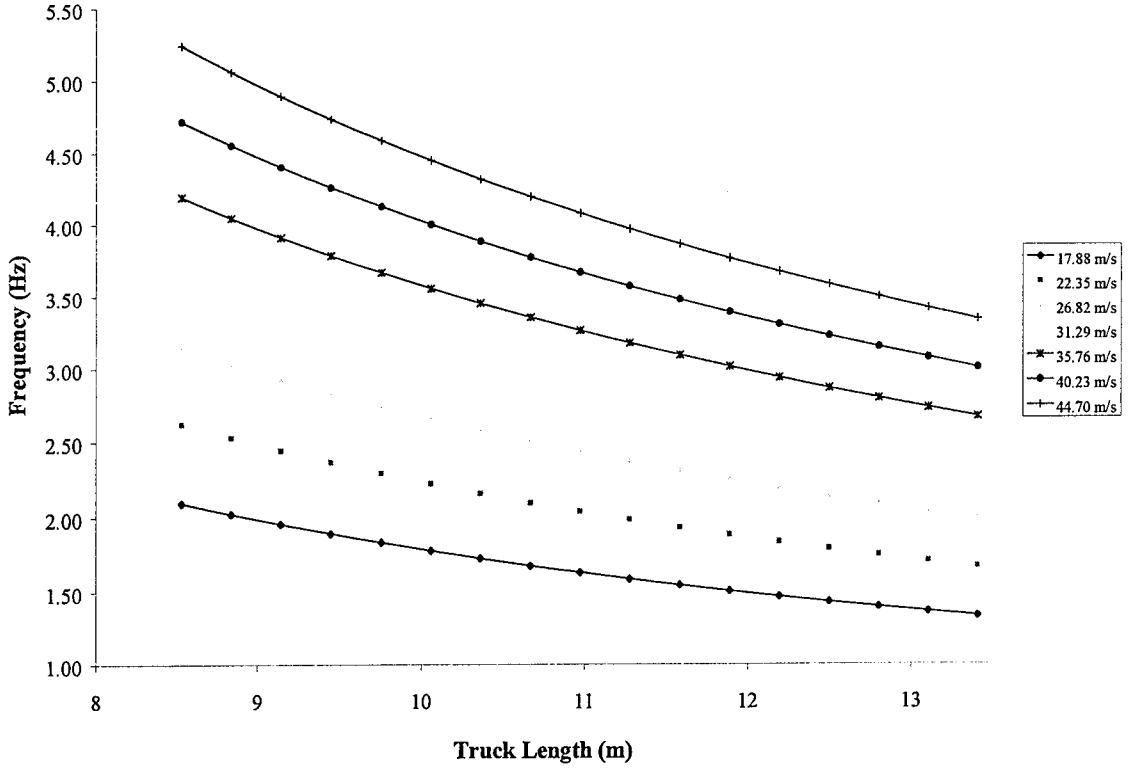

Figure 10-9 – Wheel Base Length vs. Frequency for Varying Speeds

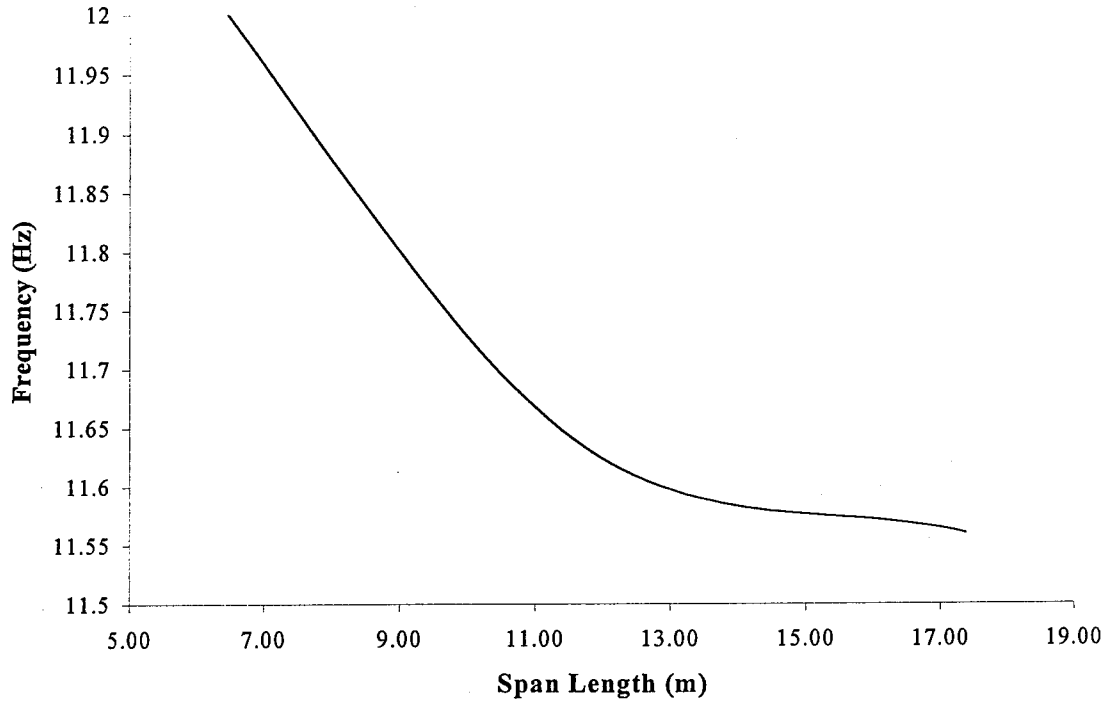

Figure 10-10 -- Span Length Versus Frequency

Figure 10-9, Wheel Base Length vs. Frequency for Varying Speeds, was included in this study in order to show how speed and wheel base length affect the frequency, also, to determine if the assumed value of 3.0 Hz was sufficient. Since the speed of a vehicle on a bridge can range from 17.88 m/s to 44.70 m/s (40mph to 100mph) this range was used in the relationship derived from Williams [36] and the truck length was based on an HS20-44 truck as shown in Figure 10-3. This relationship is:

$$f = \frac{S}{L} \qquad (10\text{-}1)$$

where, f = frequency
S = Speed of vehicle in feet per second (17.88 m/s to 44.70 m/s)
L = Length of Truck (8.53 m to 13.41 m)

The purpose in varying the span length was to determine if the length of the span has any effect on the frequency of the bridge deck. It was hypothesized that the longer the bridge deck the lower the frequency will become. This investigation was used to also determine if resonance would be reached for the longer span of the deck. As can be seen in Figure 10-10, the longer the span length is, the lower the frequency truly is. However, the span length variation was stopped at a span length of 17.37 m (57'-0"), which, is deemed a reasonable maximum span length for a typical movable bridge of the type being investigated.

The initial mode shapes for each model are shown in Figures 10-11 to 10-14. These mode shapes show an inflection in the middle, which helps to visualize the natural frequency. As the mode shape increases the number of inflections increase. Figures 10-15 and 10-16 indicate the additional mode shapes for Model 5. As can be seen in the figures the mode shapes have an additional convexity and concavity as the mode shape

number increases, which can indicate the higher frequency that occurs as the mode shape increases. Since the frequency increases as the mode shape increases, it is obvious why the fundamental mode is often considered the most crucial.

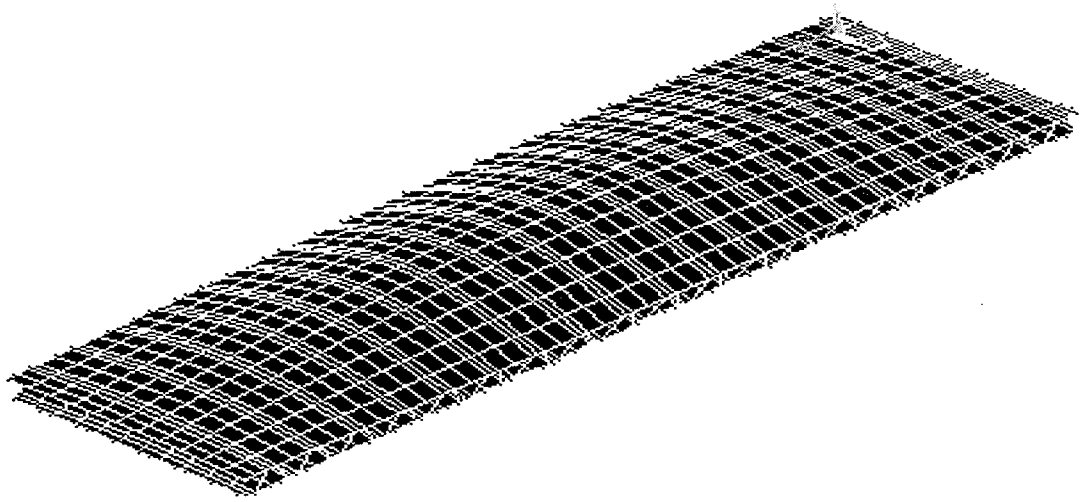

Figure 10-11 – Initial Mode Shape for Model 1 – Natural Frequency = 12.68 Hz

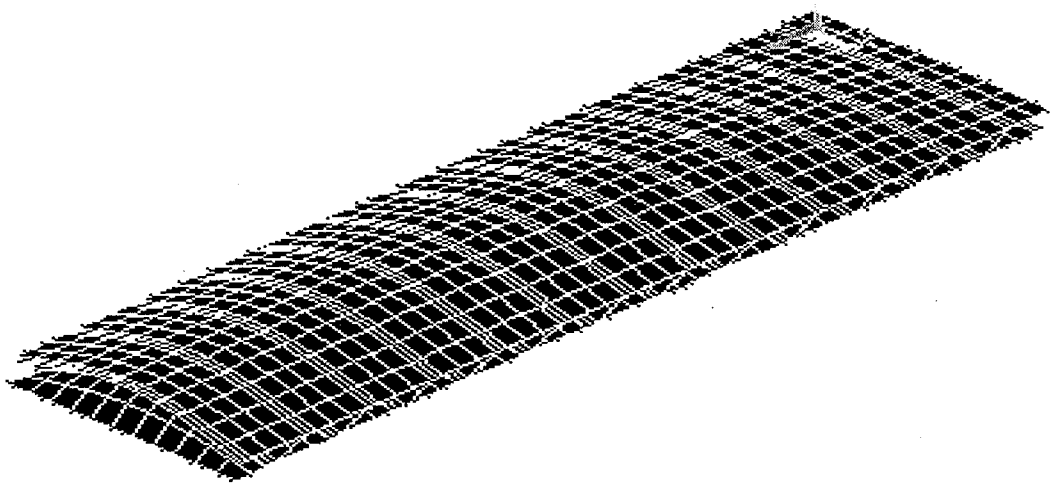

Figure 10-12 – Initial Mode Shape for Model 4 – Natural Frequency = 11.24 Hz

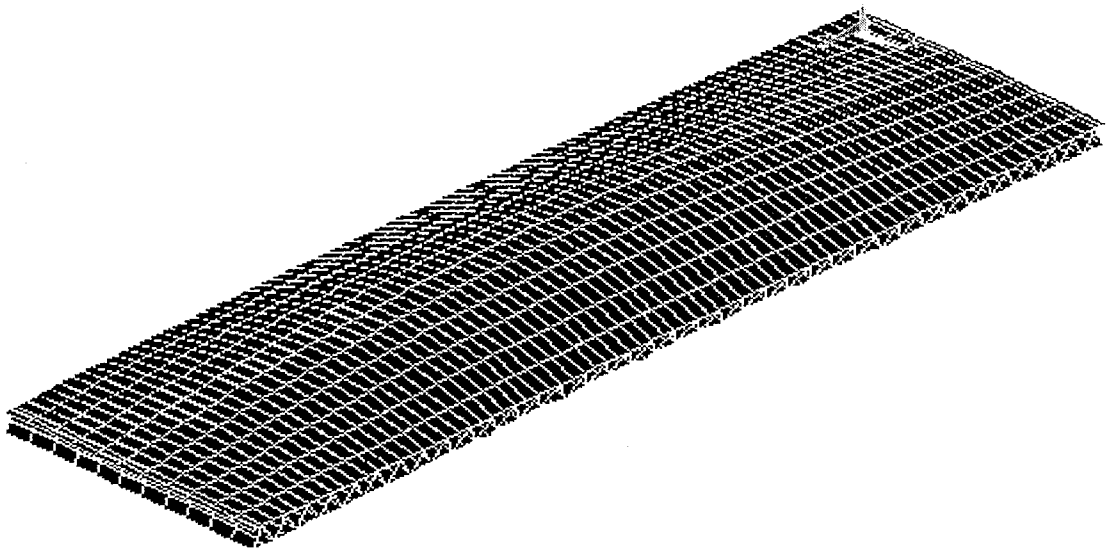

Figure 10-13 – Initial Mode Shape for Model 5 – Natural Frequency = 12.05 Hz

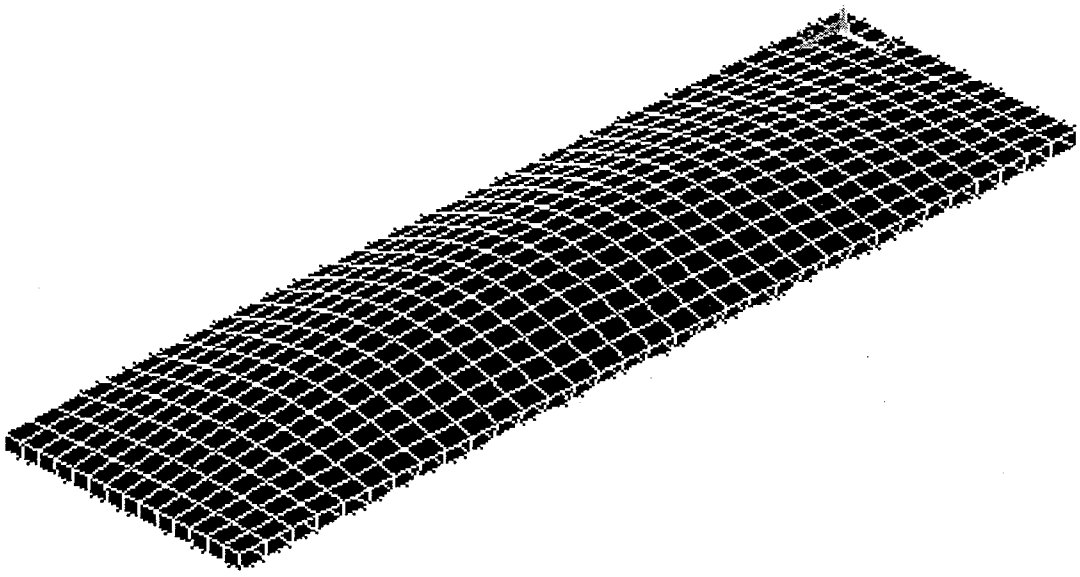

Figure 10-14 – Initial Mode Shape for Model Y – Natural Frequency = 3.98 Hz

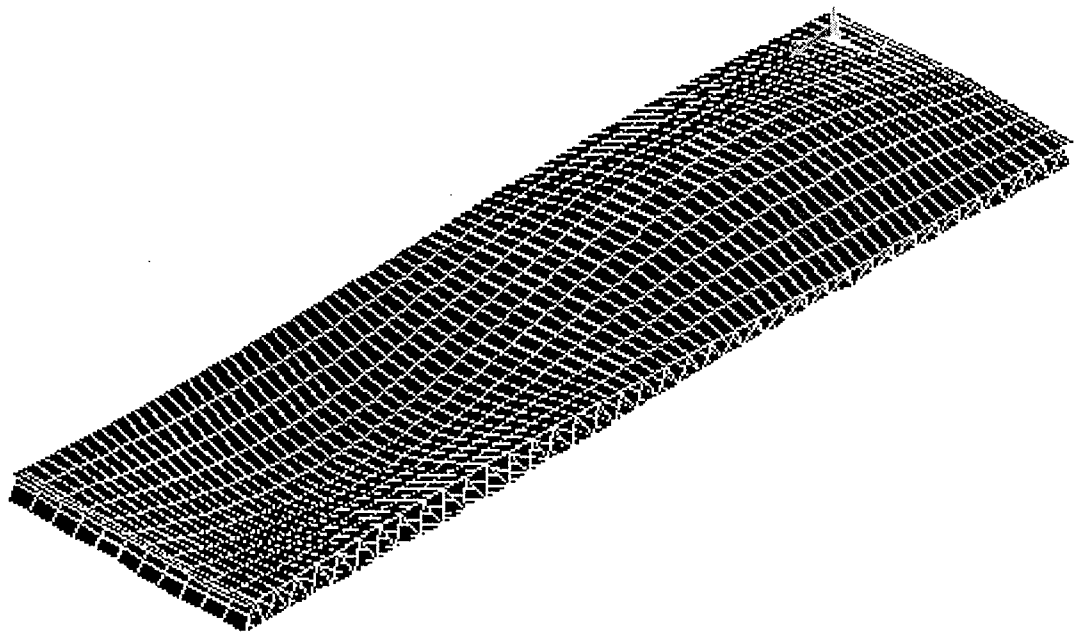

Figure 10-15 – Second Mode Shape for Model 5 – Natural Frequency = 14.11 Hz

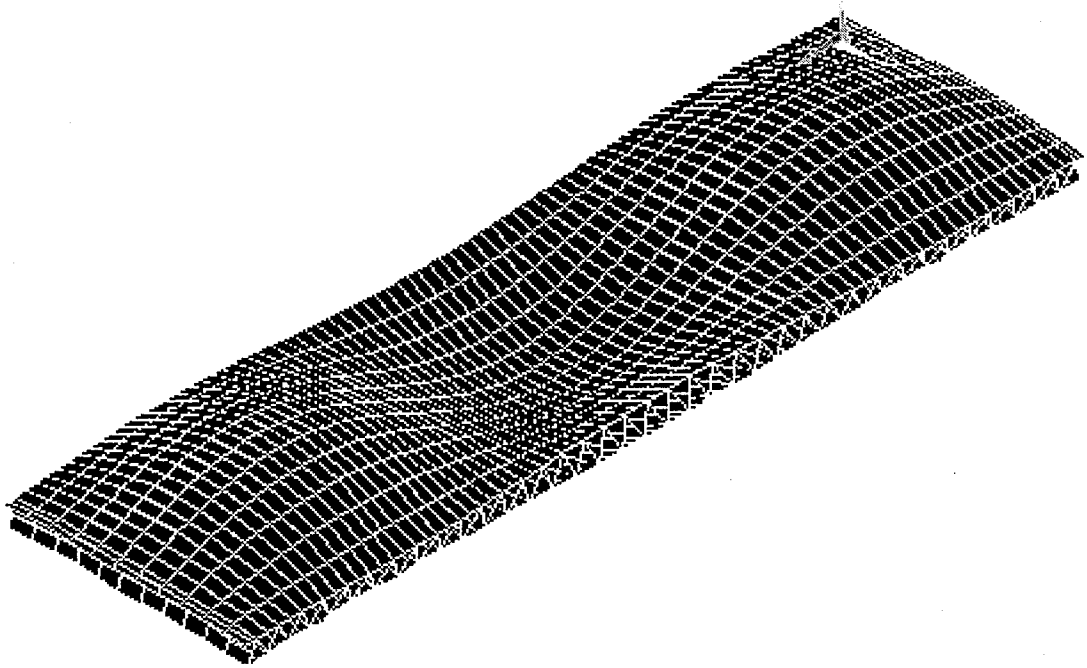

Figure 10-16 – Third Mode Shape for Model 5 – Natural Frequency = 17.97 Hz

CHAPTER 11

FORCED VIBRATION DYNAMIC ANALYSIS

Forced vibration is vibration in which the response is due to an external loading [40]. From Chapter 10 it can be summarized that Model 5 is the most viable model to utilize in this portion of the research. One purpose for the forced vibration dynamic analysis is to determine if the impact factor of 1.3 used in the static analysis portion of this research was adequate. The impact factor referred to in this chapter is equivalent to the dynamic load factor, DLF, mentioned in Chapter 8.

In order to determine the DLF, a harmonic response analysis is chosen for use in this study. This method of analysis is used to determine the steady-state response of a linear structure to loads that vary sinusoidally with time [25], it was assumed that the sinusoidal forcing function is representative of vehicular vibration on the bridge. Through this analysis the dynamic deflection, $\delta_{dynamic}$, can be determined as well as the stresses due to dynamic loading. In order to have enough data for a reasonable comparison, the static analysis on Model 5 was rerun without the impact factor of 1.3 included in the load. With this data extracted, a full analytical conclusion can be drawn for this research.

One element that goes into a dynamic analysis that has not been discussed to this point is the damping coefficient. The use of the damping coefficient is valid for every structural element because every material has an inherent damping capability. The property of damping is the ability of a structure to absorb structural vibration [40]. For this research, Table 11-1 details the damping coefficients that were obtained from Mallick [37], which are not percentages. Additionally, Mallick [37] states that Hwang and Gibson [38] have published a review of recent applications of the strain energy/finite element approach in the analysis of damping in composite materials. This approach has been used to study many aspects of damping in FRP such as the effects of fiber aspect ratio, fiber spacing, and fiber/ matrix interphase [37] and was used in determining the damping coefficients in Table 11-1.

Material	Fiber Orientation	Modulus (GPa)	Damping Factor
E glass/ Epoxy	0°	35.2	0.007
Carbon/ Epoxy	0° 22.5° 90° $[0/22.5/45/90]_S$	188.9 32.4 6.9 69	0.0157 0.0164 0.0319 0.0201
Low Carbon Steel		207	0.0017
6061 aluminum alloy		70	0.0009

Table 11-1 – Damping coefficients of Polymeric Matrix Composites [37]

In Table 11-1 the designation $[0/22.5/45/90]_S$ indicates a composite with eight layers that have fiber directions of 0°, 22.5°, 45°, and 90°. The subscript 'S' on the

outside of the brackets indicates that the composite is symmetric. This means that the first four layers have the above mentioned angles and the final four layers have angles of 90°, 45°, 22.5°, and 0°, respectively. However, for this study, no particular type of fiber orientation per layer is not specifically accounted for, since this research has been done on the macro level. The damping coefficient assumed from Table 11-1 is based on conclusions drawn from Ballard's [29] research. Although not explicitly stated as the fiber material of choice, most of the data and literature review revealed that the most common fiber type is that of E-glass. Therefore the damping coefficient of 0.007 will be used in the forced vibration dynamic analysis.

The deflection results from the dynamic analysis are given in Table 11-2. This dynamic analysis consisted of placing a wheel load in the center of the deck and varying the forcing frequency from 0 to 20 Hz. This forcing frequency range was used so the deflection due to the natural frequency, as well as, the deflection due to the vehicle frequency could be observed

Model	**Dynamic Deflection mm (in)**		**Static Defl. mm (in)**	**DLF or Impact Factor**	
	@ Vehicle Frequency = 3 Hz	**@ Natural Frequency**		**@ Vehicle Frequency = 3 Hz**	**@ Natural Freq.**
Model 1	-0.04 (-0.0015)	-0.50 (-0.019)	0.167 (0.0066)	0.239	2.99
Model 4	-0.28 (-0.0111)	0.04 (0.00154)	0.188 (0.0074)	1.49	0.212
Model 5	-0.22 (-0.00086)	0.74 (0.0292)	0.352 (0.0138)	0.625	2.10

Table 11-2 – Comparison of Dynamic Load Factors (DLF)

From Table 11-2, it can be seen that the DLF determined from this dynamic analysis is close to the 1.3 impact factor given by AASHTO. The deflection values at the vehicle frequency are the deflections that theoretically occur during normal operating conditions. The deflection values at the natural frequency are to show that a higher deflection occurs when the deck is close to resonance. However, this frequency would not be reached under normal operating conditions. These DLF values show that a dynamic analysis may be required, in some instances, to obtain more accurate stresses where, in most cases, simply applying the 1.3 impact factor to the load will yield sufficient results for design. However, a more detailed analysis utilizing a moving load would feasibly give more accurate DLF results.

From Table 11-2, Model 5 has the lowest DLF value of all three models, which further shows the potentiality of this cross section in the application discussed in this study. Figures 11-1 through 11-3 show how the deflections vary over the forcing frequency range.

One other way to show the importance of the impact factor is to compare dynamic analysis results to static analysis results. Table 11-3 shows the maximum stresses for the dynamic and static analyses. The dynamic stresses are chosen close to the natural frequency of the deck and are therefore worst case scenarios. From Table 11-3 it can be seen that the dynamic stresses are considerably higher than those from a simple static analysis are.

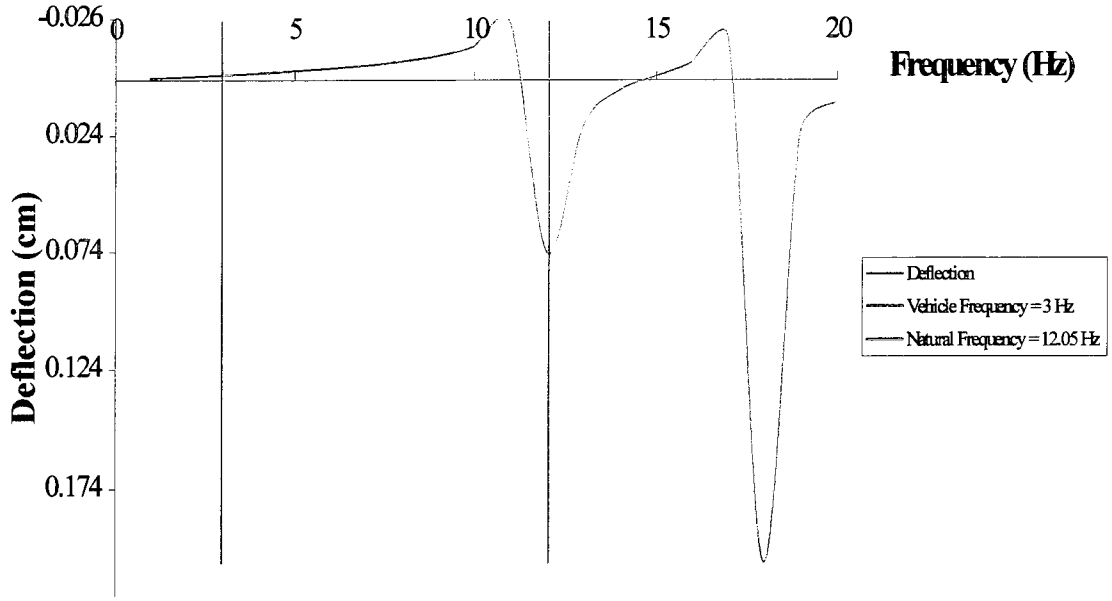

Figure 11-1 – Model 5 Deflection vs. Frequency

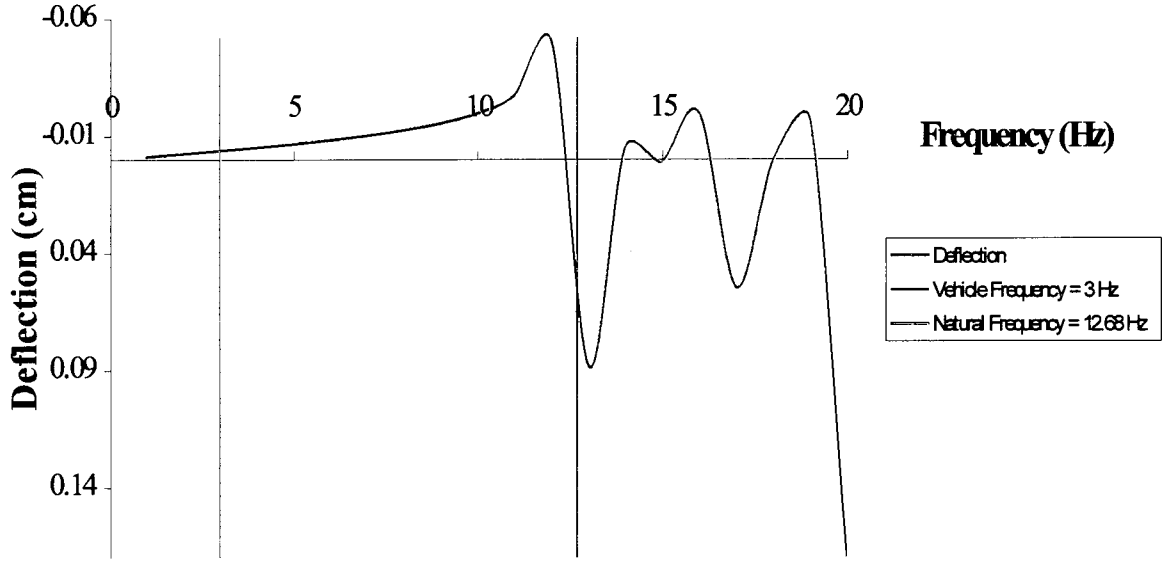

Figure 11-2 – Model 1 Deflection vs. Frequency

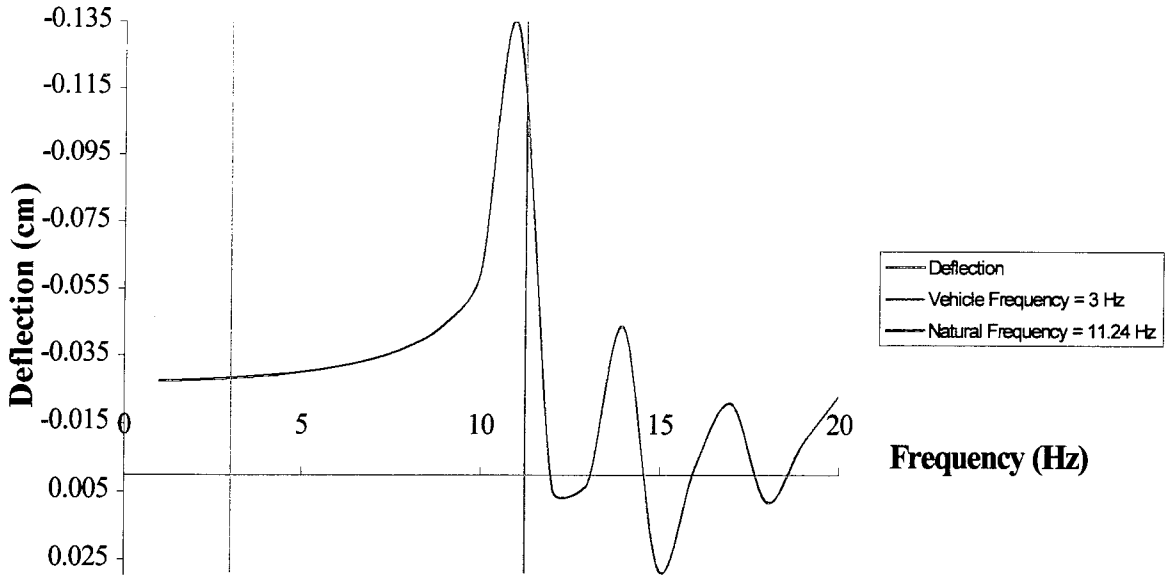

Figure 11-3 – Model 4 Deflection vs. Frequency

One other comparison that needs to be made is between the forced vibration dynamic results and the results from the static analysis with impact factor used. Table 11-3 shows the comparison of the dynamic analysis, static analysis with impact factor, and static analysis without the impact factor. Looking at Table 11-3 and the σ_x stresses, it can be seen that the dynamic analysis yields a σ_x stress of –8.827 MPa (-184356 psf) (tensile stress) while the static analysis without the impact factor yields a σ_x stress of –1.99 MPa (-41570 psf) (tensile stress). These values can be compared to show that $\sigma_{x,dynamic}$ is approximately 4 times that of $\sigma_{x,static\ w/o\ impact}$.

	σ_x MPa (psf)	σ_y MPa (psf)	σ_z MPa (psf)	τ_{xy} MPa (psf)	τ_{yz} MPa (psf)	τ_{xz} MPa (psf)
Static w/out impact	-1.99 (-41570)	-0.778 (-16257)	-3.189 (-66600)	-0.817 (-17071)	-0.372 (-7769)	-1.169 (-24407)
	0.692 (14449)	0.593 (12394)	1.099 (22953)	0.815 (17014)	0.389 (8129)	1.075 (22450)
tatic with impact	-6.373 (-133112)	-5.796 (-121053)	-18.628 (-389063)	-2.670 (-55761)	-2.202 (-45994)	-3.564 (-74438)
	2.408 (50284)	2.630 (54934)	8.180 (170839)	2.330 (48655)	2.898 (60526)	3.662 (76487)
Dynamic Analysis	-8.827 (-184356)	-6.618 (-138213)	-17.279 (-360885)	-5.810 (-121339)	-2.896 (-60493)	-5.898 (-123189)
	8.417 (175803)	4.645 (97017)	10.177 (212545)	5.246 (109565)	3.241 (67694)	6.048 (126323)

Table 11-3 – Dynamic and Static Stresses for Forced Dynamic Analysis of Model 5

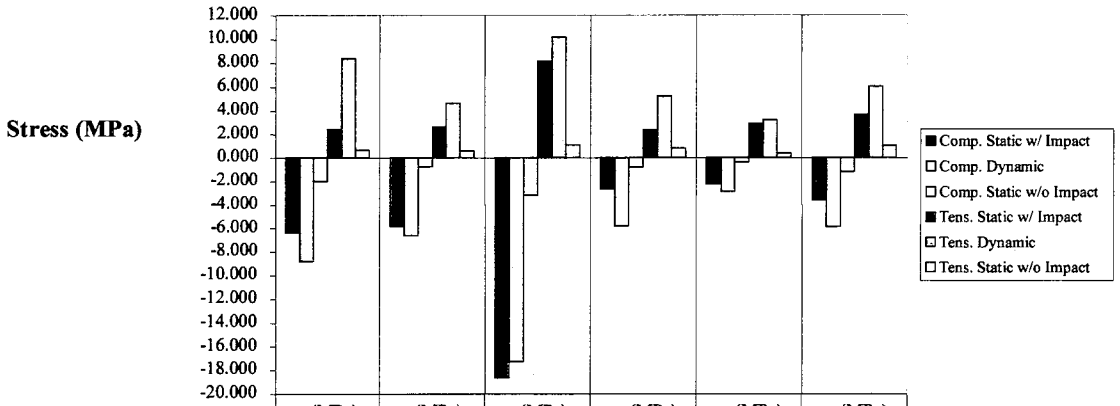

	sx (MPa)	sy (MPa)	sz (MPa)	txy (MPa)	tyz (MPa)	txz (MPa)
Comp. Static w/ Impact	-6.373	-5.796	-18.628	-2.670	-2.202	-3.564
Comp. Dynamic	-8.827	-6.618	-17.279	-5.810	-2.896	-5.898
Comp. Static w/o Impact	-1.990	-0.778	-3.189	-0.817	-0.372	-1.169
Tens. Static w/ Impact	2.408	2.630	8.180	2.330	2.898	3.662
Tens. Dynamic	8.417	4.645	10.177	5.246	3.241	6.048
Tens. Static w/o Impact	0.692	0.593	1.099	0.815	0.389	1.075

Figure 11-4 – Comparison of Dynamic Analysis, Static Analysis w/ Impact, and Static Analysis w/o Impact

One phenomenon that was seen in the forced vibration dynamic analysis was that as the frequency increased, the stress diagrams began to take the shape of the mode. Figures 11-5 to 11-8 illustrates this phenomenon.

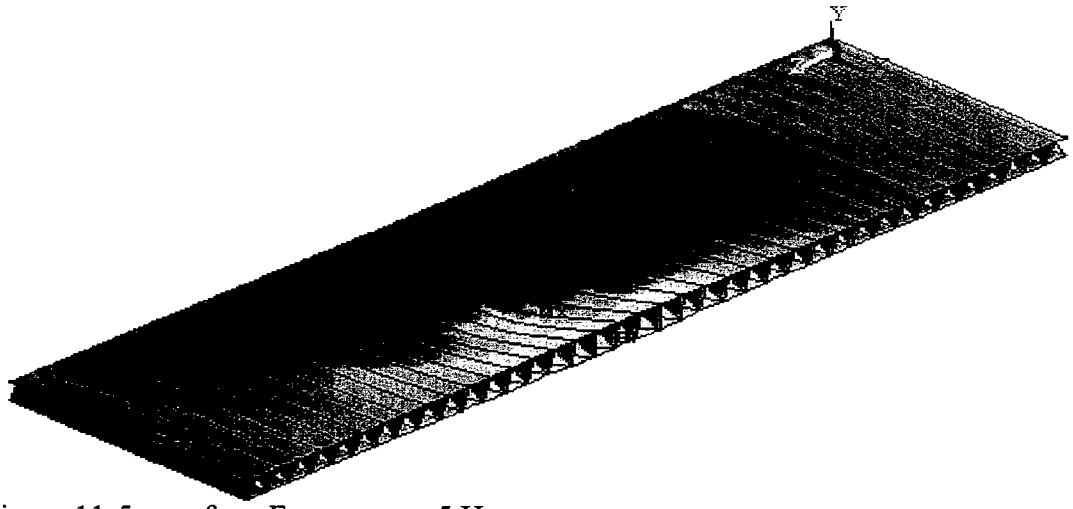

Figure 11-5 – σ_x for a Frequency = 5 Hz

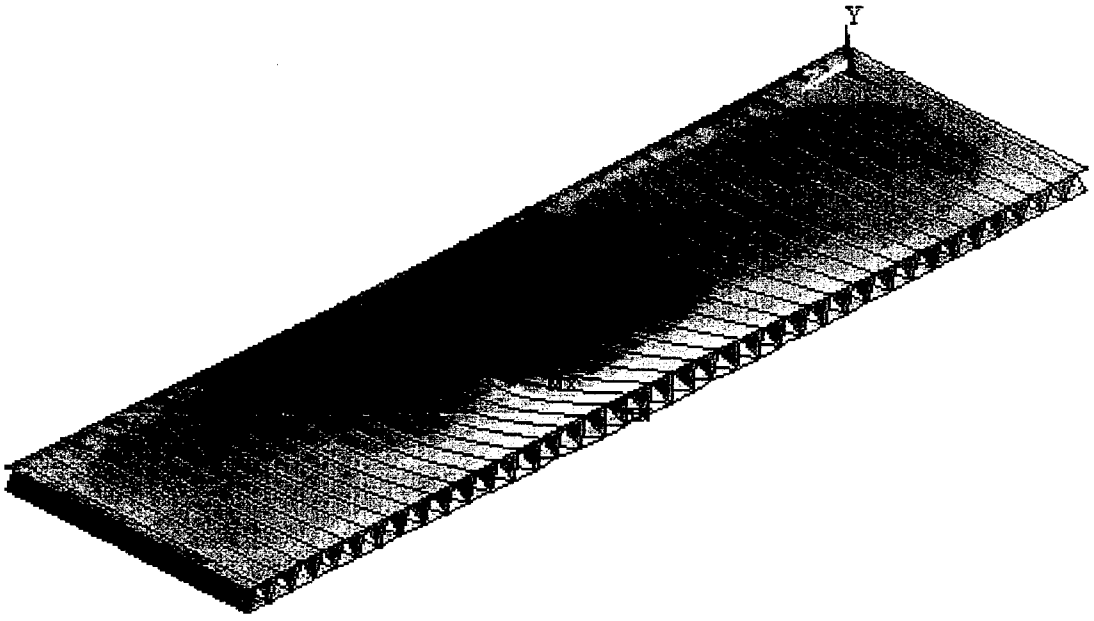

Figure 11-6 – σ_x for a Frequency = 10 Hz

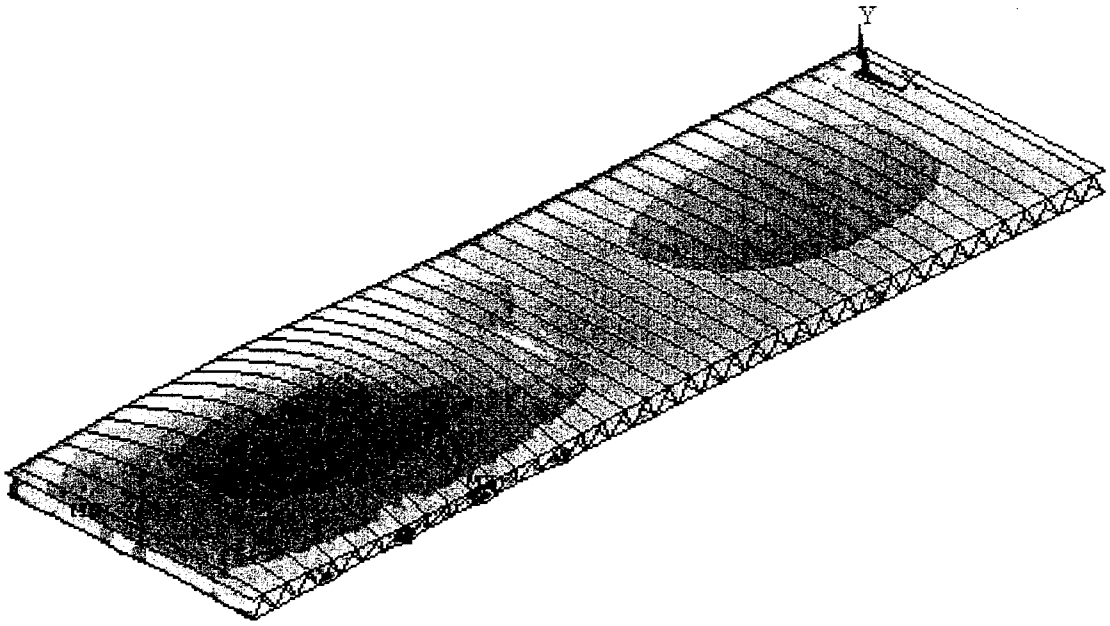

Figure 11-7 – σ_x for a Frequency = 15 Hz

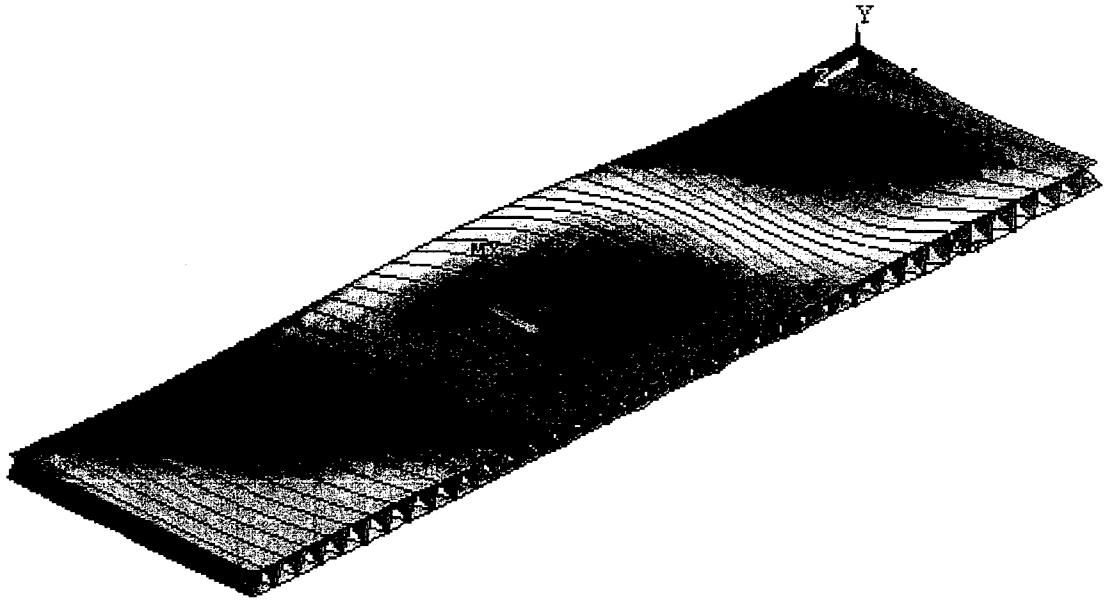

Figure 11-8 – σ_x for a Frequency = 20 Hz

CHAPTER 12

PART B : CONCLUSIONS AND RECOMMENDATIONS

12.1 Conclusions

The original intent of this research was to determine a model that could be fabricated and tested in a laboratory. From previous research by Ballard [29], tube and sheet models were statically analyzed using both hand calculations and the ANSYS 5.3 finite element computer program. From the data result of that static analysis two models were chosen as the most feasible. The 12.7 cm x 17.8 cm x 1.9 cm (5" x 7" x ¾") tubes with 1.9 cm (¾") cover sheets and the 10.2 cm x 10.2 cm x 0.64 cm (4" x 4" x ¼") with 2.54 cm (1") cover sheets were chosen for their efficiency. The reason for the tube and sheet models was that the shapes are ones from the Extren Design Manual, which were assumed to be readily available.

The research by Ballard also discovered localized shear stresses at the boundary when supported in all three translational directions, as well as, high localized buckling stresses in some of the webs close to the supports. In this study, it was suggested that sloped webs be utilized to try and reduce these stresses. Also, creating a monolithic model would help to reduce the discontinuities between the tubes. This study did not

focus on the particular attachment of the deck to the stringers; however, it is suggested that a simple epoxy adhesive would be a practical choice versus using a bolt. Although bolts are more readily available and the design of the connections is more prevalent, using the epoxy adhesive would allow for no spacing between the webs. The use of a bolt attachment would require a specific amount of spacing between the webs.

The tube and sheet models from Ballard's research were narrowed down to one tube and sheet model, Model Y, the 12.7 cm x 17.8 cm x 1.9 cm (5" x 7" x ¾") tubes with 1.9 cm (¾") cover sheets, which was further used in this study. In addition to the tube and sheet model, four monolithic models were analyzed under static conditions with an impact factor of 1.3. This impact factor is to take into account the dynamic effects of the vehicular traffic on the bridge. Another purpose of this research was to determine if this impact factor, or dynamic load factor, of 1.3 was adequate for fiber reinforced polymer. The way to determine if this impact factor was sufficient is to perform a forced vibration dynamic analysis and compare the results to a static analysis without the impact factor included in the load.

One data comparison that was performed utilized the static analysis data for all the models. The varying thickness, slope of the web, and distance between the webs was compared to see what, if any, effect these variables had on the stresses in the model. These comparisons showed that the larger the thickness then the lower the stresses became and that as the distance between the webs increases the stresses increase as well. Also, from these comparisons, the models that would be the most efficient to use in the dynamic portion of this research would be chosen. The models that were chosen for the

dynamic portion were Model 1, Model 4, Model 5 and Model Y. Model Y was chosen in order to determine how the tube and sheet models would perform under dynamic conditions.

Once the static analysis had performed and the most suitable models chosen, a free vibration dynamic analysis was performed to determine the dynamic properties, such as, the frequency and mode shape. The importance of determining the natural frequencies of the deck was to determine if the phenomenon of resonance exists. Resonance is when the natural frequencies of the bridge are close enough to the frequency of the vehicle to cause a deleterious failure. From the research by Williams [36], the frequency of a vehicle is approximately 3.0 Hz. Figure 10-9 of Chapter 10 details how the frequency of the AASHTO HS20-44 truck varies with the wheel base length and speed. The comparison of the frequencies for Model 1, Model 4, Model 5, Model Y, and the vehicle shows that Model Y's fundamental frequency is very close to the vehicle therefore, suggesting the potential for possible failure due to resonance. The conclusion that was drawn from the free vibration dynamic analysis was that the monolithic models had a high enough frequency to keep away from resonance. In order to fully determine if the monolithic models would not reach a resonant frequency Model 5 was analyzed with span lengths of 11.58 m (38'-0") and 17.37 m (57'-0"). The conclusion from this analysis was that the frequency decreased as the span length increased but not acutely enough to come to make resonance a concern during its normal use.

No model could be specifically determined as the most feasible from the free dynamic analysis, however, the static analysis showed that Model 5 performed the best. With this conclusion, the forced vibration dynamic analysis was performed to determine the dynamic deflection and therefore, the dynamic load factor. The data extracted from this analysis was compared to data from a static analysis, without the impact factor included, in order to determine the suitability of the 1.3 impact factor previously mentioned. This comparison showed that the 1.3 impact factor was adequate.

From the previous chapters and analysis, Model 5 performs the most efficiently and would be an appropriate section to use in a real life application. The only problem with this model is that an epoxy adhesive would have to be used versus a bolt since there is no space between the webs. This problem may allow for an alternative section that has spacing between the webs to be chosen as well. The previous chapters have shown that Model 1 and Model 4, monolithic models, would be sufficient as this alternate. Model Y, the tube and sheet model, was deemed insufficient due to its possibility of resonance.

12.2 Recommendations for Future Work

Although this research was to determine a feasible model for testing, this section will discuss items that need to be addressed before a full-scale deck can be implemented. The issue of connection of the FRP spans to each other and the FRP deck to the stringers has not been addressed and needs to be analyzed before the bridge deck can be used in a real life situation. Also, how the lighter FRP section with a wearing surface effects the hydraulics of the movable bridge needs to be analyzed in order to determine if the

hydraulic equipment is more than necessary. One other investigation that needs to be performed is a cost analysis. This cost analysis will show how the difference between using a steel deck configuration with a concrete deck and a FRP cross section, such as one determined in this research, will effect the cost in the long run. This cost study will analyze the cost of FRP versus concrete as well as the long term cost impact due to the quicker construction time and the fewer repairs that will be required. Therefore, it must be approached as a life cycle cost analysis.

One other element of typical structural design that has not been discussed thus far is that of fracture and fatigue. This issue is one that can be taken care of by researching the earlier application of FRP in aircraft design. The drastic changing of temperatures going from the ground to the higher altitudes shows that FRP performs very well under such extreme conditions of stress reversal. However, extensive testing is required to determine the exact fatigue effects in structural applications, as well as, the specific stresses that will occur for the sections modeled in this research.

LIST OF REFERENCES

[1] Loud, S., ed. (1995, October 16). Composites News: Infrastructure (Issue No. 33).

[2] Bettigole, R. A., (1996). Exodermic Bridge Deck on Bascule Bridges. 6th Biennial Symposium, Heavy Movable Structures, Inc.

[3] Bridge Flooring Systems. (1991). Cheswick, PA: IKG GREULICH, Inc.

[4] EXTREN Fiberglass Structural Shapes: Design Manual. (1989). Bristol, VA: Strongwell, Inc.

[5] Standard Specifications for Highway Bridges (16th ed.). (1996). Washington, DC: AASHTO, Inc.

[6] Standard Specifications for Movable Highway Bridges. (1988). Washington, DC: AASHTO, Inc.

[7] Hoa, S. V. (1995). Computer Aided Design of Polymer-Matrix Composite Structures. New York: Marcel Dekker, Inc.

[8] Loewenstein, K. L. (1993). The Manufacturing Technology of Continuous Glass Fibres (3rd ed.). New York: Elsevier

[9] Design Guide: Standard & Custom Fiberglass-Reinforced Structural Shapes (Volume 2). Creative Pultrusions, Inc.

[10] Dumlao, C., et. al. Demonstration Low Cost Modular Composite Highway Bridge. Lockheed Martin Missiles and Space, Research and Development Division, Palo Alto, CA.

[11] Pfister, T. (1996, September 23). Current FWHA Sponsored FRP Composite Research Projects. (E-Mail correspondence with T. Pfister @ ITD.STATE.ID.US). Idaho Transportation Department.

[12] Mirmiran, A., and Shahawy, M. (1997, May). Behavior of Concrete Columns Confined by Composites. J. Structural Engineering, ASCE, 123(5), 583-590.

[13] Sen, R., Mariscal, D., and Shahawy, M. (1993, September-October). Durability of Fiberglass Pretensioned Beams. ACI Structural J., 90(5), 525-533.

[14] Seible, S., Karbhari, V. (1996, August). Advanced Composites Build on Success. Civil Engineering, 44-47.

[15] (1994, July 18) Trucks Welcome on U.K. Plastics Span. ENR, 233, 22-23.

[16] Ashley, S. (1995, May). First Plastic Bridge. Mechanical Engineering, 117, 16.

[17] Bonds Mill Lift Bridge: Promotional Literature. (1997). Beckenham, Kent, UK: Maunsell Structural Plastics, Ltd

[18] (1996, April). Composite Bridge Reopens Trail to Historic Lighthouse. Civil Engineering, 96.

[19] Liao, K., et. al. Long-Term Durability of Composites in Secondary Infrastructure Applications. Northwestern University, Evanston, IL.

[20] Bruce, R. N. (1990, August 21-23). Fiber Reinforced Plastic Bridges in Chongqing 1983-1988. Developments in Structural Engineering: Proceedings of the Forth Rail Bridge Centenary Conference, 159-164.

[21] Hool, G. A.(1943). Moveable and Long-Span Steel Bridges (2nd ed.). New York: McGraw-Hill, Inc.

[22] Sixth Biennial Symposium Proceedings. (1996, Oct. 30 - Nov. 1). Middletown, NJ: Heavy Movable Structures, Inc.

[23] Bascule Span Framing Plan: Sunrise Boulevard Bridge. (1984). Fort Lauderdale, FL: Kunde Driver & Associates, Inc.

[24] Tonias, D. E. (1995) Bridge Engineering: Design Rehabilitation and Maintenance of Modern Highway Bridges. New York: McGraw-Hill, Inc.

[25] ANSYS Multi-Physics 5.3: FEA Software. (1997). Houston, PA: ANSYS, Inc.

[26] Murphy, J. (1990). PcBridge v2.60: Computer Software. Madison, WI.

[27] Xanthakos, P. P. (1994). Theory and Design of Bridges. New York : Wiley.

[28] Taly, N. (1998). Design of Modern Highway Bridges. New York: McGraw Hill.

[29] Ballard, J. (1997). Fiber Reinforced Polymer (FRP) Composite Deck for Moveable Bridges. Thesis (Master's). University of Central Florida.

[30] Timoshenko, S. (1952). History of Strength of Materials. New York: McGraw-Hill Book Co.

[31] Edwards, L.N. (1959). A Record of History and Evolution of Early American Bridges. Orono, Maine: University Press.

[32] Deflection Limitation of Bridges, (May 1958). Progress Report of the ASCE Committee on Delflection Limitations of Bridges. Proc., ASCE, 84(ST3), Paper no. 1633, pp. 1633-1 - 1633-19.

[33] Biggs, J.M. (1964). Introduction to Structural Dynamics. New York: McGraw-Hill Book Co.

[34] Fenves, S.J., Veletsos, A.S., and Siess, C.P. (1962). "Dynamic Studies of the AASHTO Road Test Bridges". Highway Res. Board Spec. Rep. 73, p 83.

[35] Waker, W.H. and Veletsos, A.S. (1963). "Response of Simple Span Highway Bridges to Moving Vehicles". Univ. Illinois, Civil Eng. Studies, Structural Res. Ser. No. 272.

[36] Williams, M. (1997). Impact of Moving Traffic Loads and Boundary Conditions on the Dynamic Response of Highway Bridges. Thesis (Master's). University of Central Florida.

[37] Mallick, P.K., ed. (1997). Composites Engineering Handbook. New York: Marcel Dekker.

[38] Hwang, S.J. and Gibson, R.F. (1992). "The Use of Strain Energy Based Finite Element Techniques in the Analysis of Various Aspects of Damping of Composite Materials and Structures". J. Compos Mater. 26(17):2585.

[39] American Society of Civil Engineers/ Rutgers University. (1997). "Tacoma Narrows". URL: http://www-civeng.rutgers.edu/asce/tacoma.html.

[40] Paz, Mario. (1991). Structural Dynamics: Theory and Computation. New York, New York: Van Nostrand Reinhold.